Avdelningen för Konstruktionsteknik
Lunds Tekniska Högskola
Box 118
221 00 LUND

Division of Structural Engineering
Faculty of Engineering, LTH
P.O. Box 118
S-221 00 LUND
Sweden

Axial load determination using modal analysis

Beräkning av axiell last genom modal analys

Stefan Fässler

2014

Report TVBK-5233
ISSN 0349-4969
ISRN: LUTVDG/TVBK-14/5233+(128pp)

Master Thesis
Supervisor: Roberto Crocetti
June 2014

Abstract

The report investigates the use of measured transversal vibrations to estimate the axial load on beams/columns.

A literary review of the basic theory is performed, which clearly shows the theoretical relation between natural frequency and axial loading of linear structural elements (strings & beams). Current journal articles show that research has been done on mathematical models as well as some experimental studies. Basic theory and current research show that the impact of support conditions is of great importance to the relation between frequency and load. Thus an approach which models the support conditions as unknowns (springs) is suggested and used in the remainder of the study. The method requires the measurement of both the natural frequency and the corresponding mode shape for calculation purposes.

The calculations are performed using both an analytical and a discrete approach. Numerical testing shows that the method is highly sensitive for the measured shape of the vibration mode. Testing of the discrete algorithm has shown stability/convergence issues if the discretization level is too detailed. However the ability to use an excess of measurement points than necessary (over-determined system) to describe the mode shape seems to overcome some stability issues.

The experimental studies to date have mainly focused on tensile tests performed on slender structures. Laboratory testing on four compressive samples with varying slenderness is performed in order to investigate the applicability on real-life structures.

Testing results show that the presented approach yields loading estimates highly sensitive to the mode shape. Estimation quality is significantly improved by the use of excess shape measurements. Also the load estimations seem to overestimate the magnitude of loading. The use of both Bernoulli-Euler and Timoshenko beams show that the former tends to yield even higher estimates of loading.

The study shows that the suggested method is promising for axial load identification, yet further investigations are required. Specifically improvements to the measurement/calculation of the mode shape are necessary.

Preface

This thesis constitutes the final part of the civil engineering program at Lund University and was written in the fall of 2013 and spring of 2014.

The initial thesis idea was supplied by Tore Nilsson, which also included a field test at production facilities owned by Stora Enso. Even though the measurement data was not usable (due to equipment malfunction), I would like to Tore Nilsson (Brosys) and Stefan Johansson (Stora Enso) for arranging the field testing.

I would also like to thank the people who made this thesis possible: my supervisor Roberto Crocetti for his guidance, Anders Sjöström for all the help with the measurement equipment and all the people who facilitated the laboratory testing in the midst of a major renovation of the research facilities.

Finally I would like to thank my wife for all her patience and support during my studies.

Lund, June 2014

Stefan Fäßler

Notation

Abbreviations

B&K	Brüel o Kjaer (Measurement equipment/software supplier)
FE(M)	Finite Element (Method)
FFT	Fast Fourier Transform
FRF	Frequency Response Function
DOF	Degree Of Freedom
MDOF	Multiple Degrees Of Freedom
SDOF	Single Degree Of Freedom
sym.	Indicates that a matrix is symmetric

Operators (X used as a placeholder)

$\dot{X},\ \ddot{X},\ \dddot{X}$	1st, 2nd and 3rd derivative with respect to time
X	**BOLD** denotes a matrix (or vector)
$\boldsymbol{X}^{e}$	Element matrix

Lower case roman letters

b	Width (of a beam)
d	Depth (of a beam)
f	Frequency [in Hz]
i	Integer (1,2,3…∞) indicating order of frequency
k	Spring stiffness
t	Time variable
u	Displacement or shape measurement
x	Coordinate along axis of object (beam, string, etc.)
y	Coordinate orthogonal to axis

Upper case roman letters

A	Cross sectional area
D	Mode shape amplitude
E	Young's modulus (of elasticity)
G	Shear modulus
I	Moment of inertia
K	Stiffness matrix
L	Length
L_{CR}	Buckling length
M	Moment
M	Mass matrix
N (N_{cr}, N_{Rd})	Axial force (Euler buckling load, design load)
S	Static moment of area
V	Shear force

Greek

ω (ω_0)	Frequency [in rad/s] (frequency of unloaded sample)
ϕ	Mode shape
ρ	Mass density
κ	Correction factor for shear stiffness
λ (λ_{rel})	Slenderness ratio (relative slenderness ratio)

Contents

Abstract i

Preface iii

Notation v

1 Introduction 1

- 1.1 Background 1
- 1.2 Aim of thesis 1
- 1.3 Method 1
- 1.4 Limitations 1
- 1.5 Outline 2

2 Vibration theory 3

- 2.1 System with a single degree-of-freedom (SDOF) 3
- 2.2 System with multiple degrees-of-freedom (MDOF) 4
- 2.3 From string to beam 5
  - 2.3.1 String 5
  - 2.3.2 Bernoulli-Euler beam 6
  - 2.3.3 Axially loaded Bernoulli-Euler beam 7
  - 2.3.4 Timoshenko beam 7
  - 2.3.5 Axially loaded Timoshenko beam 8

3 Transversal vibrations & axial load 11

- 3.1 Modeling approach when measuring existing structures 14
  - 3.1.1 Continuous solution 15
  - 3.1.2 Discretized solution (FEM) 15
- 3.2 Element matrices 17
  - 3.2.1 Spring stiffness matrix 18
- 3.3 Numerical testing & sensitivity analysis 18
  - 3.3.1 Analytical approach 19
  - 3.3.2 Discretized approach 26
- 3.4 Concluding remarks 34

4 Experimental modal analysis 37

5 Laboratory testing 39

- 5.1 Background 39
- 5.2 Test specimens 39
- 5.3 Testing procedure 40
  - 5.3.1 Compression testing procedure 40
  - 5.3.2 Modal testing procedure 41
  - 5.3.3 Modal data extraction 43
- 5.4 Modal results 43
- 5.5 Analysis of modal results 49
- 5.6 Calculation procedure 50

5.7 Results – Analytical approach 50
5.7.1 B1020 53
5.7.2 B1530 55
5.7.3 B2040 56
5.7.4 B4590 58

5.8 Analysis – Analytical approach 59

5.9 Results – Discretized approach 60
5.9.1 B1020 60
5.9.2 B1530 61
5.9.3 B2040 63
5.9.4 B4590 64

5.10 Analysis – Discretized approach 66

6 Conclusion 67

6.1 Further research 68

References 69

Appendix

A – Calculation code .... A – I
rebecchi .... A – I
reveig .... A – I
beam .... A – III
Numerical testing – Analytical approach .... A – V
Numerical testing – Discrete approach .... A – VI
Laboratory testing – Analytical approach .... A – VIII
Laboratory testing – Discrete approach .... A – IX

B – Calculation of beam properties .... B – I

C – Test results .... C – I
Driving point FRFs .... C – I
Frequency shifts at 4Z .... C – VIII

D – Calculation results .... D – I
B1020 .... D – I
B1530 .... D – VII
B2040 .... D – XIII
B4590 .... D – XIX

1 Introduction

1.1 Background

The ability to measure axial loads is of great importance in order to verify models and design assumptions. The use of strain gauges is a quite well established method to detect a change in loading, but this method requires a reference level to yield an absolute loading value.

Measuring an absolute value of loading can be accomplished for instance by lifting the structure in question or by measuring the deflection induced by applying a transversal load (for example as shown by Tullini et al. [1]). Yet given the sizes of structures and loads common in civil engineering this can be a very arduous if not impossible task.

Therefore it is of great interest to be able to determine axial loads by measuring the natural frequencies of a structure, since the effort involved is less laborious.

1.2 Aim of thesis

The objective of this report is to determine methods to estimate axial loads by experimental modal analysis. Since the presented methods should be applicable for real-life structures in civil engineering, special focus will be on structures in compression with varying slenderness.

1.3 Method

A literature study is carried out in order to discover the current methods and experimental results when determining the axial load by modal analysis. On the basis of previous research a calculation methodology is chosen and numerically tested.

Due to a lack of experimental data regarding compressive loads and no investigations regarding non-slender structures, experiments investigating the applicability on elements with varying slenderness are carried out.

1.4 Limitations

The study will focus purely on transversal vibrations of beams within the boundaries of linear elasticity (i.e. plasticity and/or longitudinal and twisting vibrations are not considered). Furthermore the only considered material is steel due to its homogeneity and well defined mechanical properties.

1.5 Outline

The thesis consists of the following chapters:

1 – Introduction

The background and aim of the study are introduced.

2 – Vibration theory

In order to understand the used concepts the basic theory of free vibration is reviewed shortly. The different components influencing the transversal vibration of an axially loaded beam are investigated by examining linear structural elements (strings & beams) with increasing complexity.

3 – Transversal vibrations & axial load

The application of transversal vibrations with regards to axial load is examined by reviewing previous research. The adopted approach is presented and numerically tested.

4 – Experimental modal analysis

A brief review of experimental modal analysis is given with specific focus on the methodology used in the laboratory testing.

5 – Laboratory testing

The testing procedure is described, which includes the practical laboratory work, the extraction of modal data and the different calculative procedures. Results and analysis of laboratory testing are presented separately for each calculative procedure.

6 – Conclusion

The conclusions drawn from previous chapters are summarized and points for improvements/further research are suggested.

2 Vibration theory

The used approach to determine the axial load by means of vibrations makes use of two different relations:

- The effect of stiffness on the natural frequency of a system
- The effect of axial load on the transversal stiffness

The former relation is illustrated by examining the free vibrations of both a single degree-of-freedom (SDOF) and a multiple degree-of-freedom (MDOF) system. In order to understand the latter phenomena, the governing differential equations for beams (and a string) are shortly reviewed and the solution with regard to natural frequency for simply supported structures is presented.

The scope of this review is limited to transversal vibrations and furthermore the effect of damping on the natural frequency is considered negligible (which is a common assumption[2]). The intent is to give a base for further discussion (in conclusions), so for more detailed derivations the reader is referred to Chopra [2] and/or Timoshenko et al. [3].

2.1 System with a single degree-of-freedom (SDOF)

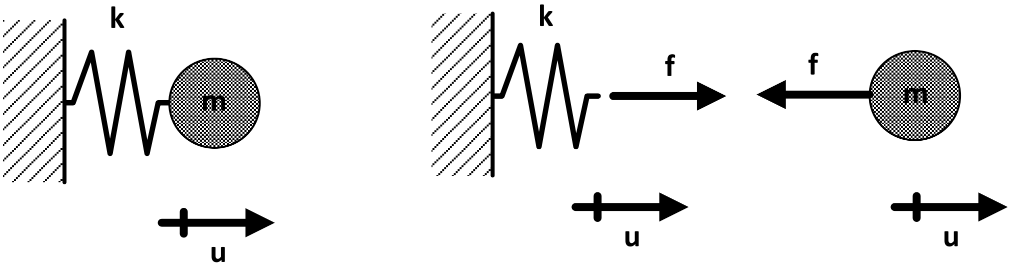

Figure 2.1 *Free vibration of a SDOF system including free body diagram*

The most basic system in structural dynamics is the free vibration of a small mass attached to a spring (see above). By Using Hooke's law together with Newton's law of motion, the equilibrium equation can be established:

$$m \cdot \ddot{u} + k \cdot u = 0 \tag{2.1}$$

This differential equation has the general solution:

$$u = A\,cos(\omega t) + B\,sin(\omega t) \tag{2.2}$$

$$\dot{u} = \omega(-A\,sin(\omega t) + B\,cos(\omega t)) \tag{2.3}$$

$$\ddot{u} = -\omega^2(A\,cos(\omega t) + B\,sin(\omega t)) = -\omega^2 u \tag{2.4}$$

Insertion in the differential equation and solving for the natural frequency yields:

$$\omega = \sqrt{\frac{k}{m}} \tag{2.5}$$

Thus if the mass is kept constant the conclusion can be made that

$$\omega \propto k \tag{2.6}$$

and that an increase in stiffness will lead to an increase in frequency and vice versa. The opposite applies if the mass is altered whilst keeping stiffness constant:

$$\omega \propto \frac{1}{m} \tag{2.7}$$

These general effects of mass and stiffness on the natural frequency also holds true for more complex approaches as will be seen later in this chapter.

2.2 System with multiple degrees-of-freedom (MDOF)

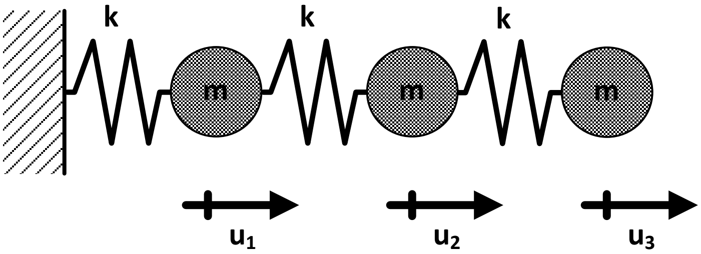

Figure 2.2 *Free vibration of a MDOF system*

The behavior of a MDOF system is exemplified by a system with three DOFs. Assuming all springs are equally stiff and all masses are equal, Hooke's law and Newton's law of motion can be used to determine the equilibrium equation for each node, which in matrix notation has the form:

$$\begin{bmatrix} 2k & -k & 0 \\ & 2k & -k \\ sym. & & k \end{bmatrix} \begin{bmatrix} u_1 \\ u_2 \\ u_3 \end{bmatrix} + \begin{bmatrix} m & 0 & 0 \\ & m & 0 \\ sym. & & m \end{bmatrix} \begin{bmatrix} \ddot{u}_1 \\ \ddot{u}_2 \\ \ddot{u}_3 \end{bmatrix} = \begin{bmatrix} 0 \\ 0 \\ 0 \end{bmatrix} \tag{2.8}$$

$$\boldsymbol{M} \cdot \ddot{\boldsymbol{u}} + \boldsymbol{K} \cdot \boldsymbol{u} = \boldsymbol{0} \tag{2.9}$$

The solution of this system is similar to the SDOF system but includes a shape vector, which describes the mode shape of the particular vibration frequency:

$$\boldsymbol{u} = (A\,cos(\omega t) + B\,sin(\omega t))\boldsymbol{\phi_n} \tag{2.10}$$

$$\dot{\boldsymbol{u}} = \omega(-A\,sin(\omega t) + B\,cos(\omega t))\boldsymbol{\phi_n} \tag{2.11}$$

$$\ddot{\boldsymbol{u}} = -\omega^2(A\,cos(\omega t) + B\,sin(\omega t))\boldsymbol{\phi_n} = -\omega^2\boldsymbol{u} \tag{2.12}$$

Insertion into the differential equation (2.9) yields the following Eigenvalue problem:

$$(\boldsymbol{K} - \omega^2 \boldsymbol{M})\boldsymbol{\phi} = \boldsymbol{0} \tag{2.13}$$

Thus there exist as many natural frequencies as the number of DOF of the system. Furthermore for the non-trivial solution (i.e. non rigid body motion) the problem is reduced to:

$$|\boldsymbol{K} - \omega^2 \boldsymbol{M}| = \boldsymbol{0} \tag{2.14}$$

As previously mentioned when examining the SDOF system, the natural frequency is proportional to the stiffness and inverse proportional to the mass of the system.

2.3 From string to beam

In order to understand the different aspects which influence the transversal vibrations of a column, the differential equations of free vibration and the resulting natural frequencies for various axially loaded elements are presented. Generally a similar ansatz as (2.10) is used for all the elements discussed:

$$y = \phi(A\,cos(\omega t) + B\,sin(\omega t)) \tag{2.15}$$

2.3.1 String

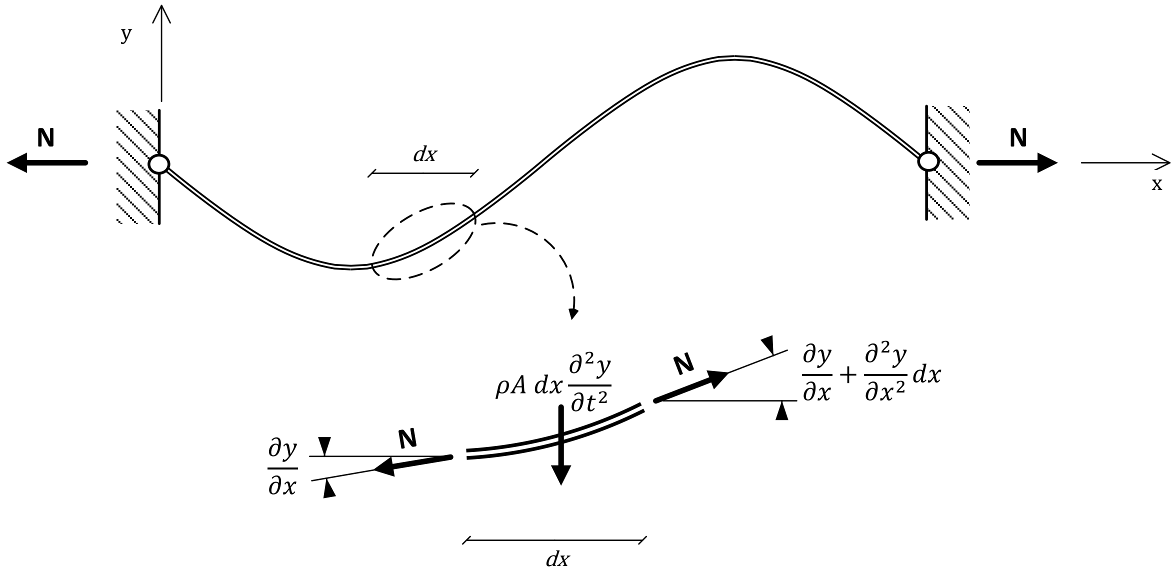
y
N
N
x
dx
$\rho A\,dx\frac{\partial^2 y}{\partial t^2}$
N
$\frac{\partial y}{\partial x} + \frac{\partial^2 y}{\partial x^2}dx$
$\frac{\partial y}{\partial x}$
N
dx

Figure 2.3 *Free vibration of a string (based on* **[3]***)*

The transversal strength/stiffness of a string is entirely dependent on the axial force (due to the low bending stiffness of the string being negligible). The differential equation of motion can easily be deduced from the dynamic equilibrium in the transversal direction:

$$N\left(\frac{\partial y}{\partial x} + \frac{\partial^2 y}{\partial x^2}dx\right) - N\frac{\partial y}{\partial x} - \rho A\,dx\frac{\partial^2 y}{\partial t^2} = 0 \tag{2.16}$$

$$N\frac{\partial^2 y}{\partial x^2} = \rho A\frac{\partial^2 y}{\partial t^2} \tag{2.17}$$

Thus for a simply supported string (fixed in both ends) the natural frequencies and corresponding mode shapes are

$$\omega_i = \frac{i\pi}{L}\sqrt{\frac{N}{\rho A}} \tag{2.18}$$

$$\phi_i = D_i\, sin\left(\frac{i\pi x}{L}\right) \tag{2.19}$$

$$(i = 1{,}23, \dots, \infty)$$

The mode shape and frequency for a given string depends therefore solely on the axial force. Furthermore the mode shape of the ith frequency will display a total of i crests/troughs.

2.3.2 Bernoulli-Euler beam

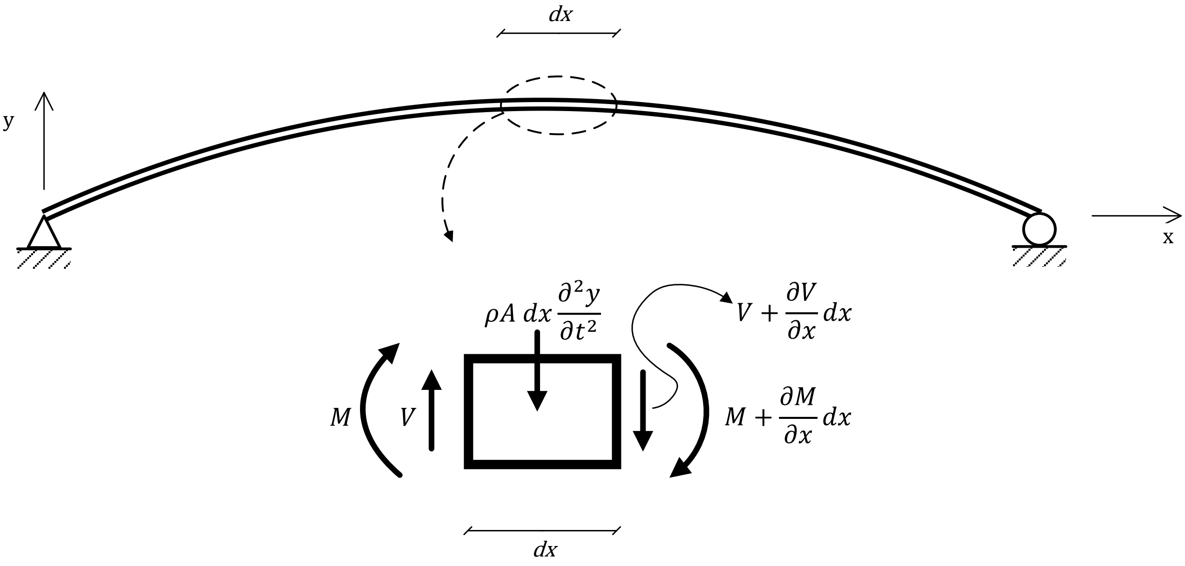

dx
y
x
$\rho A\, dx\frac{\partial^2 y}{\partial t^2}$
$V + \frac{\partial V}{\partial x}dx$
M
V
$M + \frac{\partial M}{\partial x}dx$
dx

Figure 2.4 *Free vibration of a Bernoulli-Euler beam (based on* **[3]***)*

For a Bernoulli-Euler beam the governing differential equation is determined using equilibrium equations and for a prismatic beam the differential equation has the form:

$$EI\frac{\partial^4 y}{\partial x^4} = -\rho A\frac{\partial^2 y}{\partial t^2} \tag{2.20}$$

In case of a simply supported beam the mode shape is exactly the same as for the string (see equation (2.19)) and the natural frequency is:

$$\omega_i = \left(\frac{i\pi}{L}\right)^2 \sqrt{\frac{EI}{\rho A}} \tag{2.21}$$

Note the resemblance to the simply supported string and that the effects of mass/stiffness on the natural frequency are the same as for the SDOF system.

2.3.3 *Axially loaded Bernoulli-Euler beam*

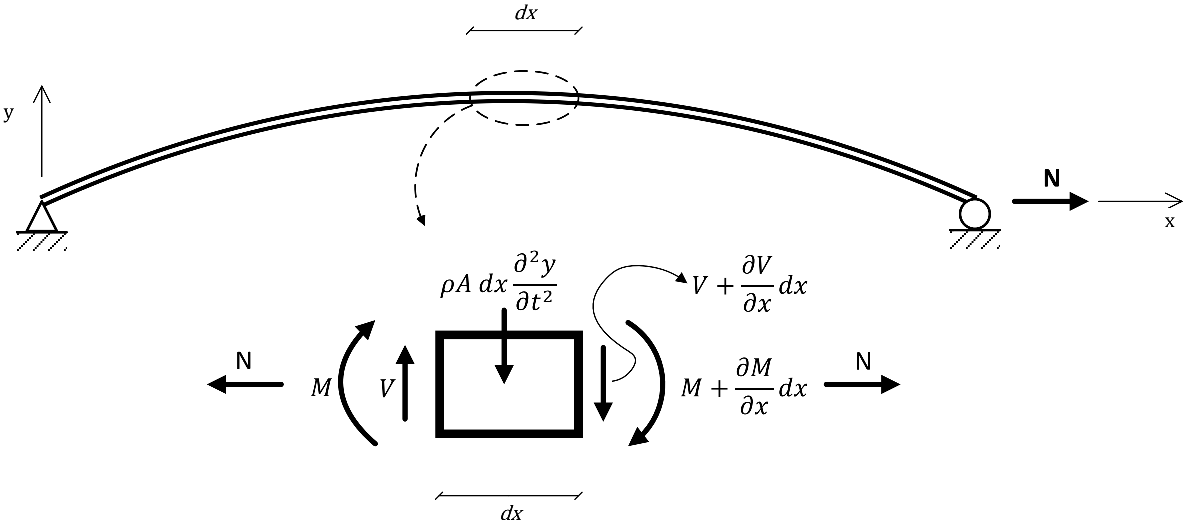
dx
y
N
x
$\rho A\, dx \frac{\partial^2 y}{\partial t^2}$
$V + \frac{\partial V}{\partial x} dx$
N
M
V
$M + \frac{\partial M}{\partial x} dx$
N
dx

Figure 2.5 *Free vibration of an axially loaded Bernoulli-Euler beam (based on* **[3]***)*

By subjecting the beam to an axial load the governing differential equation is appended by one term, which considers the influence of an axial force:

$$EI\frac{\partial^4 y}{\partial x^4} - N\frac{\partial^2 y}{\partial x^2} = -\rho A\frac{\partial^2 y}{\partial t^2} \tag{2.22}$$

When simply supported the mode shape still corresponds with the string (see equation (2.19)) and the natural frequency is:

$$\omega_i = \left(\frac{i\pi}{L}\right)^2 \sqrt{\frac{EI}{\rho A} + \frac{N}{\rho A}\left(\frac{L}{i\pi}\right)^2} \tag{2.23}$$

Note that for a negligible bending stiffness or axial force the expression reverts to the natural frequency of a string or beam respectively (see equation (2.18) & (2.21)). Also for higher frequencies (large i), the impact of the axial force diminishes.

2.3.4 *Timoshenko beam*

In elementary beam theory the depth of the beam is assumed to be small in comparison to the length; moreover the effects of rotational inertia and shear deformation of a cross sectional element are neglected. A more complete formulation of the differential equation can be proposed if these are taken into account.

During the vibration of a beam, a small element not only undergoes a translational but a rotational movement as well. The moment due to a rotating beam element is given by:

$$-\rho I \frac{\partial^3 y}{\partial x \partial t^2} dx \tag{2.24}$$

Thus the differential equation when taking into account rotational inertia for a prismatic beam is:

$$EI \frac{\partial^4 y}{\partial x^4} = -\rho A \frac{\partial^2 y}{\partial t^2} + \rho I \frac{\partial^4 y}{\partial x^2 \partial t^2} \tag{2.25}$$

The deformation of the beam is more precisely described if the cross section is allowed to rotate with respect to the neutral axis (due to shear deformation). The differential equation considering both these phenomena is:

$$EI \frac{\partial^4 y}{\partial x^4} = -\rho A \frac{\partial^2 y}{\partial t^2} + \rho I \frac{\partial^4 y}{\partial x^2 \partial t^2} + \frac{\rho I E}{\kappa G} \frac{\partial^4 y}{\partial x^2 \partial t^2} - \frac{\rho^2 I}{\kappa G} \frac{\partial^4 y}{\partial t^4} \tag{2.26}$$

The mode shape of the beam is still described by equation (2.19) and the natural frequency is determined by the following equation:

$$\omega_i^2 = \frac{EI}{\rho A}\left(\frac{i\pi}{L}\right)^4 - \left(\omega_i \frac{i\pi}{L}\right)^2 \frac{I}{A} - \left(\omega_i \frac{i\pi}{L}\right)^2 \frac{EI}{\kappa GA} + \omega_i^4 \frac{\rho I}{\kappa GA} \tag{2.27}$$

Note that for both the above equations the last three terms consider the rotational inertia, shear deformation and their combined impact respectively. By omitting the last term, which has a very small impact [3], the following expression for the natural frequency can be obtained [4]:

$$\omega = \frac{\left(\frac{i\pi}{L}\right)^2 \sqrt{\frac{EI}{\rho A}}}{\sqrt{1 + \frac{I}{A}\left(\frac{i\pi}{L}\right)^2 + \frac{EI}{\kappa GA}\left(\frac{i\pi}{L}\right)^2}} \tag{2.28}$$

It can clearly be seen that the influence of the discussed factors (2nd and 3rd term of the denominator) increases for the higher natural frequencies; however for the lower frequencies of more common beams the impact is negligible as has been exemplified by Timoshenko [3] and further studied by Abramovich and Elishakoff [5]. It should also be noted that these corrections lead to a **lowering** of the calculated frequency (see equation (2.21)).

2.3.5 Axially loaded Timoshenko beam

The most complete description of a beam element is thus the axially loaded Timoshenko beam and its free vibration is governed by the following differential equation [6]:

$$EI\left(1+\frac{N}{\kappa AG}\right)\frac{\partial^4 y}{\partial x^4}-N\frac{\partial^2 y}{\partial x^2}=-\rho A\frac{\partial^2 y}{\partial t^2}+\rho I\left(1+\frac{N}{\kappa AG}+\frac{E}{\kappa G}\right)\frac{\partial^4 y}{\partial x^2\partial t^2}-\frac{\rho^2 I}{\kappa G}\frac{\partial^4 y}{\partial t^4} \tag{2.29}$$

A simple expression for the natural frequency is not possible, even for the simply supported case which has been used so far.

3 Transversal vibrations & axial load

The expressions for the natural frequency in a string and an axially loaded Bernoulli-Euler beam (equation (2.18) & (2.23)) clearly show that a compressive axial force will lower the natural frequency of the structure. The same is true for the Timoshenko beam although this demands a numerical analysis as for instance Abramovich [7] has performed. Thus by measuring the natural frequency of a column it is theoretically possible to calculate the axial load.

Note that there is a close relationship between the free vibration and the buckling of beams. As has been pointed out by Abramovich [7], an exclusion of the time derivatives from the differential equations will result in a buckling analysis. An approximate[1] relation between natural frequency and the buckling load has been developed by Galef [9], which holds true for most single span support conditions of Bernoulli-Euler beams [8]:

$$\left(\frac{\omega}{\omega_0}\right)^2 = 1 - \frac{N}{N_{cr}} \tag{3.1}$$

Table 3.1 *Support conditions for which* (3.1) *holds true (in grey)*

	Free	Pinned	Sliding	Clamped
Free			■	■
Pinned		■	■	■
Sliding	■	■	■	■
Clamped	■	■	■	■

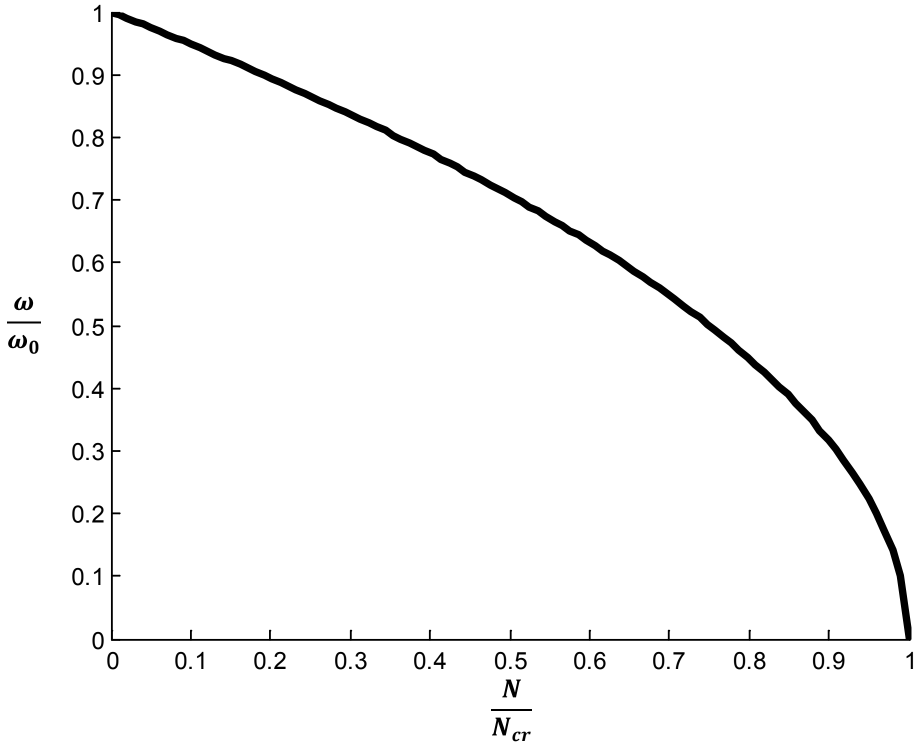

Figure 3.1 *Relationship between compressive axial load and natural frequency for certain single-span beams*

---

[1] The expression is in fact exact for the support conditions in Table 3.1, which has been shown by Bokaian. [8]

This relationship does not hold for Timoshenko beams [7], where a small divergence is seen at half the critical buckling load (see Figure 3.2). Also note that the unloaded fundamental frequency for a Timoshenko beam is not the same as for a Bernoulli-Euler beam.

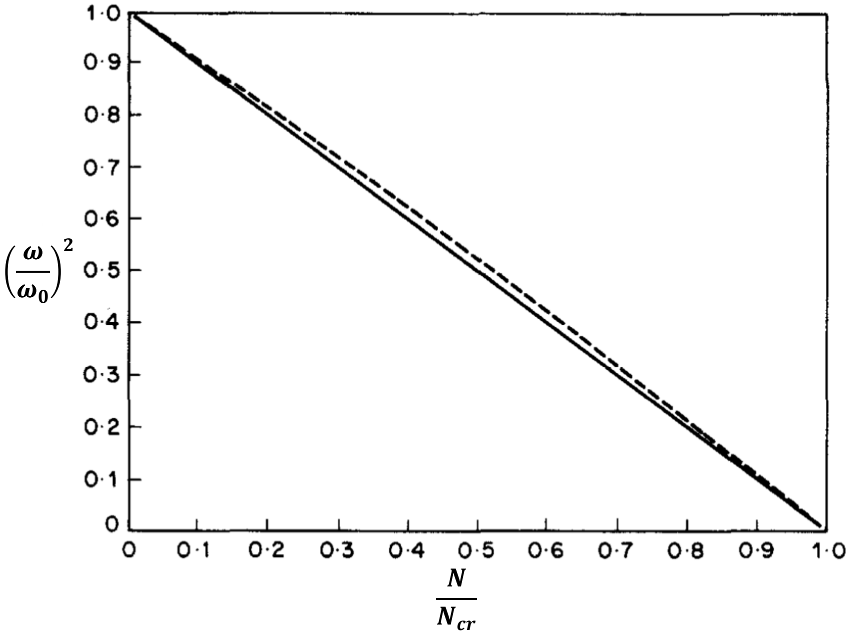

Figure 3.2 *Load vs frequency; Simply supported Bernoulli-Euler beam (solid) and Timoshenko beam (dotted);* **[7]**

Thus the calculation of compressive axial forces by means of transversal frequency is in essence a dynamic version of buckling analysis. In buckling slender beams conform to the standard Euler curve, whilst for bulkier cross sections plasticity influences the load bearing capacity (see Figure 3.3) and purely elastic buckling is not limiting.

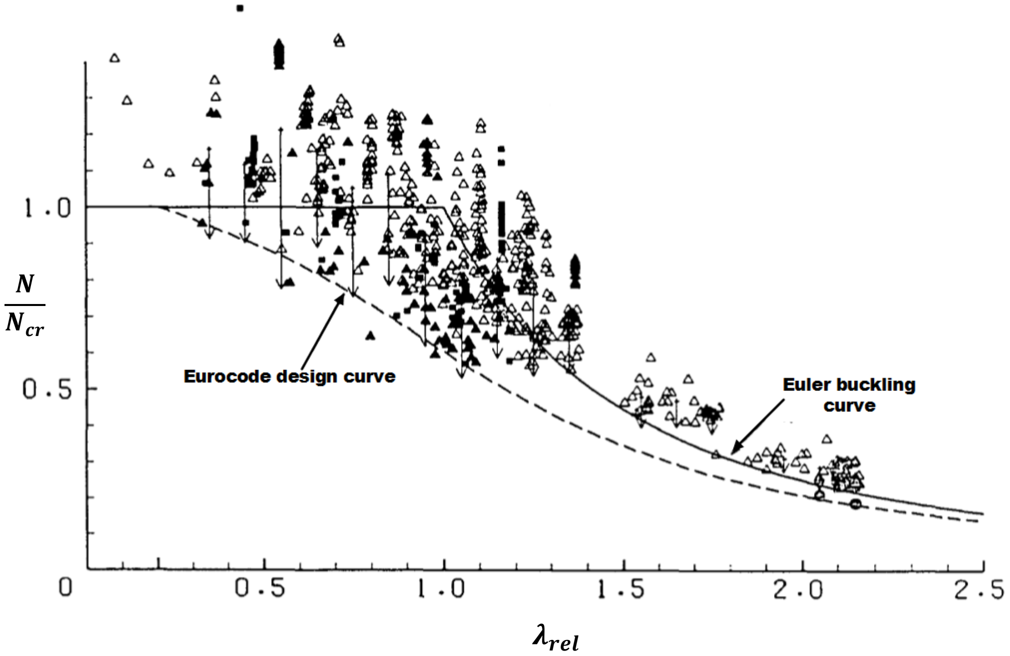

Figure 3.3 *Load bearing capacity vs slenderness;* **[10]** *(modified notation)*
Testing specimen variability vs Design curve & Euler buckling curve

An extensive amount of work has been done to confirm the link between axial load and bending frequency, however a large amount of this has been purely theoretical/numerical (e.g. Bokaian [8]). The conducted studies that have included experimental testing have dealt with slender structures and have mainly focused on tensile tests (e.g. Virgin and Plaut [11], Rebecchi et al. [12], etc.). Testing has mainly been performed on metal specimens, although one body of work has dealt with timber (Laux [13]).

Although buckling theory diverges from load capacity for beams of decreasing slenderness, the same might not be true for the effect on natural frequency as long as testing is done within the elastic range. This is particularly of interest within civil engineering, since structures in this field are generally designed with intermediate slenderness and are supposed to experience loads within the elastic range under normal service life conditions.

It should however be mentioned that the impact of axial force on transversal frequency will greatly diminish with decreasing slenderness. This can easily be observed by studying equation (2.23), where a very large bending stiffness of the Bernoulli-Euler beam, clearly leads to a diminished impact of axial load on natural frequency.

This may also be realized by the fact that the buckling load greatly increases with increasing stiffness and thus a change in the load/buckling load ratio will demand greater change in loading. This in turn is proportional to the frequency as can be seen in the Galef equation (3.1).

Aside from the stiffness due to the cross section of the beam or the beam theory used, the support stiffness also has a considerable impact on the unloaded natural frequency of the beam and thus the frequency shift under load, which has been shown by numerical investigations by Amba-Rao [14]:

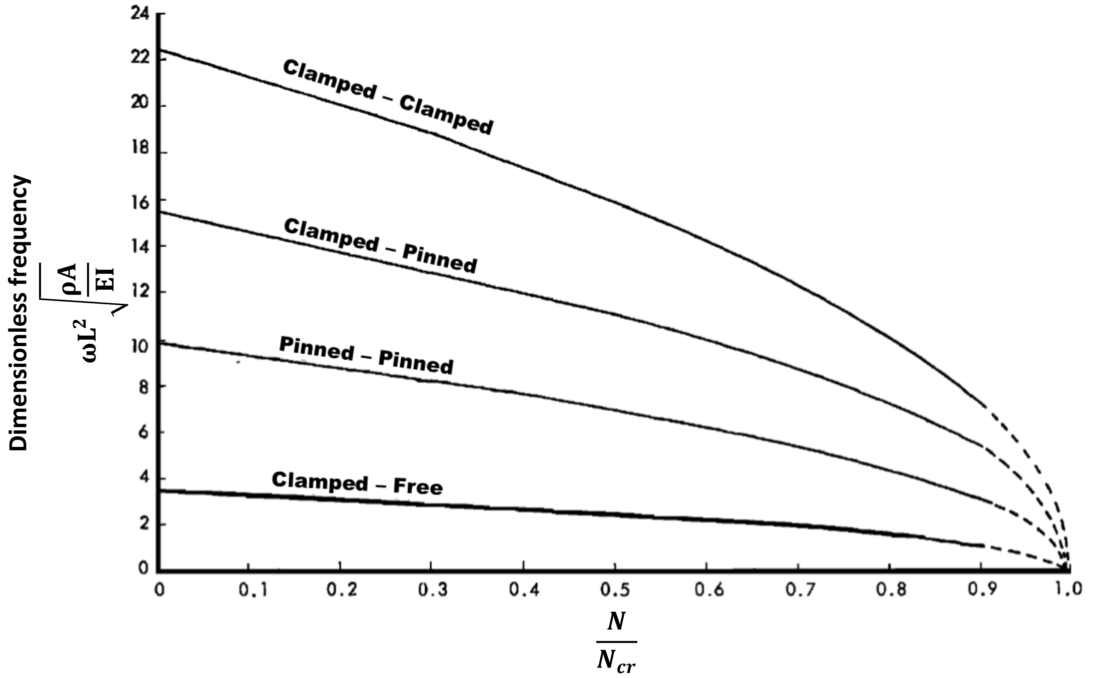

Figure 3.4 *Load vs frequency, effects of support stiffness ;* **[14]** *(modified notation)*

3.1 Modeling approach when measuring existing structures

In order to determine the axial load using modal data, the used model must conform to the real structure. The following conditions should therefore be met in the modeling procedure:

- Well described geometry of the tested sample (exact dimensions including possible imperfections as curvatures)
- Known material stiffness of the tested structure (Young's modulus)
- The structure should be operating within its elastic range
- Well modeled support conditions

Support conditions in particular can be difficult to model accurately, since joints in buildings rarely constitute a clear case such as a true hinge or a true clamp. Therefore it is advantageous to model the supports with springs, which has the further advantage that parts of a structure can be analyzed independently (e.g. a column being part of a frame structure).

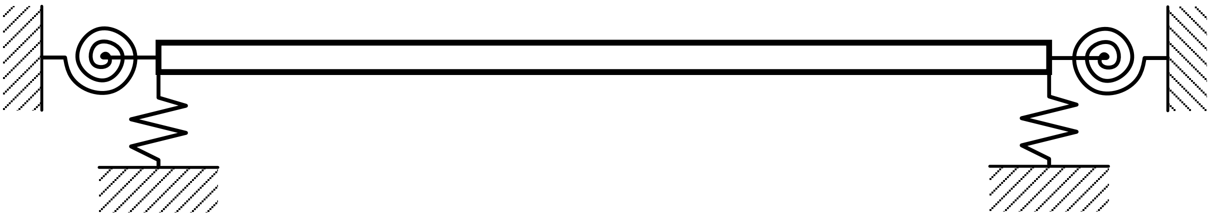

Figure 3.5 *Beam with spring supports*

Introducing spring supports involve 4 additional unknown quantities (besides the axial load), which theoretically can be solved in two ways:

- Measuring several frequencies
- Measuring frequency(ies) and identifying the corresponding mode shape(s)

Experimental work by Livingston et al. suggests that employing higher natural frequencies results in less accuracy and greater variation even though more measurements than necessary are made [15]. Thus using only frequencies with a model such as suggested in Figure 3.5 would demand at least the five lowest transversal frequencies (assuming a lack of symmetry) and is therefore not advisable. An approach employed by Rebecchi et al. using only the fundamental frequency with the corresponding mode shape seems to give satisfactory results. [12]

Both the above mentioned approaches make use of the Bernoulli-Euler beam although in the case of Rebecchi et al. the solution is obtained analytically (a continuous model), whilst Livingston uses a discretized approach (FEM). There have however been studies employing a Timoshenko model like Amabili et al. [16] or Laux [13].

It should be mentioned that the above approaches also yield estimates for the support conditions of the beam model (see Figure 3.5). In the case of work done by Tullini et al. [17] (preceding Rebechi et al.) the calculated values of the springs stiffness are not a satisfactory estimation of support condition as Laux [13] points out. However since the main aim of this investigation is to determine the axial loads, there is no reason to dismiss the methods, yet the results regarding support conditions should be regarded purely as a byproduct.

In this report both the continuous and the FE method will be used and in the latter both a Bernoulli-Euler and a Timoshenko beam element will be employed.

3.1.1 Continuous solution

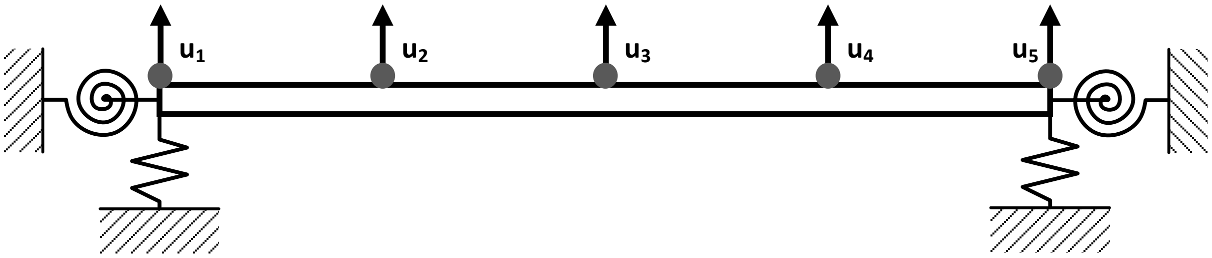

Figure 3.6 *Beam with springs & measurement points*

According to Rebecchi et al. by measuring the frequency and the corresponding mode shape in five points with an even spacing, the axial load can be determined using the equation below. The measured input parameters ($u_1 - u_5$ & ω) and the resulting load (N) have been highlighted in bold.

$$\frac{\boldsymbol{u_2}+\boldsymbol{u_4}}{\boldsymbol{u_3}}=\frac{\frac{\boldsymbol{u_1}+\boldsymbol{u_5}}{\boldsymbol{2u_3}}+1+2\cos\left(\frac{q_1}{4}\right)\cosh\left(\frac{q_2}{4}\right)}{\cos\left(\frac{q_1}{4}\right)+\cosh\left(\frac{q_2}{4}\right)} \tag{3.2}$$

Where

$$q_1^2=\frac{1}{2}\left(\sqrt{n^2+4\lambda^4}-n\right),\qquad q_2^2=\frac{1}{2}\left(\sqrt{n^2+4\lambda^4}-n\right)=q_1^2+n$$

$$n=\frac{\boldsymbol{N}L^2}{EI},\qquad \lambda^4=\boldsymbol{\omega}^2\frac{\rho AL^4}{EI}$$

Note that the measurement points do not have to be evenly spaced for the method to be used, but in that case the application is not as straightforward and the solution requires solving the math numerically. For obvious reasons the measured mode shape should not have a nodal point at the middle measurement point (u_3) if the equation above is to be used.

3.1.2 Discretized solution (FEM)

This solution employs the Eigenvalue problem of a MDOF system (see equation (2.13)). Assuming both the frequency and the mass matrix of the beam is known, the stiffness matrix may be divided into three parts.

$$(\boldsymbol{K_0}+N\cdot\boldsymbol{K_G}+\boldsymbol{K_k}-\omega^2\boldsymbol{M})\boldsymbol{\phi}=\boldsymbol{0} \tag{3.3}$$

$\boldsymbol{K_0}$ Stiffness matrix accounting for the axially unloaded beam

$\boldsymbol{K_G}$ Stiffness matrix accounting for the effect of axial load

$\boldsymbol{K_k}$ Stiffness matrix introducing the support springs

Thus the equation above consists of 5 unknown entities within the parenthesis (axial load and four spring stiffness values). The mode shape on the other hand consists of the measured mode shape points, whilst the remaining parts are unknown.

This matrix equation yields a system of equations that can be solved by means of a non-linear least square method, as for instance MATLAB's lsqnonlin function. However a straightforward solving of the equation system will entail solving for all the variables (including the unknown elements of the shape vector).

The use of finite elements yields an approximate solution that requires using a well discretized system for convergence. Thus numerous beam elements are needed for a satisfactory solution which in turn yields a large amount of variables in the above system. Theoretically this system of equations can of course be solved, but finding a numeric solution can be very demanding from a computational standpoint.

Since the only variable of real interest in the equation system is the axial load, a reduction of the problem can be made by condensing the system to the measured DOFs only. In order to explain this approach equation (3.3) is reformulated:

$$\boldsymbol{S\phi} = \mathbf{0} \tag{3.4}$$

Where

$$\boldsymbol{S} = \boldsymbol{K_0} + N \cdot \boldsymbol{K_G} + \boldsymbol{K_k} - \omega^2 \boldsymbol{M}$$

The shape vector ($\boldsymbol{\phi}$) contains both the measured parts of the shape as well as unknowns. The system is now rearranged so that all the known elements of $\boldsymbol{\phi}$ are collected at the top. In order for the equation system not to change, the corresponding columns of $\boldsymbol{S}$ must be moved to the front of the matrix. The same shift is made to the rows of $\boldsymbol{S}$, which has no effect on the system since all elements of $\mathbf{0}$ are zero. This last operation is done in order to insure that a later matrix inversion is possible (see equation (3.8)).

When all known elements of the shape are collected the equation system can be divided into parts separating the known and unknown elements of the shape (subscript a and b respectively):

$$\begin{bmatrix} \boldsymbol{S_{aa}} & \boldsymbol{S_{ab}} \\ \boldsymbol{S_{ba}} & \boldsymbol{S_{bb}} \end{bmatrix} \begin{bmatrix} \boldsymbol{\phi_a} \\ \boldsymbol{\phi_b} \end{bmatrix} = \begin{bmatrix} \mathbf{0}_{\boldsymbol{a}} \\ \mathbf{0}_{\boldsymbol{b}} \end{bmatrix} \tag{3.5}$$

This equation system can be split into two separate matrix equations and rearranged to remove the unknown shape parameters ($\boldsymbol{\phi_b}$) from the system:

$$\boldsymbol{S_{aa}\phi_a} + \boldsymbol{S_{ab}\phi_b} = \mathbf{0}_{\boldsymbol{a}} \tag{3.6}$$

$$\boldsymbol{S_{ba}\phi_a} + \boldsymbol{S_{bb}\phi_b} = \mathbf{0}_{\boldsymbol{b}} \tag{3.7}$$

(3.7)

$$\boldsymbol{\phi_b} = \boldsymbol{S_{bb}^{-1}}(\mathbf{0}_{\boldsymbol{b}} - \boldsymbol{S_{ba}\phi_a}) = -\boldsymbol{S_{bb}^{-1}S_{ba}\phi_a} \tag{3.8}$$

(3.6)+(3.8)

$$\boldsymbol{S_{aa}\phi_a} - \boldsymbol{S_{bb}S_{bb}^{-1}S_{ba}\phi_a} = \mathbf{0}_{\boldsymbol{b}} \tag{3.9}$$

$$(\boldsymbol{S_{aa}} - \boldsymbol{S_{bb}S_{bb}^{-1}S_{ba}})\boldsymbol{\phi_a} = \mathbf{0}_{\boldsymbol{b}} \tag{3.10}$$

Thus a discretized system with e.g. 1000 DOFs can be passed to a non-linear solver (such as lsqnonlin) with only five unknowns.

Unlike the analytical approach, mode shapes with a central nodal point can be accepted. However zero values in the same DOF as the spring constants, lead to the spring constant to be eliminated from the equation system. The non-linear solver will thus not be able find a solution for this variable. A quick fix to this solution is assigning an arbitrary value to the particular spring constant.

3.2 Element matrices

Timoshenko beam element matrices developed by Kosmatka [18] are used. By setting the factor θ to zero and excluding the mass matrix due to rotational inertia $\mathbf{M_R}$, the elements revert to a normal Bernoulli-Euler beam. Note that the following matrices do not contain longitudinal degrees of freedom, which are normally considered to be uncoupled from the translational and rotational deformation.

The stiffness matrix of a beam element is given by one 1st order component and one geometric component (due to axial load):

$$\boldsymbol{K^e} = \boldsymbol{K_0^e} + \boldsymbol{K_G^e} \tag{3.11}$$

$$\boldsymbol{K_0^e} = \frac{EI}{(1+\theta)L^3}\begin{bmatrix} 12 & 6L & -12 & 6L \\ & (4+\theta)L^2 & -6L & (2-\theta)L^2 \\ & & 12 & -6L \\ sym. & & & (4+\theta)L^2 \end{bmatrix} \tag{3.12}$$

$$\boldsymbol{K_G^e} = \frac{1}{30L(1+\theta)^2}\begin{bmatrix} 36+60\theta+30\theta^2 & 3L & -(36+60\theta+30\theta^2) & 3L \\ & (4+5\theta+2{,}5\theta^2)L^2 & -3L & -(1+5\theta+2{,}5\theta^2) \\ & & 36+60\theta+30\theta^2 & -3L \\ sym. & & & (4+5\theta+2{,}5\theta^2)L^2 \end{bmatrix} \tag{3.13}$$

Where
$$\theta = \frac{12}{L^2}\frac{EI}{\kappa GA} \tag{3.14}$$

In an equal manner the mass matrix is given by the sum of the translational component and the rotational component:

$$\boldsymbol{M^e} = \boldsymbol{M_T^e} + \boldsymbol{M_R^e} \tag{3.15}$$

$$\boldsymbol{M_T^e} = \frac{\rho AL}{210(1+\theta)^2}\begin{bmatrix} (70\theta^2+147\theta+78) & (35\theta^2+77\theta+44)\frac{L}{4} & (35\theta^2+63\theta+27) & -(35\theta^2+63\theta+26)\frac{L}{4} \\ & (7\theta^2+14\theta+8)\frac{L^2}{4} & (35\theta^2+63\theta+26)\frac{L}{4} & -(7\theta^2+14\theta+6)\frac{L^2}{4} \\ & & (70\theta^2+147\theta+78) & -(35\theta^2+77\theta+44)\frac{L}{4} \\ sym. & & & (7\theta^2+14\theta+8)\frac{L^2}{4} \end{bmatrix} \tag{3.16}$$

$$\boldsymbol{M_R^e} = \frac{\rho I}{30(1+\theta)^2L}\begin{bmatrix} 36 & -(15\theta-3)L & -36 & -(15\theta-3)L \\ & (10\theta^2+5\theta+4)L^2 & (15\theta-3)L & (5\theta^2-5\theta-1)L^2 \\ & & 36 & (15\theta-3)L \\ sym. & & & (10\theta^2+5\theta+4)L^2 \end{bmatrix} \tag{3.17}$$

Where
$$\theta = \frac{12}{L^2}\frac{EI}{\kappa GA} \tag{3.18}$$

3.2.1 Spring stiffness matrix

Although this is not an element matrix per se, the implementation of the spring supports can be done by adding the stiffness of the springs at the appropriate DOFs. What is actually done is an assembly of the springs stiffness elements followed by a static condensation (see [19] for a thorough review). Thus the stiffness matrix introducing spring supports for a beam as in Figure 3.5 can be written as (all non-filled positions being zero):

$$\boldsymbol{K_k} = \begin{bmatrix} k_1 & & & & \\ & k_2 & & & \\ & & \ddots & & \\ & & & k_3 & \\ & & & & k_4 \end{bmatrix} \tag{3.19}$$

3.3 Numerical testing & sensitivity analysis

The presented calculation approaches are tested numerically. A beam with the same geometric and material properties as in the laboratory tests (B2040 see chapter 5.2) is chosen and modelled as simply supported.

Table 3.2 *Beam properties*

Length		1	L	$[m]$
Depth		10	d	$[mm]$
Width		20	b	$[mm]$
Slenderness ratio		242,1	λ	
Relative slenderness ratio		3,2	λ_{rel}	
Buckling load		7,1	N_{cr}	$[kN]$
Design load		6,1	N_{Rd}	$[kN]$
Unloaded theoretical natural frequency	1st	36,6	ω_0	$[Hz]$
	2nd	118,7		
	3rd	247,7		

The analytical equations for natural frequency and mode shape (equation (2.23) and (2.19) respectively) are used to establish input values for calculations. The measurement points used for calculations are chosen according to the laboratory testing setup.

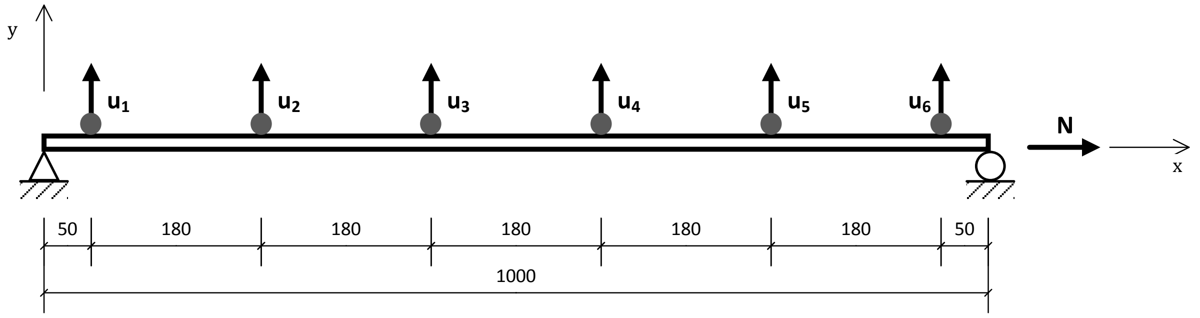

Figure 3.7 *Beam used for numeric testing [mm]*

Using the mode shapes/frequencies the loads are calculated using the various approaches and then checked against the loads used to calculate the input values (frequencies and mode shape).

3.3.1 Analytical approach

Since the setup includes six measurement points, calculations can be performed using the five measurement points at either end. Due to the symmetry of the shape and point placement using both set of points is redundant and only the left five will be used.

Compressive loads ranging from zero up to the Euler buckling load are used to calculate the first three natural frequencies at each loading level. These frequencies are then used to calculate the compressive force by means of the analytical approach (see chapter 3.1.1).

In order to check the robustness of the method a sensitivity analysis is performed as well. Percentage errors (up to ± 10 %) are applied to the input parameters and the resulting error in load calculation is determined. The elastic modulus, material density, the frequency and the mode shape are investigated.

Error analysis of the mode shape is not straightforward since a difference in total magnitude has no impact. Instead a relative error of the terms $(u_1 + u_5)$, $(u_2 + u_4)$ and u_3 will change the results using equation (3.2). Remaining parameters such as length and cross sectional properties can generally be measured with quite high certainty even in situ and are therefore not part of the sensitivity analysis.

3.3.1.1 Results

The calculated loads using the first three natural frequencies are the **exact same** load that was used to calculate the input parameters. A detailed presentation of the results e.g. by means of a table is therefore meaningless and will be omitted.

The presented results of the sensitivity analysis compare the impact on the first three frequencies at 60 % of the first Euler buckling load. Also the impact of varying loading level is presented for the first natural frequency.

Note that the y-axis scaling used for Young's modulus, density and frequency is ± 2 %, whilst a scaling of ± 10 % is used for the shape parameters. The error for each input/output parameter is calculated according to:

$$Error = \frac{Faulty\ value - True\ value}{True\ value} \tag{3.20}$$

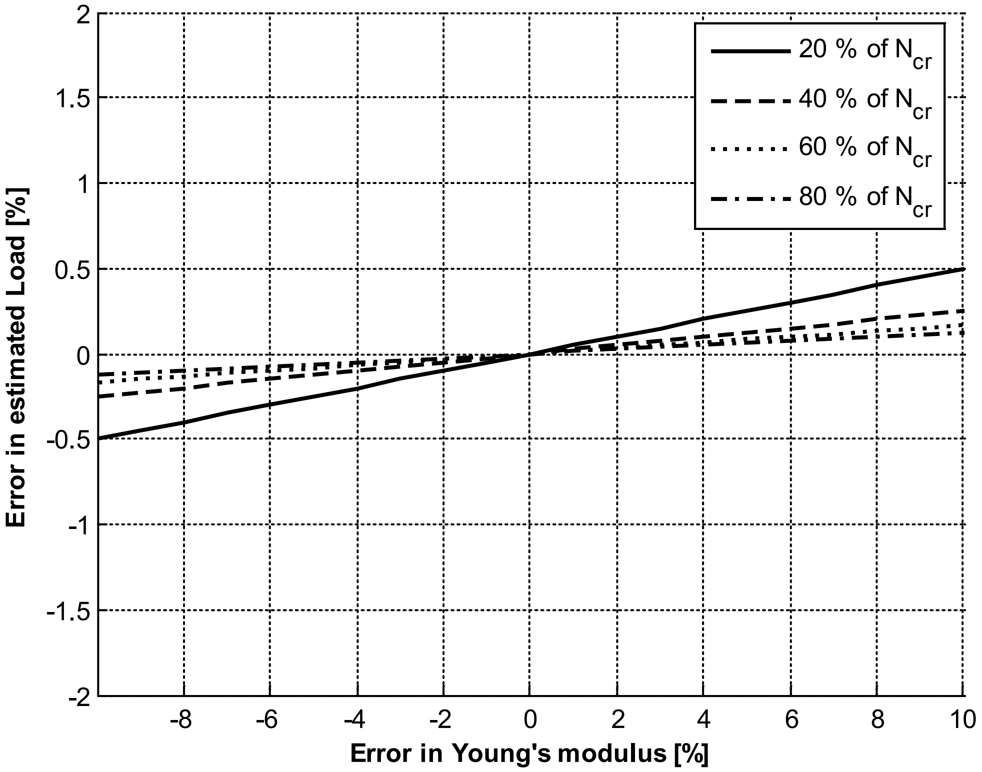

Figure 3.8 *Sensitivity of calculated load with respect to Young's modulus at 60 % of theoretical buckling load*

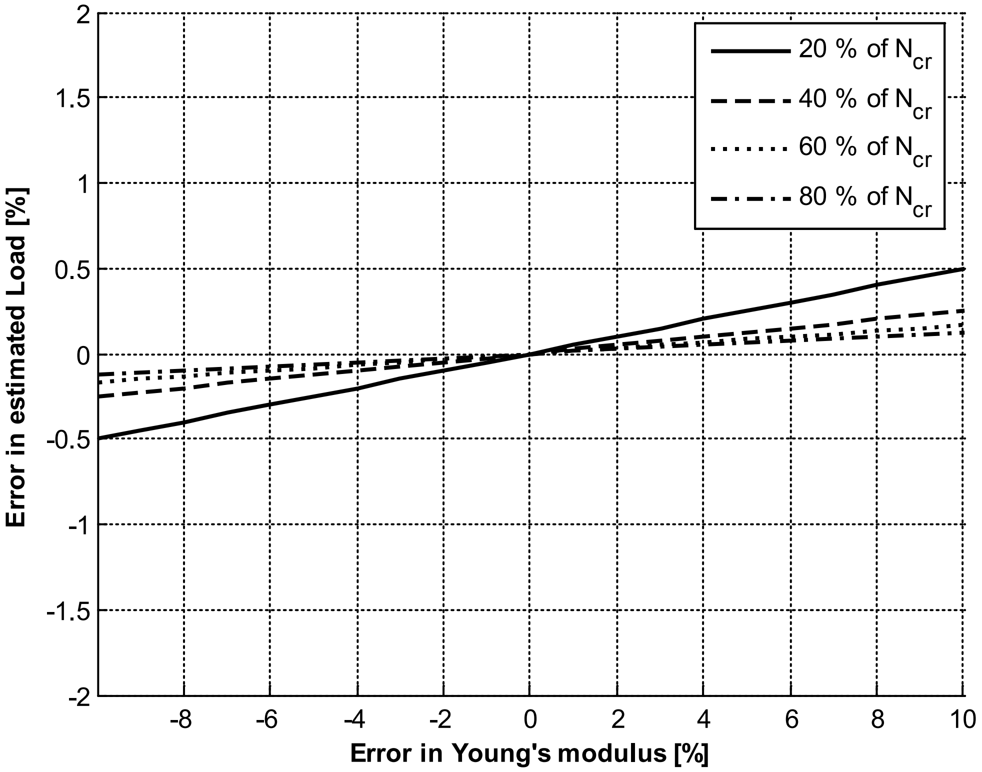

Figure 3.9 *Sensitivity of calculated load with respect to Young's modulus for 1st natural frequency*

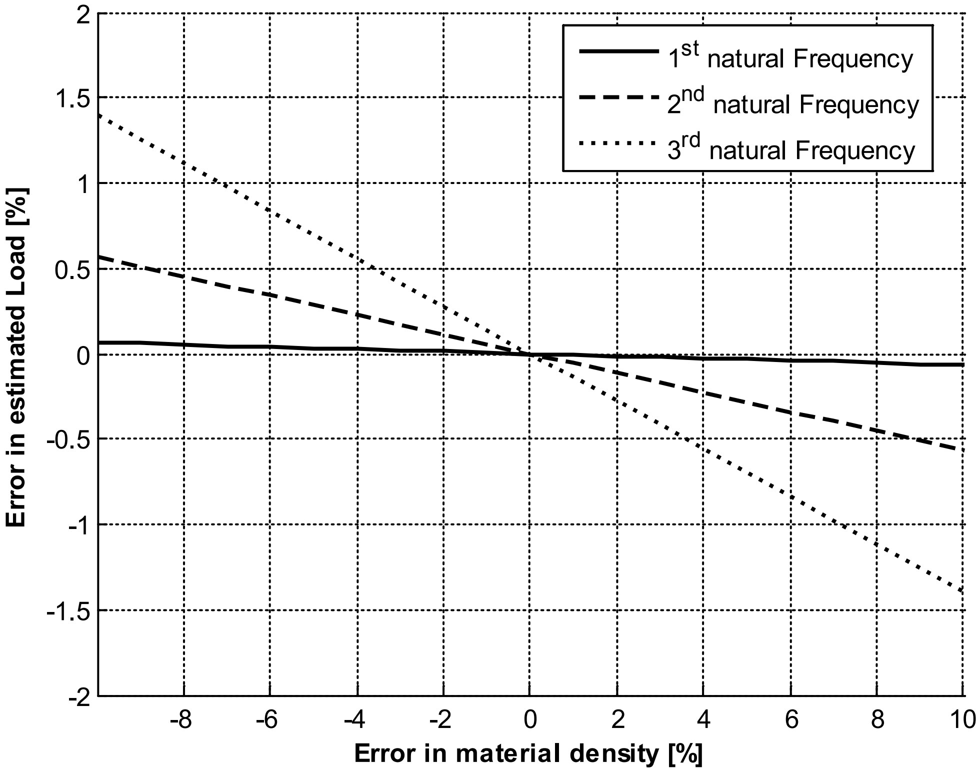

Figure 3.10 *Sensitivity of calculated load with respect to density at 60 % of theoretical buckling load*

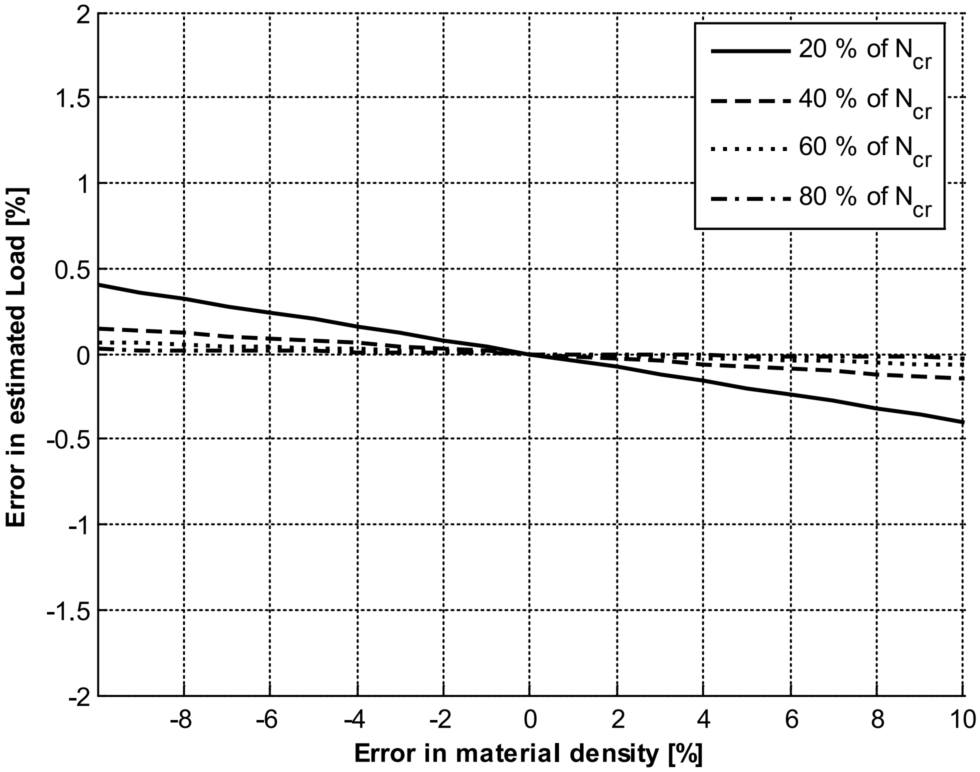

Figure 3.11 *Sensitivity of calculated load with respect to density for 1st natural frequency*

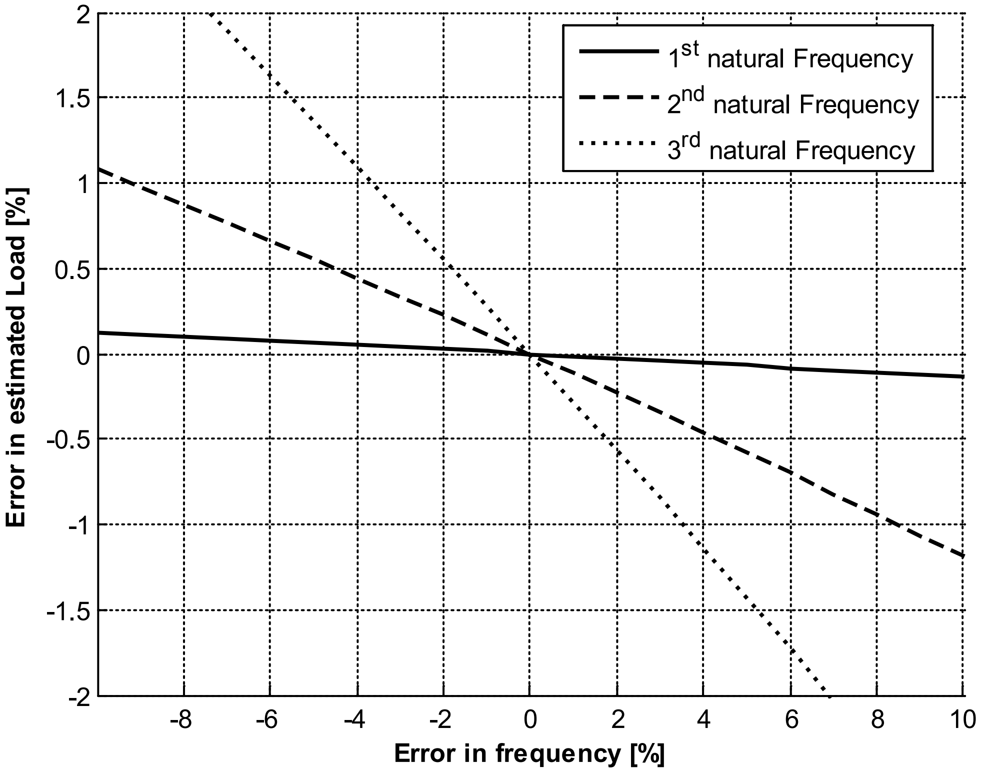

Figure 3.12 *Sensitivity of calculated load with respect to frequency at 60 % of theoretical buckling load*

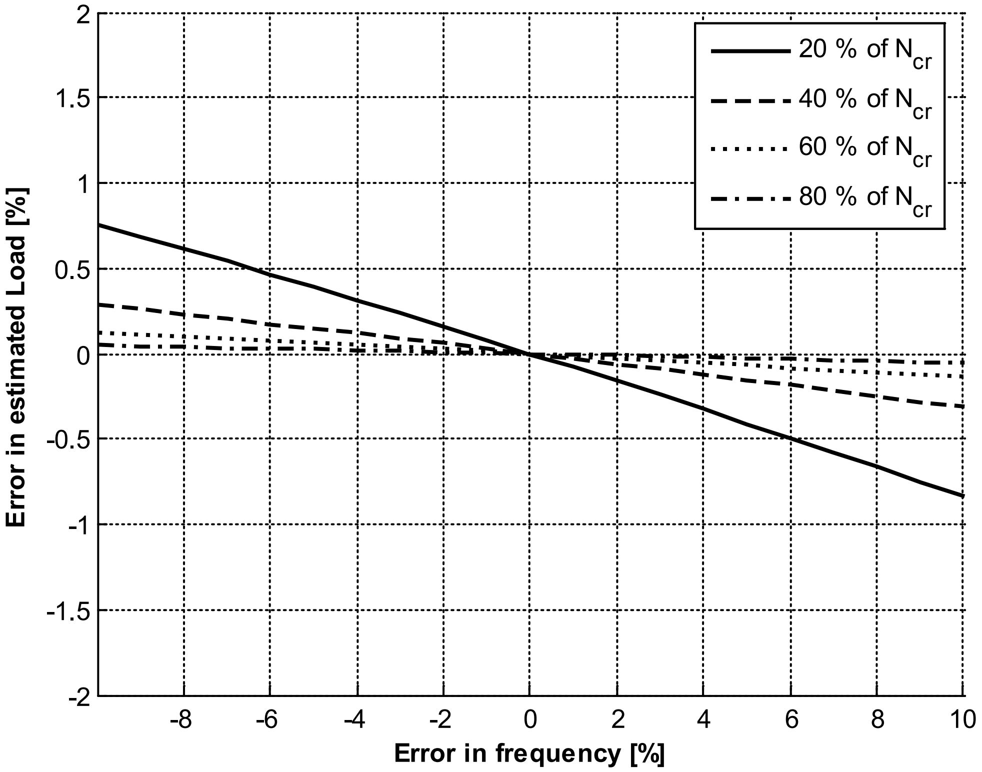

Figure 3.13 *Sensitivity of calculated load with respect to frequency for 1st natural frequency*

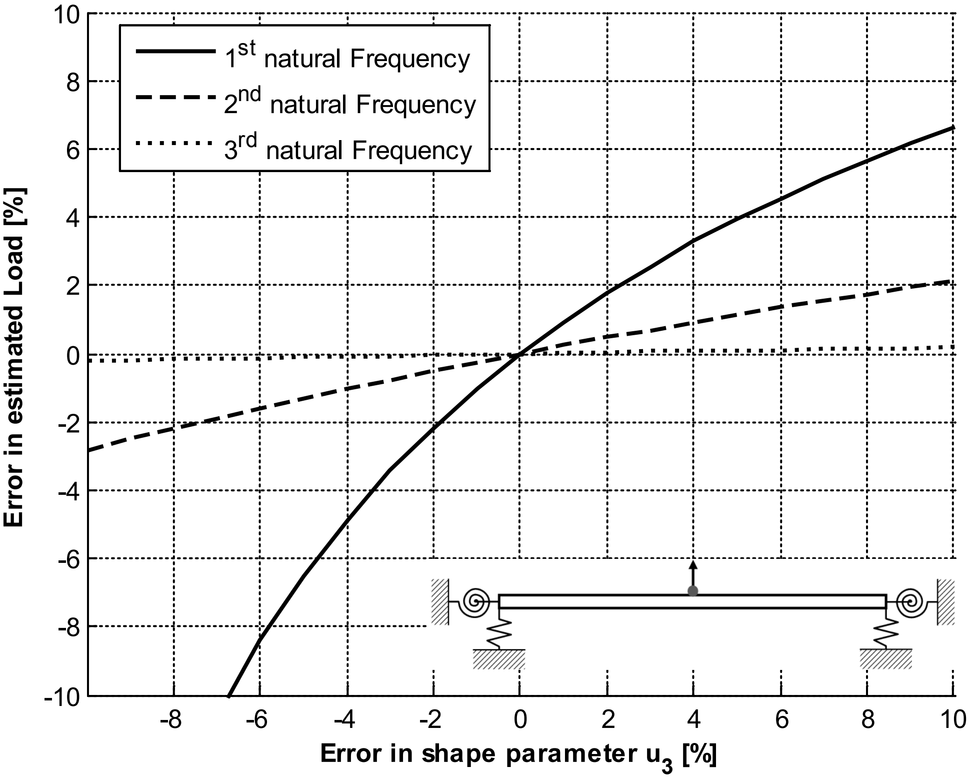

Figure 3.14 *Sensitivity of calculated load with respect to u_3 at 60 % of theoretical buckling load*

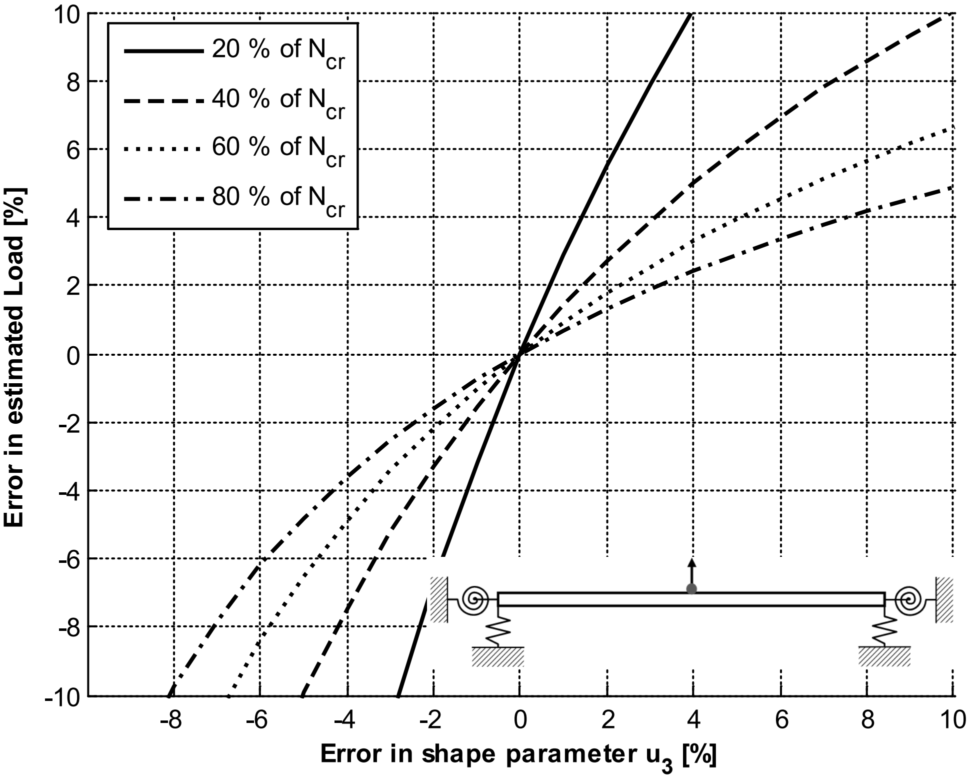

Figure 3.15 *Sensitivity of calculated load with respect to u_3 for 1st natural frequency*

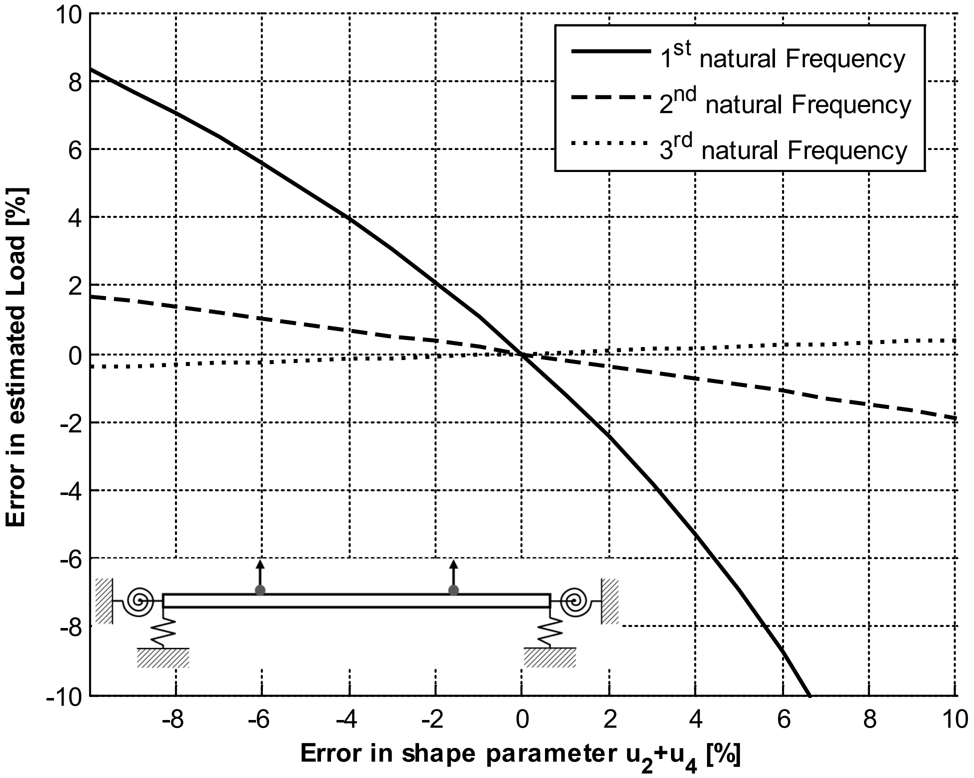

Figure 3.16 *Sensitivity of calculated load with respect to* u_2+u_4 *at 60 % of theoretical buckling load*

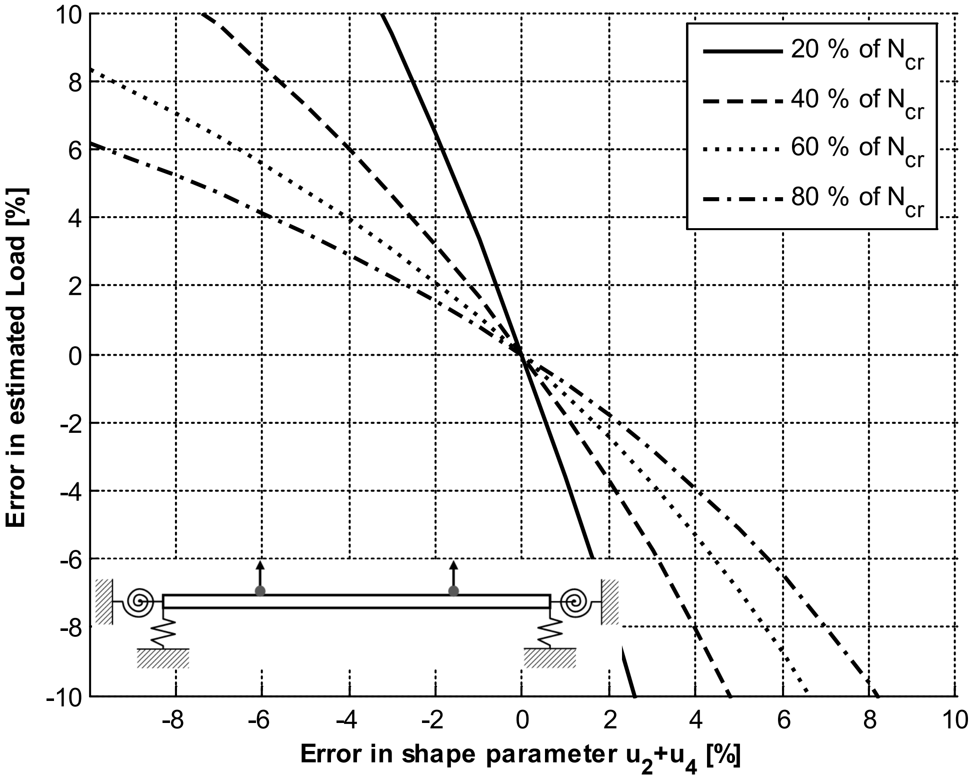

Figure 3.17 *Sensitivity of calculated load with respect to* u_2+u_4 *for 1st natural frequency*

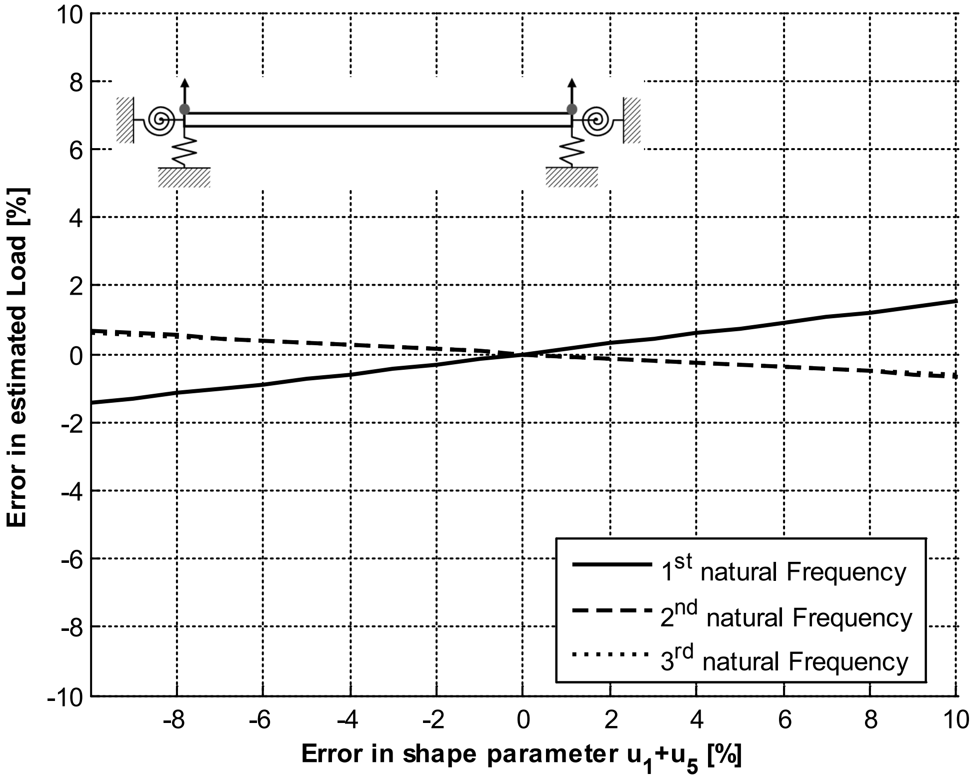

Figure 3.18 *Sensitivity of calculated load with respect to* u_1+u_5 *at 60 % of theoretical buckling load*

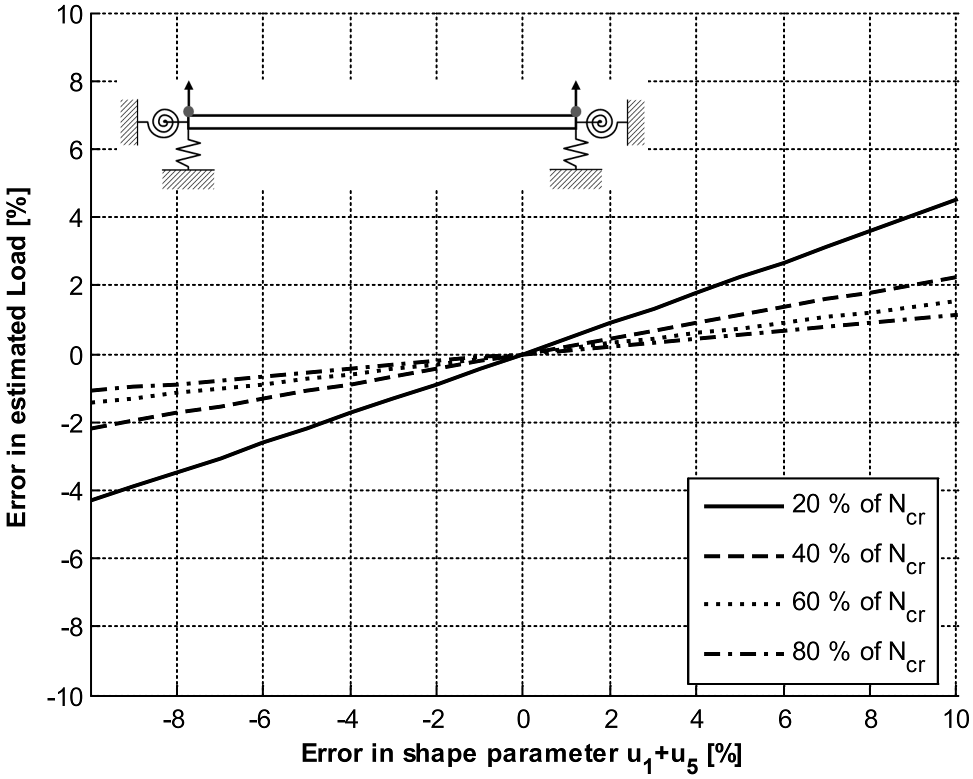

Figure 3.19 *Sensitivity of calculated load with respect to* u_1+u_5 *for 1st natural frequency*

3.3.1.2 Analysis of the results

A general trend in all the figures is a smaller error for larger loads. Higher orders of natural frequencies yield larger errors with respect to Young's modulus, density and frequency, whilst the opposite is true with respect to the shape.

The largest error impact on load estimation is clearly due to the various shape parameters. Also the innermost shape parameters (u_3 and u_2+u_4) produce the largest error within this group. The remaining parameters (E, ρ and ω) yield manageable errors (< 3 % at 10 % input error) with the frequency being the most sensitive.

Thus when estimating axial loads on samples with well-defined material properties (such as steel) the largest source of error will probably be the modal properties (i.e. the frequency and vibration shape) of the structure.

Note that only one type of beam (simply supported) with only the chosen shape point distribution has been analyzed. The drawn conclusions will therefore be applicable for the laboratory setup, which is similar. However applying the performed sensitivity analysis to a more general case might prove erroneous.

3.3.2 Discretized approach

The discretized approach is tested using the same six measurement points as shown in Figure 3.7. Calculations employ the left five as well as all six measurement points, the latter constituting an over-determined system. In order to exclude any differences due to the six point setup being symmetrical, a system using five symmetrical points is employed as well (see Figure 3.20)

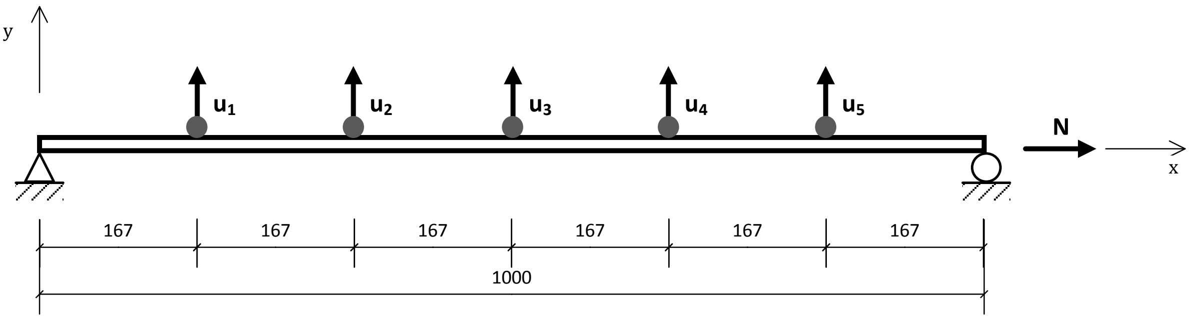

Figure 3.20 *Alternative setup for discretized approach (5 point symmetric) [mm]*

Simulations are performed using up to four beam elements between measurement points in order to determine any convergence issues.[2] As previously calculations are performed for the first three natural frequencies for compressive loads up to the Euler buckling load.

Furthermore the effect of considering shear deformation and rotational inertia is investigated by performing calculations using both a Bernoulli-Euler and a Timoshenko beam. In both cases the input data is determined using the analytical equations for a Bernoulli-Euler beam (see equations (2.19) and (2.21)).

3.3.2.1 Results

As can be seen in the figures below the discrete algorithm can diverge if more than two beam elements are used between the measurement points. Also the 2nd natural frequency seems to be numerically difficult to determine when using only five measurement points, however the use of an over-determined system (six points) seems to overcome this (see Figure 3.24 – Figure 3.26).

---

[2] I.e. up to 16 and 20 beam elements are used for the 5 point and 6 point systems respectively.

Some initial tests using a non-condensed system were performed as well to insure that the divergence issues were not due to the matrix inversion in condensation (see chapter 3.1.2). It was found that the issues remained even with the full system. Due to the time needed for computation being shorter using the condensed approach, it was employed throughout the remainder of the study.

Note that as a bi-product of the calculation numerical values for the spring constants are determined. However these values do not represent a physical representation of the actual springs since in most cases some negative values are obtained even if the load estimation is exact.

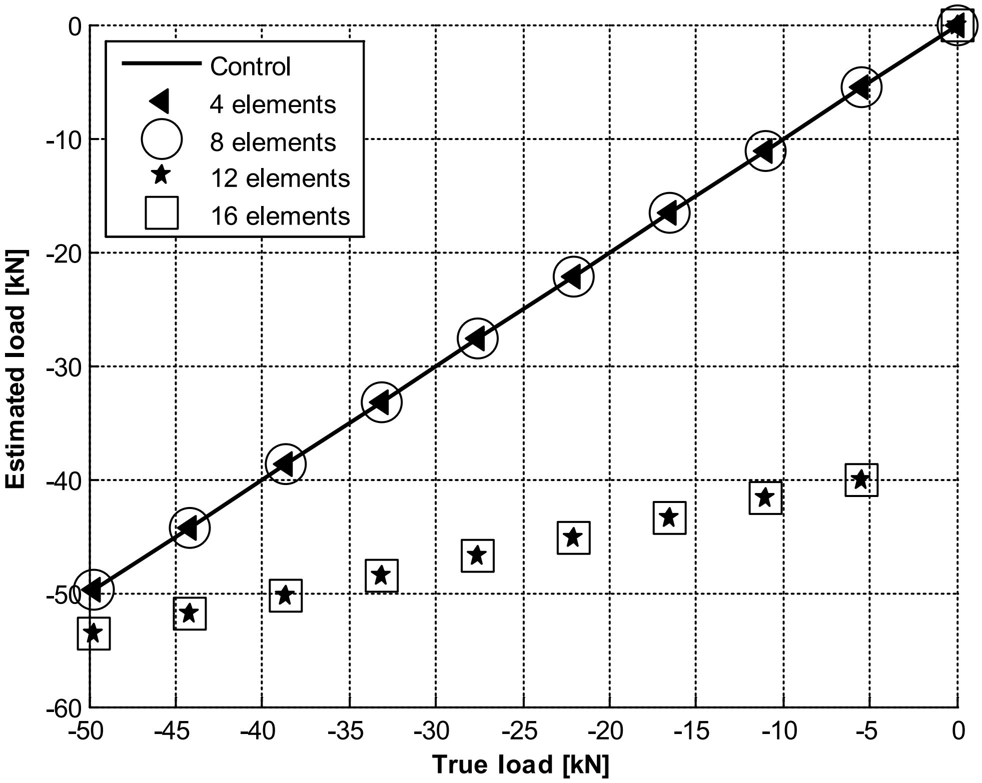

Figure 3.21 *Level of discretization; 1st natural frequency, 5symmetric points*

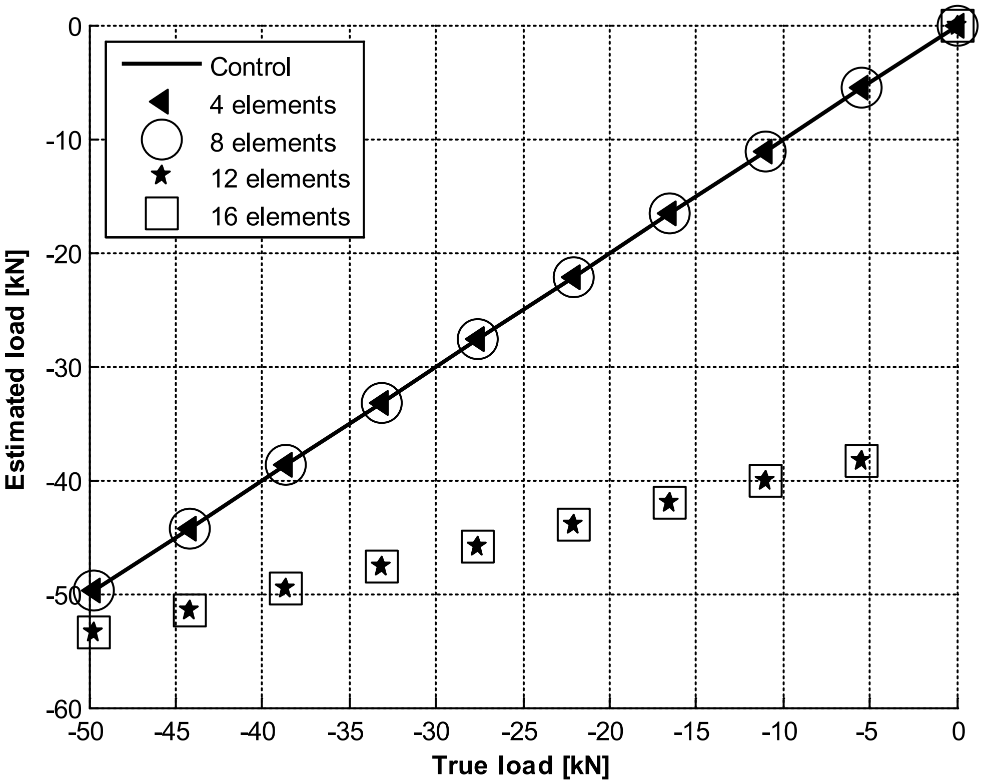

Figure 3.22 *Level of discretization; 1st natural frequency, 5non-symmetric points*

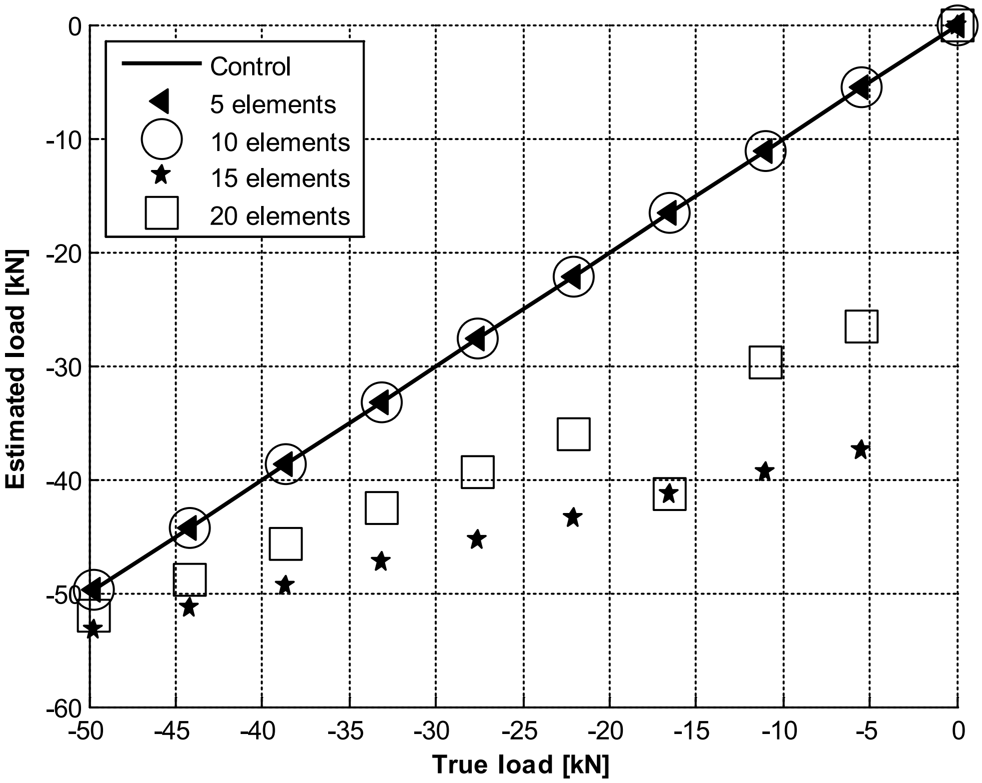

Figure 3.23 *Level of discretization; 1st natural frequency, 6 points (over-determined)*

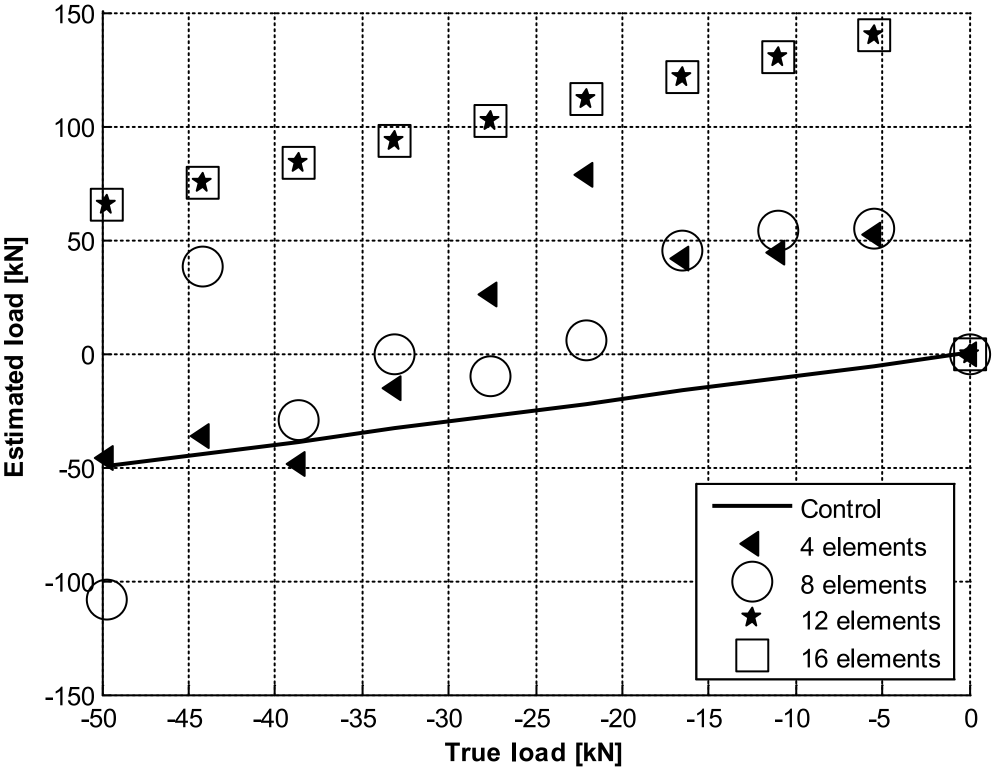

Figure 3.24 *Level of discretization; 2nd natural frequency, 5 symmetric points*

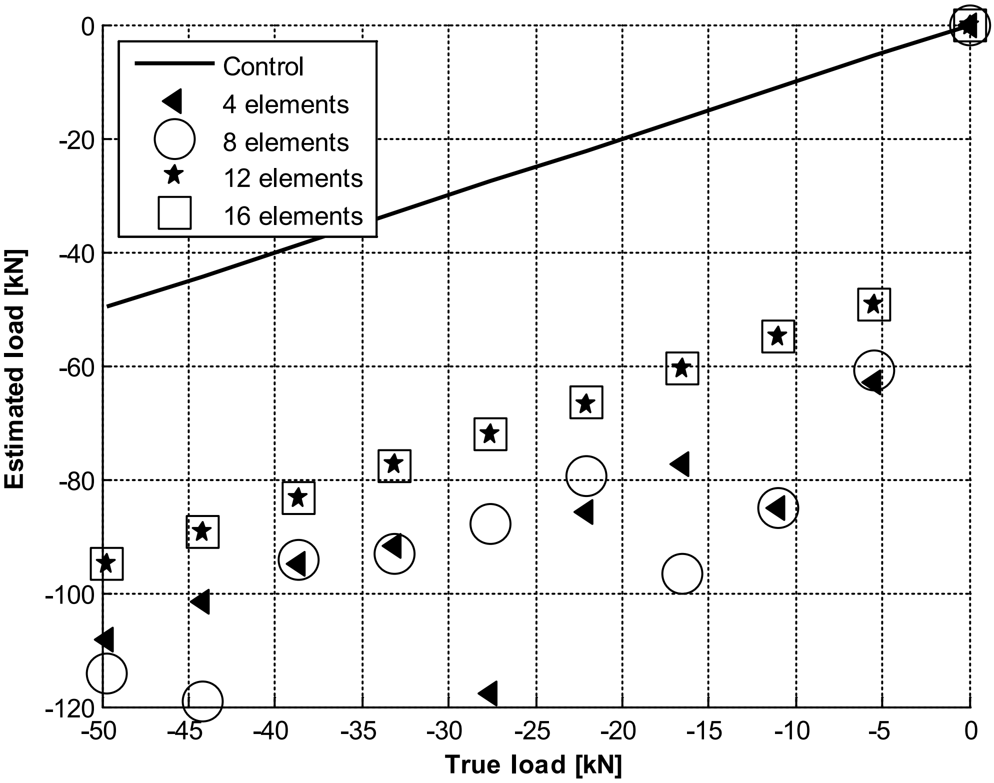

Figure 3.25 *Level of discretization; 2nd natural frequency, 5 non-symmetric points*

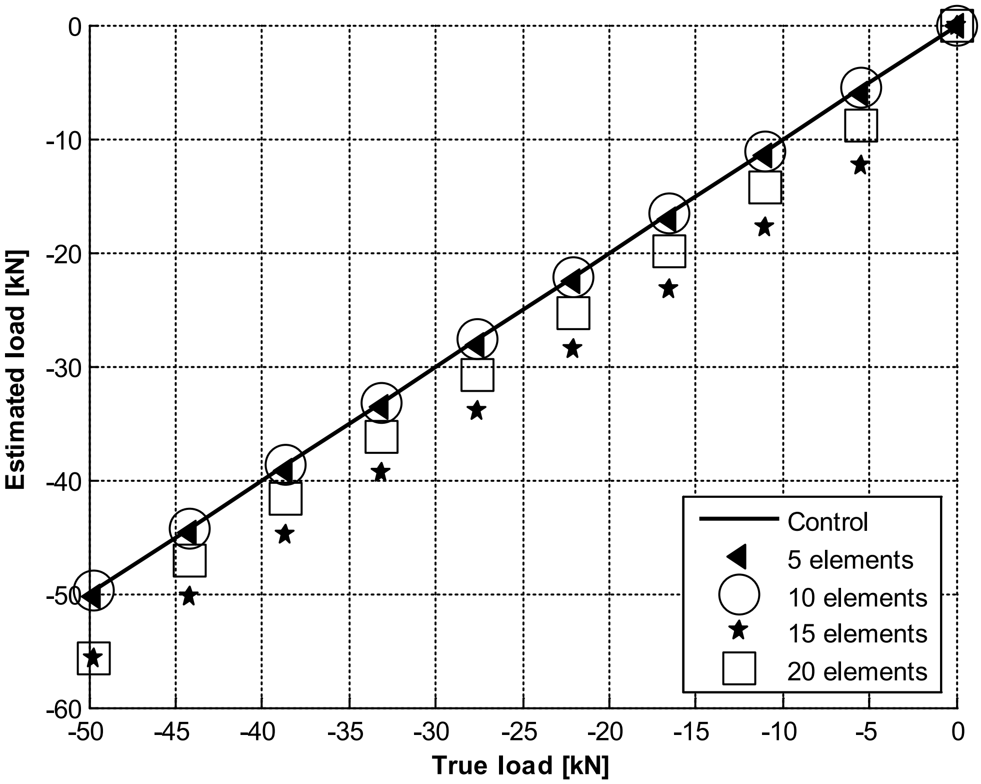

Figure 3.26 *Level of discretization; 2nd natural frequency, 6 points (over-determined)*

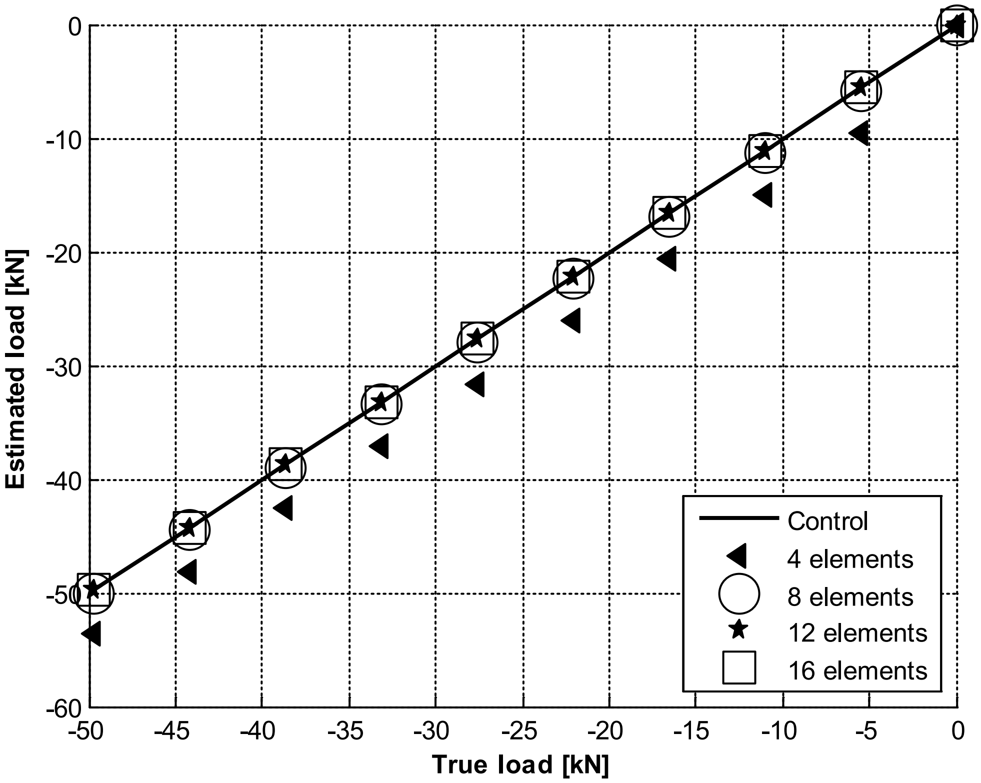

Figure 3.27 *Level of discretization; 3rd natural frequency, 5symmetric points*

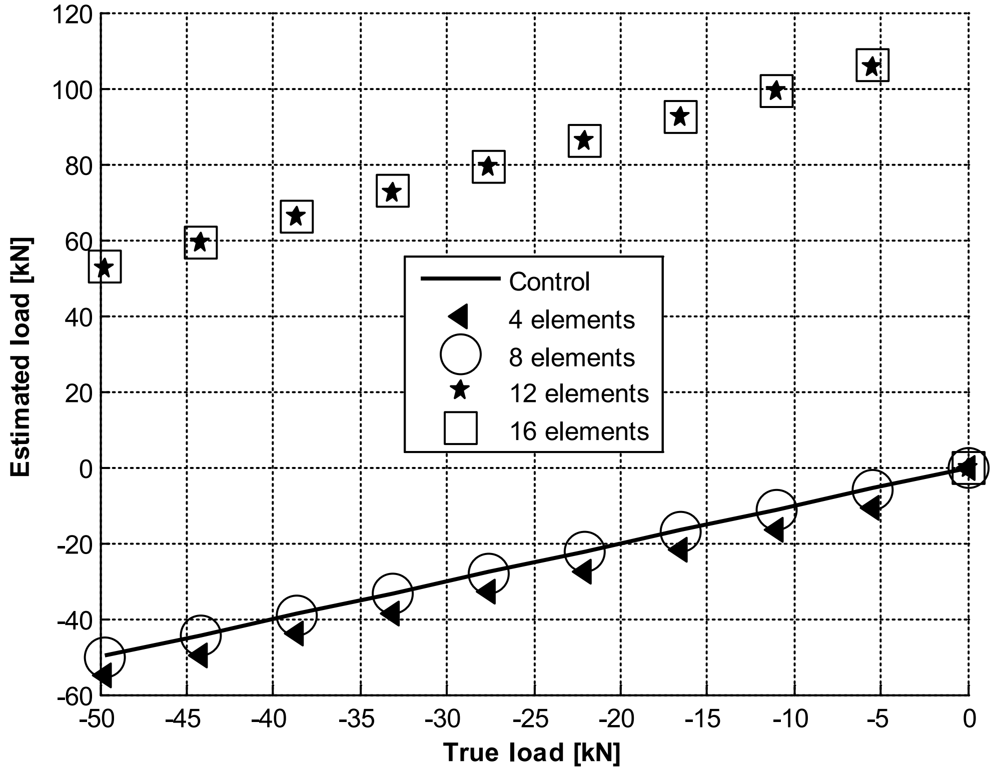

Figure 3.28 *Level of discretization; 3^{rd} natural frequency, 5non-symmetric points*

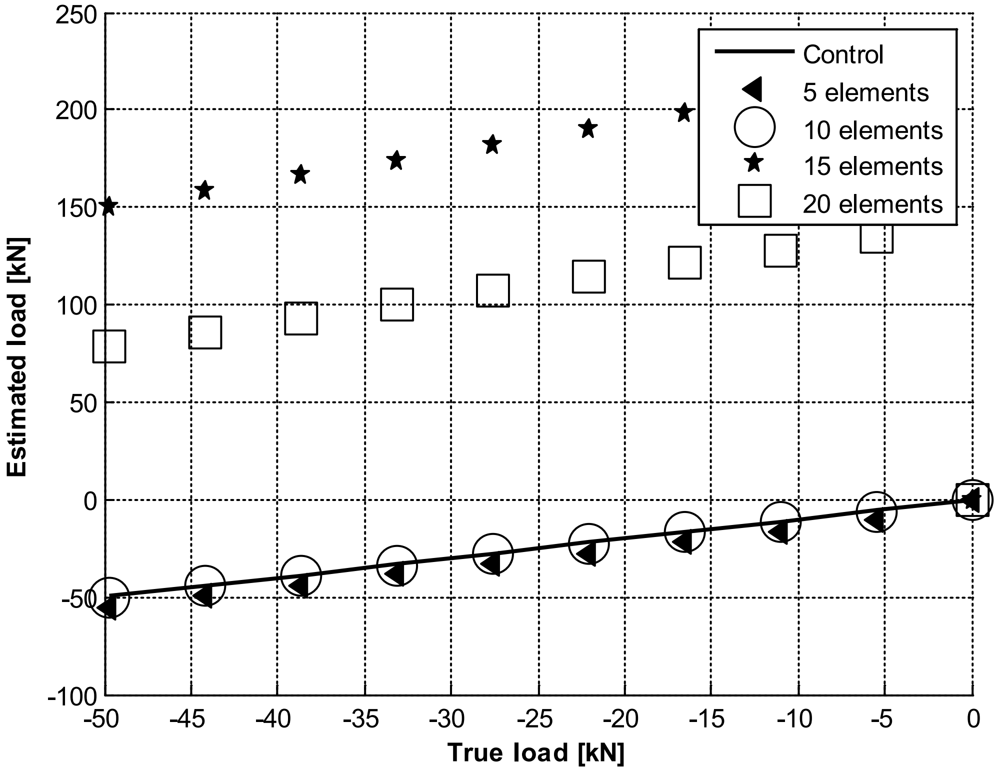

Figure 3.29 *Level of discretization; 3^{rd} natural frequency, 6 points (over-determined)*

The use of Timoshenko beam elements proves to have no impact on stability and convergence issues. Compared to standard beam theory (Bernoulli-Euler) a lower estimation of load magnitude is obtained.

The difference between the two beam theories becomes more pronounced with an increasing order of frequency and appears to be unaffected by the choice of measurement points. The figures below show the results for the over-determined system (six points) using a total of ten elements:

Note that the "true" load is the input according to Bernoulli-Euler theory and the difference seen using Timoshenko theory is not an error, but the difference due to beam formulation.

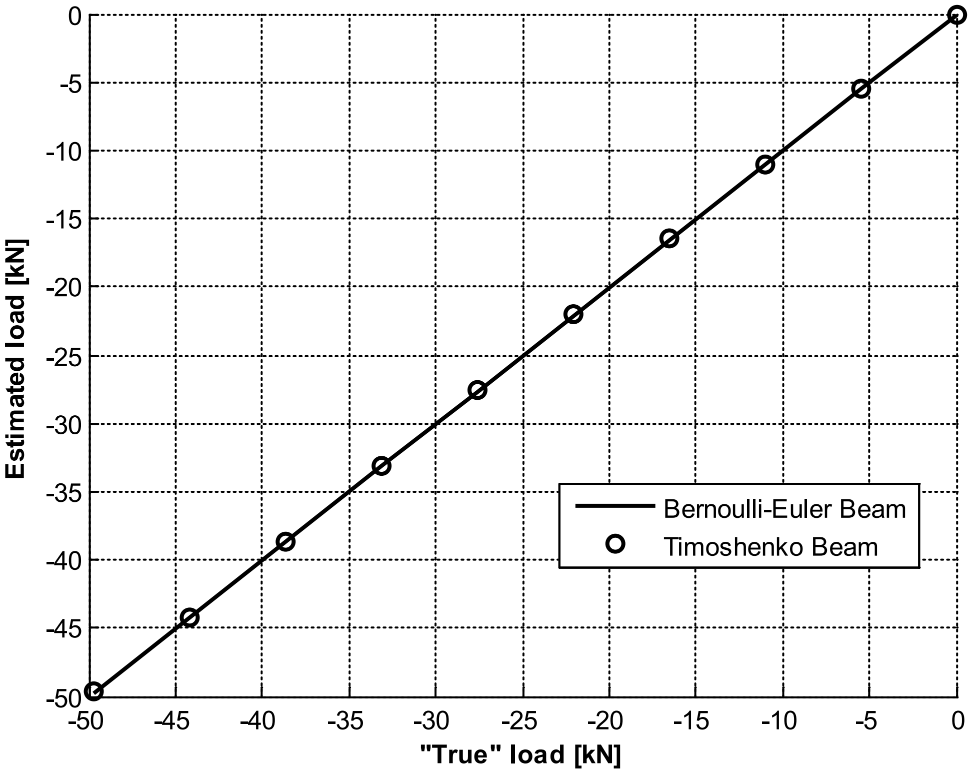

Figure 3.30 *Bernoulli-Euler vs Timoshenko beam; 1st natural frequency, 6 points (over-determined)*

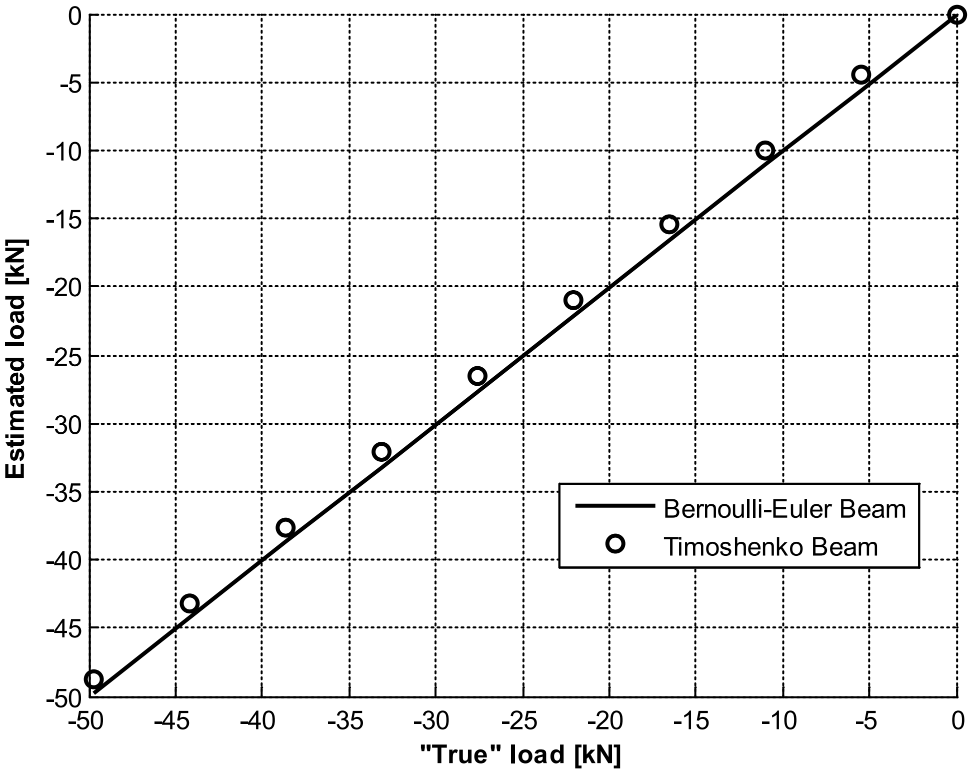

Figure 3.31 *Bernoulli-Euler vs Timoshenko beam; 2nd natural frequency, 6 points (over-determined)*

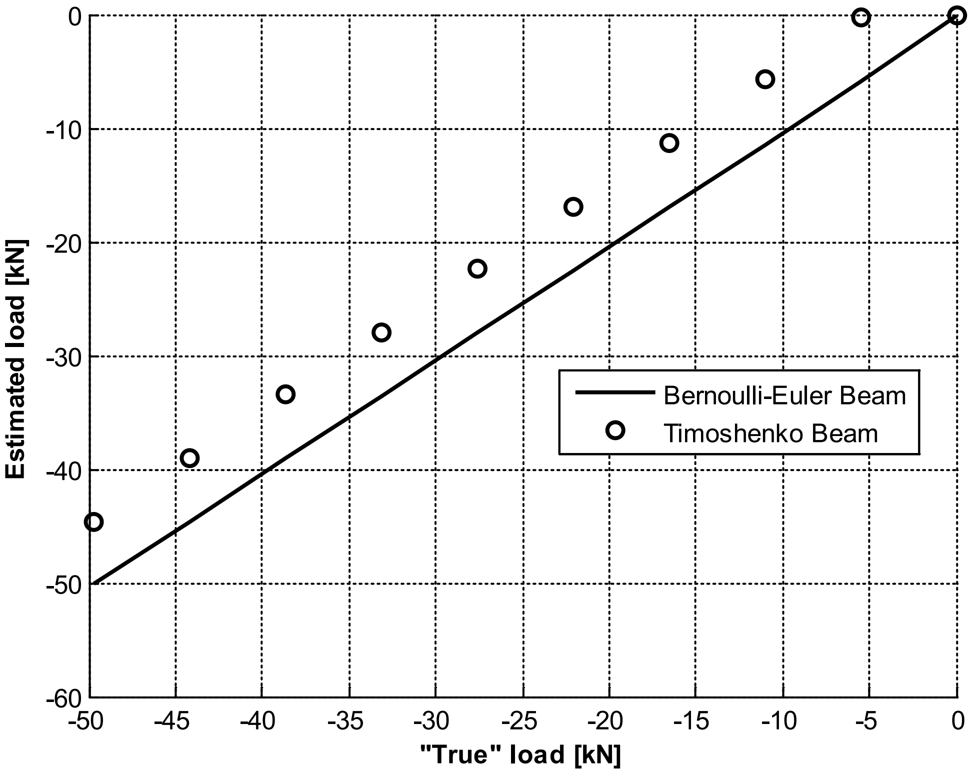

Figure 3.32 *Bernoulli-Euler vs Timoshenko beam; 3rd natural frequency, 6 points (over-determined)*

3.3.2.2 Analysis of the results

The divergence issues were unexpected prior to numerical testing and the underlying cause (high discretization of the beam) was tedious to determine. The reason for this effect is not known at the time of publication.

The magnitude and direction of divergence varies from case to case. The divergence differs for each frequency and there is also a difference for the 3rd natural frequency when using the different measurement inputs (see Figure 3.27 - Figure 3.29). Thus the vibration shape seems to have a major influence on divergence.

The influence of vibration shape on the algorithm is also apparent in the 2nd natural frequency, where no proper solution is obtained when employing the minimum 5 measurement points. However the use of an over-determined system (6 points) appears to overcome some shape specific stability issues of the algorithm as the correct solution is obtained for the 2nd frequency (see Figure 3.26).

The use of Timoshenko elements yields a lower load magnitude in compression with a significant difference already in the 3rd natural frequency (approximately 10 % of the buckling load). Since the Timoshenko beam provides a more complete description of an actual structure[3], the large difference implies a clear inadequacy of standard beam theory at higher frequencies. Given that only a simple rectangular cross section has been examined, the difference due to beam theories could be substantial in other cases.

3.4 Concluding remarks

For both the presented methods MATLAB was used to solve the equations and the code is presented in appendix A – Calculation code. The continuous method (in the presented form) is somewhat more straightforward to implement and yields the exact solution to the Bernoulli-Euler beam's differential equation. The discretized approach only yields an approximate solution and since the use of too many elements results in a diverging solution the method in the presented form should be used with caution. However there are a few advantages using a discretized approach:

- A non-prismatic beam can be used (i.e. varying cross sections)
- Mode shape measurement points can easily be rearranged
- A variety of numerical improvements could be made, such as:
  - Use of an over-determined system (more measurement points than necessary)
  - Use of several frequencies (solving several equation systems simultaneously)
  - Weighting parts of the equation (e.g. load and/or spring constants)

Even though these methods are not used in this report (aside from the over-determined system), the possibility of further development is promising in order to refine the technique implemented in this study.

Both the sensitivity analysis and the testing of the discretized algorithm show the large impact of the vibration shape on measurement results. Thus measuring several points of the vibration shape and using the discretized approach with an over-determined system might overcome measurement errors in this highly sensitive parameter.

---

[3] Note that the "true" loading values are determined using the analytical solution according to Bernoulli-Euler beam theory.

The possibility of using both Bernoulli-Euler and Timoshenko beam theory is a significant advantage of the discretized approach. Since the more complete Timoshenko theory should deliver a more accurate estimation it is preferable. However since Bernoulli-Euler beams seem to yield an overestimation of loading magnitude, this could be employed to produce a margin of safety. Note that numerical testing has only been done for a small selection of rectangular beams in compression and that the overestimation of Bernoulli-Euler beam theory might not hold true for the general case.

4 Experimental modal analysis

In the laboratory and field testing experimental modal analysis has been performed. A short review of the most important parts of this is given in this chapter, which is mainly based on Avitabile's article [20]. For a more in depth description of modal analysis the Avitabile's collection of articles [21] or the book from Maia and Silva [22] are recommended.

The modal characteristics of a structure (i.e. its dynamic properties) can be described by the modes (the natural frequency and corresponding mode shape) of the structure.[4] In order to detect these, two different approaches can be taken:

- Exciting the structure in several different locations
- Measuring the response in several different locations

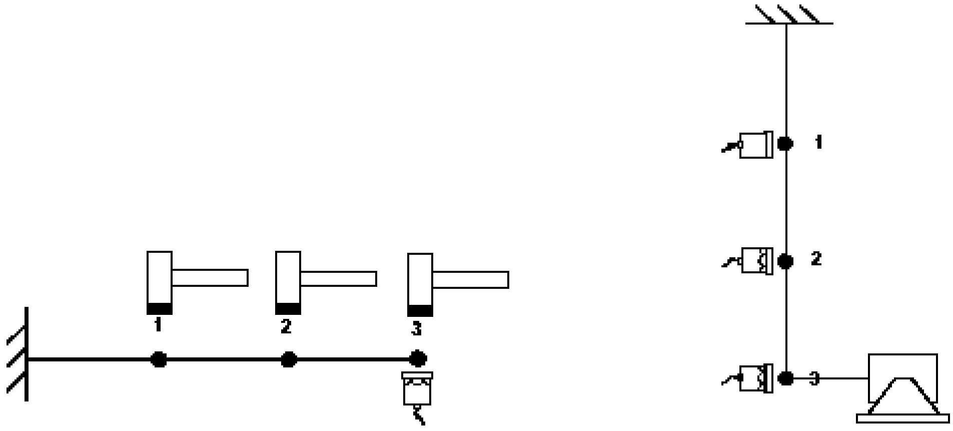

Figure 4.1 *Multiple impact vs multiple measurement;* **[20]**

Either way, care must be taken to pick enough (and the correct) measurement/excitation locations so that all the desired modes can be detected.

Once a measurement is made the experimental data contains the applied force and the response (displacement, velocity or acceleration) of the structure over time. In order to determine the natural frequencies and mode shapes both these signals must be transformed from the time domain to the frequency domain, which is done using a Fast Fourier Transformation (FFT). Finally by normalizing the response of the structure with respect to the excitation yields the frequency response function (FRF). By analyzing the FRFs of a structure the mode(s) (frequency and shape) can be determined.

However in real-life experiments the results are not as ideal as in theory. Therefore the transformation of a recorded time signal to a FRF is somewhat more laborious. First the analogous signal must be cleansed from high frequency noise by means of filters and then the signal is digitalized. The signal should be a periodic representation of the complete response for a successful FFT otherwise certain frequencies could be lost in the transformation (leakage). A weighting (window functions) of the signal is applied in order to avoid a distortion in the frequency domain. The steps of this process are shown in Figure 4.2.

---

[4] For sake of simplicity damping is neglected.

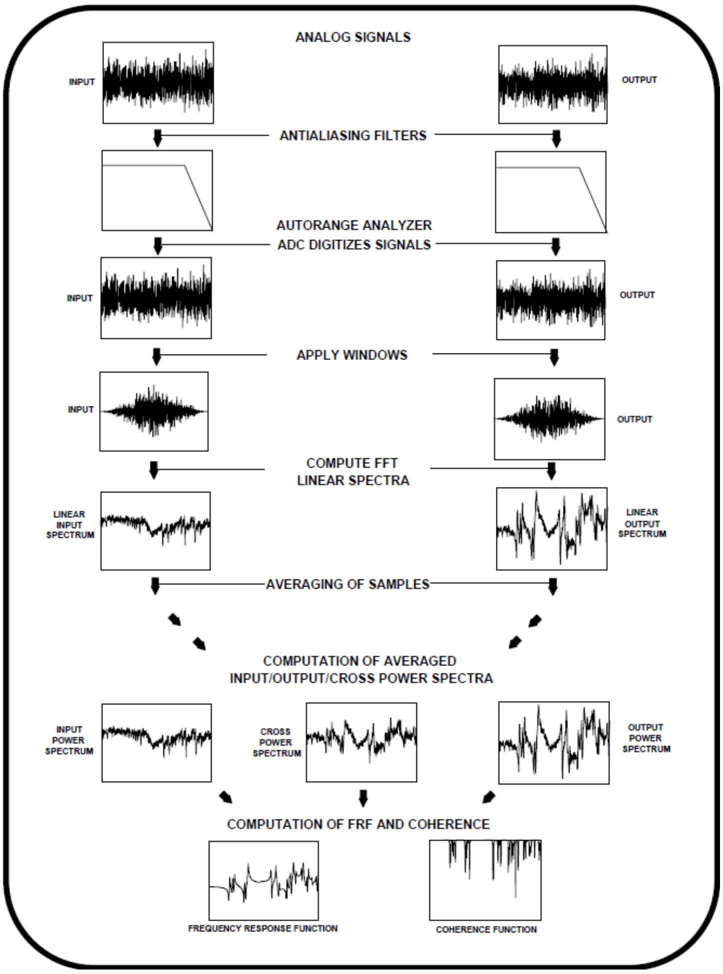
ANALOG SIGNALS
INPUT
OUTPUT
ANTIALIASING FILTERS
AUTORANGE ANALYZER
ADC DIGITIZES SIGNALS
INPUT
OUTPUT
APPLY WINDOWS
INPUT
OUTPUT
COMPUTE FFT
LINEAR SPECTRA
LINEAR INPUT SPECTRUM
LINEAR OUTPUT SPECTRUM
AVERAGING OF SAMPLES
COMPUTATION OF AVERAGED
INPUT/OUTPUT/CROSS POWER SPECTRA
INPUT POWER SPECTRUM
CROSS POWER SPECTRUM
OUTPUT POWER SPECTRUM
COMPUTATION OF FRF AND COHERENCE
FREQUENCY RESPONSE FUNCTION
COHERENCE FUNCTION

Figure 4.2 *Signal processing;* **[20]**

In the performed experiments Brüel & Kjaer (B&K) equipment with the accompanying software was used both to measure and process the dynamic response of the structures. The measurement software (B&K Pulse Labshop) performs all of the steps depicted in Figure 4.2.

The data was then extracted using the analysis software B&K Pulse Reflex, which also allowed visualization and animation of the mode shape. This is important in order to exclude undesired modes, which in this case could be biaxial bending or twisting modes. The surrounding structure such as the test rig could also be excited by the impact, which would need to be excluded from the analysis and can be detected visually.

The software also has more advanced analytical capabilities, which estimate the modal parameters of the analyzed structure. These methods are in essence curve fitters that attempt to find all the modal parameters of a test specimen, so that a numerical simulation using the determined parameters will yield the same response as recorded during testing.

While the complexity of the advanced curve fitters certainly is impressive, they have not been employed in this study. The main problem is that the algorithms are designed to determine model parameters that satisfy numerous qualities (including damping). The drawback being that the estimation of the undamped parameters might be compromised for damping.

Use of the polynomial z algorithm included in the software was tested, which gave very scattered/distorted results. Therefore the choice was made to estimate the modes by picking the peaks of the FRF diagrams.

5 Laboratory testing

5.1 Background

The aim of the laboratory testing is twofold:

- To experimentally check the suggested calculation model on compressive samples and to compare the different calculation approaches (i.e. the discretized approach for both beam theories and the analytical approach)
- To check the applicability of this approach on samples with diminishing slenderness

5.2 Test specimens

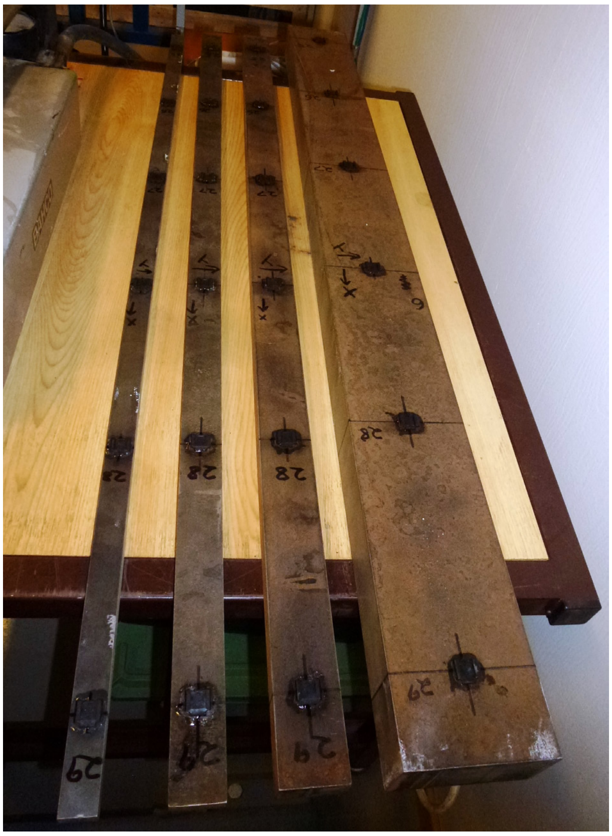

Figure 5.1 *Test specimens*

The laboratory testing is performed on four steel beams with rectangular cross sections with the width/depth ratio of 2. This should insure that especially bending frequencies in the measured (weaker) direction are triggered and a minimal impact of biaxial bending and torsion. The following properties are common for all test samples:

Table 5.1 *Material properties*

Young's modulus	210	$\boldsymbol{E}$ $[\boldsymbol{GPa}]$
Poisson's ratio	0,3	$\boldsymbol{\nu}$
Shear modulus	$\frac{E}{2(1+\nu)} = 80{,}8$	$\boldsymbol{G}$ $[\boldsymbol{GPa}]$
Characteristic yield strength	355	$\mathfrak{f}_y$ $[\boldsymbol{MPa}]$

Initially the testing equipment was thought to provide flat contact surfaces to the samples at both ends. Thus sample cross sections where chosen corresponding to the relative slenderness ratio

(λ_{rel}) of 0,5, 1, 1,5 and 2 assuming a rigid supports at high loads. However the upper contact surface turns out to resemble a pinned connection. The sample properties assuming a fixed/pinned connection are presented in the table below:[5]

Table 5.2 *Specimen properties*

		B1020	B1530	B2040	B4590		
Length		1				L	$[m]$
Depth		10	15	20	45	d	$[mm]$
Width		20	30	40	90	b	$[mm]$
Slenderness ratio		242,1	161,4	121,1	53,8	λ	
Relative slenderness ratio		3,2	2,1	1,6	0,7	λ_{rel}	
Buckling load		7,1	35,8	113,1	2899,1	N_{cr}	$[kN]$
Design load		6,1	28,5	82,0	1038,2	N_{Rd}	$[kN]$
Unloaded theoretical natural frequency	**1st**	36,6	55,0	73,3	164,9	ω_0	$[Hz]$
	2nd	118,7	178,1	237,5	534,4		
	3rd	247,7	371,6	495,5	1114,8		

5.3 Testing procedure

The testing procedure consists of three main components:

- The stepwise compression of the sample up to the maximum design load according to Eurocode
- The modal testing at each load step
- The extraction of modal data

5.3.1 *Compression testing procedure*

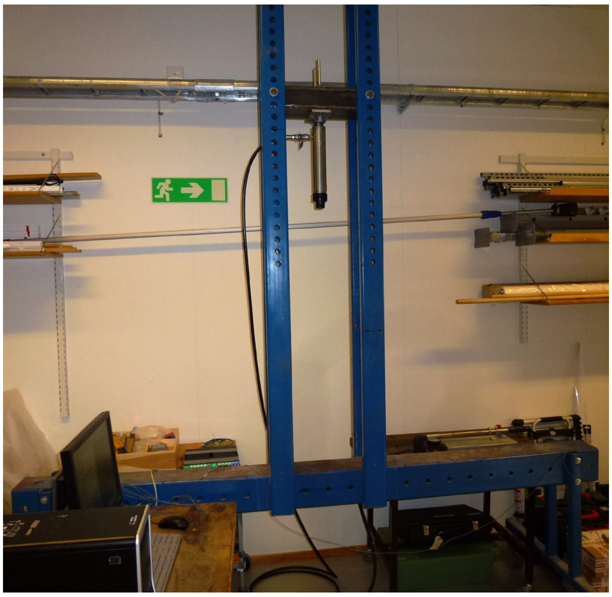

Figure 5.2 *Testing rig*

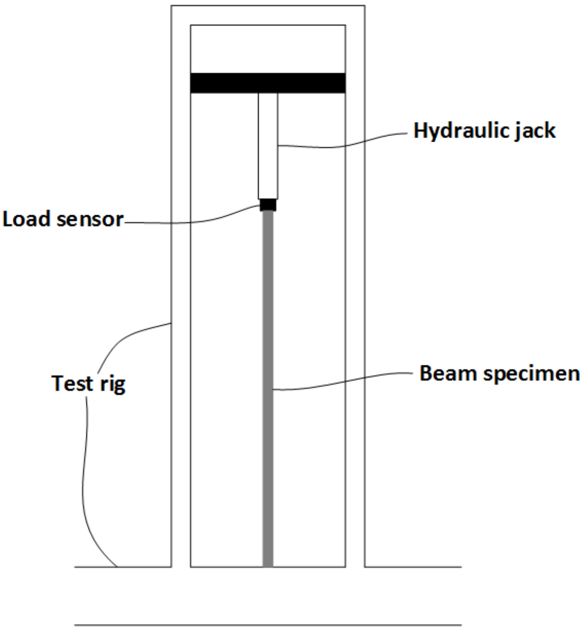

Figure 5.3 *Test setup*

---

[5] The detailed calculations determining the various properties are found in appendix B – Calculation of beam properties.

The compression of samples is performed using a test rig with a hydraulic jack. The lower end of the samples is placed directly on the flat surface of the rig, which is assumed to resemble a fixed connection at higher loads (see Figure 5.4). The upper end of the samples is connected to a load measuring cell, which in turn is fixed to the hydraulic jack. The connecting surface of the load measuring cell is beveled and therefore the connection can be thought of as pinned (see Figure 5.5).

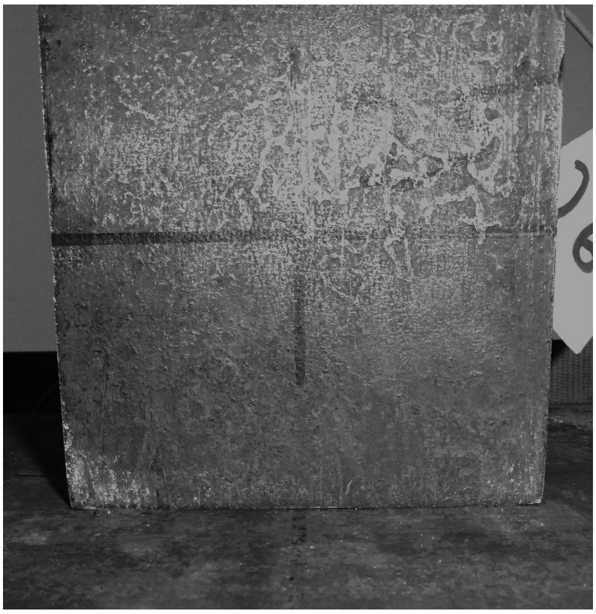
Figure 5.4 *Lower connecting surface (fixed at high loads)*

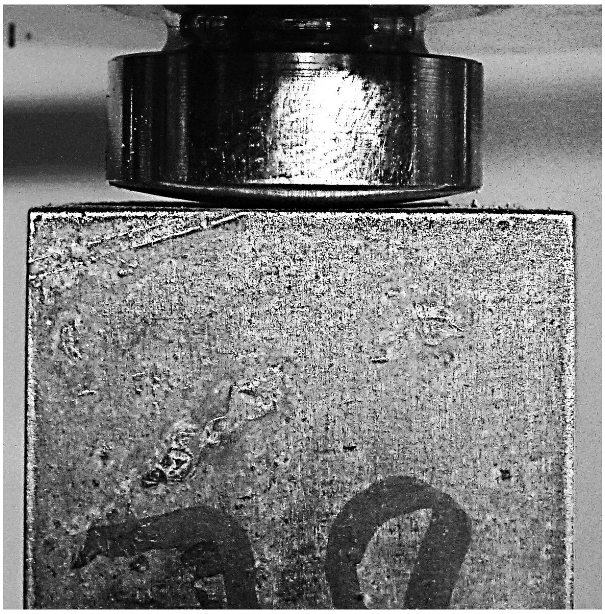
Figure 5.5 *Upper connecting surface (pinned at high loads)*

Loading is applied in steps by gradually increasing the load[6] up until the approximate design load[7] with an upper limit of 100 kN[8]. However the exact final loading is determined in situ according to the reactions of the specimen. The actual load levels used in testing are shown in the table below[9]:

Table 5.3 *Load levels [kN]*

	B1020	B1530	B2040	B4590
1st	1,1	5,1	10,0	10,0
2nd	2,0	10,0	30,0	30,0
3rd	3,4	15,0	50,0	50,0
4th	3,8	20,0	54,7	70,0
5th		25,0		90,0
6th		30,1		

Due to dissipating pressure of the hydraulic jack, the loading level needs to be constantly adjusted. Thus the actual loading is maintained within a precision of 0,1 kN.

5.3.2 Modal testing procedure

The response of the beams is measured using a total of six accelerometers, whereof five of the sensors (B&K Type 4507 001) measure response in one direction only. One of the sensors (B&K

---

[6] The testing equipment does not allow a controlled lowering of the load.

[7] According to Eurocode SS-EN 1993-1-1

[8] The upper limit of the load measuring cell

[9] Levels with visible deflections are highlighted in grey.

Type 4524b) measures a tri-axial response and this data is used to exclude bi-axial and twisting modes. The tri-axial sensor is also more sensitive than the others and thus the data from this sensor can be considered more reliable.

The sensors are placed along the midline of the beam with a vertical spacing of 18 mm (see Figure 5.6). The placing of the tri-axial sensor is quite central in order to yield high displacements in both the uniaxial direction (desirable due to higher sensitivity) and three-dimensional movement (for exclusion purposes).

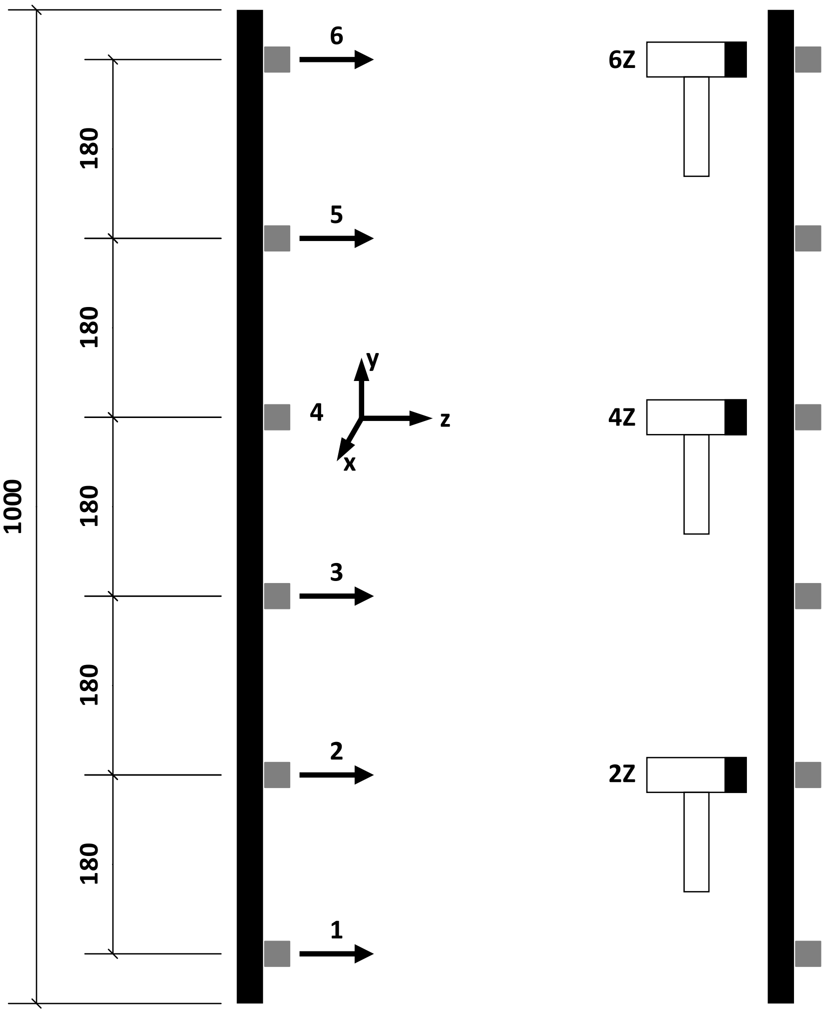

Figure 5.6 *Beam dimensions, accelerometer positioning & impact points [mm]*

The response is induced using a modal testing hammer (Type 8206) with a plastic tip at three different sensor locations yet at the rear of the structure (see Figure 5.6). Excitation at each impact location is induced a total of five times to produce an average response.

The sensor response is allowed to die down between impacts in order to ensure a clean relation between impact and response. Furthermore the signal of the modal testing hammer is monitored both manually and with a double hit detector (part of the measurement software) to insure that a clean impact is induced.

5.3.3 Modal data extraction

The measurement software used (B&K Pulse Labshop) automatically determines the frequency response at every impact location by averaging the five measurements. The chosen sampling rate allows frequencies up to 1,6 kHz to be detected with differences as small as 0,25 Hz.

The modal frequencies/shapes are determined by peak-picking of the FRF diagrams. This is done in the following steps:

- A visual assessment of each natural frequency is made by inspecting the three driving point FRFs[10] and the preliminary frequency and mode shape are obtained. At this point certain frequency peaks are excluded from further analysis:
    - The response of the tri-axial accelerometer is used in order to only include pure uniaxial bending modes.
    - Modes that seem to be highly impacted by outside interference are dismissed, e.g. rigid body modes and modes that clearly indicate the beam being part of a vibration of the larger structure (test rig)
- The frequency and accompanying mode shape for each impact location is determined separately:
    - The exact frequency is chosen by considering mainly the driving point FRF and the FRF at the point of maximum displacement in the vibration shape.
    - The frequencies are only included if deviations from the preliminary frequency (previous step) are within reason.

The frequency (in Hz) and the complex vibration shape (in m/s^2) are then exported from the program for numerical treatment in MATLAB.

5.4 Modal results

The final loading levels in the three most slender test specimens (i.e. all aside from B4590) also entailed a visible deflection of the specimen (see Figure 5.7). Therefore the data from the highest loading level (and possibly the second highest as well) is outside the applicable range for the suggested methods, which assume a non-deformed geometry. This data will be included in the remainder of the report, yet it should be noted that results from these loading levels are questionable.

As previously mentioned the testing has been performed assuming fixed-pinned support conditions, yet the deformation shape of the most slender beam (B1020) clearly resembled pinned-pinned conditions at the highest two loading levels. Thus the ultimate load was reached much sooner than expected, why only two loading levels with non-deformed geometry have been tested.

It should also be mentioned that the testing rig was not perfectly suited for modal testing. The hydraulic jack was affixed to the rig with pins (see Figure 5.2). Thus in the unloaded state the jack was hanging from the pins, whilst at high loads the jack pressed the pins upwards. Thus small movements were possible in the rig setup, which could influence testing.

---

[10] The FRF of a measurement with coinciding sensor and impact location

Furthermore the loading direction of the jack was not necessarily perfectly aligned with the test specimens. The vertical alignment of the jack, rig and the specimen, where never checked in specific detail.

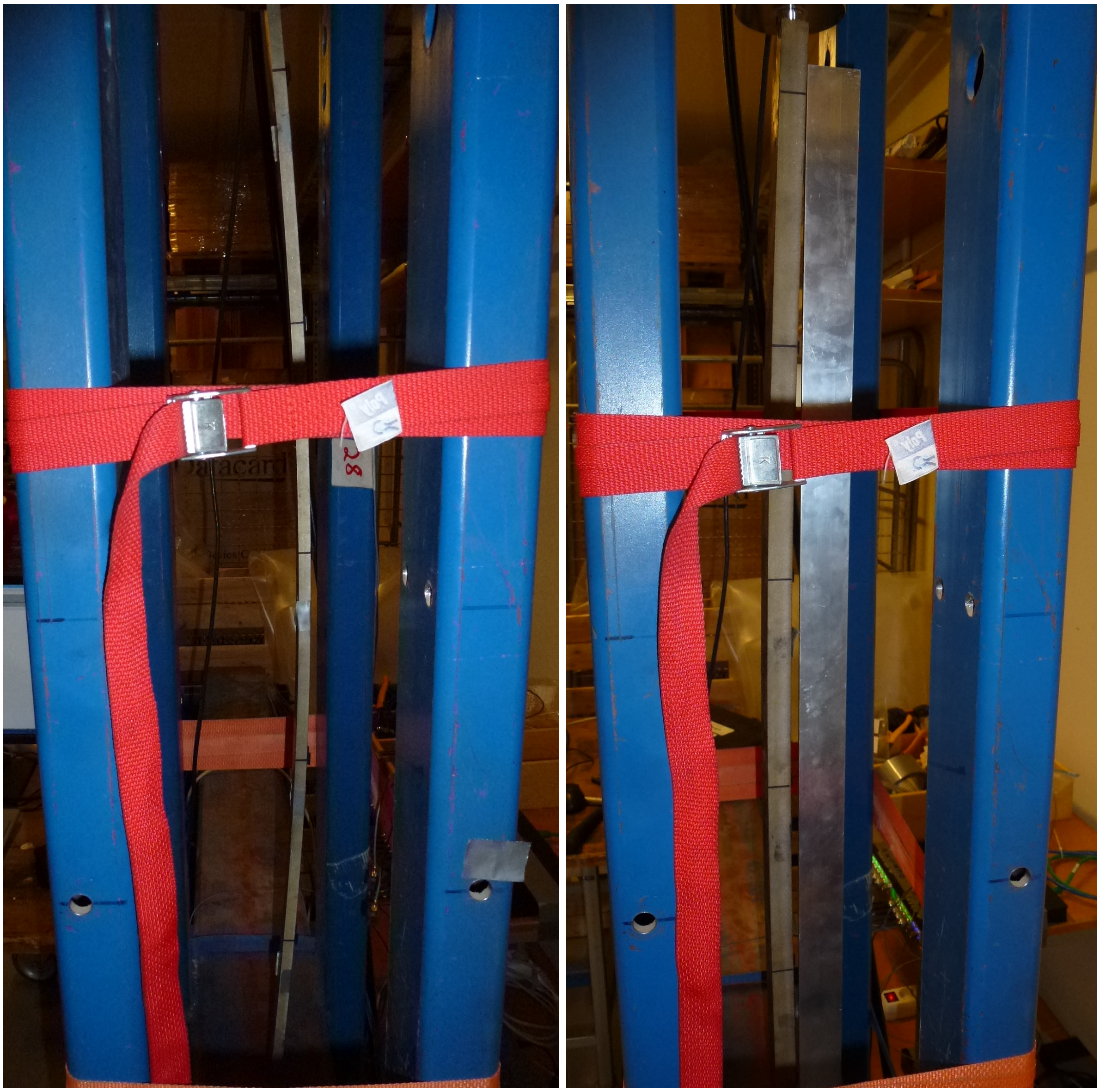

Figure 5.7 *Deformation of the beams at highest loading level (left: B1020 right: B2040 with reference ruler)*

The first three bending frequencies can be identified for all but the stockiest beam (only 2 for B4590) by examining the driving point FRFs together with FRF based mode shape visualization. The clarity of the first bending mode in particular can vary greatly depending on which impact location is examined as can be seen in Figure 5.8[11]. There is also a clear shift in frequency which for instance can be seen in Figure 5.9[12].

---

[11] FRF diagrams for each loading level are found in appendix C – Test results.

[12] FRF diagrams showing the frequency shift (at 4Z) for each beam are found in appendix C – Test results.

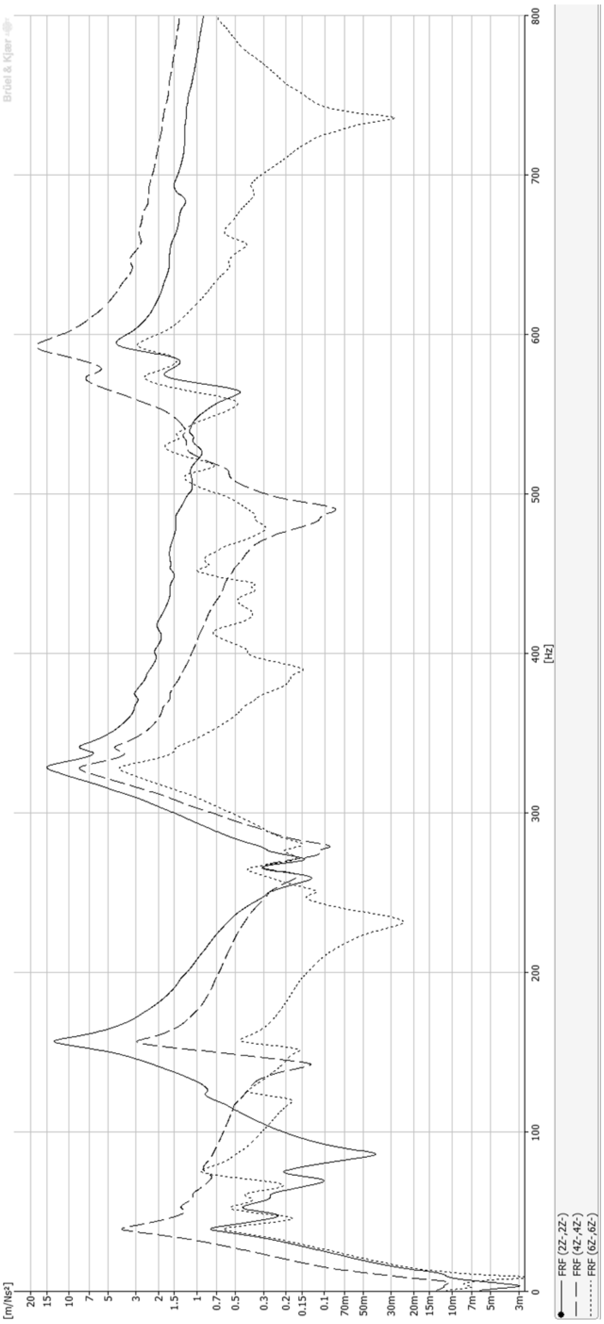

Figure 5.8 *Driving point FRF for B1530 at 10 kN*

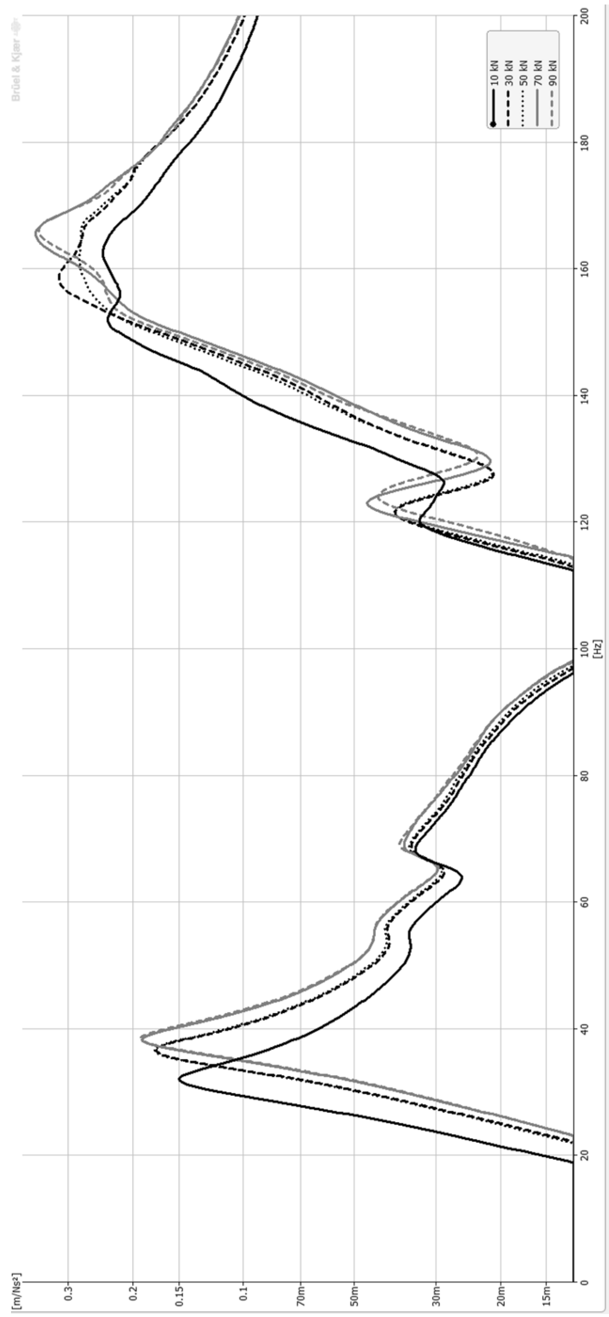

Figure 5.9 *Driving point FRF for B4590 at 4Z*

Natural frequencies are identified by picking the peaks of the FRF diagrams in conjunction with a visualization of the mode shape. The mode shapes are used in order to ensure that only true uniaxial bending modes are included. The selection can at times be difficult as the initial peaks for beam B2040 show. By examining the shape the third peak can be identified as the "true" bending mode.

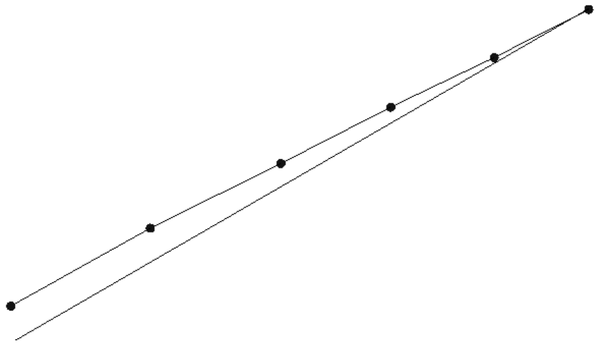

Figure 5.10 *Mode shape B2040 1st peak*

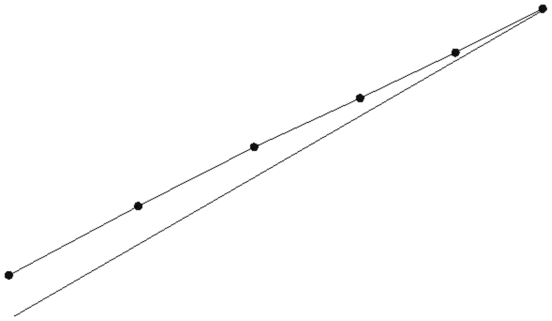

Figure 5.11 *Mode shape B2040 2nd peak*

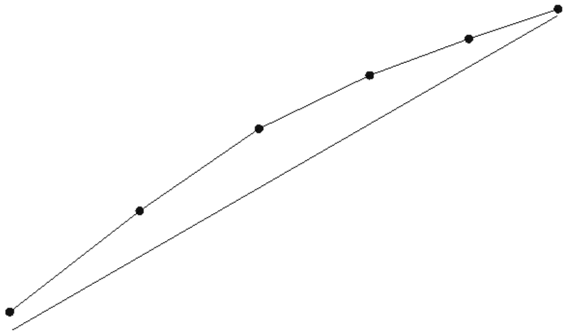

Figure 5.12 *Mode shape B2040 3rd peak*

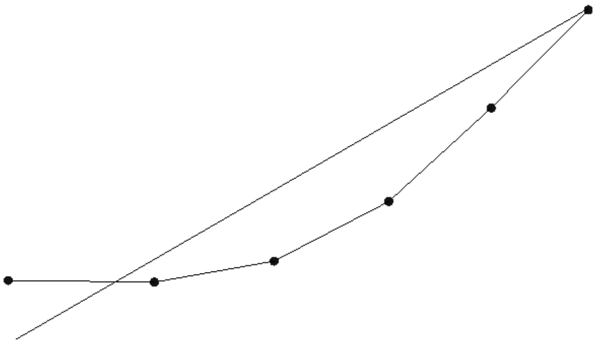

Figure 5.13 *Mode shape B2040 4th peak*

The first three natural frequencies for the specimens thus have a form (once again only the first two apply for B4590) which resemble sine waves with a number of crests/troughs equal to the frequency order. The presented shapes are from specimen B1530 in particular, but the shapes of the remaining specimens are similar:

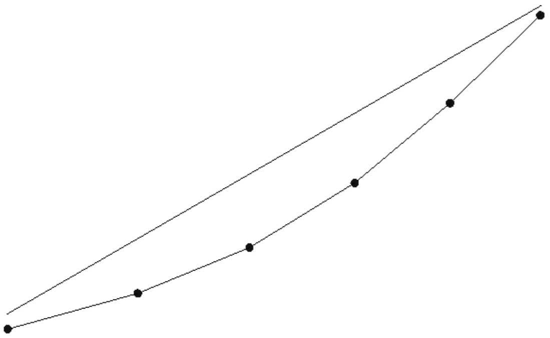

Figure 5.14 *1st mode shape*

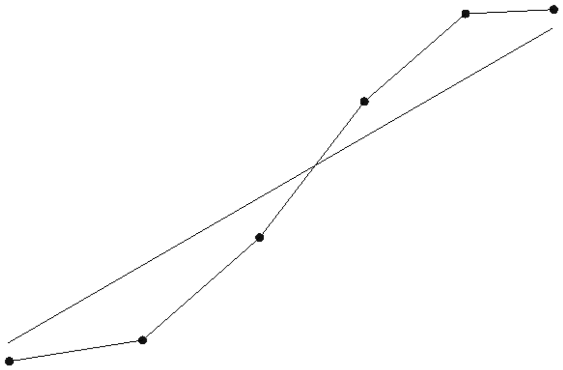

Figure 5.15 *2nd mode shape*

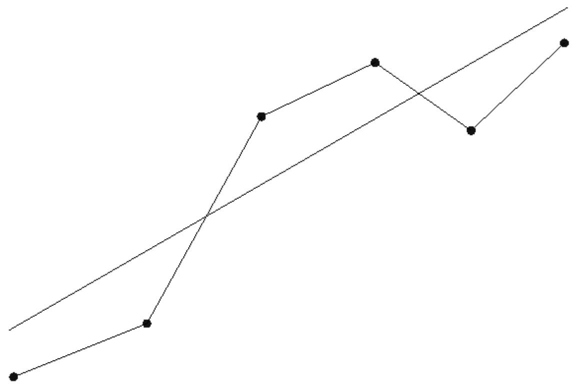

Figure 5.16 *3rd mode shape*

In order to examine the frequency shift with respect to loading, the normalized frequencies are plotted. Only the results for impact at location 4Z are shown, yet since the difference in frequency between the impact locations is rather small this data can be considered representative for the other impact locations as well.

Frequency normalization is performed by division with the frequency at initial loading. Thus the figures show the frequency ratio with respect to the lowest loading.

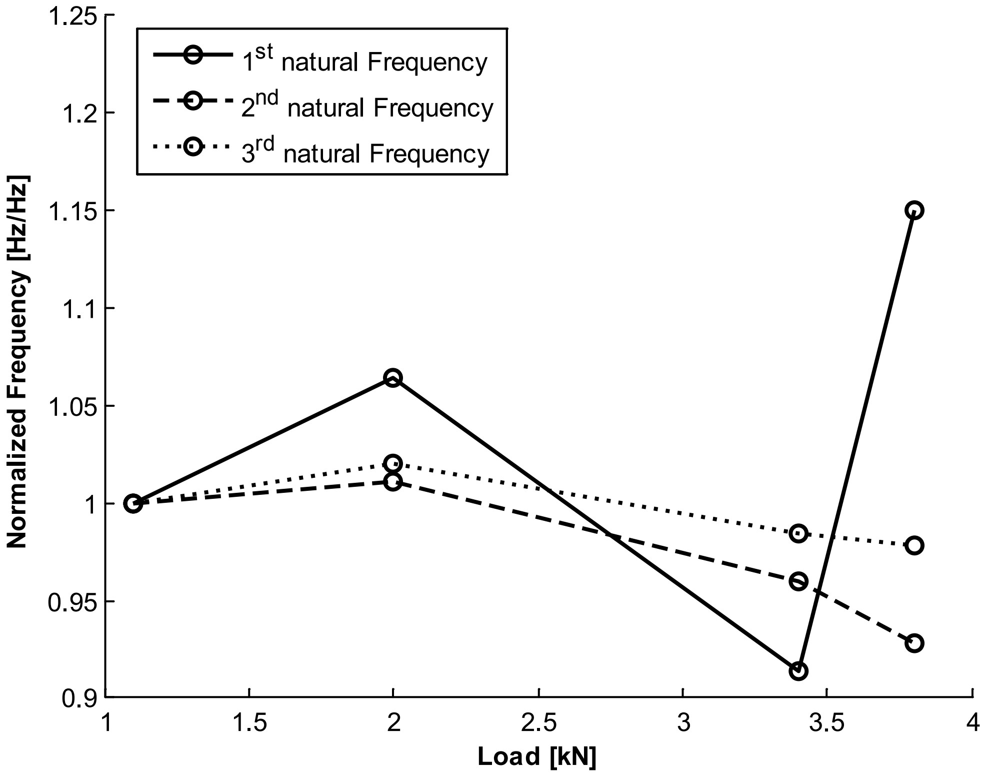

Figure 5.17 *Frequency variation vs loading B1020*

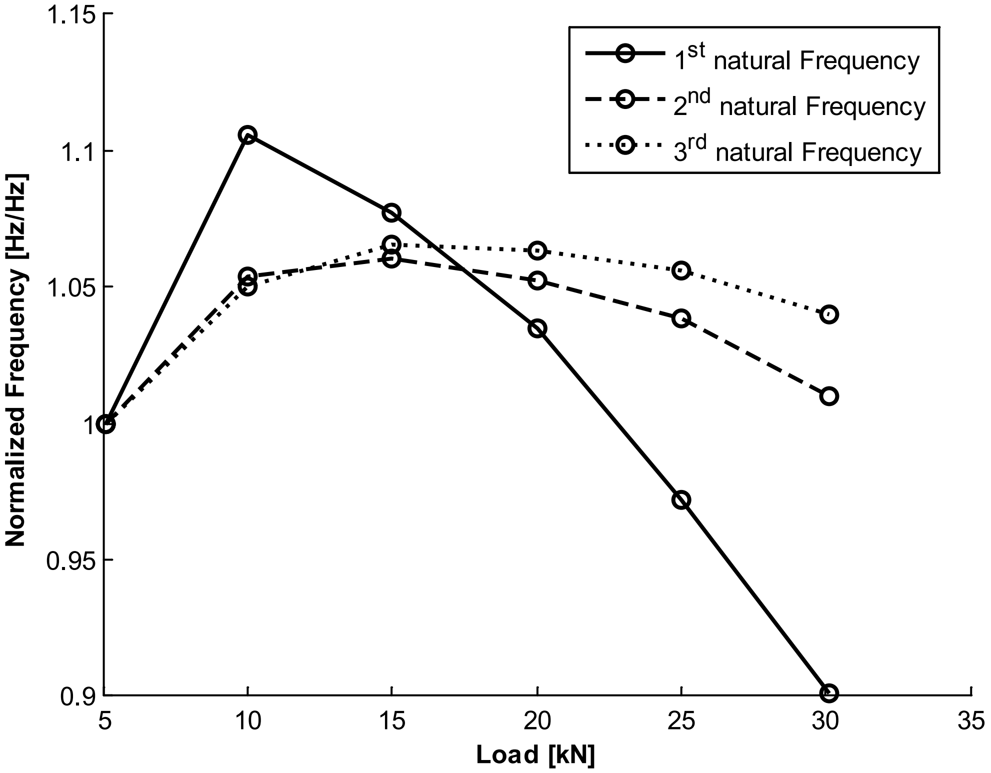

Figure 5.18 *Frequency variation vs loading B1530*

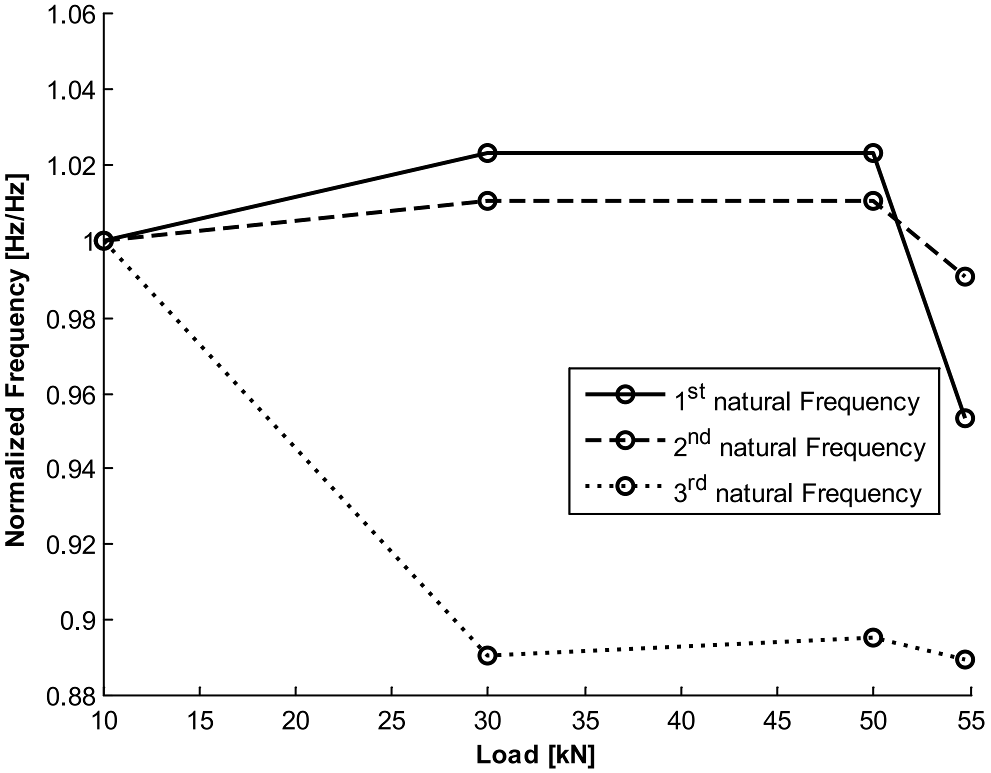

Figure 5.19 *Frequency variation vs loading B2040*

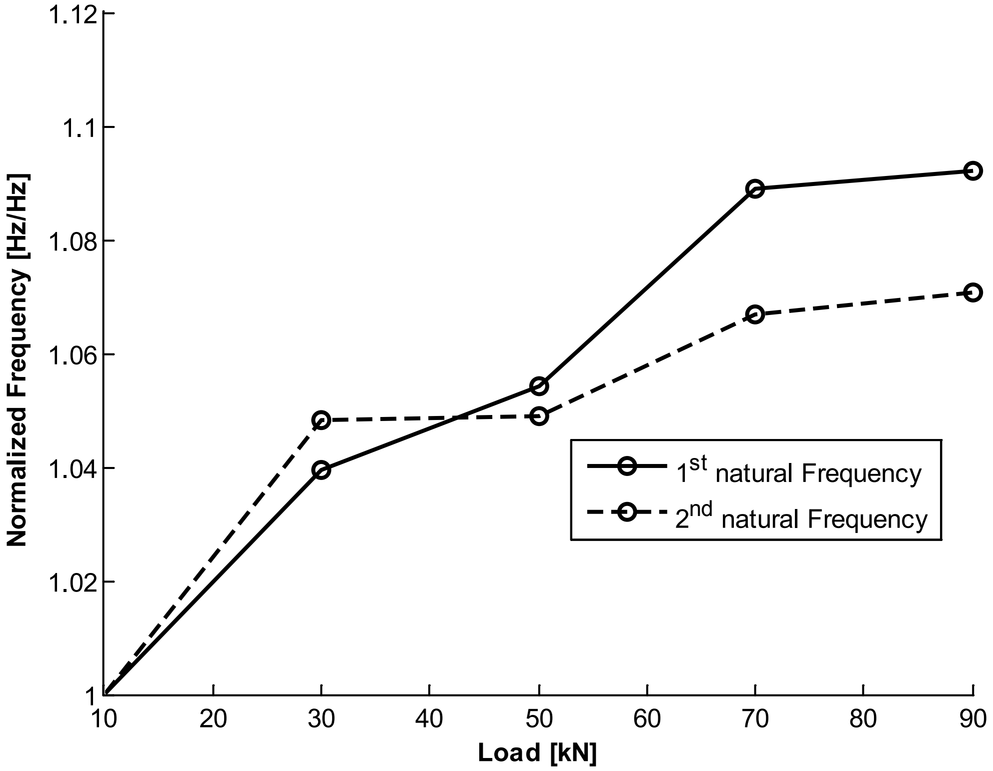

Figure 5.20 *Frequency variation vs loading B4590*

Beam B4590 clearly deviates from the remaining test samples as the frequency consistently increases with increasing load (see Figure 5.20).

The trend in the two most slender specimens is an initial increase followed by a decrease in frequency (note that the final loading values are deformed geometry and are only included for completeness sake).

The first two frequencies in B2040 display a mix of the other two behaviors by increasing at first and then remaining somewhat stable. The third frequency of B2040 does not follow any other behavior patterns in the lab data and no simple explanation for this exists. However this frequency is among the higher ones (> 400 Hz) and the FRF shape near this frequency is fairly noisy.[13]

5.5 Analysis of modal results

The assumption prior to testing was that boundary conditions would resemble fixed-pinned supports at high loads. Given the ultimate loads for B1530 and B2040 this assumption seems to hold true for all but the most slender beam. However this assumption is made for higher loads and rotational resistance at the fixed end is highly dependent on the axial load.

An increase in compressive loading yields a lowering in frequency theoretically as can be seen in equations (2.23) and (3.1). However these relations assume unchanging support conditions and therefore the initial increase in frequency could be due to a stiffening of support conditions. E.g.

---

[13] See driving point FRF for B2040 in appendix C – Test results

as the load increases the lower end of the beam is less prone to end rotation, due to it being pressed against the contact surface.

The same explanation model could be applied to stockier beams as B4590, where the increase in axial loading is very small with respect to the buckling load. Yet the impact on support stiffening might be considerable. Therefore the increase in frequency could solely depend on support stiffening, whilst the frequency change due to the effect of axial load on lateral stiffness is negligible.

Thus the change in frequency over the various loading levels is influenced both by a stiffening of the supports and a weakening of the transversal stiffness. Depending on the dimensions of the beam these factors are influenced differently by loading.

This in turn makes it difficult to exactly discern the effect of loading on the frequency. Thus the exact determination of loading conditions is of the utmost importance if the axial load is to be determined. Thus the use of spring supports is recommendable, since loading effects might be considerable regarding support conditions.

5.6 Calculation procedure

The axial load is calculated using the analytical Bernoulli-Euler beam approach described in chapter 3.1.1. The necessary input consists of a measured frequency and the corresponding mode shape in the form of five evenly spaced measurements (in m/s^2).[14]

However the output data from the laboratory setup yields six measurement points per mode shape and thus the upper and lower set of points (see Figure 5.6) are used and possible result differences are investigated. Also up to three frequencies can been detected for each loading level of a beam and three different impact positions have been employed. Thus up to $2 \cdot 3 \cdot 3 = 18$ different load calculations are performed for each load step of each beam.

Given the high sensitivity with respect to mode shape the discretized approach is employed using all six measurement points. Calculations are performed using both Bernoulli-Euler and Timoshenko beam theory. The former is used in order to compare results between the analytical and discretized approach. Then the more exact Timoshenko element is used to investigate the differences between the two theories.

Due to the amount of data only a portion of the results are presented within the report.[15]

5.7 Results – Analytical approach

The estimated loads show poor coherence with the actual loading (measured with the loading cell) as can be seen in the following four figures, which show the results for the using the lower sensor group at impact position 4Z.

In the following figures tensile forces are defined as positive and compressive forces as negative. Thus values above the control line imply an overestimation of the compressive force, whilst values below imply an underestimation of compressive force/estimation of tensile force.

---

[14] The calculation code used is found in appendix A – Calculation code.

[15] Remaining figures can be found in appendix D – Calculation results.

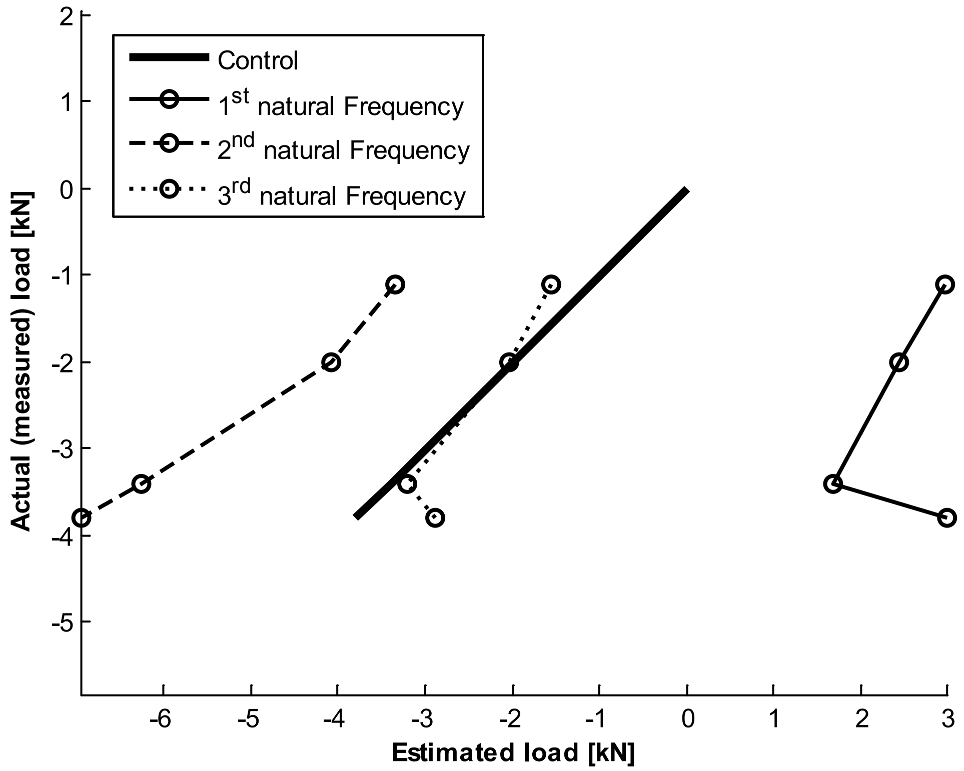

Figure 5.21 *B1020 Calculated load vs actual load (4Z lower sensors)*

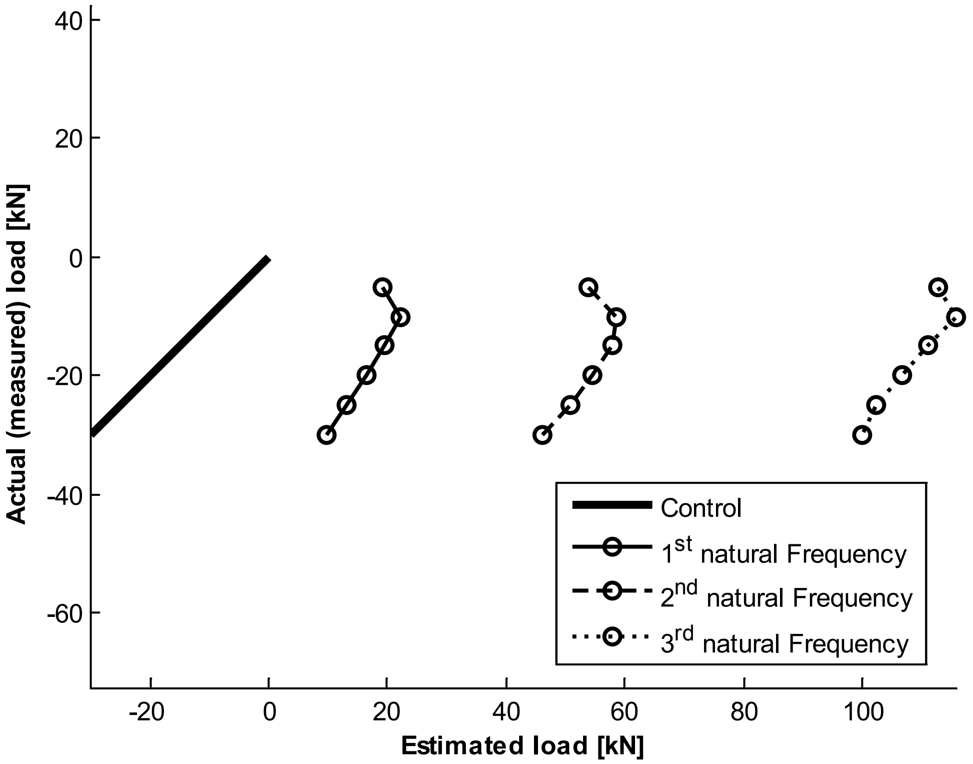

Figure 5.22 *B1530 Calculated load vs actual load (4Z lower sensors)*

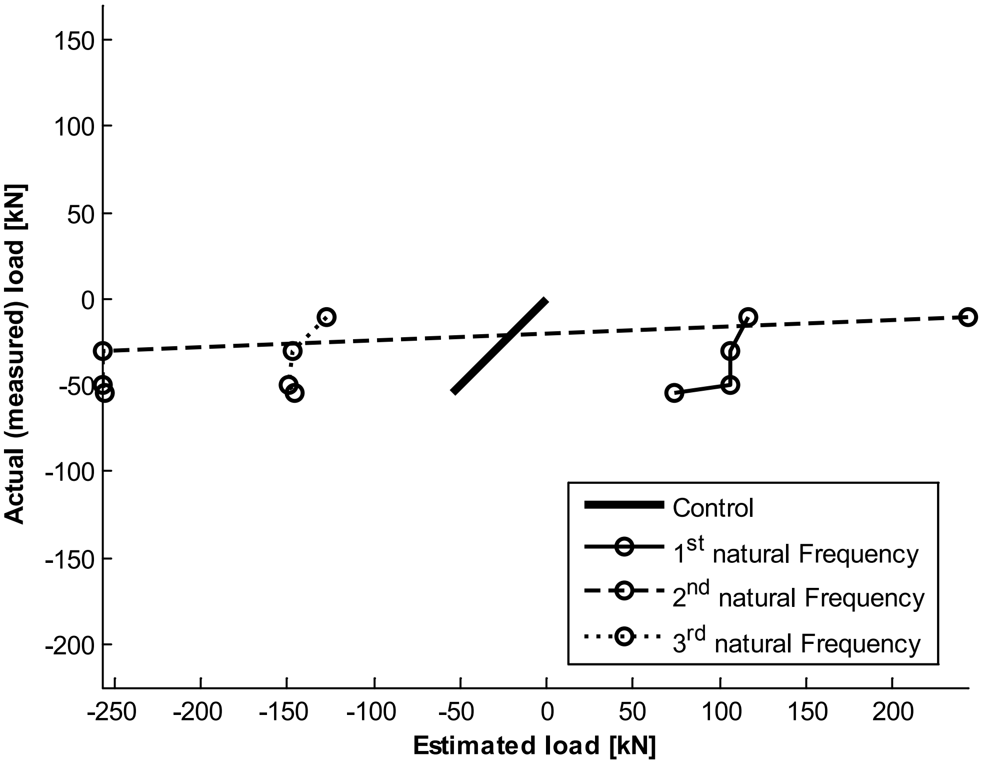

Figure 5.23 *B2040 Calculated load vs actual load (4Z lower sensors)*

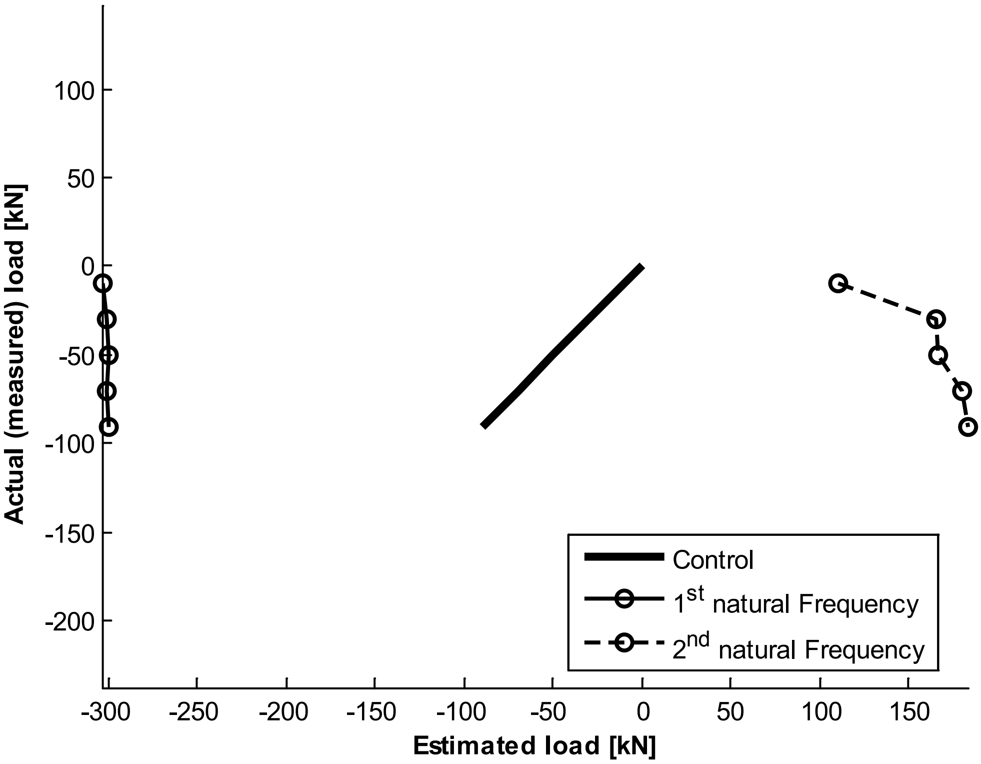

Figure 5.24 *B4590 Calculated load vs actual load (4Z lower sensors)*

Only for the most slender beam some of the calculated loads seem to be within an acceptable range to be considered estimates (even if they are poor). The calculated loads for stockier samples are far from the actual load, although in some cases (e.g. Figure 5.22) the change in loading seems to be well mirrored in the calculated loads.

Due to the poor results regarding estimation, the focus of the examination will be to discern trends in the data. Therefore the remaining results will be plotted in the form of actual loading level vs estimation error (in %), where the error is calculated according to:

$$Error = \frac{N_{calc} - N_{true}}{N_{true}} \tag{5.1}$$

Thus using a negative sign convention for compressive axial forces the following will apply:

Table 5.4 *Load levels [kN]*

	Range		Consequence
Positive percentage	$0\ \%$	∞	Overestimation of compressive force
Negative percentage	$0\ \%$	$-100\ \%$	Underestimation of compressive force
	$-100\ \%$	$-\infty$	Tensile force estimated

Due to the large amount of data and figures the results are examined for each beam independently. To improve readability the shown figures are exclusively for impact location 4Z, whilst remaining plots are found in the appendix.

5.7.1 B1020

In this specimen the 2nd and 3rd natural frequency (especially the latter) yield decent approximations for the loading. The 1st frequency on the other hand yields poor estimations which even vary in sign (tensile/compressive) depending on sensor group.

The estimation is improved at higher loading levels aside from the ultimate load (deformed geometry) and results using the upper sensor group are slightly better.

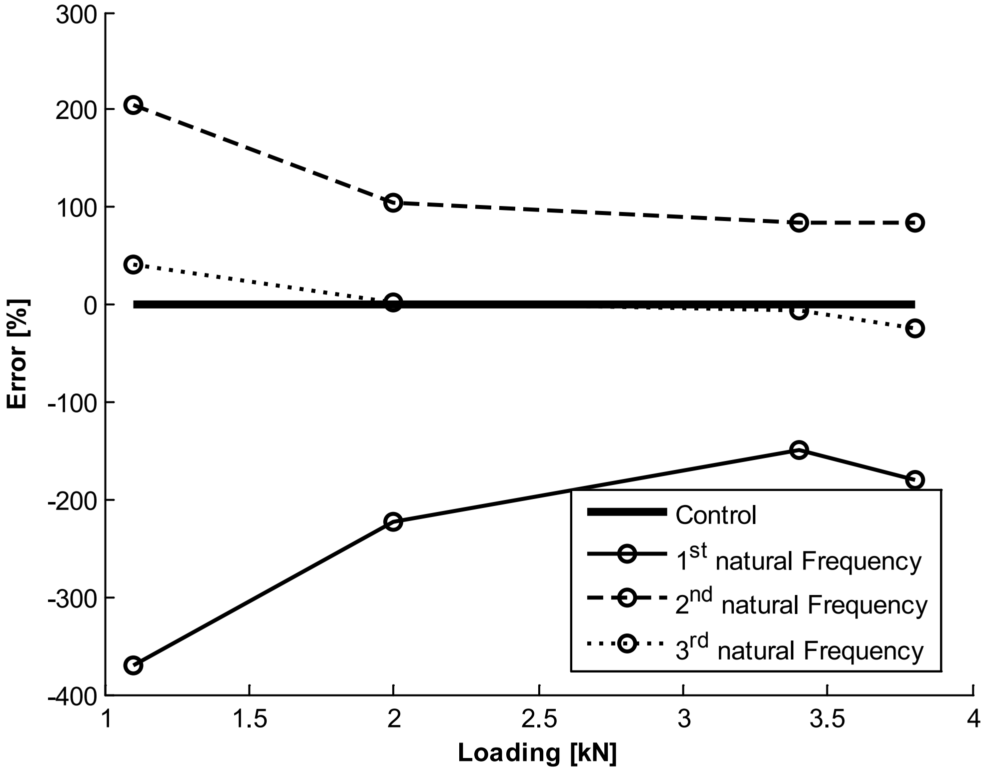

Figure 5.25 *B1020 Error vs actual load (4Z lower sensors)*

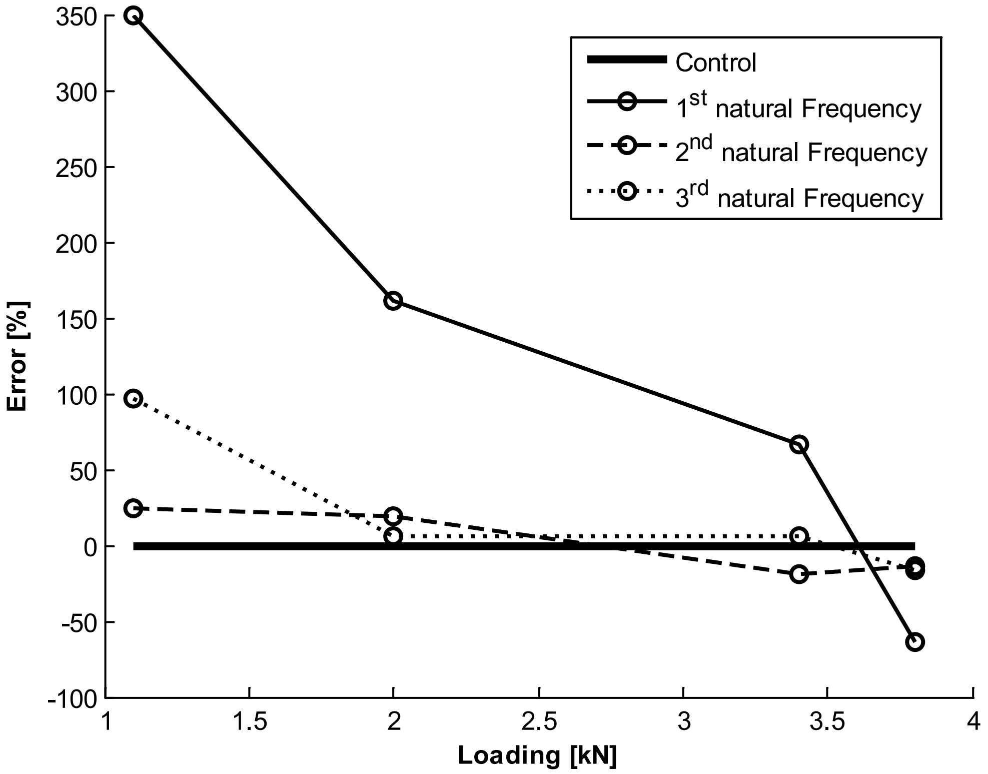

Figure 5.26 *B1020 Error vs actual load (4Z upper sensors)*

5.7.2 B1530

Compared to the previous sample the estimations are very poor, yielding tensile forces many times higher than the actual compressive force. In this specimen the lowest frequency yields the best results and the upper sensor group gives somewhat better results for the 1st natural frequency.

The estimates mimic the change in force found in the loading levels (see Figure 5.22). Note that the convergence of the estimation is **only apparent** and due to the initially small denominator in equation (5.1). The convergence of the curves does **not** imply a dramatic improvement in estimation.

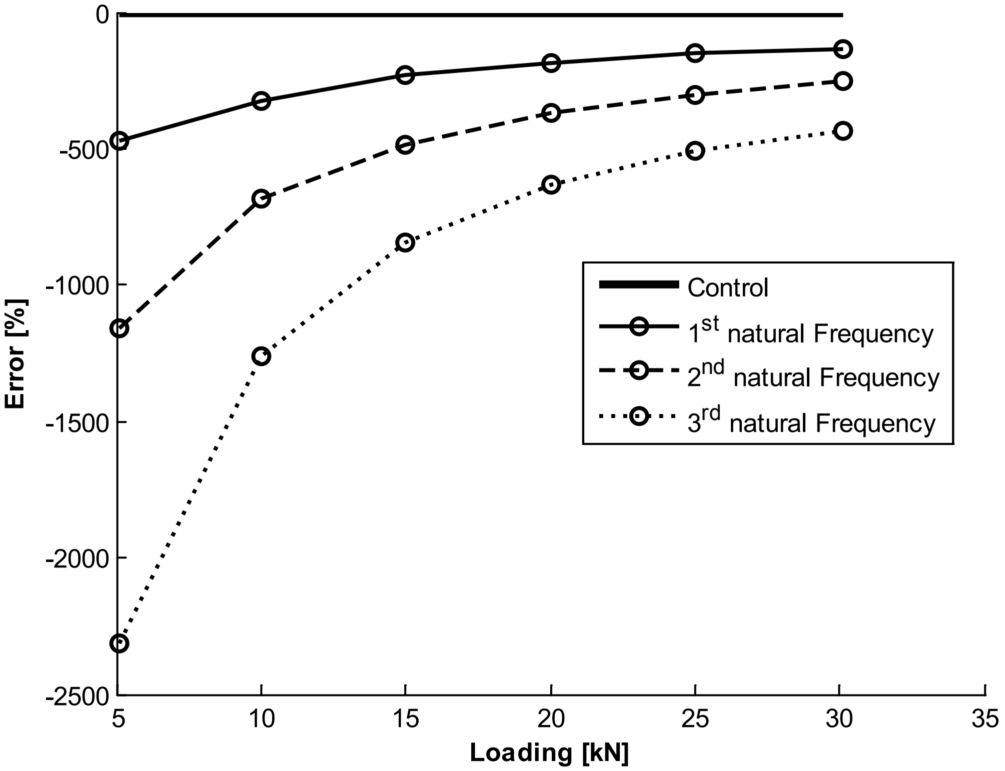

Figure 5.27 *B1530 Error vs actual load (4Z lower sensors)*

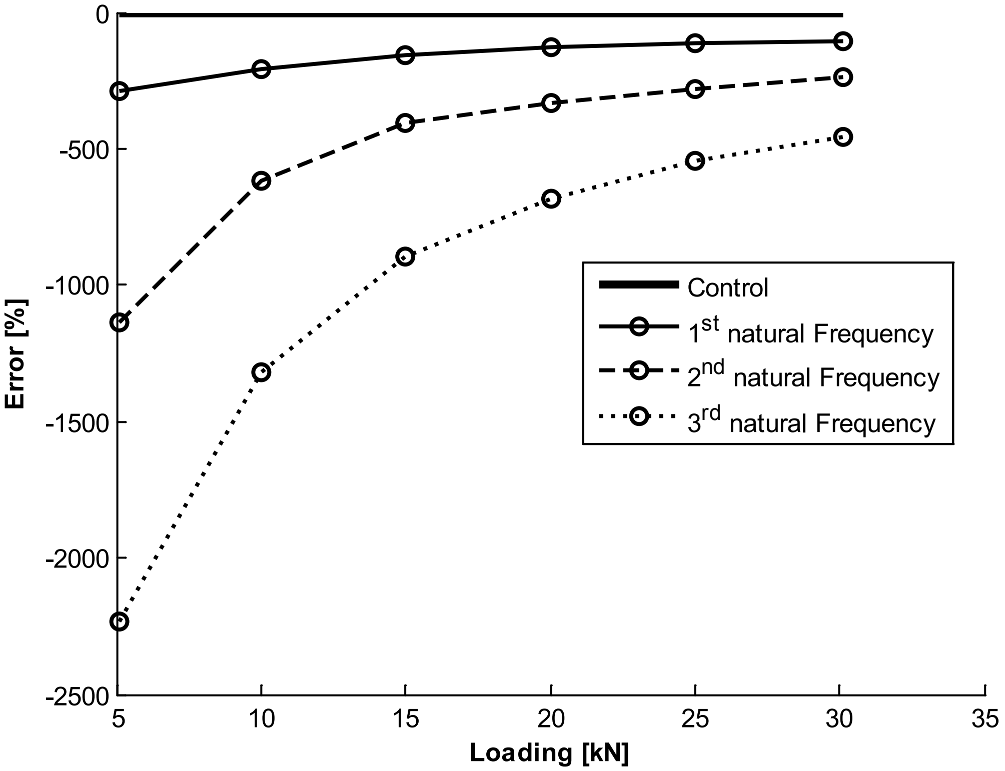

Figure 5.28 *B1530 Error vs actual load (4Z upper sensors)*

5.7.3 B2040

Note that also for this specimen the apparent convergence in the following figures depends on the initially small denominator. The estimations for the specimen are poor and compared to sample B1530 the change in force does not mimic the loading level as clearly.

In this specimen the estimation using the 2nd natural frequency yields the greatest error, while the remaining two frequencies yield similar errors although with different signs (tensile/compressive). Furthermore the upper sensor group yields slightly better results for the 1st and 2nd frequency (observe the difference in y-axis scaling in the two figures).

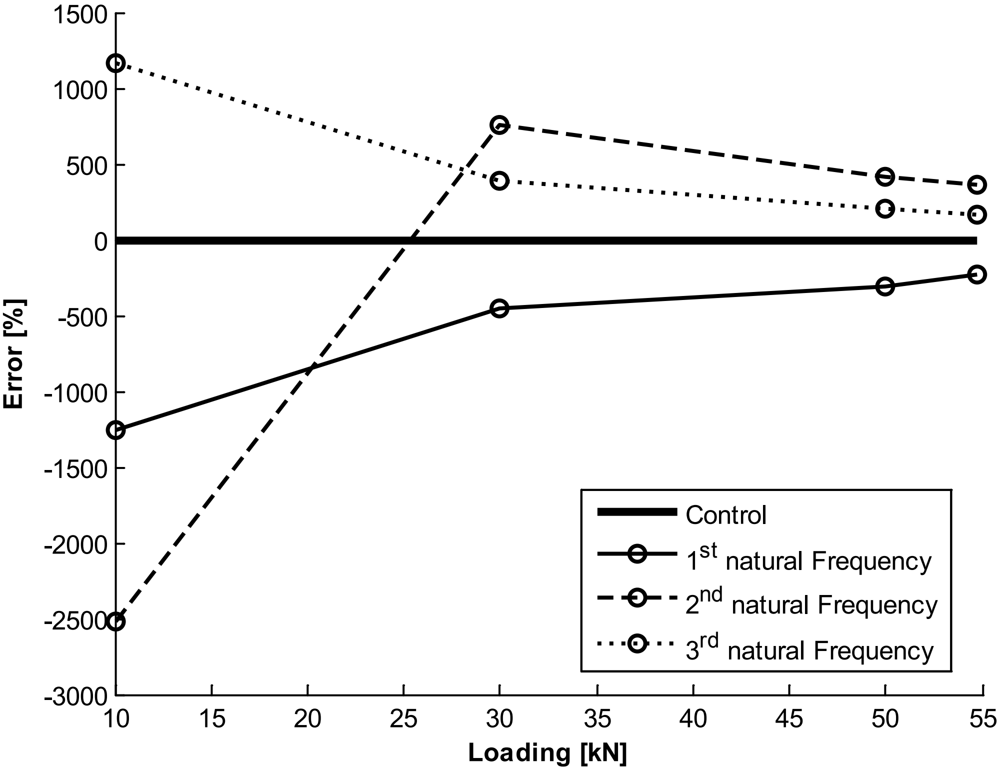

Figure 5.29 *B2040 Error vs actual load (4Z lower sensors)*

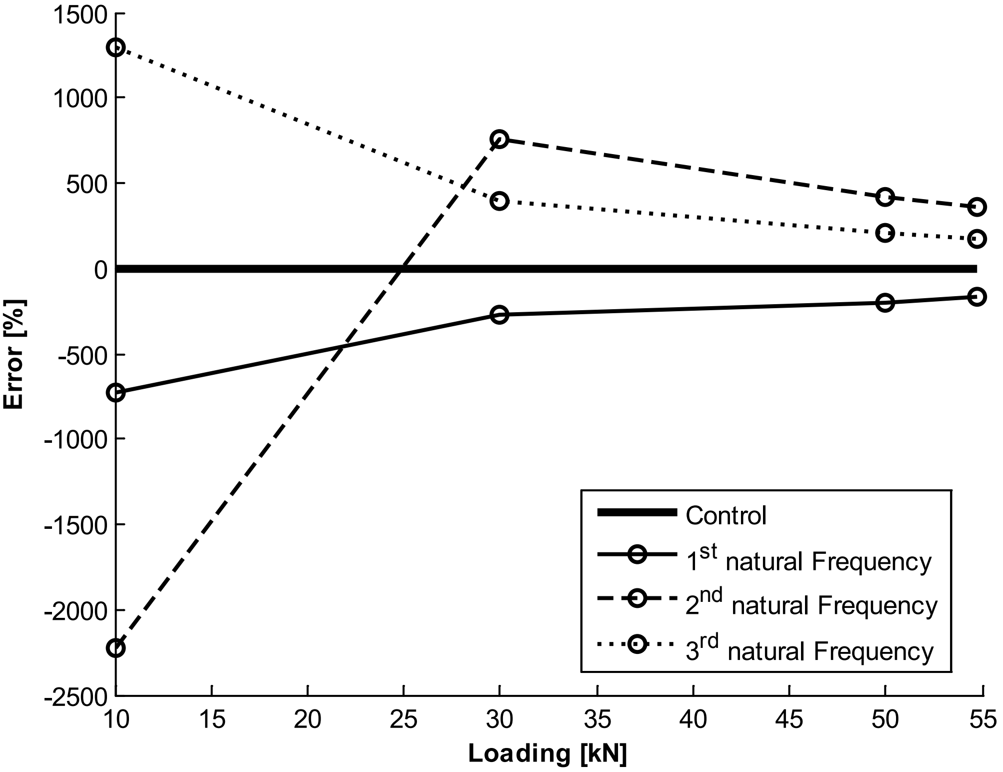

Figure 5.30 *B2040 Error vs actual load (4Z upper sensors)*

5.7.4 B4590

The results for this sample are very poor and there is no clear correlation to the actual loading. The apparent convergence in the following figures is clearly only apparent as the estimation using the 2nd natural frequency clearly worsens with increased loading (see Figure 5.24).

The 2nd natural seems to yield slightly better values when using the lower sensor group. Given the large estimation error and the fact that the estimated load is either unchanged (1st frequency) or lightens (2nd frequency) with higher load (see Figure 5.24), a detailed comparison of the estimations is excessive.

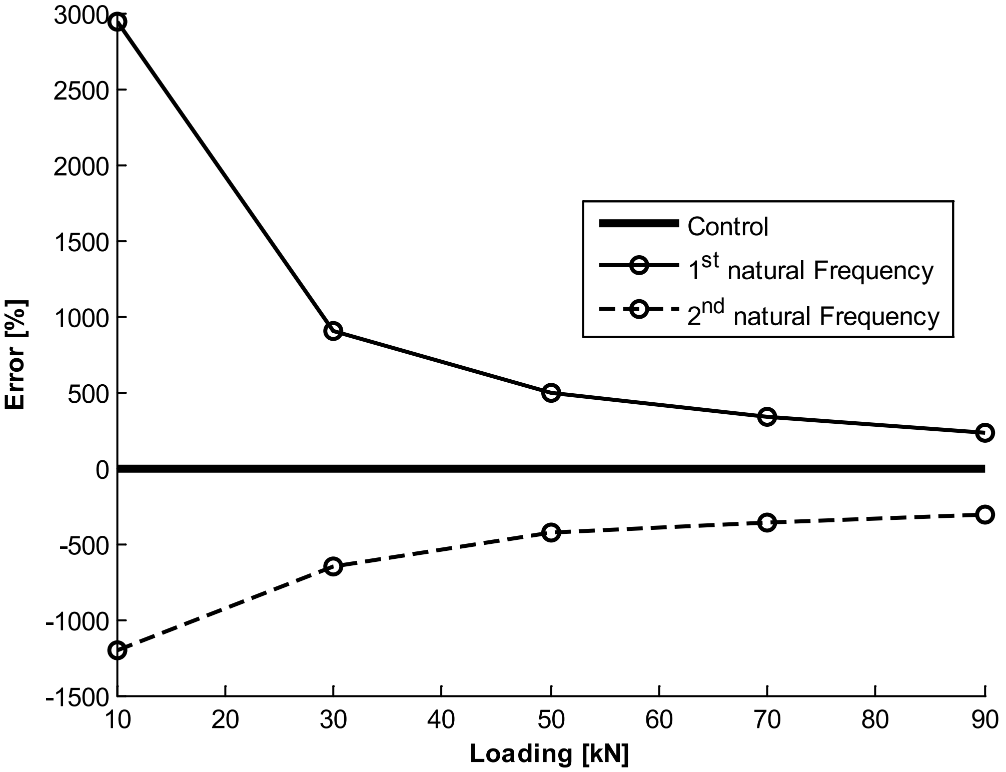

Figure 5.31 *B4590 Error vs actual load (4Z lower sensors)*

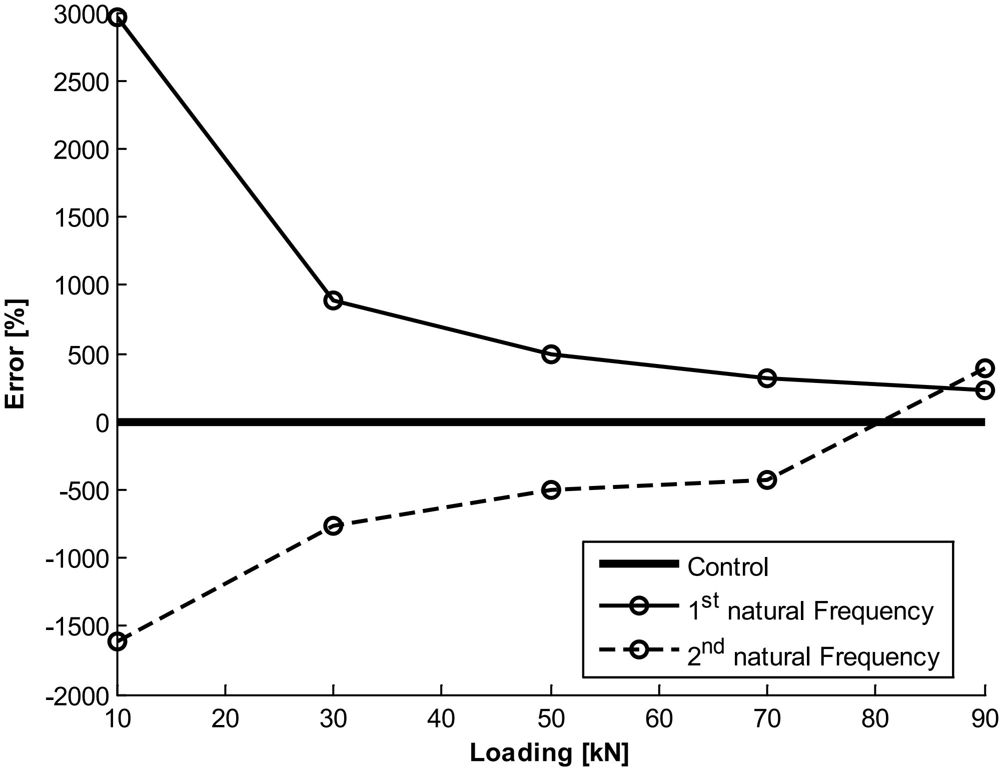

Figure 5.32 *B4590 Error vs actual load (4Z upper sensors)*

5.8 Analysis – Analytical approach

The somewhat decent results from B1020 and the mimicry with respect to load change in B1530 clearly show that load estimation is better for slender specimens. The natural frequencies in bending are determined by two components, transversal stiffness and axial loading (equation). Thus the bending frequency of a very slender specimen is mainly influenced by the axial load. However the scale of deterioration in estimation quality as slenderness decreases is remarkable.

There is no clear trend regarding which impact position yields the best result, why one position is focused upon (4Z). This is unexpected since the clarity of natural frequencies differs between the various driving point FRFs.[16]

Also none of the natural frequencies (1st, 2nd or 3rd) appear to be significantly better or worse in terms of load estimation quality. Even more remarkable is the fact that no clear correlation exists with respect to the frequency clarity in the various FRF diagrams. For instance the difficulty of specifying the 1st mode of B2040 was discussed in chapter 5.4, yet the load estimation using the 1st frequency is closest to the actual loading values.

Finally the results using the upper sensor group are slightly better at times. The support condition at the upper end is more flexible and deflection at the upper end is a little larger. Thus the vibration shape could be easier to detect clearly at the upper end (due to larger magnitude), which in turn could explain the improvement in load estimation.

---

[16] See the various driving point FRFs in appendix C – Test results.

5.9 Results – Discretized approach

Results are presented by plotting estimated loads against measured loads for each beam at position 4Z.[17] Unless specifically stated standard beam theory (Bernoulli-Euler) is used.

The estimation results have been significantly improved when using an over-determined system for all beams aside from B4590. Furthermore the load estimation tends to be higher than the actual loading level.

5.9.1 B1020

The load estimation is very good for the 3rd frequency producing an estimation error of < 10 % for the 2nd and 3rd loading level. Aside from the 1st natural frequency the method produces a load estimation that is higher than the actual value. Use of Timoshenko elements improves accuracy of good estimations to an error of ± 3 %.

Note that the geometry was visibly deformed in the final two loading levels.

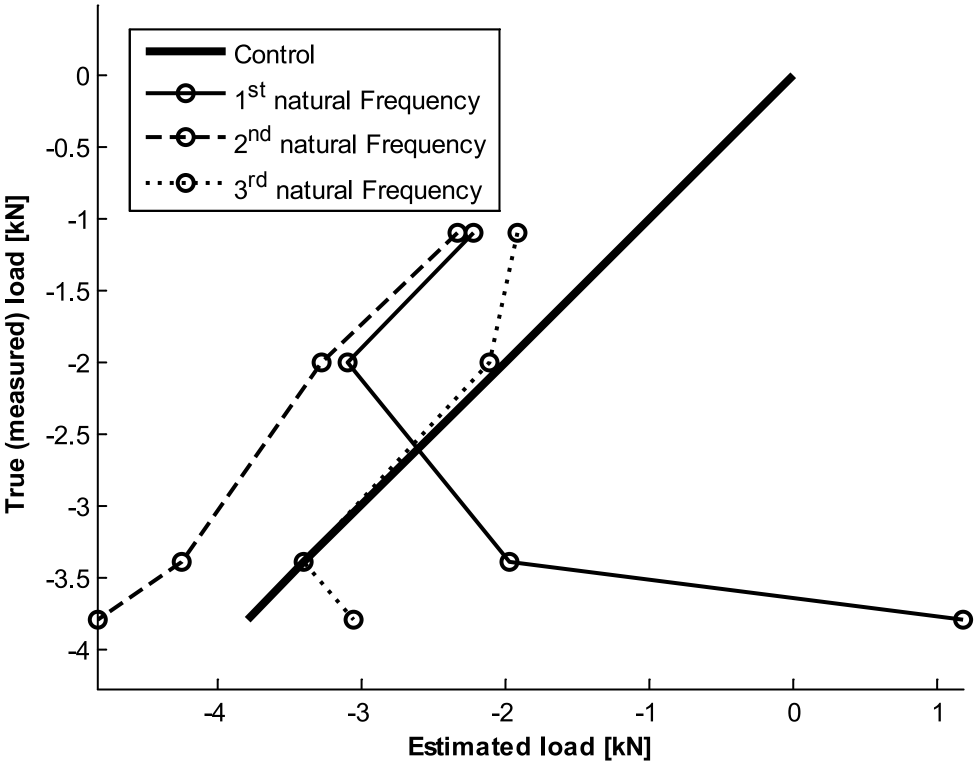

Figure 5.33 *B1020 Calculated load vs actual load (4Z all sensors)*

---

[17] Remaining figures (other impact positions & error plots) can be found in appendix D – Calculation results.

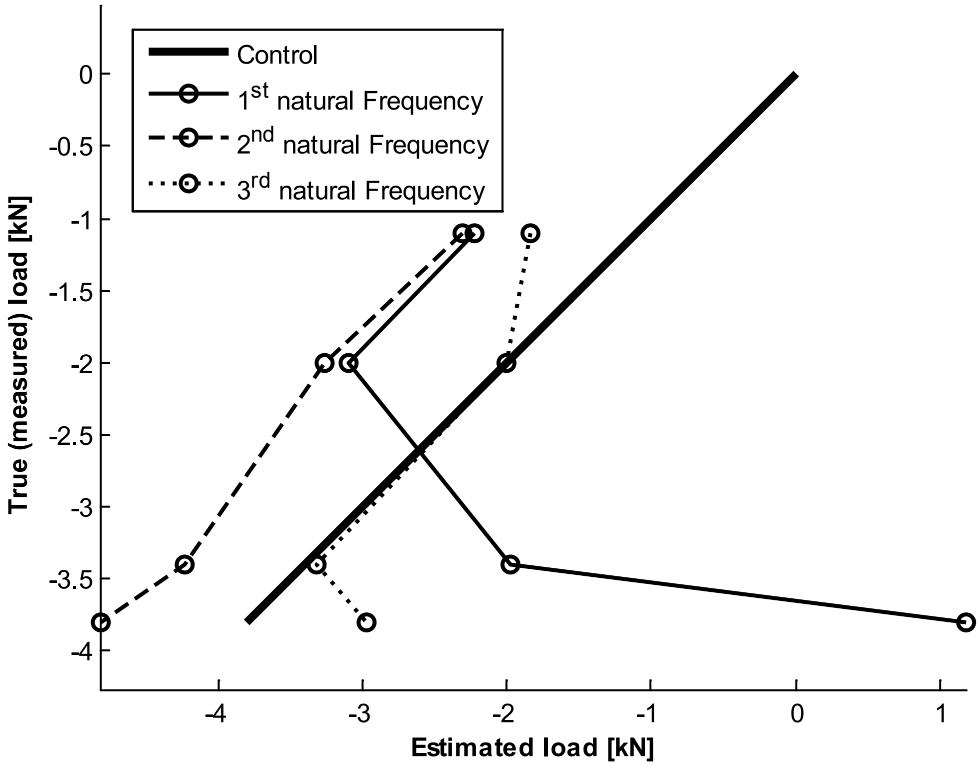

Figure 5.34 *B1020 Calculated load vs actual load (4Z all sensors); Timoshenko elements*

5.9.2 B1530

The increase in loading is nicely mimicked by the estimations of all frequencies. The 3rd frequency yields the best estimation with an error of 20 % and 15 % using Bernoulli-Euler elements and Timoshenko elements respectively.

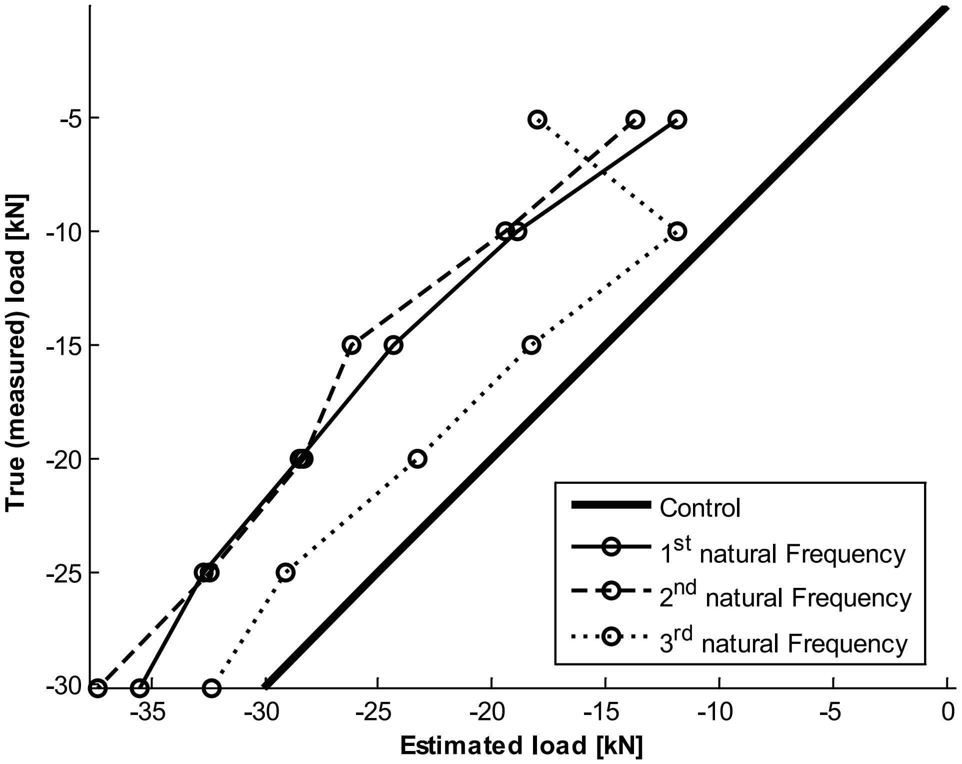

Figure 5.35 *B1530 Calculated load vs actual load (4Z all sensors)*

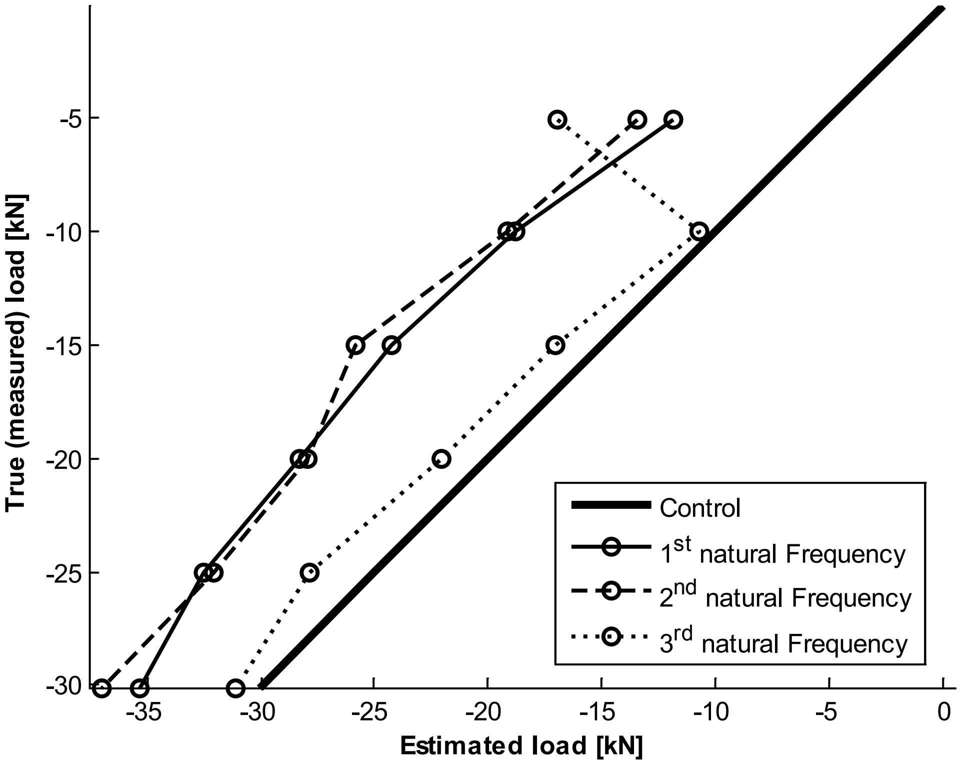

Figure 5.36 *B1530 Calculated load vs actual load (4Z all sensors) ; Timoshenko elements*

5.9.3 B2040

The estimation quality is poorer and estimations are more scattered compared to the two previous specimens. The lowest natural frequency yields the worst estimation, whilst the 2nd and 3rd natural frequency yield similar results. The least scatter is seen when using the 2nd frequency (approximately 50-100 % error).

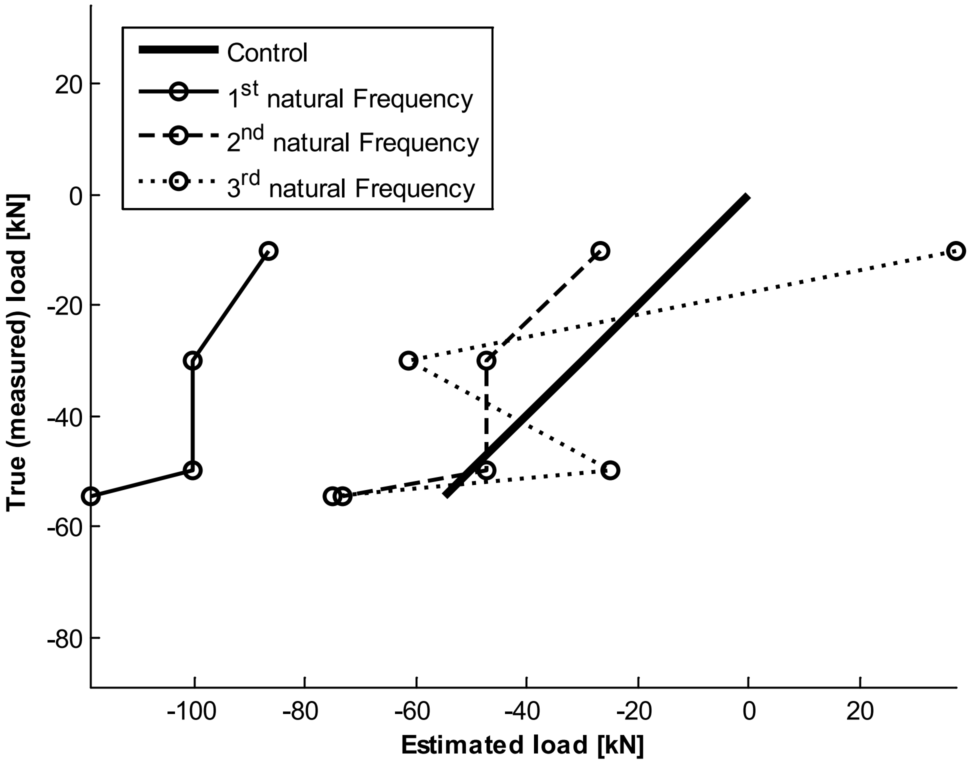

Figure 5.37 *B2040 Calculated load vs actual load (4Z all sensors)*

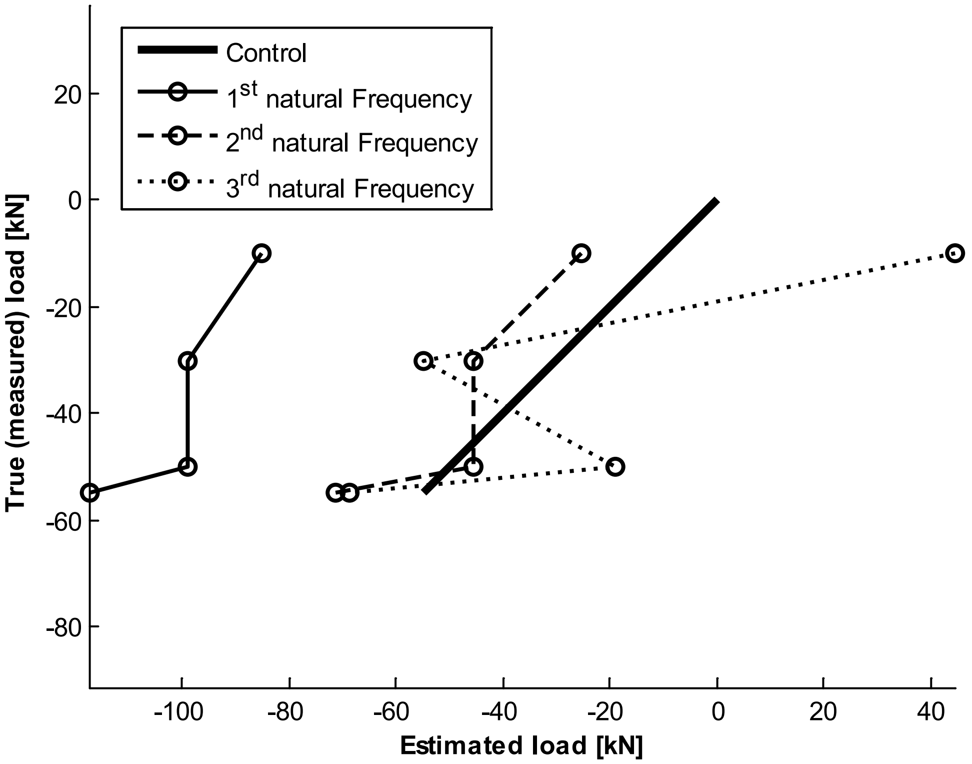

Figure 5.38 *B2040 Calculated load vs actual load (4Z all sensors) ; Timoshenko elements*

5.9.4 B4590

The estimation quality in this particular sample is still very poor even with the use of an over-determined system. However the estimations obtained are consistently of higher magnitude than the measured loading level.

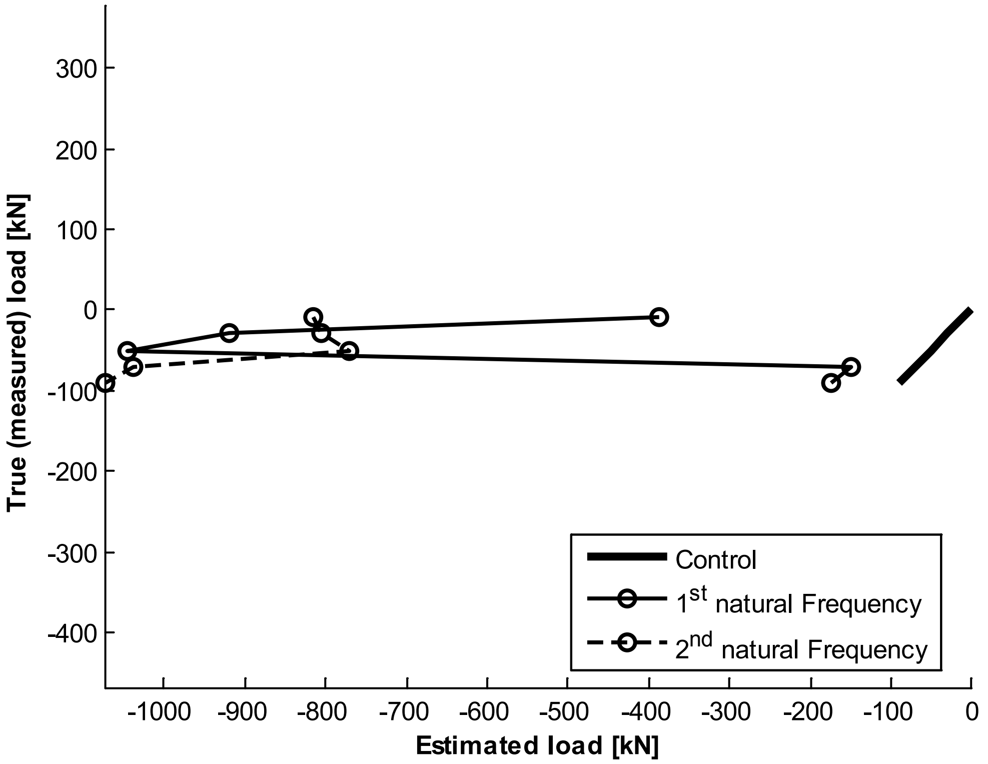

Figure 5.39 *B4590 Calculated load vs actual load (4Z all sensors)*

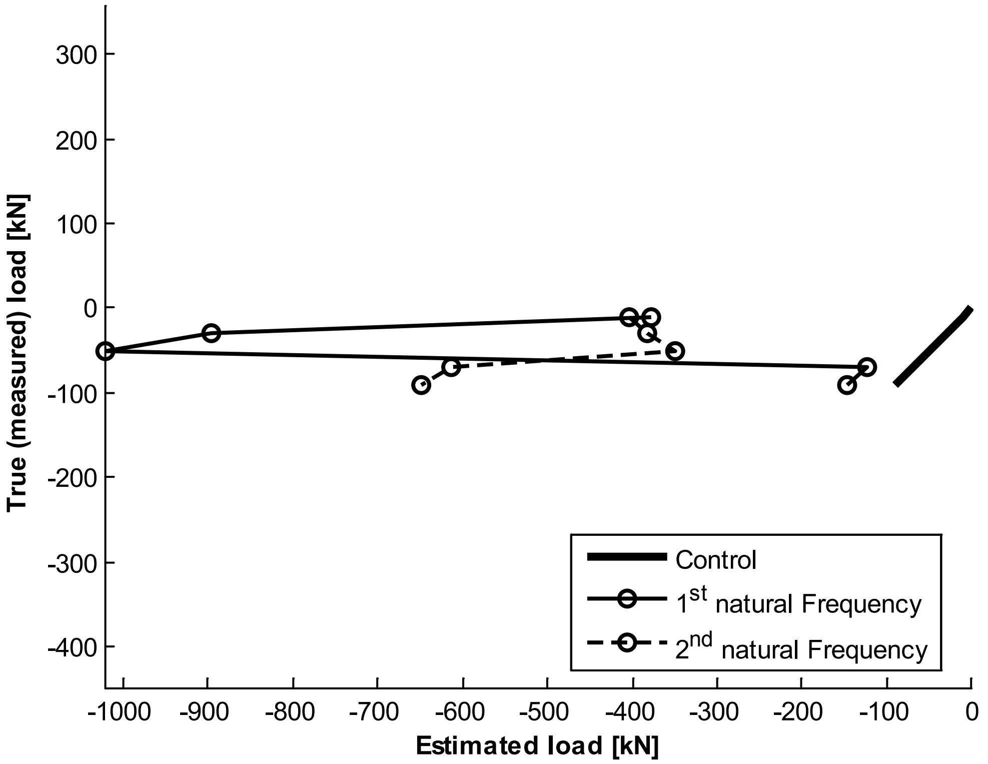

Figure 5.40 *B4590 Calculated load vs actual load (4Z all sensors) ; Timoshenko elements*

5.10 Analysis – Discretized approach

The results are significantly improved by using the discrete approach with an over-determined system compared to the analytical approach. The numerical testing only showed a small difference in load estimation between the analytical and discrete approach. Thus the improvement in estimation quality must be due to the improved shape approximation by using six measurement points.

As previously there have been no clear trends regarding the impact position.[18]

The estimation quality appears to be much better for slender specimens considering the poor results for the stockiest specimen (B4590). However that particular specimen is loaded with less than 10 % of the design load[19], whilst remaining beams are loaded close to the failure load. Given that the first loading level tends to yield the worst estimations,[20] the inferior estimation quality could be due to low loading.

Interestingly the estimation quality has been best for the higher frequencies. In the sensitivity analysis[21] the error magnitude with respect to shape parameters clearly decreased for higher frequencies. Therefore the shape parameters seem to be the most influencing factor with respect to estimation error.

The use of both Bernoulli-Euler and Timoshenko beams shows that the former tends to overestimate the loading. However that the difference would be as pronounced was not anticipated. The results using the over-determined system show a general overestimation of loading, which is positive if a margin of safety is considered.[22] The use of Bernoulli-Euler beams could be specifically used to increase this margin.

---

[18] Remaining results can be found in appendix D – Calculation results

[19] Corresponds approximately to 3 % of the Euler buckling load

[20] See Figure 5.31 – Figure 5.36

[21] See chapter 3.3.1

[22] Assuming an overestimation increases the margin of safety.

6 Conclusion

The study has shown that there is a clear theoretical link between the bending frequency and axial load. Particularly the Galef equation[23] relating natural frequency and buckling load demonstrates this nicely. However the impact of boundary conditions is substantial which can clearly be seen in the numerical studies of beams with different support conditions (i.e. Amba-Rao [14]).

The use of assumed support conditions would be very imprecise, which is clearly shown by the modal results of the experiments. The increase in frequency after the first loading level occurs in all specimens, which is attributed to the change in (stiffening of) the support conditions. Thus the modelling of support conditions as unknown springs circumvents the need of support assumptions quite elegantly. Particularly for real real-world use the exact support conditions can be very hard to determine (e.g. a bolted column footing).

The analytical approach in the presented form is straightforward and fairly easy to implement. The major drawbacks are the limitation to a prismatic Bernoulli-Euler beam and the use of only five measurement points. The discrete approach on the other hand is more versatile, allowing the use of non-prismatic beams (by change of elements), the more complete Timoshenko beam theory and an excess of measurement points. However the issue of convergence remains a serious concern.

Both the numerical and experimental work shows the high level of sensitivity regarding mode shape, which can be seen in:

- The sensitivity analysis itself
- The improvement in estimation, when using an over-determined discretized approach compared to the analytical approach
- The fact that the best estimations in the over-determined approach are found in the 3rd frequency, which also yielded the smallest error in the sensitivity analysis with respect to shape.

Thus the measurement of the mode shape seems to be the factor influencing estimation quality the most in the used calculation model. This suggests that an improvement in this area (e.g. by measuring even more shape points) could further enhance estimation quality.

The extraction of natural frequencies and mode shapes has not been given an in-depth treatment in the report. As previously mentioned the use of more advanced modal analysis[24] has not been employed, instead the FRFs from a single impact location have been used. An appropriate algorithm for the task (i.e. specialized for undamped frequency and shape) could improve the data extracted from testing. However this matter has not been investigated further due to time constraints.

Experimental results indicate that the presented approach yields better results for slender specimens, particularly when examining the poor estimations of the stockiest beam. However one must consider that the relative loading level[25] is very low for the specific beam and the sensitivity analysis as well as the Galef equation indicates higher estimation errors at low loading levels. Thus the load estimation might be considerably improved even for non-slender specimens if the loading is high enough compared to the buckling load.

---

[23] See equation (3.1)

[24] As for instance included in the B&K software

[25] < 10 % of the design load and < 3 % of the Euler buckling load

The study indicates that higher frequencies or an increase in measurement points would improve results. Given the limited testing[26] caution is advised regarding these indications. Furthermore there are certain improvements that could be made to the experimental procedure such as the use of more sensitive sensors (i.e. the tri-axial sensors) or a better suited testing rig (especially regarding the boundary conditions).

Overall the suggested approach cannot be used practically in its current form; however the results indicate that the approach is promising given further development, especially considering a better estimation/measurement of the mode shape. On a positive note the estimations using the over-determined discrete approach show a tendency to overestimate loading. Thus the method seems to yield estimates on the safe side regarding the remaining load bearing capacity.

6.1 Further research

The following points are suggestions regarding further research and improvement of the suggested approach.

- Improved vibration shape estimation/measurement
    - Determining whether using even more measurement points would improve estimation quality further. It remains to be seen if the discrete approach converges/is stable if increasing the number of measurement points. An over-determined shape could also be employed for the analytical approach. A possible approach could be to measure the vibration shape in several points and curve fitting it to a sine wave, thereafter extracting the desired five points from the fitted curve.
    - Determining an appropriate algorithm for extraction of undamped frequency and shape from several impact locations. Alternatively in the discrete approach the equation systems for several impacts (and/or frequencies) could be concatenated.
- Further experimental work with a larger series and variation of test specimens (including the examination of higher frequencies)
- Studies regarding other cross section types. In particular open cross sections (e.g. I-beams) could be of interest due to their low torsional stiffness.

---

[26] Only 4 beams with very similar support conditions, cross section types (rectangular) and lengths were used. Also calculations were limited to the 3 lowest natural frequencies.

References

[1] Tullini N, Rebecchi G, Laudiero F. Bending tests to estimate the axial force in tie-rods. Mechanics Research Communications 2012;44:57–64.

[2] Chopra AK. Dynamics of structures : theory and applications to earthquake engineering. Upper Saddle River, N.J.: Pearson/Prentice Hall; 2007.

[3] Timoshenko S, Young DH, Weaver W. Vibration problems in engineering. 4th ed. New York: Wiley; 1974.

[4] Abramovich H, Elishakoff I. Application of the Krein's method for determination of natural frequencies of periodically supported beam based on simplified Bresse-Timoshenko equations. Acta Mechanica 1987;66:39–59.

[5] Abramovich H, Elishakoff I. Influence of shear deformation and rotary inertia on vibration frequencies via Love's equations. Journal of Sound and Vibration 1990;137:516–22.

[6] Howson WP, Williams FW. Natural frequencies of frames with axially loaded Timoshenko Members. Journal of Sound and Vibration 1973;26:503–15.

[7] Abramovich H. Natural frequencies of Timoshenko beams under compressive axial loads. Journal of Sound and Vibration 1992;157:183–9.

[8] Bokaian A. Natural frequencies of beams under compressive axial loads. Journal of Sound and Vibration 1988;126:49–65.

[9] Galef AE. Bending Frequencies of Compressed Beams. The Journal of the Acoustical Society of America 2005;44:643–643.

[10] Fukumoto Y, Itoh Y. Evaluation of multiple column curves using the experimental database approach. Journal of Constructional Steel Research 1983;3:2–19.

[11] Virgin LN, Plaut RH. Axial load effects on the frequency response of a clamped beam. IMAC-XXI: Conference and Exposition on Structural Dynamics 2003.

[12] Rebecchi G, Tullini N, Laudiero F. Estimate of the axial force in slender beams with unknown boundary conditions using one flexural mode shape. Journal of Sound and Vibration 2013;332:4122–35.

[13] Laux S. Estimation of axial load in timber beams using resonance frequency analysis. Masters Thesis. Chalmers University of Technology, 2012.

[14] Amba-Rao CL. Effect of End Conditions on the Lateral Frequencies of Uniform Straight Columns. The Journal of the Acoustical Society of America 2005;42:900–1.

[15] Livingston T, Béliveau JG, Huston DR. Estimation of axial load in prismatic members using flexural vibrations. Journal of Sound and Vibration 1995;179:899–908.

[16] Amabili M, Carra S, Collini L, Garziera R, Panno A. Estimation of tensile force in tie-rods using a frequency-based identification method. Journal of Sound and Vibration 2010;329:2057–67.

[17] Tullini N, Laudiero F. Dynamic identification of beam axial loads using one flexural mode shape. Journal of Sound and Vibration 2008;318:131–47.

[18] Kosmatka JB. An improved two-node finite element for stability and natural frequencies of axial-loaded Timoshenko beams. Computers & Structures 1995;57:141–9.

[19] Dahlblom O, Olsson K-G. Strukturmekanik : modellering och analys av ramar och fackverk. Lund: Studentlitteratur; 2010.

[20] Avitabile P. Experimental modal analysis a simple non-mathematical presentation. S V Sound and Vibration 2001;35:20–31.

[21] Avitabile P. Modal Space - In Our Own Little World. Modal Space - In Our Own Little World 2014.

[22] Maia NMM, Montalvão e Silva JM. Theoretical and experimental modal analysis. Taunton: Research Studies Press; 1997.

Appendix

A – Calculation code

rebecchi

```
function  f0 = rebecchi(N, omega, v, m, L, E, I)
% f0 = rebecchi(N, omega, v, m, L, E, I)
% In combination with fzero:
% N = fzero(@(N) rebecchi(N, omega, v, m, L, E, I), initial guess)
%----------------------------------------------------------------------------
% PURPOSE
%   This function is used as an input to fzero (or similar) in order to
%   calculate the axial force in a slender beam using one flexural mode
%   shape according to Rebecchi et al
%   (Journal of Sound and Vibration 332, 2013)
%
% INPUT:    N       Axial force [N], the function is solved for this
%                   constant using a function handle (@)
%           omega   Circular frequency (omega) [rad/s]
%           v       Mode shape amplitudes (1-5) at equidistant points in
%                   beam
%           m       mass per unit length [kg/m]
%           L       Length of beam [m]
%           E       Young's modulus [Pa]
%           I       2nd moment of area [m^4]
%
% OUTPUT:   f0      Transcendental equation (should be zero)
%----------------------------------------------------------------------------

%----------------------------------------------------------------------------
% LAST MODIFIED:    S Fässler    2014-04-18
%----------------------------------------------------------------------------

%% Extract mode shape
v1 = v(1);  v2 = v(2);  v3 = v(3);  v4 = v(4);  v5 = v(5);

%% Define parameters
lambda4 = (omega^2*m*L^4) / (E*I);
n = N*L^2 / (E*I);

q1 = (( (n^2+4*lambda4)^(1/2) - n )/2)^(1/2);
q2 = (q1^2 + n)^(1/2);

%% Transcendental equation
f0 = ...
    ( (v1 + v5)/(2*v3) + 1 + 2*cos(q1/4)*cosh(q2/4) ) ...
    / ( cos(q1/4)+cosh(q2/4) ) ...
    - (v2+v4)/v3;
%--------------------------------------end-----------------------------------
```

reveig

```
function f0 = reveig(x,K0,KG,M,omega,meas)
% f0 = reveig(x,K0,KG,M,omega,meas)
% In combination with lsqnonlin:
% x = lsqnonlin(@(x) reveig(x,K0,KG,M,omega,meas), initial guess)
%----------------------------------------------------------------------------
% PURPOSE
%   This function is used as an input to lsqnonlin (or fsearchmin with
%   minor alterations) in order to calculate the unknown parameters in the
%   solved eigen value problem:
%                   (K - omega^2*M)*phi = 0
%
%   A condensation is performed to minimize computative effort.
%
% INPUT:    x       Unknowns, consisting of
%                   [Normal force, spring constants]
%           K0      Stiffness matrix (1st order)
%           KG      Stiffness matrix (2nd order)
%           M       Mass matrix
%           omega   Measured angular eigenfrequencies [rad/s]
%           meas    Measured mode shape deflections/accelerations
%                      Measurement 1          Measurement 2
%                   [deflection1    DOF       deflection1   DOF ...
%                    deflection2    DOF       deflection2   DOF
%                    ...                                          ]
%
%           E       Young's modulus [Pa]
%           I       2nd moment of area [m^4]
%
% OUTPUT:   f0      Concatenated eigen value problem (should be zero)
%---------------------------------------------------------------------------

%---------------------------------------------------------------------------
% LAST MODIFIED:    S Fässler    2014-05-08
%---------------------------------------------------------------------------

%% Size calculations
nbr_dof = size(K0,1);
nbr_freq = length(omega);           % nr of frequencies measured
nbr_meas =  size(meas,1);           % nr of measurement points

%% Introducing spring constants
KK = zeros(nbr_dof);
KK_sys = [];
for i = 1:nbr_freq
    KK(1,1) = x(4*i-2);          KK(end-1,end-1) = x(4*i);
    KK(2,2) = x(4*i-1);          KK(end,end) = x(4*i+1);
    KK_sys = blkdiag(KK_sys,KK);
end

%% Constructing system matrices & concatenating if several frequencies are
used
K0_sys = kron(eye(nbr_freq) , K0);
KG_sys = kron(eye(nbr_freq) , KG);
w2M_sys = kron( diag(omega.^2) , M );

%% Determining rows for condensation & concatentating measurements
top = ...
    ones(nbr_meas,1) * colon(0,nbr_dof,nbr_dof*(nbr_freq-1)) ...
    + meas(:,colon(2,2,2*nbr_freq));
bottom = colon(1,nbr_dof*nbr_freq);
bottom(top) = [];
phi = meas(:,colon(1,2,2*nbr_freq-1));
phi = phi(:);

%% Shifting rows & columns for condensation
% Rows
K0_sys  = [K0_sys(top,:) ; K0_sys(bottom,:)];
```

```
KG_sys  = [KG_sys(top,:) ; KG_sys(bottom,:)];
KK_sys  = [KK_sys(top,:) ; KK_sys(bottom,:)];
w2M_sys = [w2M_sys(top,:) ; w2M_sys(bottom,:)];

% Columns (for inverse of submatrix to be possible)
K0_sys  = [K0_sys(:,top) , K0_sys(:,bottom)];
KG_sys  = [KG_sys(:,top) , KG_sys(:,bottom)];
KK_sys  = [KK_sys(:,top) , KK_sys(:,bottom)];
w2M_sys = [w2M_sys(:,top) , w2M_sys(:,bottom)];

%% Constructing & condensing system matrix
SYS = K0_sys + KK_sys + x(1)*KG_sys - w2M_sys;
a = 1:size(phi,1);          b = (size(phi,1)+1):nbr_dof;
%SYS_star = SYS(a,a)-SYS(a,b)*inv(SYS(b,b))*SYS(b,a);
SYS_star = SYS(a,a)-SYS(a,b)*(SYS(b,b)\SYS(b,a));

%% Solving eigen value problem
f0 = SYS_star*phi;
%------------------------------------end----------------------------------
```

beam

```
function [K0e,KGe,MTe,MRe] = beam(ex,ey,ep)
% [K0e,KGe,MTe,MRe] = beam(ex,ey,ep)
%-------------------------------------------------------------------------
% PURPOSE
%   Compute all partial stiffness & mass matrices for a two dimensional
%   4-node beam element.
%   Timoshenko beam theory is used if a shear modulus and a shear
%   correction factor are given. (Otherwise according to Bernoulli-Euler
%   theory). Matrices according to Kosmatka (Journal of Computers &
%   Structures; 1995)
%
% INPUT:     ex = [x1 x2]
%            ey = [y1 y2]                Element node coordinates
%
%            ep = [E A I rho (G ks)]     Element properties,
%                                         E: Young's modulus
%                                         A: Cross section area
%                                         I: Moment of inertia
%                                         rho: material density
%                                         G: Shear modulus
%                                         ks: shear correction factor
%
%
% OUTPUT:    K0e: 1st order stiffness matrix
%            KGe: Stiffness component due to 2nd order effects
%            MTe: Mass matrix with repect to translational movement
%            MTe: Mass matrix with repect to rotational movement
%
%            All matrices are 4x4
%-------------------------------------------------------------------------

%-------------------------------------------------------------------------
% LAST MODIFIED:    S Fässler    2014-02-27
%-------------------------------------------------------------------------

%% Assigning input data
b = [ex(2)-ex(1) ; ey(2)-ey(1)];
L = sqrt(b'*b);      n  = b/L;
E = ep(1);           A = ep(2);
```

```
I = ep(3);          rho = ep(4);

if length(ep) == 6
    Gm = ep(5);
    ks = ep(6);
    phi = 12*E*I / (ks*Gm*A*L^2);
else
    phi = 0;
end

%% Computing stiffness matrices
Kl0e = E*I / ( (1+phi)*L^3 ) *...
       [12     6*L         -12     6*L;
        6*L (4+phi)*L^2     -6*L    (2-phi)*L^2;
        -12 -6*L            12      -6*L;
        6*L (2-phi)*L^2     -6*L    (4+phi)*L^2];

KlGe = 1 / ( 30*L*(1+phi)^2 ) *...
       [36+60*phi+30*phi^2      3*L                         ...
       -(36+60*phi+30*phi^2)    3*L;
        3*L                    (4+5*phi+2.5*phi^2)*L^2      ...
        -3*L                    -(1+5*phi+2.5*phi^2)*L^2;
        -(36+60*phi+30*phi^2)   -3*L                        ...
        36+60*phi+30*phi^2      -3*L;
        3*L                     -(1+5*phi+2.5*phi^2)*L^2    ...
        -3*L                    (4+5*phi+2.5*phi^2)*L^2];

%% Computing mass matrices
MlTe = rho*A*L / ( 210*(1+phi)^2 ) *...
       [70*phi^2+147*phi+78           (35*phi^2+77*phi+44)*L/4      ...
        35*phi^2+63*phi+27          -(35*phi^2+63*phi+26)*L/4;
        (35*phi^2+77*phi+44)*L/4      (7*phi^2+14*phi+8)*L^2/4      ...
        (35*phi^2+63*phi+26)*L/4    -(7*phi^2+14*phi+6)*L^2/4;
        35*phi^2+63*phi+27            (35*phi^2+63*phi+26)*L/4      ...
        70*phi^2+147*phi+78         -(35*phi^2+77*phi+44)*L/4;
        -(35*phi^2+63*phi+26)*L/4     -(7*phi^2+14*phi+6)*L^2/4     ...
        -(35*phi^2+77*phi+44)*L/4   (7*phi^2+14*phi+8)*L^2/4];

MlRe = rho*I / ( 30*L*(1+phi)^2 ) *...
       [36                 -(15*phi-3)*L             ...
       -36            -(15*phi-3)*L;
        -(15*phi-3)*L      (10*phi^2+5*phi+4)*L^2    ...
        (15*phi-3)*L    (5*phi^2-5*phi-1)*L^2;
        -36                (15*phi-3)*L              ...
        36            (15*phi-3)*L;
        -(15*phi-3)*L      (5*phi^2-5*phi-1)*L^2     ...
        (15*phi-3)*L    (10*phi^2+5*phi+4)*L^2];

%% Transforming from local to global coordinates
G = [n(1)    0    0    0;
      0      1    0    0;
      0      0  n(1)   0;
      0      0    0    1];

K0e = G'*Kl0e*G;    KGe = G'*KlGe*G;
MTe = G'*MlTe*G;    MRe = G'*MlRe*G;
%-------------------------------------end----------------------------------
```

Numerical testing – Analytical approach

```
% Numtest_Analytical.m
%--------------------------------------------------------------------------
% PURPOSE
%   This routine performs numerical simulations of axial load determination
%   by means of modal data.
%   The modal properties of a simply supported Bernoulli-Euler beam
%   (analytical solution) is used to test the proposed models.
%
%   The analytical model (rebecchi.m) is checked for the first three
%   bending frequencies and several loading levels.
%
%   Furthermore a sensitivity analysis is performed on material and modal
%   parameters employing the analytical approach.
%--------------------------------------------------------------------------

%--------------------------------------------------------------------------
% LAST MODIFIED:    S Fässler    2014-04-24
%--------------------------------------------------------------------------

%% Cleaning workspace/command window
clear,clc

%% Geometric & Material data
L = 1;      E = 210e9;      rho = 7850;         h = 20e-3;
b = 2*h;    A = b*h;        I = b*h^3/12;
ny = 0.3;   G = E/2/(1+ny); ks = 10*(1+ny)/(12+11*ny);
ep = [E A I rho G ks];
% Choice of shape data (emulate lab testing)
x = colon(50e-3,180e-3,1);  L_samp = x(end) - x(1:2);
% Initial guess for loading
N0 = -1e5;

%% Analytical frequency and shape for a B-E beam (simply supported)
n_step = 0.1;                                      % Load discretization
freqnr = transpose(colon(1,3));                    % Frequencies examined
N = -pi^2*E*I/L^2 * colon(0,n_step,1-n_step);      % Axial forces examined
% Mode shapes (1 row per frequency)
v = sin(freqnr*pi*x/L);
% Frequency table (Rows: Frequencies    Columns: Force)
omega = ( (freqnr*pi/L).^2*ones(1,size(N,2)) ) ...
    .* sqrt( E*I/rho/A + (L./freqnr/pi).^2 * N/rho/A );

%% Solving analytical approach (Rebecchi)
N_A = zeros( size(omega) );
for i = colon( 1 , size(omega,1) ) % Loop over frequencies
    for j = colon( 1 , size(omega,2) ) % Loop over loads
        N_A(i,j) = ...
            fzero(@(N) ...
            rebecchi(N, omega(i,j), v(i,:), rho*A, L_samp(2), E, I),...
            N0);
    end
end

%% Sensitivity testing (Manual positioning of err(k))
err = colon(9,0.1,11)/10;
std = ones(size(err));
N_A = zeros( [size(omega) length(err) 6]);
for err_type = 1:6
```

```
    switch err_type
        case 1 % Checking Frequency
            err_c = {err std std std std std};
        case 2 % Checking Young's modulus
            err_c = {std err std std std std};
        case 3 % Checking Density
            err_c = {std std err std std std};
        case 4 % Checking shape (v3)
            err_c = {std std std err std std};
        case 5 % Checking shape (v2 & v4)
            err_c = {std std std std err std};
        case 6 % Checking shape (v1 & v5)
            err_c = {std std std std std err};
    end
    for k = colon( 1 , length(err ) )
        for i = colon( 1 , size(omega,1) ) % Loop over frequencies
            for j = colon( 1 , size(omega,2) ) % Loop over loads
                N_A(i,j,k,err_type) = ...
                    fzero(@(N) ...
                    rebecchi(N, omega(i,j)*err_c{1}(k), ...
                    v(i,:).*[err_c{6}(k), err_c{5}(k), err_c{4}(k), ...
                    err_c{5}(k), err_c{6}(k), 1], ...
                    rho*err_c{3}(k)*A, L_samp(2), E*err_c{2}(k), I), N0);
            end
        end
    end
end
%-------------------------------------end----------------------------------
```

Numerical testing – Discrete approach

```
% NumTest_Discrete.m
%--------------------------------------------------------------------------
% PURPOSE
%   This routine performs numerical simulations of axial load determination
%   by means of modal data.
%   The modal properties of a simply supported Bernoulli-Euler beam
%   (analytical solution) is used to test the proposed models.
%
%   The discrete model (reveig.m) is checked for the first three
%   bending frequencies and several loading levels.
%
%   Varying amount of elements and measurement points can be employed and
%   both Bernoulli-Euler and a Timoshenko beam theory are investigated.
%--------------------------------------------------------------------------

%--------------------------------------------------------------------------
% LAST MODIFIED:    S Fässler    2014-05-09
%--------------------------------------------------------------------------

%% Cleaning workspace/command window
clear,clc

%% Geometric & Material data
L = 1;      E = 210e9;      rho = 7850;         h = 20e-3;
b = 2*h;    A = b*h;        I = b*h^3/12;
ny = 0.3;   G = E/2/(1+ny); ks = 10*(1+ny)/(12+11*ny);
ep = [E A I rho G ks];

%% Frequency and shape for a B-E beam (simply supported)
n_step = 0.1;                                       % Load discretization
```

```
freqnr = transpose(colon(1,3));                 % Frequencies examined
N = -pi^2*E*I/L^2 * colon(0,n_step,1-n_step);   % Axial forces examined

%% Analytical
x = colon(50e-3,180e-3,1);
v_6 = sin(freqnr*pi*x/L);       % Mode shapes (1 row per frequency)
x = colon(1/6,1/6,5/6);
v_5 = sin(freqnr*pi*x/L);
% Frequency table (Rows: Frequencies    Columns: Force)
omega = ( (freqnr*pi/L).^2*ones(1,size(N,2)) ) ...
    .* sqrt( E*I/rho/A + (L./freqnr/pi).^2 * N/rho/A );

clearvars -EXCEPT v_* ep N omega

%% Create discretized system for BE beam
el_xtra = 5;                    % Elements between each measurement point
nbr_elem = [4 4 5]*el_xtra;
L = [2/3 0.18*4 0.18*5];
ex = [zeros(3,1) L'./nbr_elem'];        ey = [0 0];
for i = 1:3
    edof{i} = [colon(1,nbr_elem(i))' ...
        colon(1,2,nbr_elem(i)*2)' * ones(1,4) + ...
        ones(nbr_elem(i),1)*colon(0,3)];
    nbr_dof{i} = max(max(edof{i}(:,2:end)));
    el_dofs{i} = [1 ; edof{i}( colon(el_xtra,el_xtra,edof{i}(end,1) ), 4)];
    K0{i} = zeros(nbr_dof{i});    KG{i} = zeros(nbr_dof{i});
    M{i} = zeros(nbr_dof{i});
    [K0e,KGe,MTe,~] = beam(ex(i,:),ey,ep(1:4));
    for j = 1:nbr_elem(i)
        indx = edof{i}(j,2:end);
        K0{i}(indx,indx) = K0{i}(indx,indx) + K0e;
        KG{i}(indx,indx) = KG{i}(indx,indx) + KGe;
        M{i}(indx,indx) = M{i}(indx,indx) + MTe;
    end
end

%% solve reveig for BE-beam
options = optimset(...
    'MaxIter',2e3,'MaxFunEvals',2e3,'TolFun',1e-10,'TolX',1e-10);
for i=1:size(omega,2)       % Loop over loads
    N0 = N(i)*1.1;
    for j=1:size(omega,1)   % Loop over frequencies
        k=1;                % 5 point symmetric shape
        N_BE{i,j,k} = lsqnonlin(@(x) reveig5(x,K0{k},KG{k},M{k},...
            omega(j,i),[v_5(j,:)' el_dofs{k}]),...
            [ N0 zeros(1,4)],[],[],options);
        k=2;                % 5 point non-symmetric shape
        N_BE{i,j,k} = lsqnonlin(@(x) reveig5(x,K0{k},KG{k},M{k},...
            omega(j,i),[v_6(j,1:5)' el_dofs{k}]),...
            [ N0 zeros(1,4)],[],[],options);
        k=3;                % 6 point symmetric shape
        N_BE{i,j,k} = lsqnonlin(@(x) reveig5(x,K0{k},KG{k},M{k},...
            omega(j,i),[v_6(j,:)' el_dofs{k}]),...
            [ N0 zeros(1,4)],[],[],options);
    end
end

%% Create discretized system for Timoshenko beam
for i = 1:3
    K0{i} = zeros(nbr_dof{i});    KG{i} = zeros(nbr_dof{i});
    M{i} = zeros(nbr_dof{i});
    [K0e,KGe,MTe,MRe] = beam(ex(i,:),ey,ep);
    for j = 1:nbr_elem(i)
        indx = edof{i}(j,2:end);
        K0{i}(indx,indx) = K0{i}(indx,indx) + K0e;
        KG{i}(indx,indx) = KG{i}(indx,indx) + KGe;
        M{i}(indx,indx) = M{i}(indx,indx) + MTe + MRe;
    end
end

%% solve reveig for Timoshenko beam
for i=1:size(omega,2)       % Loop over loads
    N0 = N(i)*1.1;
    for j=1:size(omega,1)   % Loop over frequencies
        k=1;                % 5 point symmetric shape
        N_T{i,j,k} = lsqnonlin(@(x) reveig5(x,K0{k},KG{k},M{k},...
            omega(j,i),[v_5(j,:)' el_dofs{k}]),...
            [ N0 zeros(1,4)],[],[],options);
        k=2;                % 5 point non-symmetric shape
        N_T{i,j,k} = lsqnonlin(@(x) reveig5(x,K0{k},KG{k},M{k},...
            omega(j,i),[v_6(j,1:5)' el_dofs{k}]),...
            [ N0 zeros(1,4)],[],[],options);
        k=3;                % 6 point symmetric shape
        N_T{i,j,k} = lsqnonlin(@(x) reveig5(x,K0{k},KG{k},M{k},...
            omega(j,i),[v_6(j,:)' el_dofs{k}]),...
            [ N0 zeros(1,4)],[],[],options);
    end
end
%-------------------------------------end-----------------------------------
```

Laboratory testing – Analytical approach

```
% LabTest Analytical
%-------------------------------------------------------------------------
% PURPOSE
%   This routine calculates the axial load given modal data from laboratory
%   testing using an analytical approach. The subroutine rebecchi.m is
%   required.
%
% INPUT:    PureFRFBeamData.mat     Matlab data file containing lab results
%
% OUTPUT:   Result                  Cell structure with calculated loads
%-------------------------------------------------------------------------

%-------------------------------------------------------------------------
% LAST MODIFIED:    S Fässler    2014-04-30
%-------------------------------------------------------------------------

%% Function controls & manual inputs
clc, clear, load('PureFRFBeamData.mat')
L = 0.9 - 0.18;         % Length of beamsection analysed

%% Determining input sizes
nbr_beams = size(Beam,2);                       % Nr of beams
nbr_imp = size(Beam{1,1}.Freq,3);               % Nr of impact locations
nbr_accp = length(Beam{1,1}.Shape{1,1,1})-4;    % Nr of sensor positions
(from bottom up)

nbr_loads = zeros(1,nbr_beams);         nbr_freq = nbr_loads;
Result = cell(size(Beam));
for i = 1 : nbr_beams    % Determining calculations per beam
```

```
    nbr_loads(i) = size(Beam{1,i}.Freq,1);
    nbr_freq(i) = size(Beam{1,i}.Freq,2);
    Result{i} = zeros(nbr_loads(i), nbr_freq(i), nbr_imp, nbr_accp);
end
% Index: Result{Beamnr}(Loadlevel , Freqnr, Impactloc, Accposition)

%% Calculation loop
for i = 1 : nbr_beams                       % Loop beam types
    for j = 1 : nbr_loads(i)                % Loop loading levels
        GuessForce = -1.5*Beam{i}.Force(j);
        for k = 1 : nbr_freq(i)             % Loop frequencies
            for q = 1 : nbr_imp             % Loop impact locations
                for r = 1 : nbr_accp        % Loop sensor groups
                    if Beam{i}.Freq(j,k,q) == 0
                        break
                    end
                    fprintf(...
                        'Beam:%3d\t\tLoad 
level:%3d\t\tFreqeuncy:%3d\t\tImpact Loaction:%3d\t\tSensor 
Group:%3d\t\n',...
                        i,j,k,q,r)
                    Result{i}(j, k, q, r) = ...
                        fzero(@(N) rebecchi(...
                        N,...
                        Beam{i}.Freq(j,k,q),...
                        Beam{i}.Shape{j,k,q}( (1:5)-1+r ),...
                        epBeam.m(i), L, epBeam.E, epBeam.I(1)),...
                        GuessForce);
                end
            end
        end
    end
end
disp('FIN'), save('Lab_Ana')
%-------------------------------------end-----------------------------------
```

Laboratory testing – Discrete approach

```
% LabTest Analytical
%--------------------------------------------------------------------------
% PURPOSE
%   This routine calculates the axial load given modal data from laboratory
%   testing using a discrete approach. The subroutine reveig.m is required.
%
% INPUT:    PureFRFBeamData.mat     Matlab data file containing lab results
%
% OUTPUT:   ResultDs                Cell structure with calculated loads
%--------------------------------------------------------------------------

%--------------------------------------------------------------------------
% LAST MODIFIED:    S Fässler    2014-04-30
%--------------------------------------------------------------------------

%% Function controls & manual inputs
clc, clear, load('PureFRFBeamData.mat')
L = 0.9;                    % Length of beamsection analysed

%% Determining input sizes
nbr_beams = size(Beam,2);                       % Nr of beams
nbr_imp = size(Beam{1,1}.Freq,3);               % Nr of impact locations
```

```
nbr_loads = zeros(1,nbr_beams);         nbr_freq = nbr_loads;
ResultD = cell(size(Beam));
for i = 1 : nbr_beams   % Determining calculations per beam
    nbr_loads(i) = size(Beam{1,i}.Freq,1);
    nbr_freq(i) = size(Beam{1,i}.Freq,2);
    ResultD{i} = zeros(nbr_loads(i), nbr_freq(i), nbr_imp);
end
% Index: ResultD{Beamnr}(Loadlevel , Freqnr, Impactloc)

%% Preparing calculation
nbr_el_bt = 2;          %Nr of elements between beams
nbr_el = 5*nbr_el_bt;
ex = [0 L/nbr_el];      ey = [0 0];
edof = [colon(1,nbr_el)' ...
    colon(1,2,nbr_el*2)'*ones(1,4) + ones(nbr_el,1)*colon(0,3)];
nbr_dof = max(max(edof(:,2:end)));
el_dofs = [1 ; edof( colon(nbr_el_bt,nbr_el_bt,edof(end,1) ) , 4)];

options = ...
    optimset('MaxIter',5e3,'MaxFunEvals',5e3,'TolFun',1e-12,'TolX',1e-12);
%% Calculation loop
for i = 1 : nbr_beams                       % Loop beam types
    ep = ...
        [epBeam.E epBeam.A(i) epBeam.I(i) epBeam.rho ...
        epBeam.G epBeam.kappa];
    [K0e,KGe,MTe,MRe] = beam(ex,ey,ep); % Full ep for Timoshenko 1:4 for BE
    K0 = zeros(nbr_dof);    KG = zeros(nbr_dof);
    M = zeros(nbr_dof);
    for r = 1:nbr_el
        indx = edof(r,2:end);
        K0(indx,indx) = K0(indx,indx) + K0e;
        KG(indx,indx) = KG(indx,indx) + KGe;
        M(indx,indx) = M(indx,indx) + MTe + MRe;    % Remove MRe for BE
    end
    for j = 1 : nbr_loads(i)                % Loop loading levels
        GuessForce = -1.1*Beam{i}.Force(j);
        for k = 1 : nbr_freq(i)             % Loop frequencies
            for q = 1 : nbr_imp             % Loop impact locations
                %for r = 1 : nbr_accp        % Loop sensor groups
                if Beam{i}.Freq(j,k,q) == 0
                    break
                end
                fprintf(...
                    'Beam:%3d\t\tLoad level:%3d\t\tFrequency:%3d\t\tImpact
Loaction:%3d\t\n',...
                    i,j,k,q)
                ResultD{i, j, k, q} = ...
                    lsqnonlin(@(x) reveig5(...
                    x,K0,KG,M,...
                    Beam{i}.Freq(j,k,q),...
                    [Beam{i}.Shape{j,k,q} , el_dofs]),...
                    [GuessForce zeros(1,4)],[],[],options);
                %end
                ResultDs{i}(j,k,q) = ResultD{i, j, k, q}(1);
            end
        end
    end
end
disp('FIN'), save('Lab_Disc')
%-------------------------------------end----------------------------------
```

B – Calculation of beam properties

$f_y := 355\,MPa$ $\gamma_{M1} := 1{,}0$ $E := 210\,GPa$

$L := 1\,m$ $\beta := 0{,}699$ $\rho := 7850\,\dfrac{kg}{m^3}$ $d := \begin{pmatrix}10\\15\\20\\45\end{pmatrix} mm$ $b := d \cdot 2 = \begin{pmatrix}20\\30\\40\\90\end{pmatrix} mm$

$\alpha := 0{,}49$ $L_{cr} := L \cdot \beta = 0{,}699\,m$

```
for n := 1 ; n ≤ length(d) ; n := n + 1
    $A_n := b_n \cdot d_n$
```

```
for n := 1 ; n ≤ length(d) ; n := n + 1
    $I_n := \dfrac{b_n \cdot (d_n)^3}{12}$
```

```
for n := 1 ; n ≤ length(d) ; n := n + 1
    $i_n := \sqrt{\dfrac{I_n}{A_n}}$
```

```
for n := 1 ; n ≤ length(d) ; n := n + 1
    $\lambda_{rel_n} := \dfrac{L_{cr}}{i_n \cdot \pi} \cdot \sqrt{\dfrac{f_y}{E}}$
```

```
for n := 1 ; n ≤ length(d) ; n := n + 1
    for m := 1 ; m ≤ 3 ; m := m + 1
        $\omega_{0_{n\,m}} := \dfrac{1}{2 \cdot \pi} \cdot \left[(4 \cdot m + 1) \cdot \dfrac{\pi}{4}\right]^2 \cdot \dfrac{1}{L^2} \cdot \sqrt{\dfrac{E \cdot I_n}{\rho \cdot A_n}}$
```

```
for n := 1 ; n ≤ length(d) ; n := n + 1
    $\lambda_n := \dfrac{L_{cr}}{i_n}$
```

```
for n := 1 ; n ≤ length(d) ; n := n + 1
    $\phi_n := \dfrac{1 + \alpha \cdot \left(\lambda_{rel_n} - 0{,}2\right) + {\lambda_{rel_n}}^2}{2}$
```

```
for n := 1 ; n ≤ length(d) ; n := n + 1
    $\chi_n := \dfrac{1}{\phi_n + \sqrt{{\phi_n}^2 - {\lambda_{rel_n}}^2}}$
```

```
for n := 1 ; n ≤ length(d) ; n := n + 1
    $\chi_n :=$ if $\dfrac{1}{\phi_n + \sqrt{{\phi_n}^2 - {\lambda_{rel_n}}^2}} < 1$
        $\dfrac{1}{\phi_n + \sqrt{{\phi_n}^2 - {\lambda_{rel_n}}^2}}$
    else
        1,0
```

```
for n := 1 ; n ≤ length(d) ; n := n + 1
    $N_{Rd_n} := \dfrac{\chi_n \cdot f_y \cdot A_n}{\gamma_{M1}}$
```

```
for n := 1 ; n ≤ length(d) ; n := n + 1
    $N_{cr_n} := \dfrac{E \cdot I_n \cdot \pi^2}{{L_{cr}}^2}$
```

$A = \begin{pmatrix}200\\450\\800\\4050\end{pmatrix} mm^2$ $I = \begin{pmatrix}1666{,}6667\\8437{,}5\\26666{,}6667\\6{,}8344 \cdot 10^5\end{pmatrix} mm^4$ $i = \begin{pmatrix}2{,}8868\\4{,}3301\\5{,}7735\\12{,}9904\end{pmatrix} mm$

$\phi = \begin{pmatrix}6{,}2487\\3{,}2003\\2{,}0945\\0{,}8715\end{pmatrix}$ $\chi = \begin{pmatrix}0{,}086\\0{,}1784\\0{,}2887\\0{,}7221\end{pmatrix}$ $\lambda = \begin{pmatrix}242{,}14\\161{,}43\\121{,}07\\53{,}81\end{pmatrix}$ $\lambda_{rel} = \begin{pmatrix}3{,}17\\2{,}11\\1{,}58\\0{,}7\end{pmatrix}$

$N_{Rd} = \begin{pmatrix}6{,}1\\28{,}5\\82{,}0\\1038{,}2\end{pmatrix} kN$ $N_{cr} = \begin{pmatrix}7{,}1\\35{,}8\\113{,}1\\2899{,}1\end{pmatrix} kN$ $\omega_0 = \begin{pmatrix}36{,}6 & 118{,}7 & 247{,}7\\55 & 178{,}1 & 371{,}6\\73{,}3 & 237{,}5 & 495{,}5\\164{,}9 & 534{,}3 & 1114{,}8\end{pmatrix} Hz$

C – Test results

Driving point FRFs

B1020

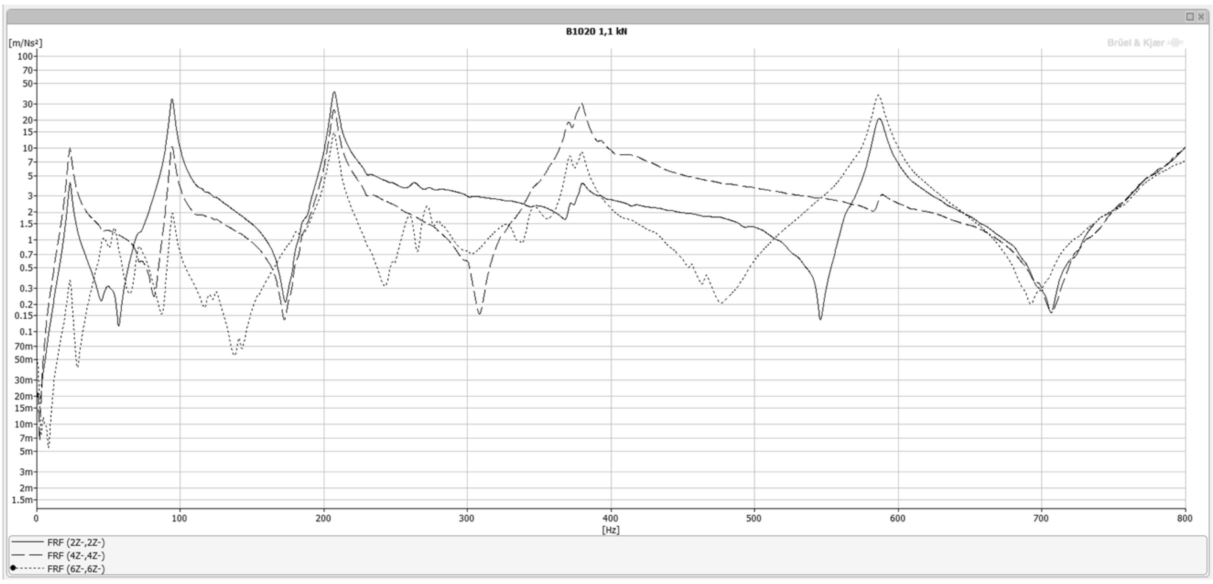

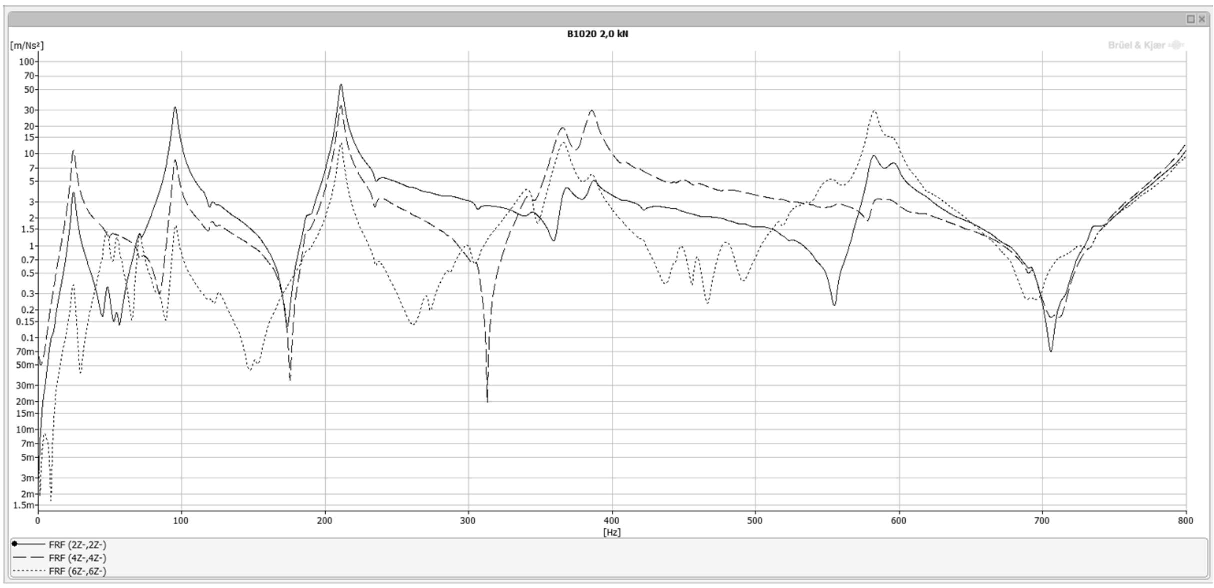

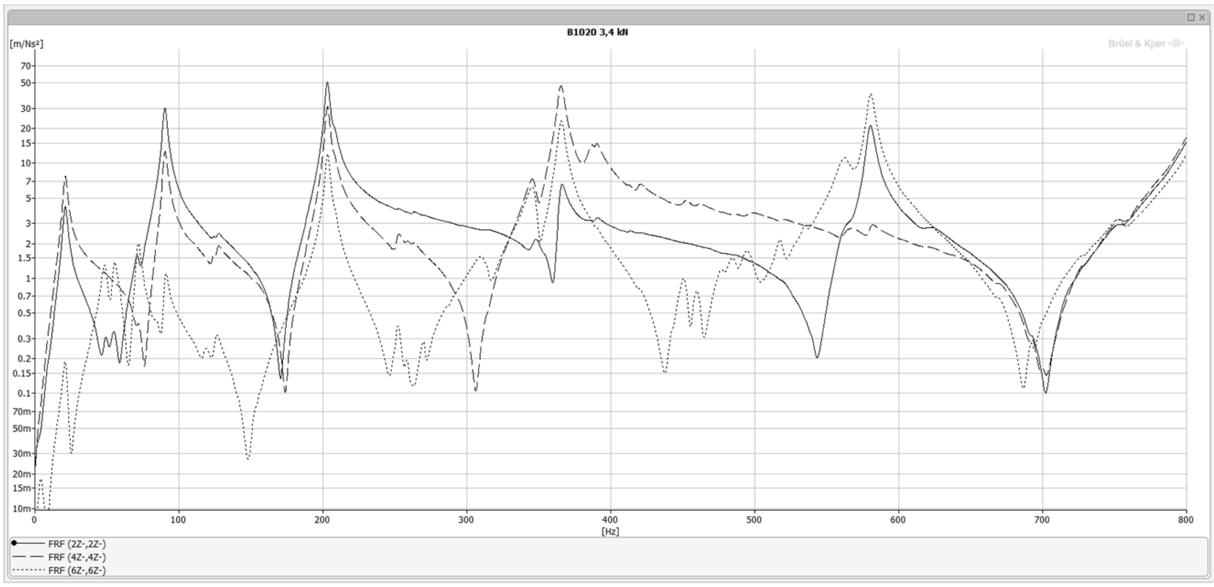
B1020 3,4 kN
Brüel & Kjær
[m/Ns²]
70
50
30
20
15
10
7
5
3
2
1.5
1
0.7
0.5
0.3
0.2
0.15
0.1
70m
50m
30m
20m
15m
10m
0
100
200
300
400
500
600
700
800
[Hz]
FRF (2Z-,2Z-)
FRF (4Z-,4Z-)
FRF (6Z-,6Z-)

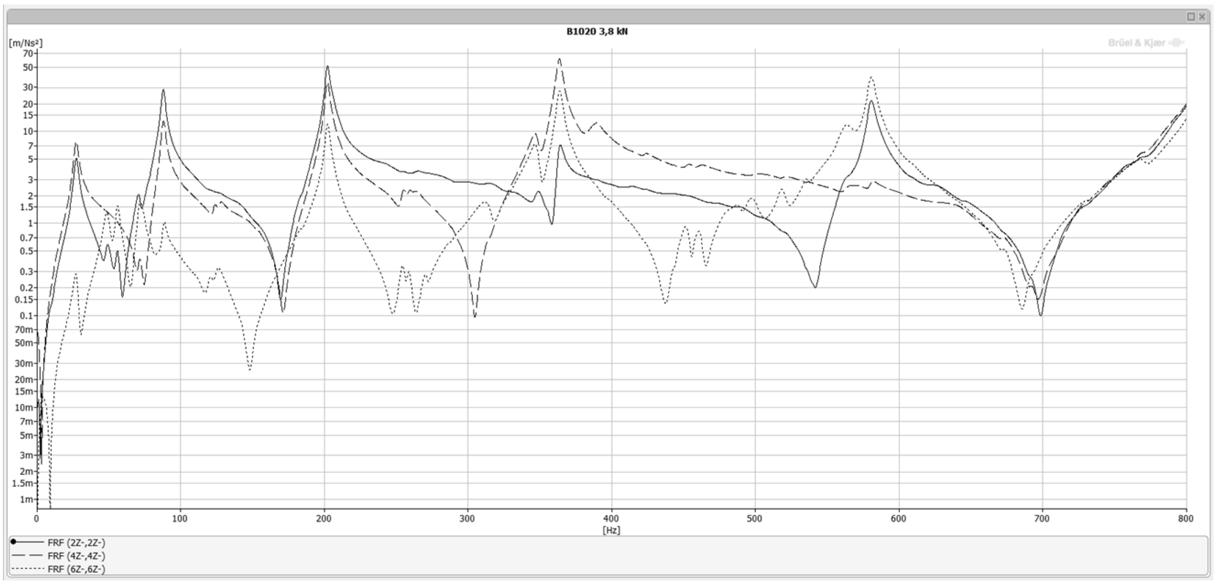
B1020 3,8 kN
Brüel & Kjær
[m/Ns²]
70
50
30
20
15
10
7
5
3
2
1.5
1
0.7
0.5
0.3
0.2
0.15
0.1
70m
50m
30m
20m
15m
10m
7m
5m
3m
2m
1.5m
1m
0
100
200
300
400
500
600
700
800
[Hz]
FRF (2Z-,2Z-)
FRF (4Z-,4Z-)
FRF (6Z-,6Z-)

B1530

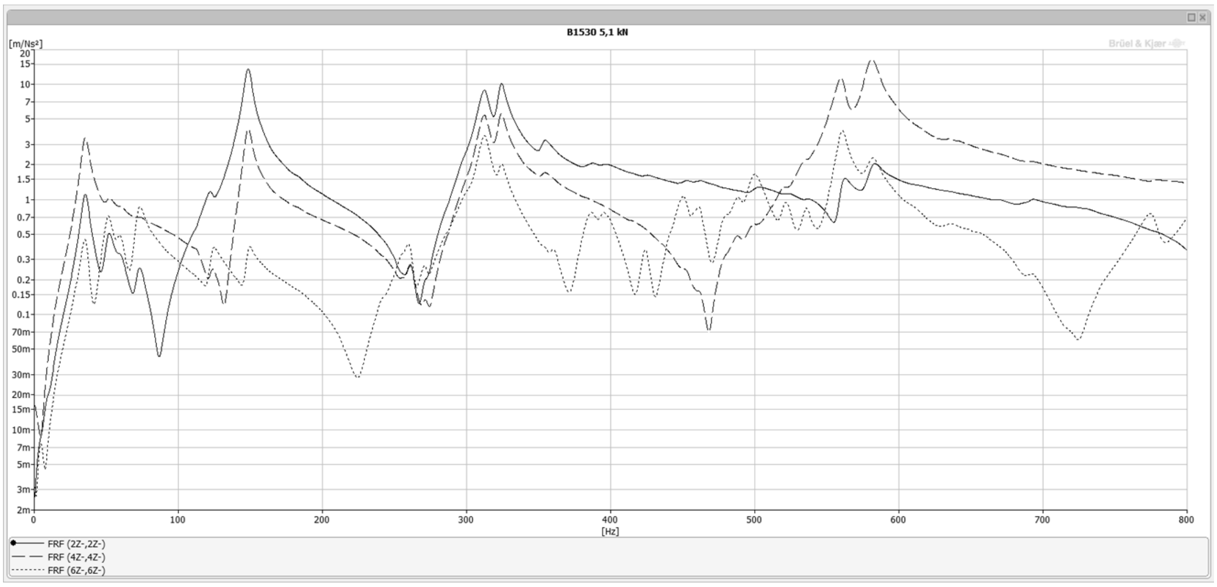
B1530 5,1 kN
Brüel & Kjær
[m/Ns²]
20
15
10
7
5
3
2
1.5
1
0.7
0.5
0.3
0.2
0.15
0.1
70m
50m
30m
20m
15m
10m
7m
5m
3m
2m
0
100
200
300
400
500
600
700
800
[Hz]
FRF (2Z-,2Z-)
FRF (4Z-,4Z-)
FRF (6Z-,6Z-)

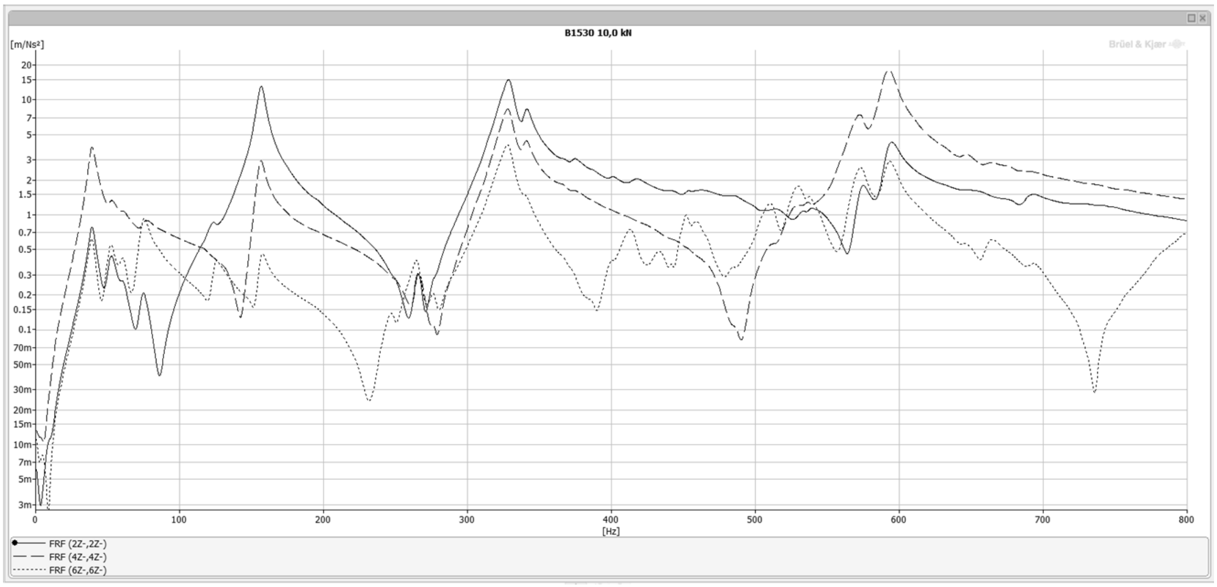
B1530 10,0 kN
Brüel & Kjær
[m/Ns²]
20
15
10
7
5
3
2
1.5
1
0.7
0.5
0.3
0.2
0.15
0.1
70m
50m
30m
20m
15m
10m
7m
5m
3m
0
100
200
300
400
500
600
700
800
[Hz]
FRF (2Z-,2Z-)
FRF (4Z-,4Z-)
FRF (6Z-,6Z-)

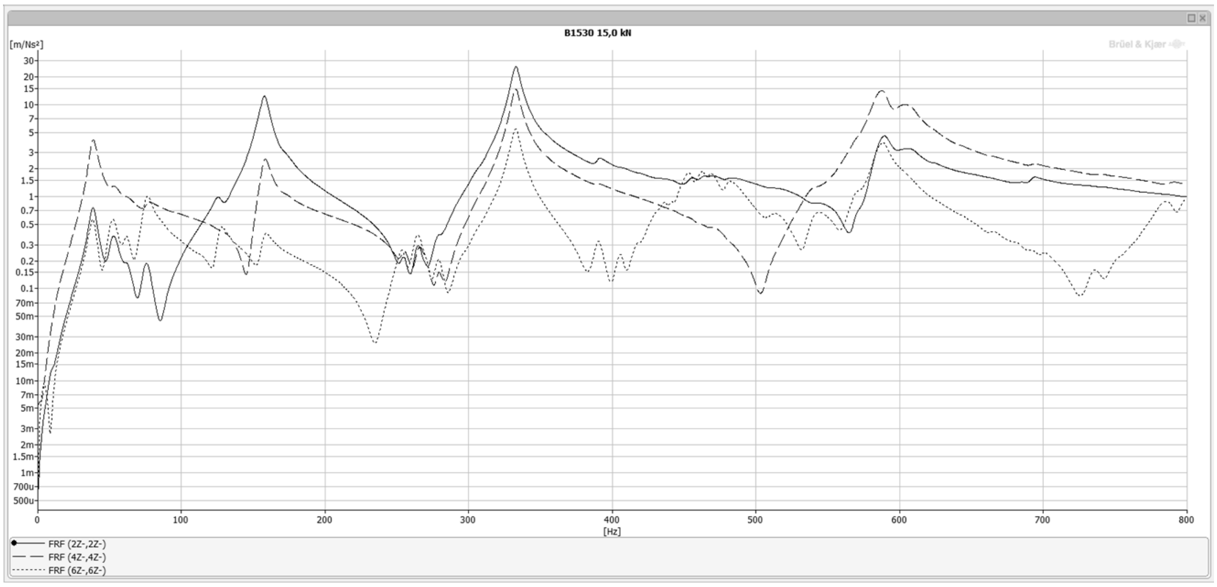
B1530 15,0 kN
Brüel & Kjær
[m/Ns²]
30
20
15
10
7
5
3
2
1.5
1
0.7
0.5
0.3
0.2
0.15
0.1
70m
50m
30m
20m
15m
10m
7m
5m
3m
2m
1.5m
1m
700u
500u
0
100
200
300
400
500
600
700
800
[Hz]
FRF (2Z-,2Z-)
FRF (4Z-,4Z-)
FRF (6Z-,6Z-)

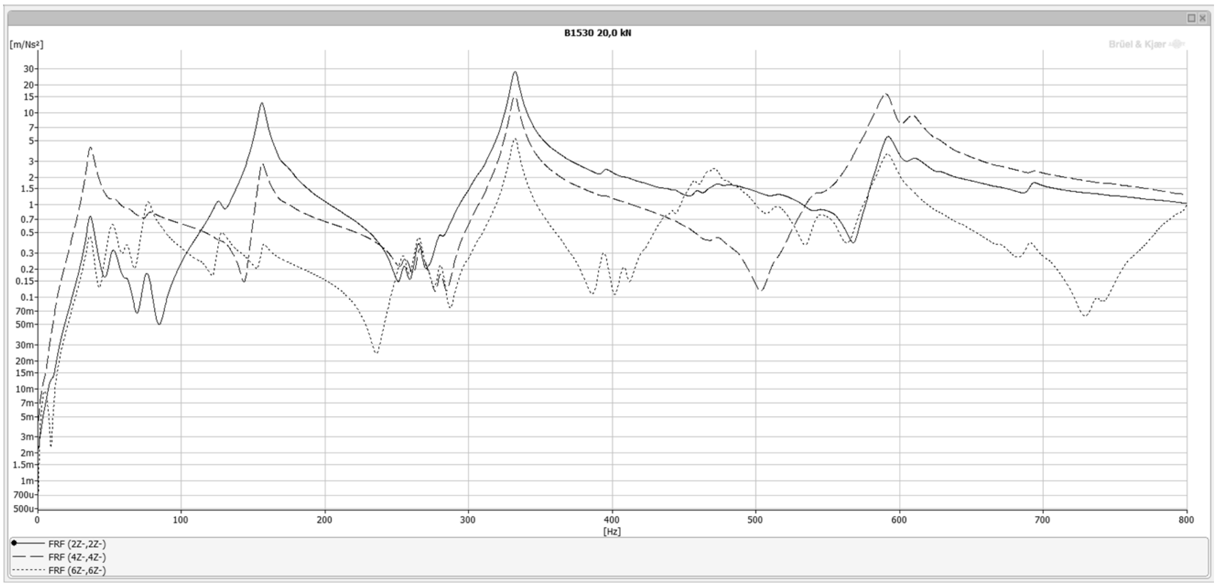
B1530 20,0 kN
Brüel & Kjær
[m/Ns²]
30
20
15
10
7
5
3
2
1.5
1
0.7
0.5
0.3
0.2
0.15
0.1
70m
50m
30m
20m
15m
10m
7m
5m
3m
2m
1.5m
1m
700u
500u
0
100
200
300
400
500
600
700
800
[Hz]
FRF (2Z-,2Z-)
FRF (4Z-,4Z-)
FRF (6Z-,6Z-)

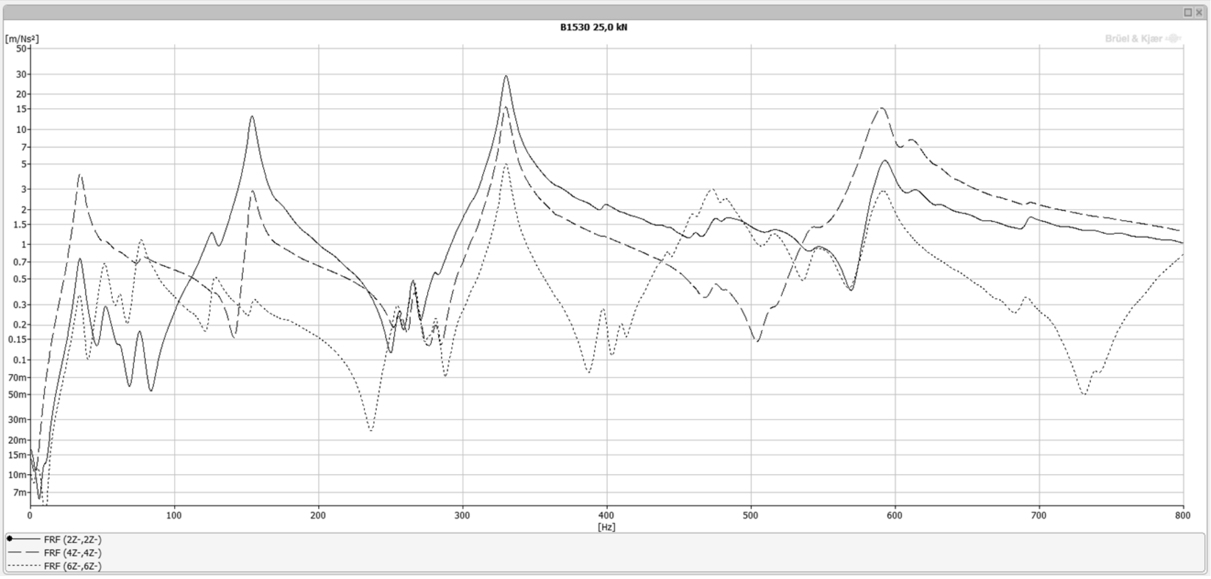
B1530 25,0 kN
Brüel & Kjær
[m/Ns²]
50
30
20
15
10
7
5
3
2
1.5
1
0.7
0.5
0.3
0.2
0.15
0.1
70m
50m
30m
20m
15m
10m
7m
0
100
200
300
400
500
600
700
800
[Hz]
FRF (2Z-,2Z-)
FRF (4Z-,4Z-)
FRF (6Z-,6Z-)

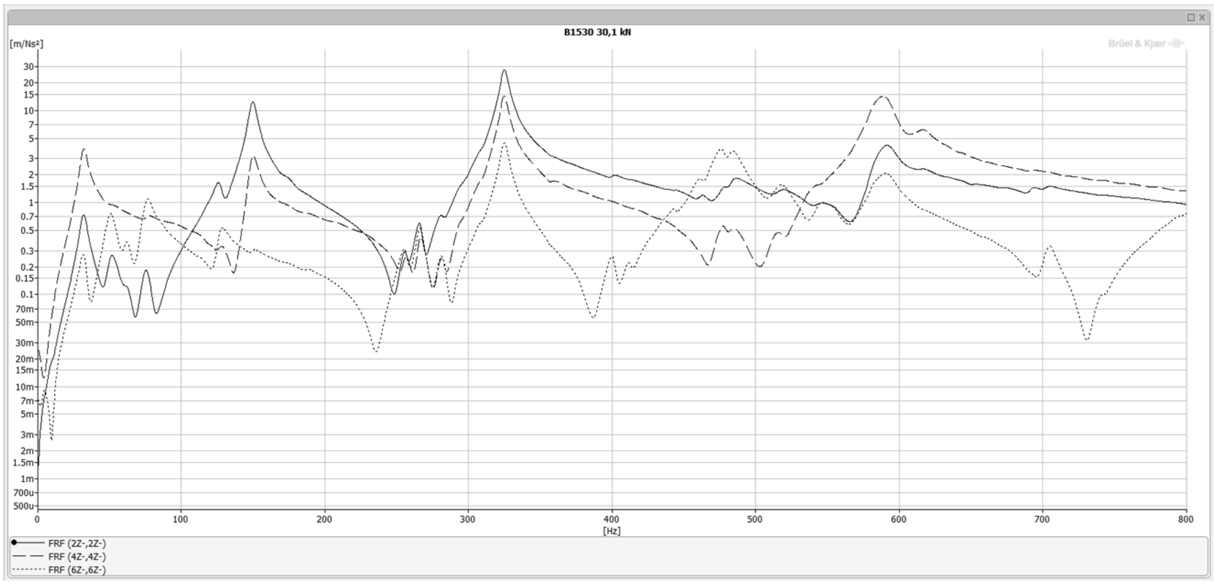
B1530 30,1 kN
Brüel & Kjær
[m/Ns²]
30
20
15
10
7
5
3
2
1.5
1
0.7
0.5
0.3
0.2
0.15
0.1
70m
50m
30m
20m
15m
10m
7m
5m
3m
2m
1.5m
1m
700u
500u
0
100
200
300
400
500
600
700
800
[Hz]
FRF (2Z-,2Z-)
FRF (4Z-,4Z-)
FRF (6Z-,6Z-)

B2040

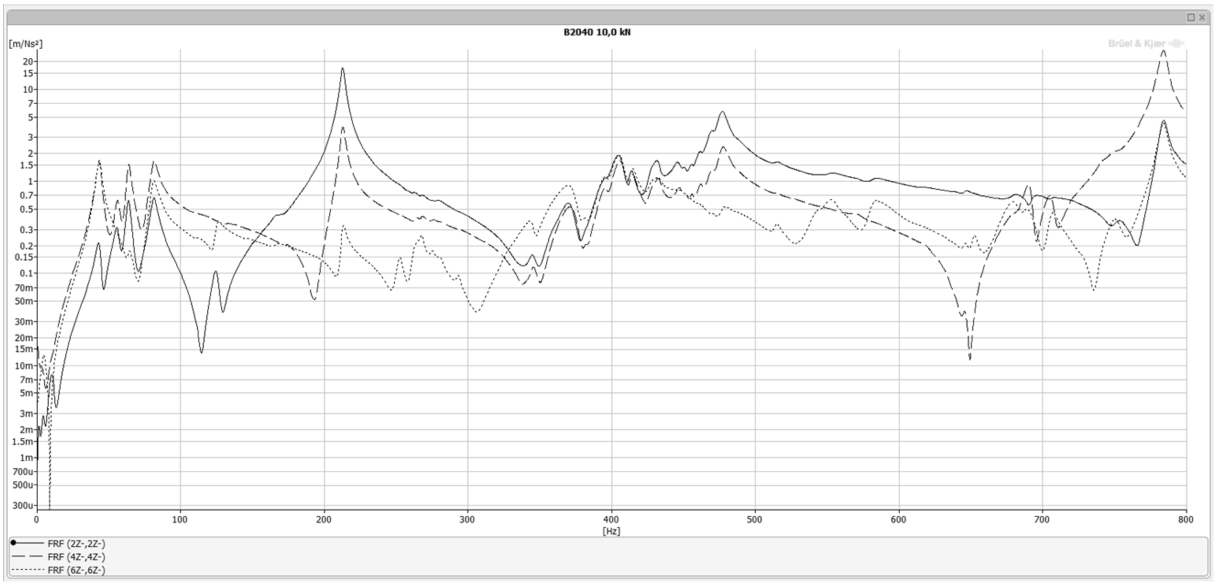
B2040 10,0 kN
Brüel & Kjær
[m/Ns²]
20
15
10
7
5
3
2
1.5
1
0.7
0.5
0.3
0.2
0.15
0.1
70m
50m
30m
20m
15m
10m
7m
5m
3m
2m
1.5m
1m
700u
500u
300u
0
100
200
300
400
500
600
700
800
[Hz]
FRF (2Z-,2Z-)
FRF (4Z-,4Z-)
FRF (6Z-,6Z-)

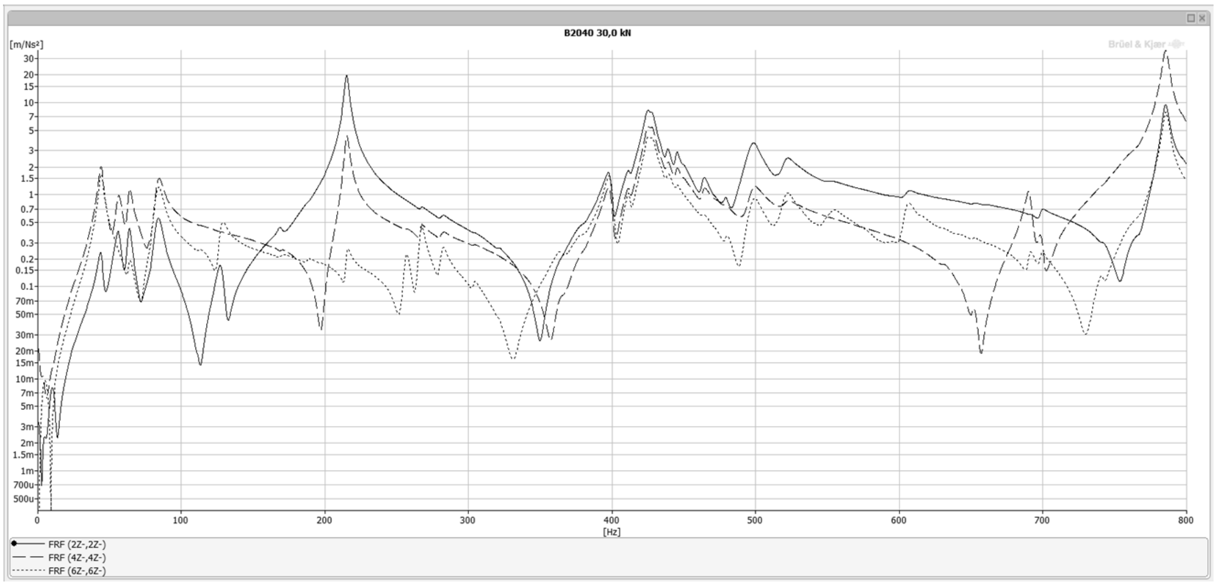
B2040 30,0 kN
Brüel & Kjær
[m/Ns²]
30
20
15
10
7
5
3
2
1.5
1
0.7
0.5
0.3
0.2
0.15
0.1
70m
50m
30m
20m
15m
10m
7m
5m
3m
2m
1.5m
1m
700u
500u
0
100
200
300
400
500
600
700
800
[Hz]
FRF (2Z-,2Z-)
FRF (4Z-,4Z-)
FRF (6Z-,6Z-)

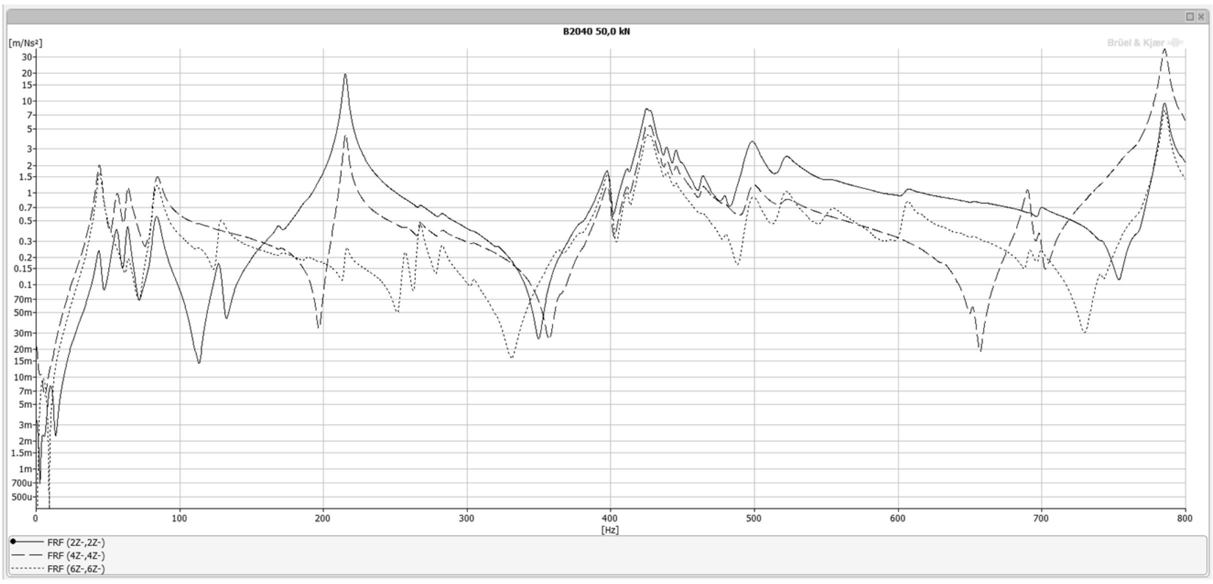
B2040 50,0 kN
Brüel & Kjær
[m/Ns²]
30
20
15
10
7
5
3
2
1.5
1
0.7
0.5
0.3
0.2
0.15
0.1
70m
50m
30m
20m
15m
10m
7m
5m
3m
2m
1.5m
1m
700u
500u
0
100
200
300
400
500
600
700
800
[Hz]
FRF (2Z-,2Z-)
FRF (4Z-,4Z-)
FRF (6Z-,6Z-)

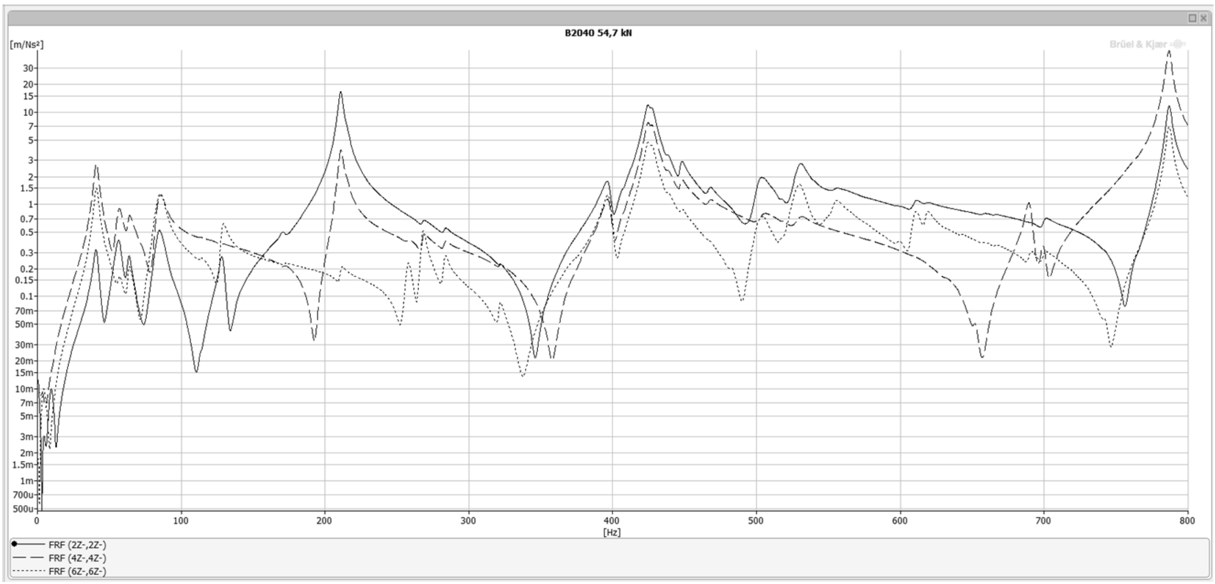
B2040 54,7 kN
Brüel & Kjær
[m/Ns²]
30
20
15
10
7
5
3
2
1.5
1
0.7
0.5
0.3
0.2
0.15
0.1
70m
50m
30m
20m
15m
10m
7m
5m
3m
2m
1.5m
1m
700u
500u
0
100
200
300
400
500
600
700
800
[Hz]
FRF (2Z-,2Z-)
FRF (4Z-,4Z-)
FRF (6Z-,6Z-)

B4590

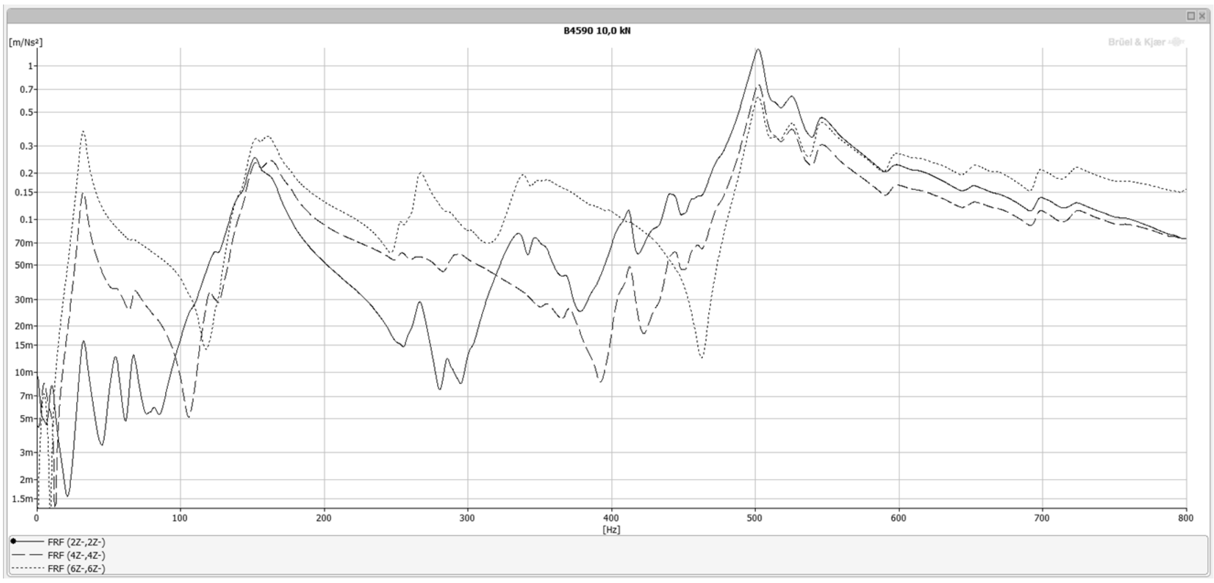
B4590 10,0 kN
Brüel & Kjær
[m/Ns²]
1
0.7
0.5
0.3
0.2
0.15
0.1
70m
50m
30m
20m
15m
10m
7m
5m
3m
2m
1.5m
0
100
200
300
400
500
600
700
800
[Hz]
FRF (2Z-,2Z-)
FRF (4Z-,4Z-)
FRF (6Z-,6Z-)

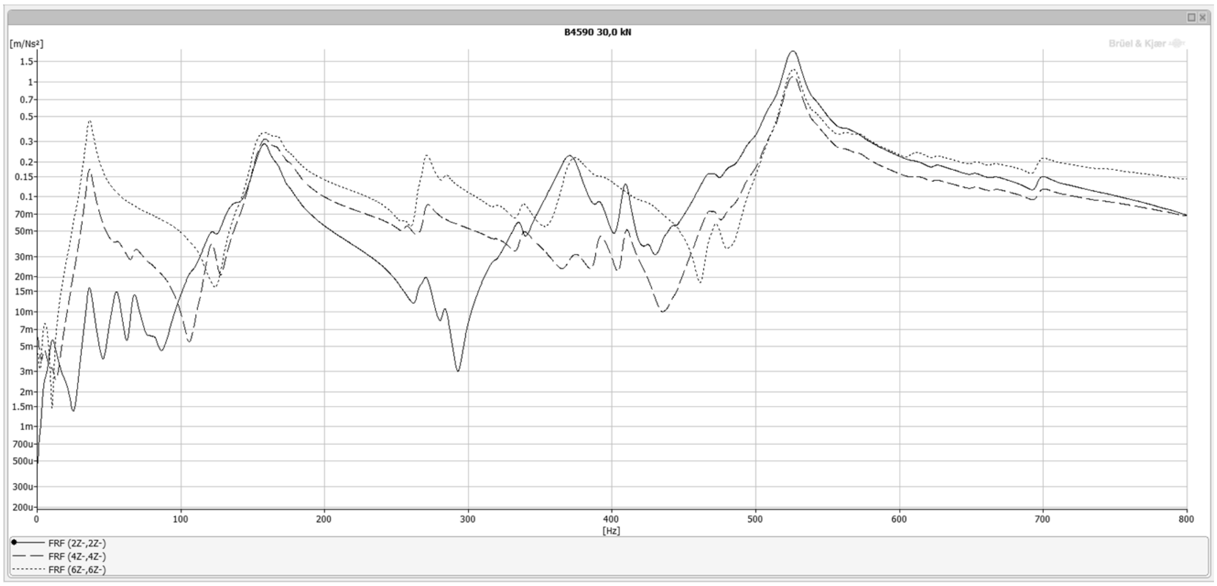
B4590 30,0 kN
Brüel & Kjær
[m/Ns²]
1.5
1
0.7
0.5
0.3
0.2
0.15
0.1
70m
50m
30m
20m
15m
10m
7m
5m
3m
2m
1.5m
1m
700u
500u
300u
200u
0
100
200
300
400
500
600
700
800
[Hz]
FRF (2Z-,2Z-)
FRF (4Z-,4Z-)
FRF (6Z-,6Z-)

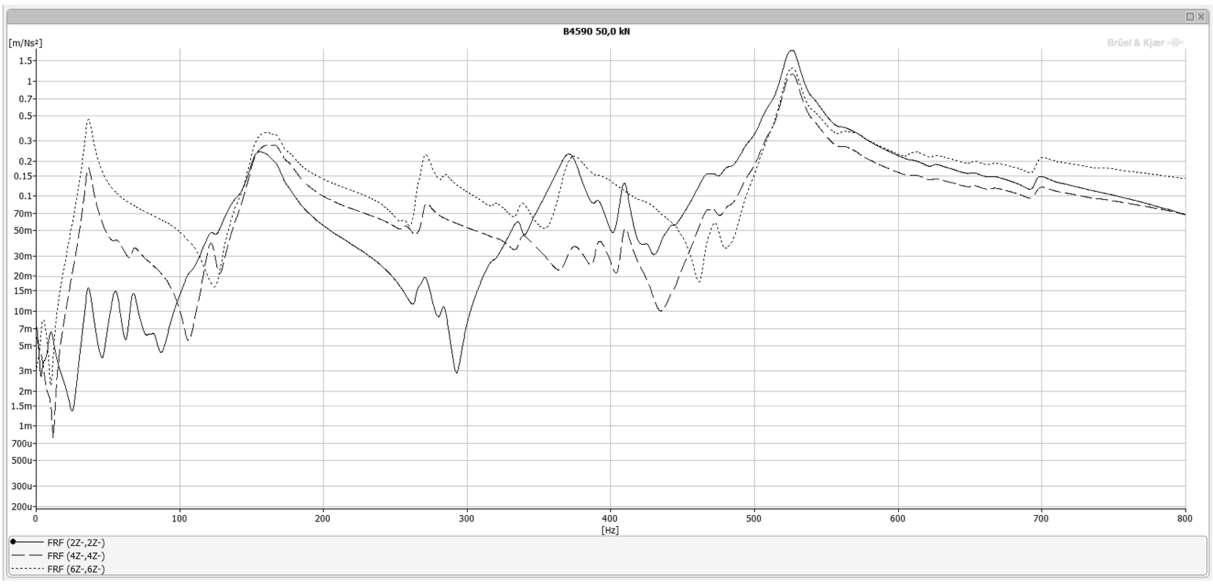
B4590 50,0 kN
Brüel & Kjær
[m/Ns²]
1.5
1
0.7
0.5
0.3
0.2
0.15
0.1
70m
50m
30m
20m
15m
10m
7m
5m
3m
2m
1.5m
1m
700u
500u
300u
200u
0
100
200
300
400
500
600
700
800
[Hz]
FRF (2Z-,2Z-)
FRF (4Z-,4Z-)
FRF (6Z-,6Z-)

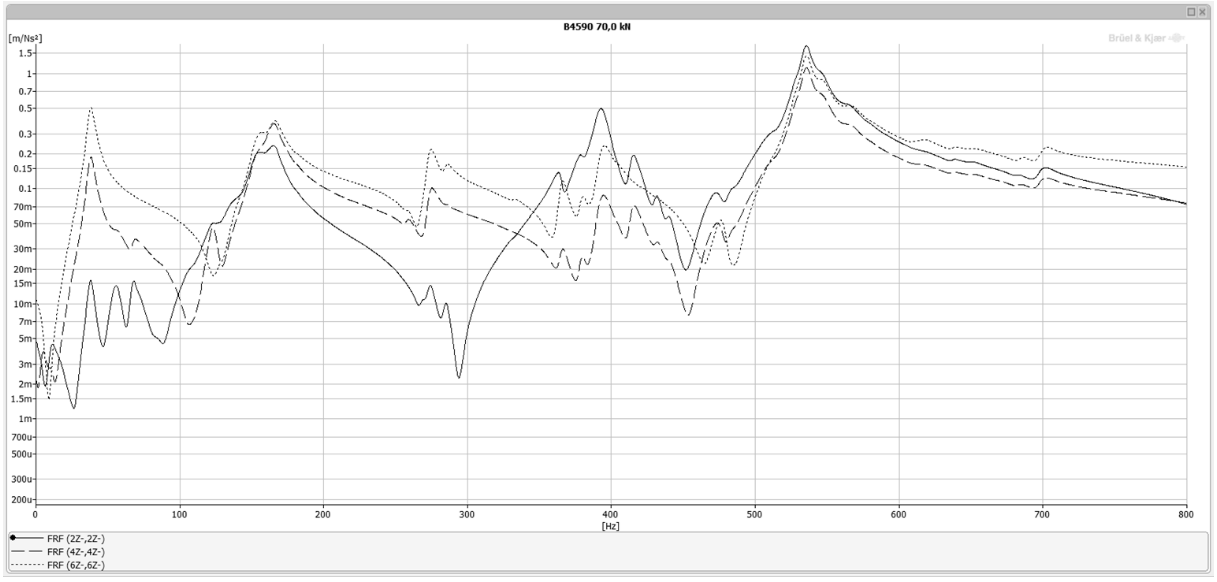
B4590 70,0 kN
Brüel & Kjær
[m/Ns²]
1.5
1
0.7
0.5
0.3
0.2
0.15
0.1
70m
50m
30m
20m
15m
10m
7m
5m
3m
2m
1.5m
1m
700u
500u
300u
200u
0
100
200
300
400
500
600
700
800
[Hz]
FRF (2Z-,2Z-)
FRF (4Z-,4Z-)
FRF (6Z-,6Z-)

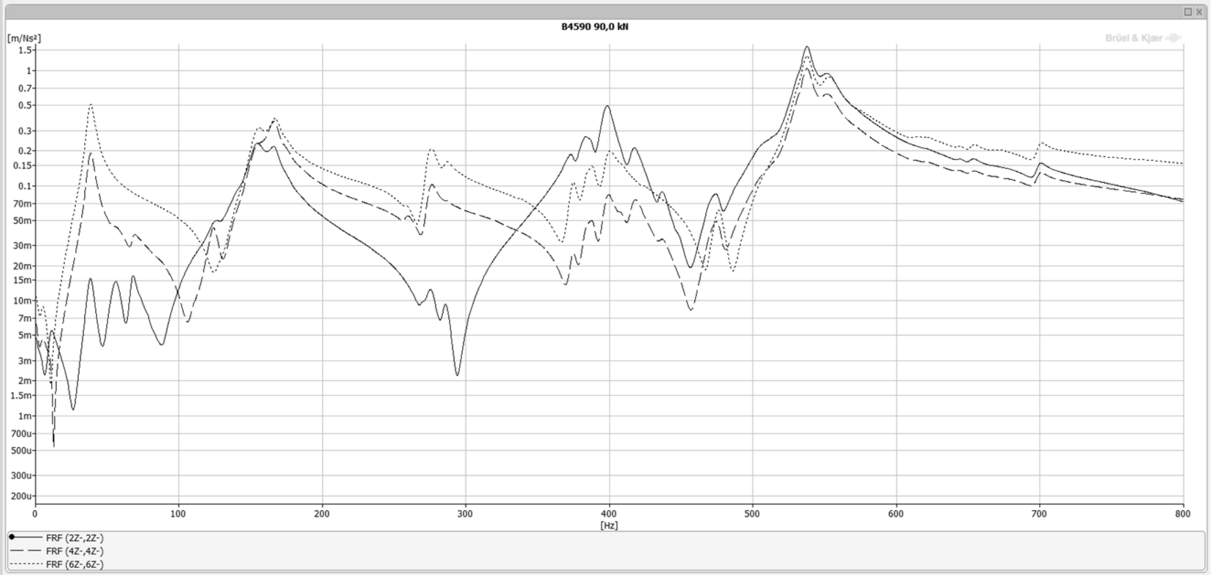
B4590 90,0 kN
Brüel & Kjær
[m/Ns²]
1.5
1
0.7
0.5
0.3
0.2
0.15
0.1
70m
50m
30m
20m
15m
10m
7m
5m
3m
2m
1.5m
1m
700u
500u
300u
200u
0
100
200
300
400
500
600
700
800
[Hz]
FRF (2Z-,2Z-)
FRF (4Z-,4Z-)
FRF (6Z-,6Z-)

Frequency shifts at 4Z

B1020

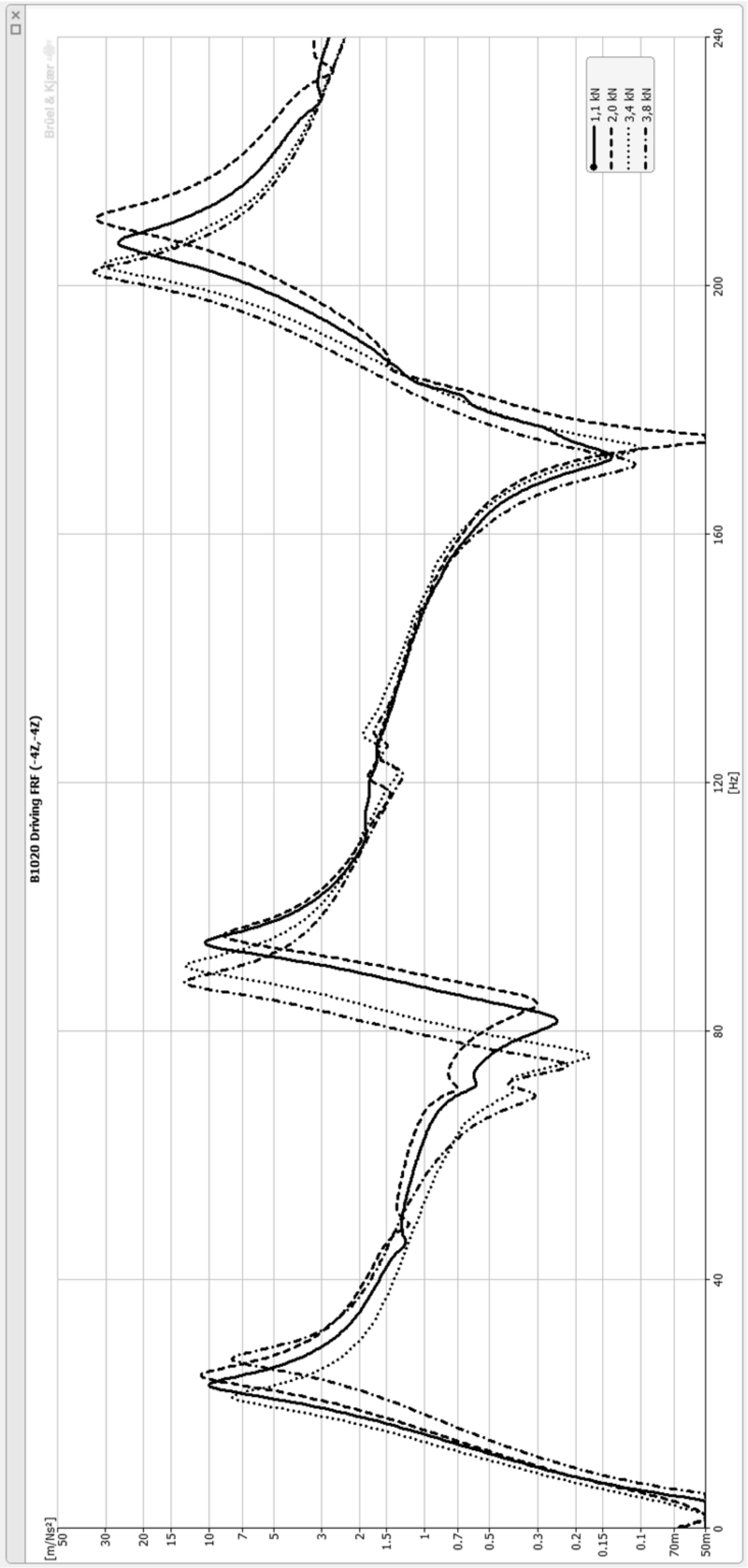

B1530

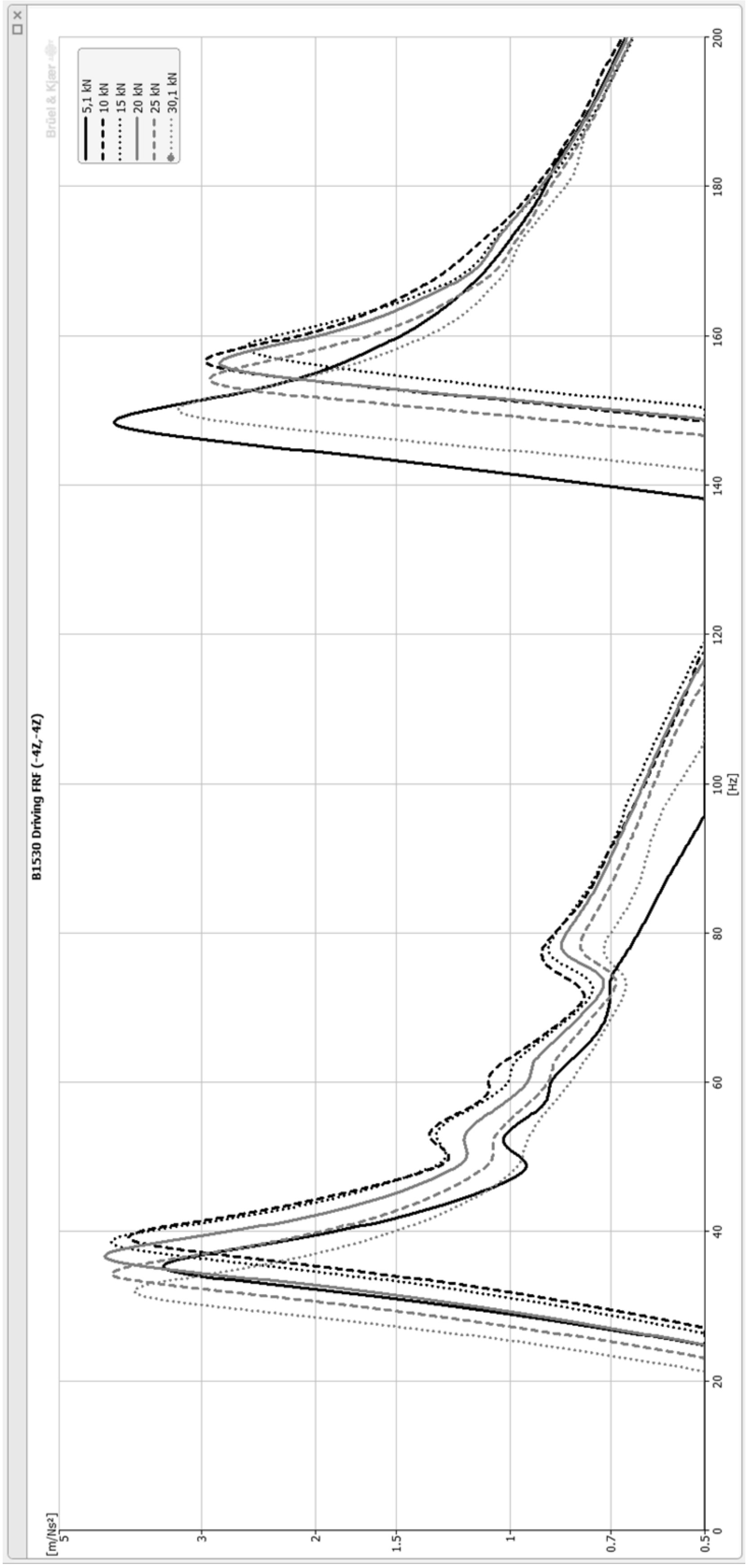
B1530 Driving FRF (-4Z,-4Z)
Brüel & Kjær
5,1 kN
10 kN
15 kN
20 kN
25 kN
30,1 kN
[m/Ns²]
5
3
2
1.5
1
0.7
0.5
0
20
40
60
80
100
120
140
160
180
200
[Hz]

B2040

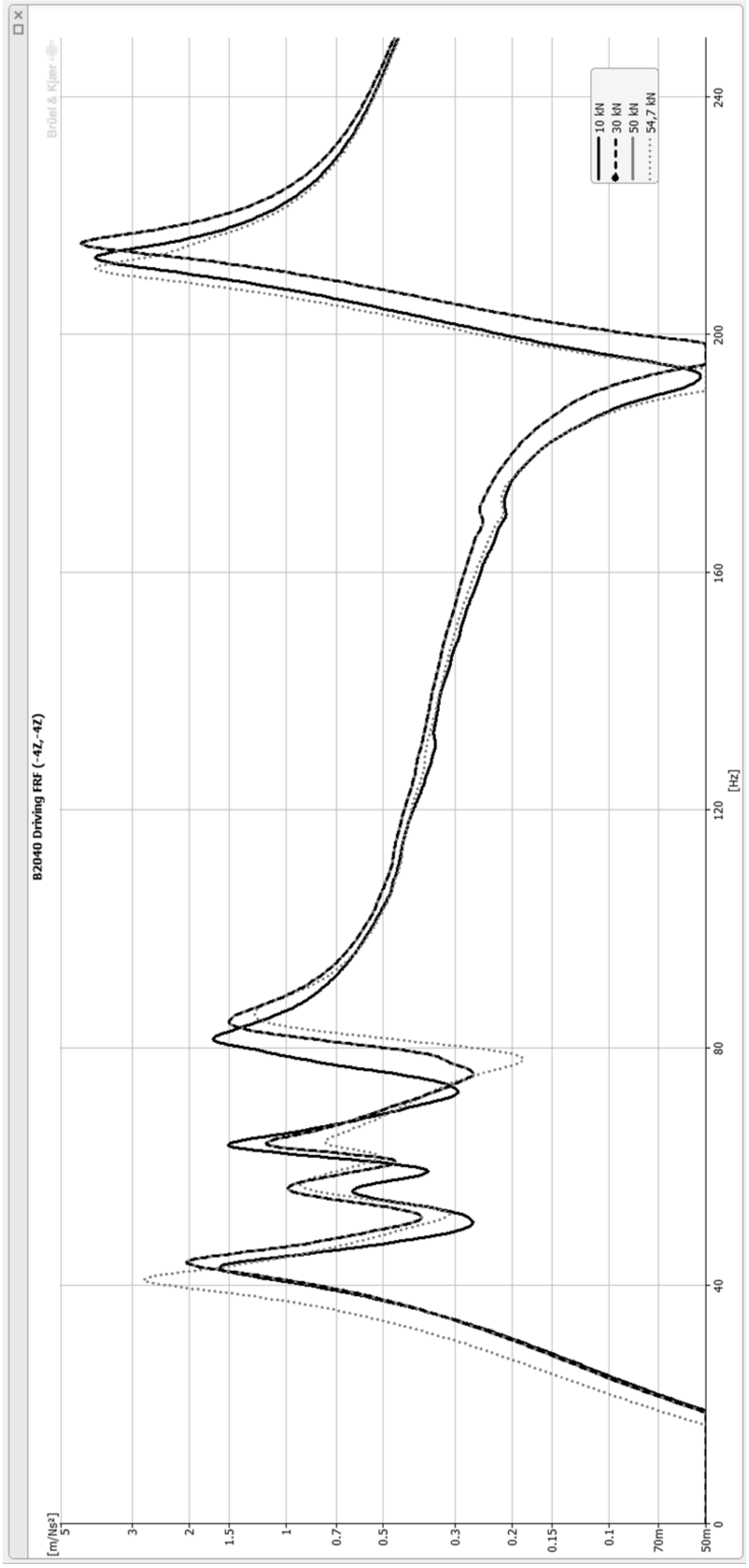
B2040 Driving FRF (-4Z,-4Z)
Brüel & Kjær
[m/Ns²]
5
3
2
1.5
1
0.7
0.5
0.3
0.2
0.15
0.1
70m
50m
0
40
80
120
160
200
240
[Hz]
10 kN
30 kN
50 kN
54,7 kN

B4590

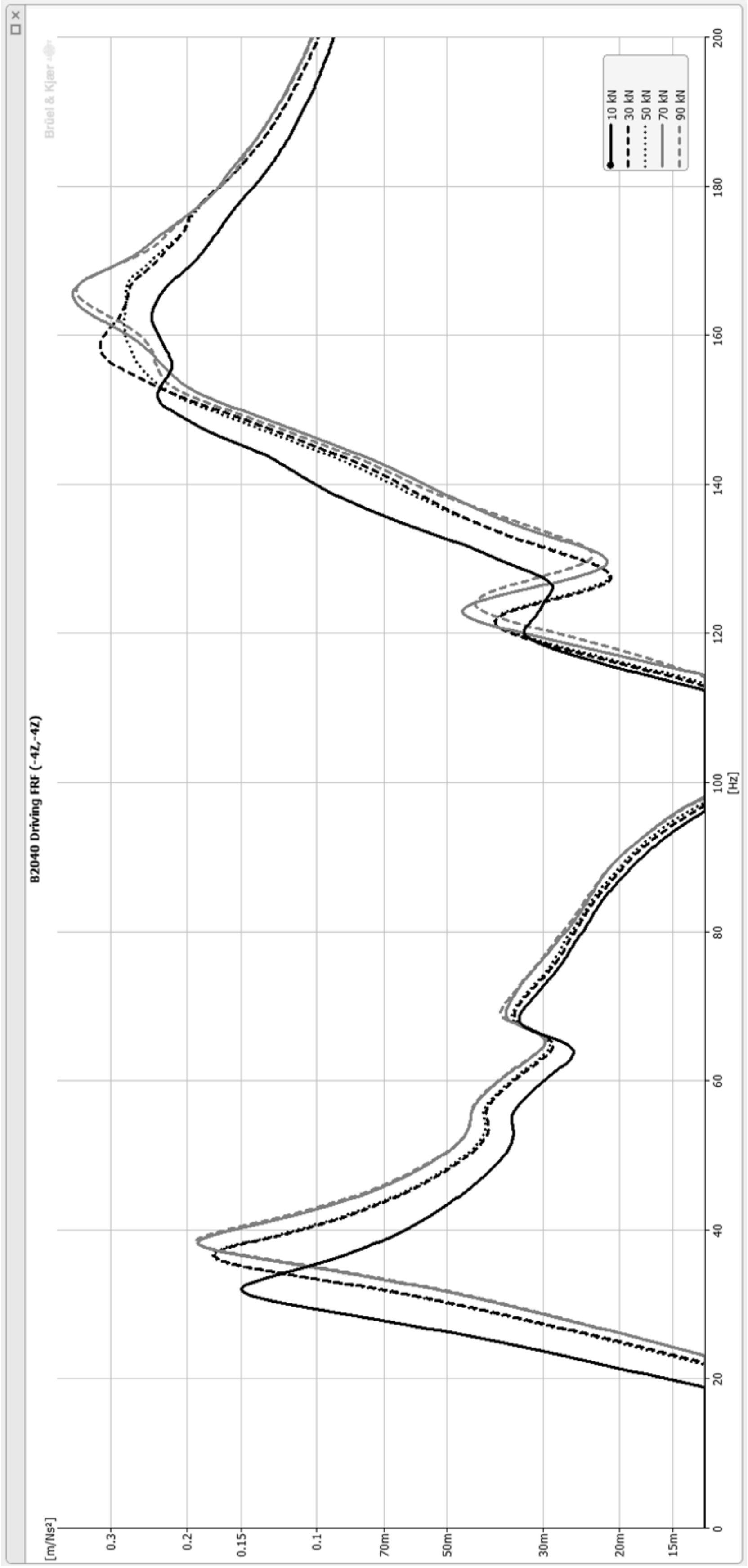
B2040 Driving FRF (-4Z,-4Z)
[m/Ns²]
0.3
0.2
0.15
0.1
70m
50m
30m
20m
15m
0
20
40
60
80
100
120
140
160
180
200
[Hz]
10 kN
30 kN
50 kN
70 kN
90 kN
Brüel & Kjær

D – Calculation results

B1020

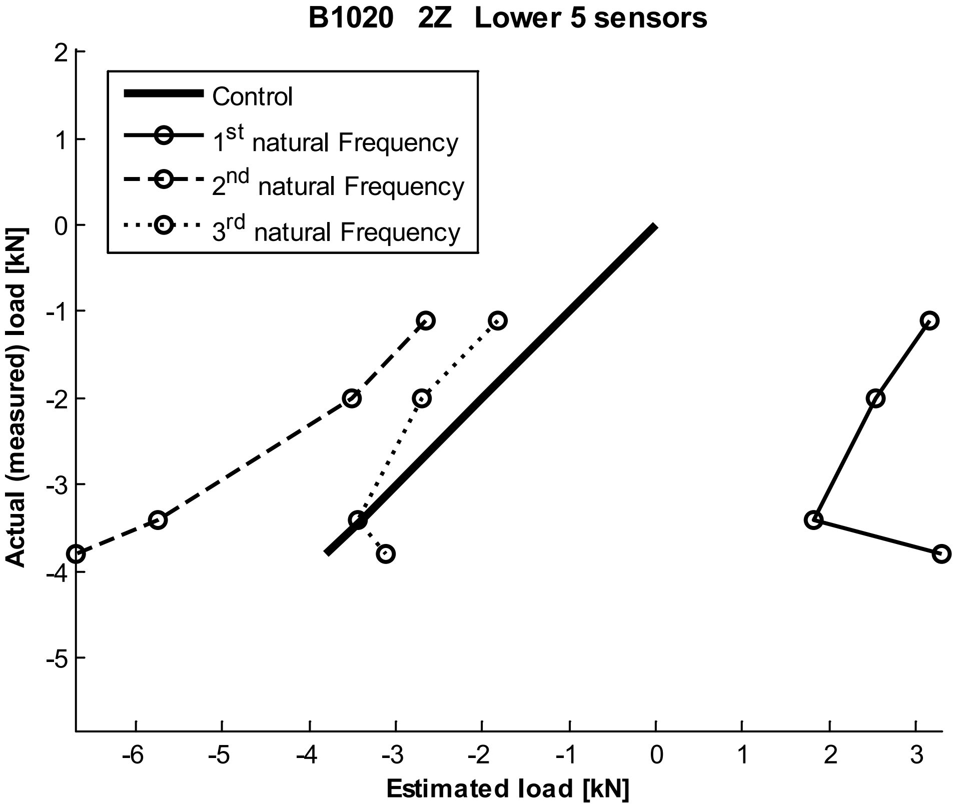

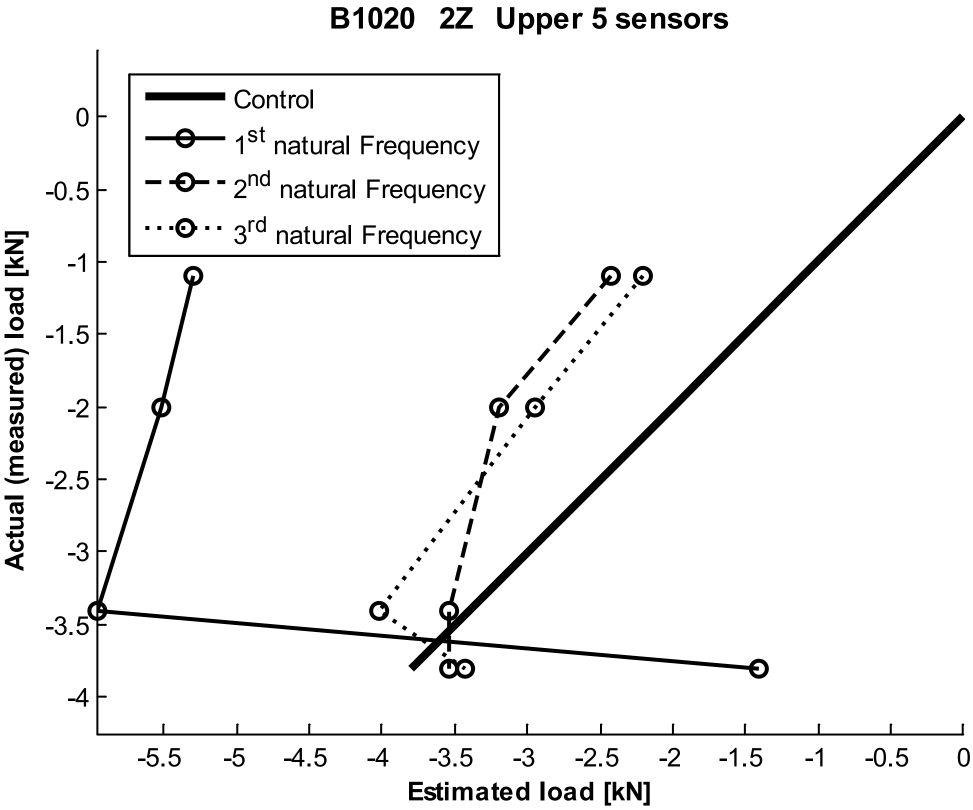

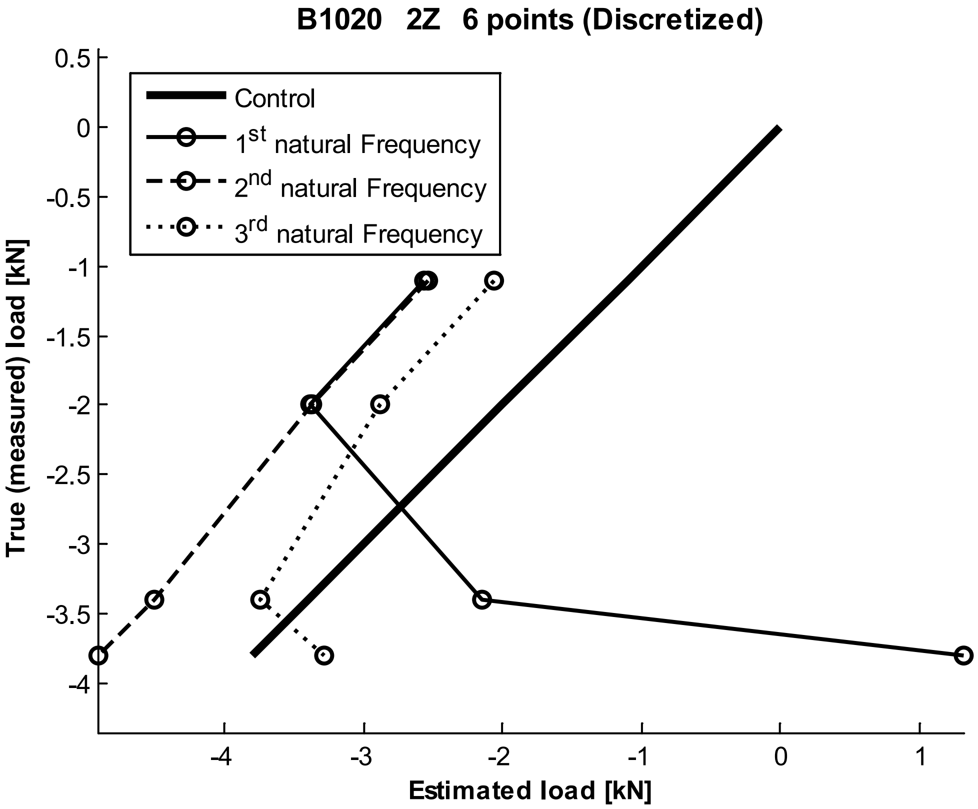

B1020 2Z 6 points (Discretized)

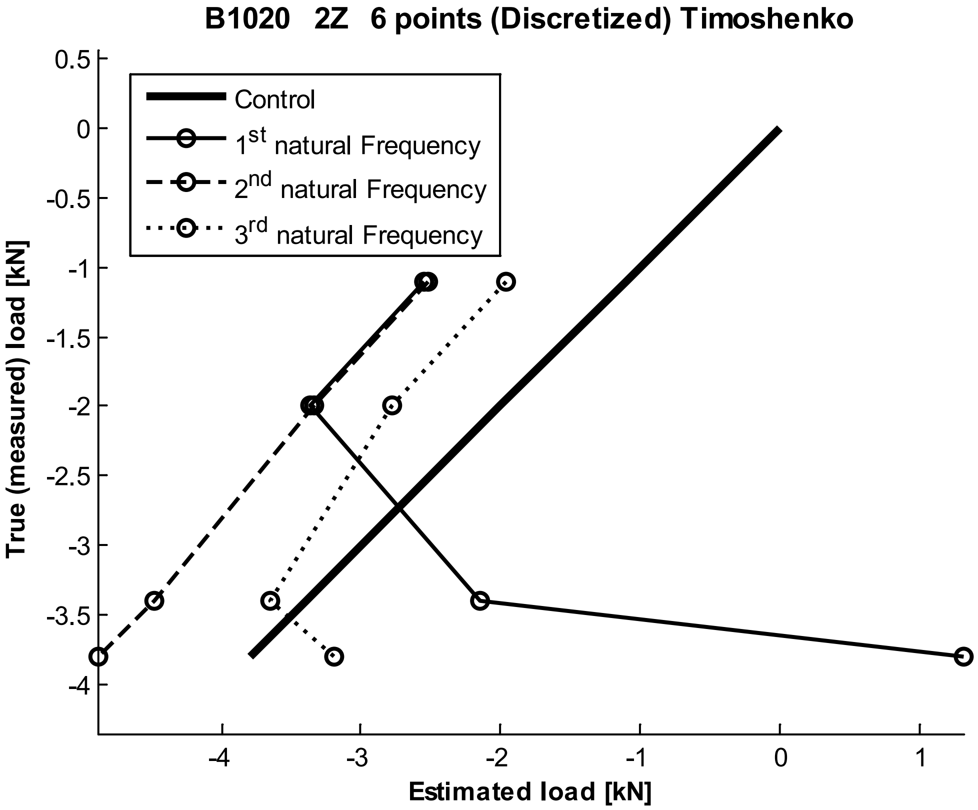

B1020 2Z 6 points (Discretized) Timoshenko

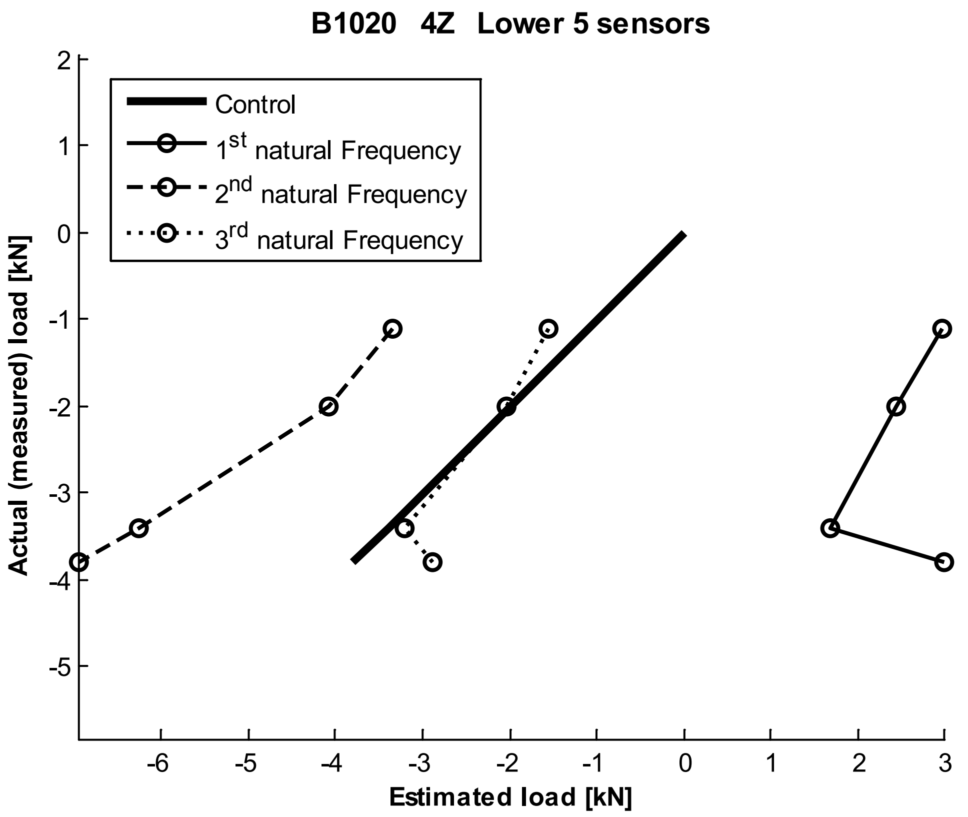
B1020 4Z Lower 5 sensors
Control
1st natural Frequency
2nd natural Frequency
3rd natural Frequency
Actual (measured) load [kN]
2
1
0
-1
-2
-3
-4
-5
-6
-5
-4
-3
-2
-1
0
1
2
3
Estimated load [kN]

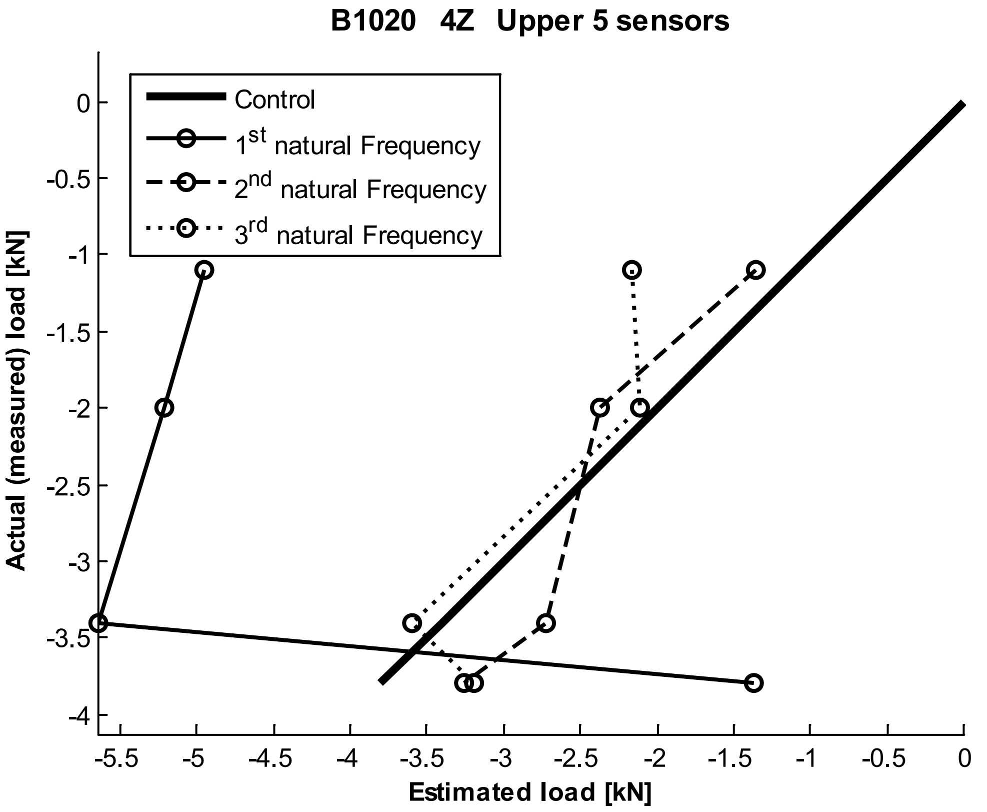
B1020 4Z Upper 5 sensors
Control
1st natural Frequency
2nd natural Frequency
3rd natural Frequency
Actual (measured) load [kN]
0
-0.5
-1
-1.5
-2
-2.5
-3
-3.5
-4
-5.5
-5
-4.5
-4
-3.5
-3
-2.5
-2
-1.5
-1
-0.5
0
Estimated load [kN]

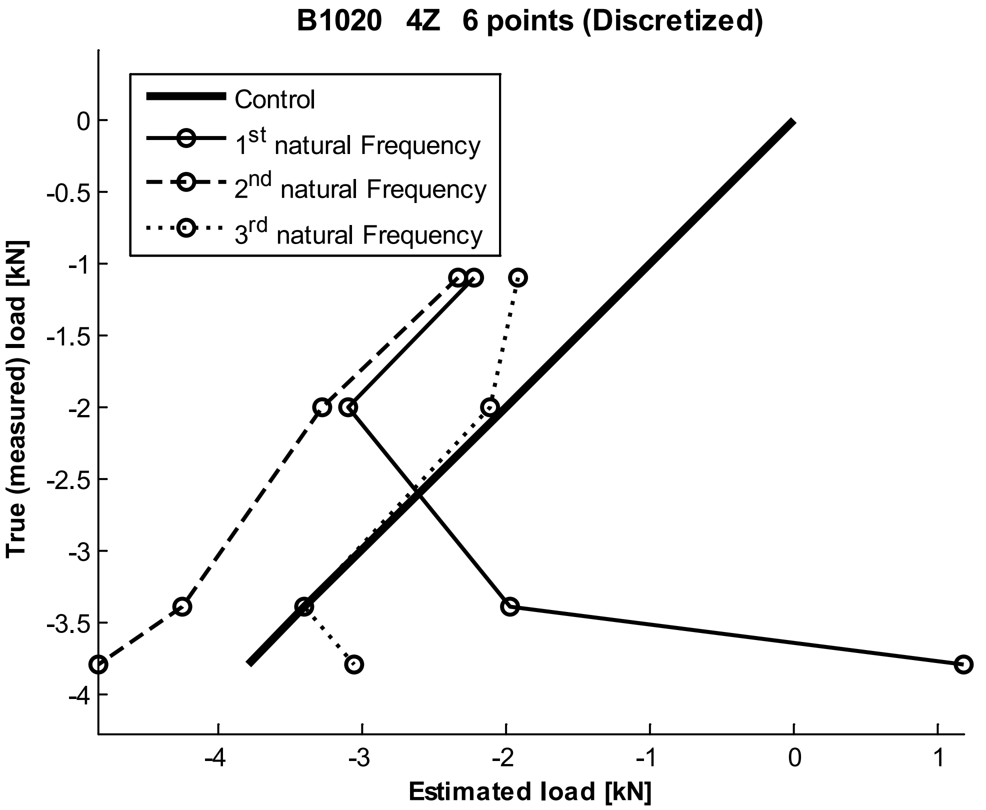
B1020 4Z 6 points (Discretized)
Control
1st natural Frequency
2nd natural Frequency
3rd natural Frequency
True (measured) load [kN]
Estimated load [kN]
0
-0.5
-1
-1.5
-2
-2.5
-3
-3.5
-4
-4
-3
-2
-1
0
1

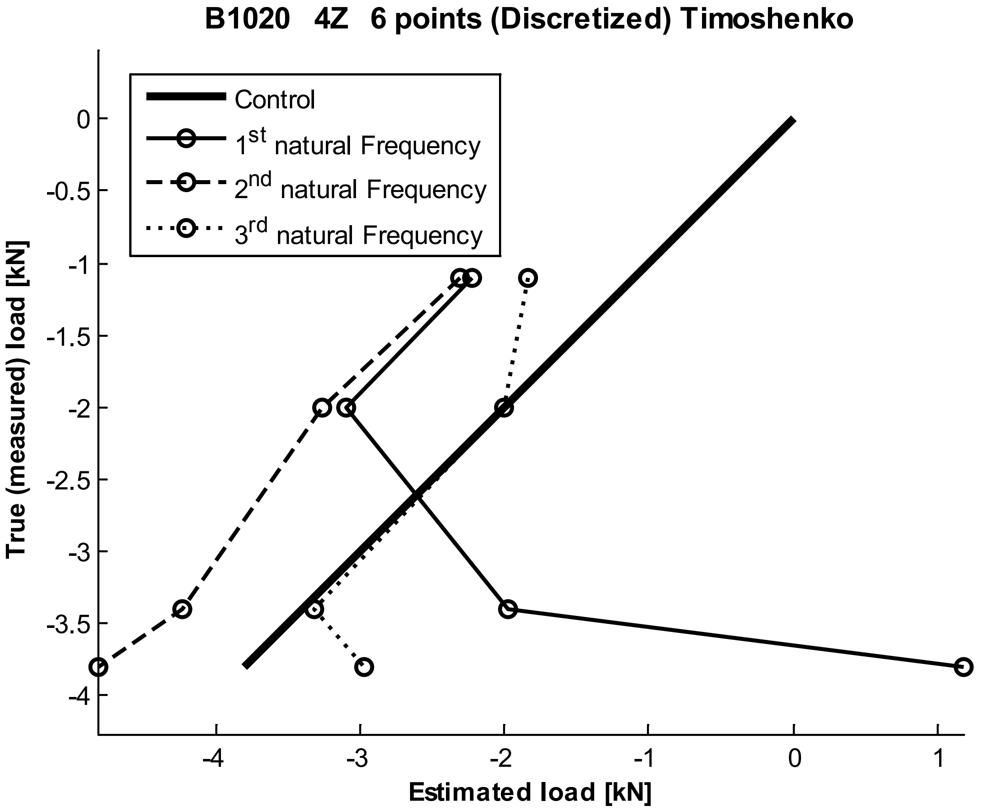
B1020 4Z 6 points (Discretized) Timoshenko
Control
1st natural Frequency
2nd natural Frequency
3rd natural Frequency
True (measured) load [kN]
Estimated load [kN]
0
-0.5
-1
-1.5
-2
-2.5
-3
-3.5
-4
-4
-3
-2
-1
0
1

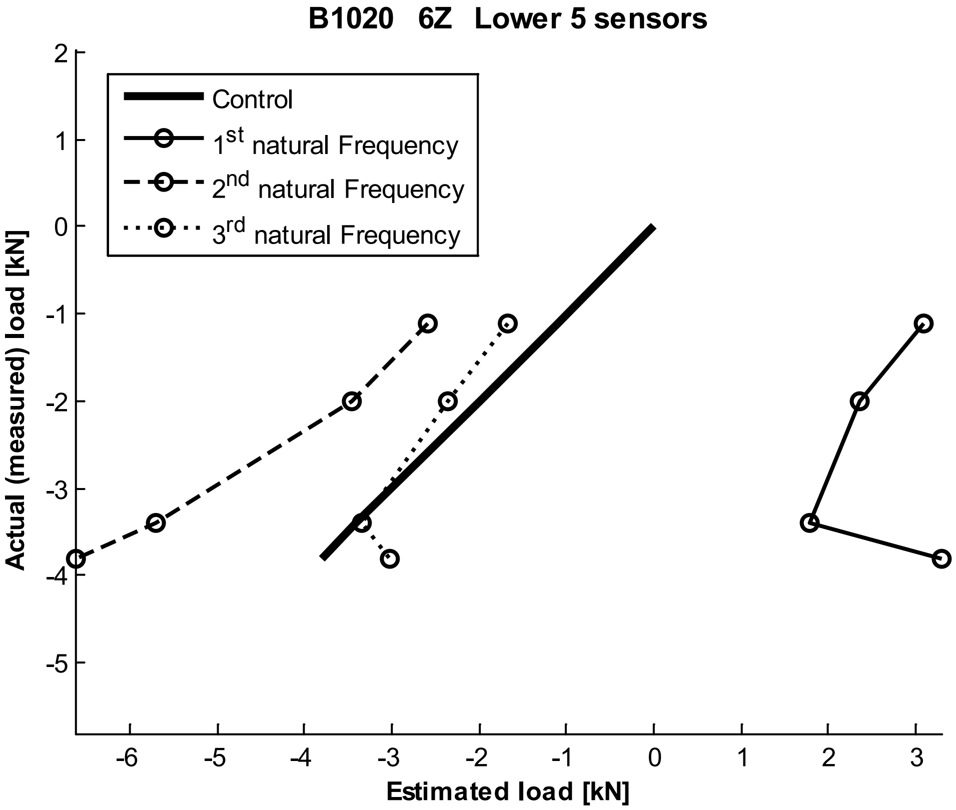
B1020 6Z Lower 5 sensors
Control
1st natural Frequency
2nd natural Frequency
3rd natural Frequency
Actual (measured) load [kN]
Estimated load [kN]
2
1
0
-1
-2
-3
-4
-5
-6
-5
-4
-3
-2
-1
0
1
2
3

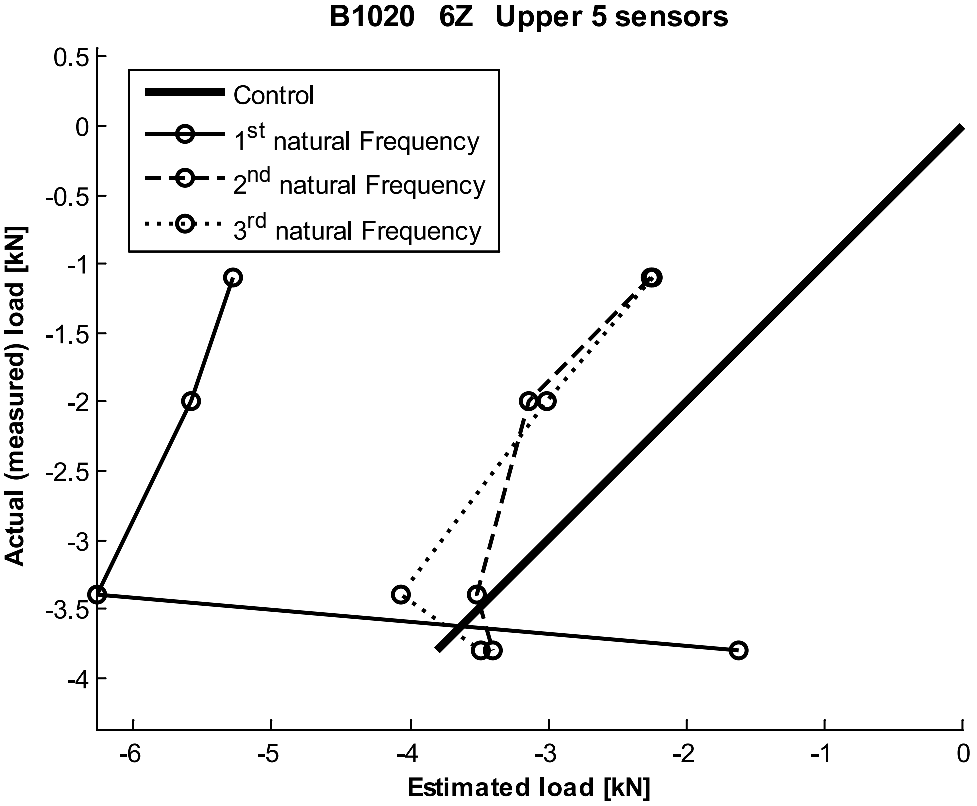
B1020 6Z Upper 5 sensors
Control
1st natural Frequency
2nd natural Frequency
3rd natural Frequency
Actual (measured) load [kN]
Estimated load [kN]
0.5
0
-0.5
-1
-1.5
-2
-2.5
-3
-3.5
-4
-6
-5
-4
-3
-2
-1
0

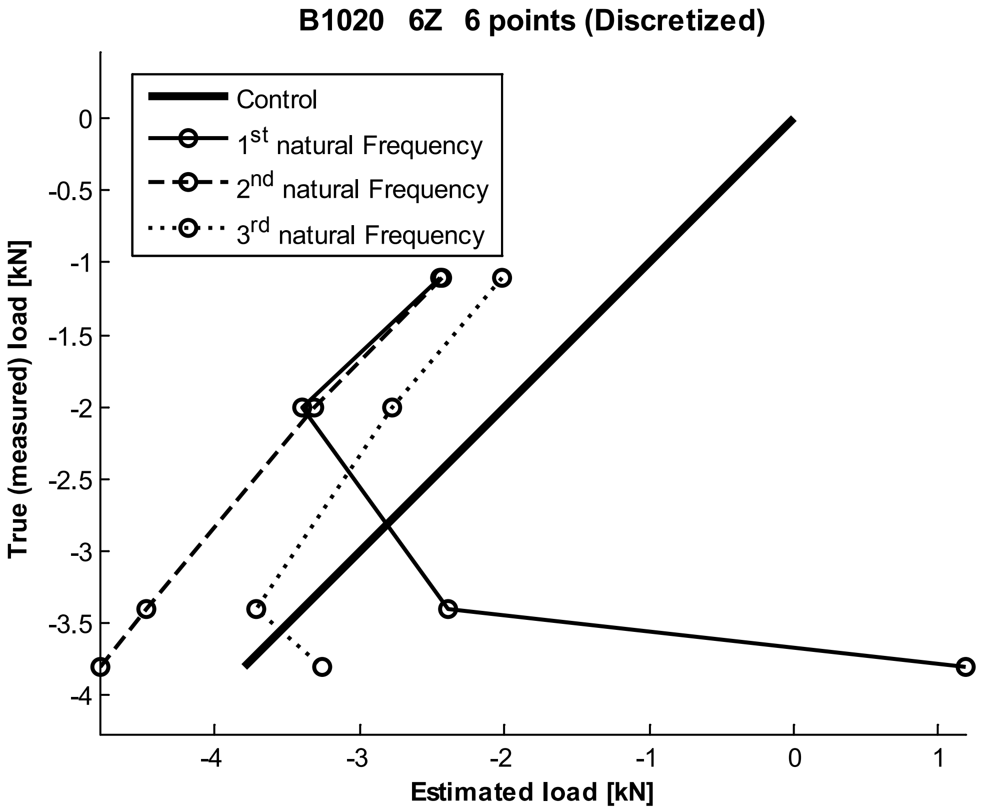
B1020 6Z 6 points (Discretized)
Control
1st natural Frequency
2nd natural Frequency
3rd natural Frequency
True (measured) load [kN]
0
-0.5
-1
-1.5
-2
-2.5
-3
-3.5
-4
-4
-3
-2
-1
0
1
Estimated load [kN]

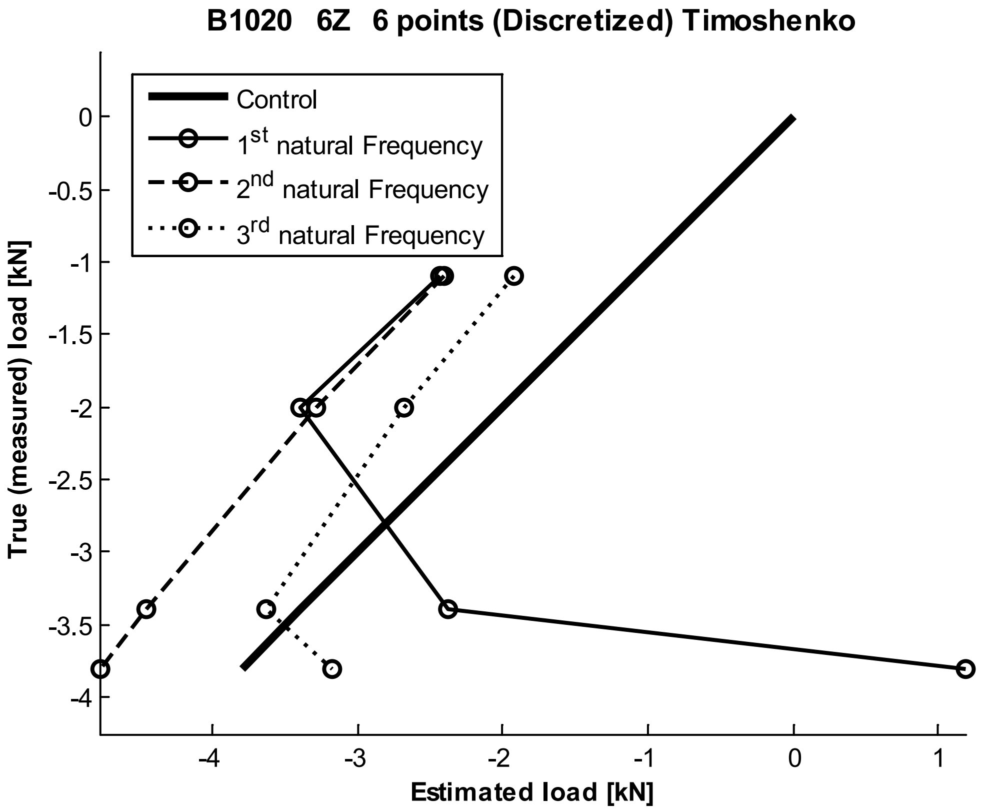
B1020 6Z 6 points (Discretized) Timoshenko
Control
1st natural Frequency
2nd natural Frequency
3rd natural Frequency
True (measured) load [kN]
0
-0.5
-1
-1.5
-2
-2.5
-3
-3.5
-4
-4
-3
-2
-1
0
1
Estimated load [kN]

B1530

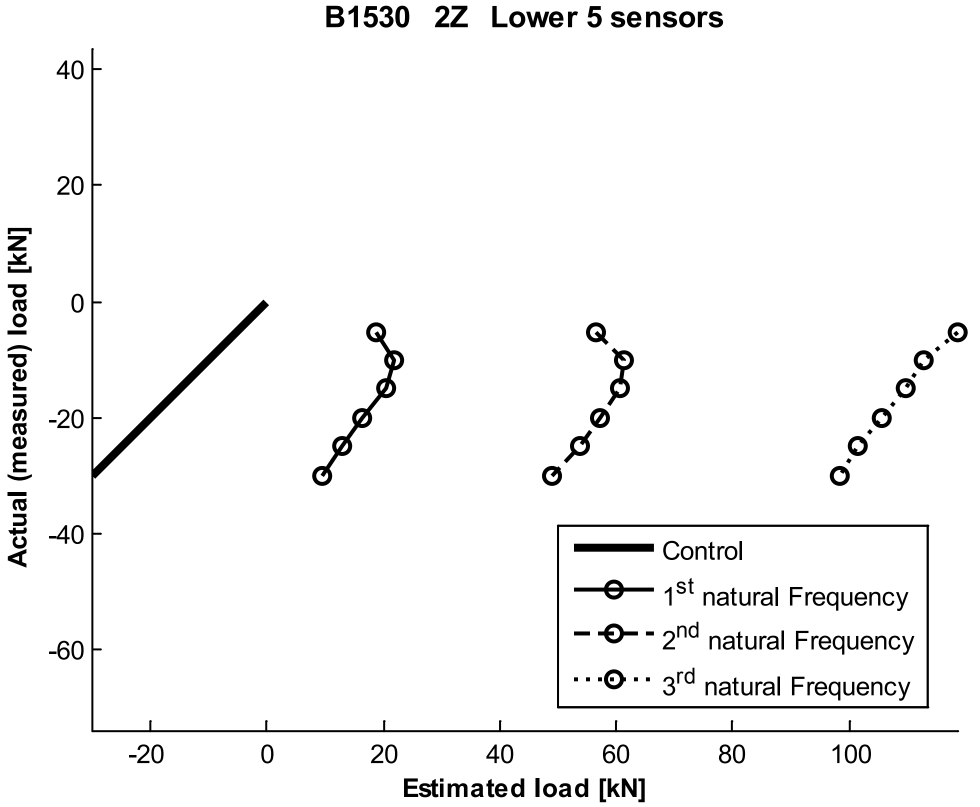
B1530 2Z Lower 5 sensors
Actual (measured) load [kN]
Estimated load [kN]
40
20
0
-20
-40
-60
-20
0
20
40
60
80
100
Control
1st natural Frequency
2nd natural Frequency
3rd natural Frequency

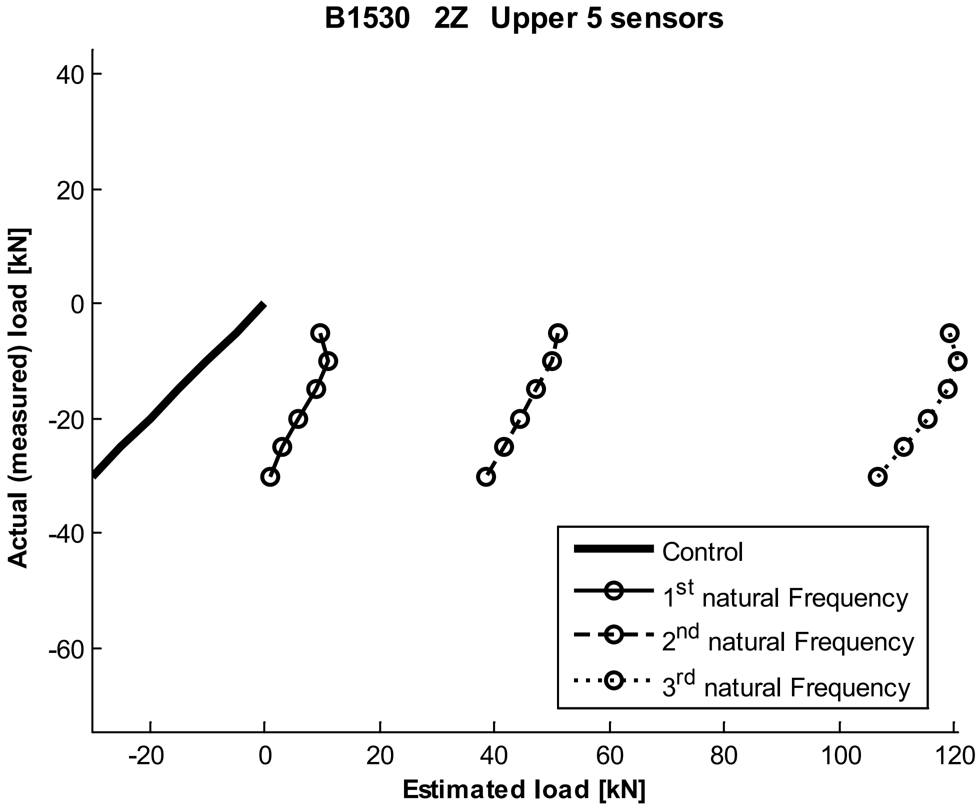
B1530 2Z Upper 5 sensors
Actual (measured) load [kN]
Estimated load [kN]
40
20
0
-20
-40
-60
-20
0
20
40
60
80
100
120
Control
1st natural Frequency
2nd natural Frequency
3rd natural Frequency

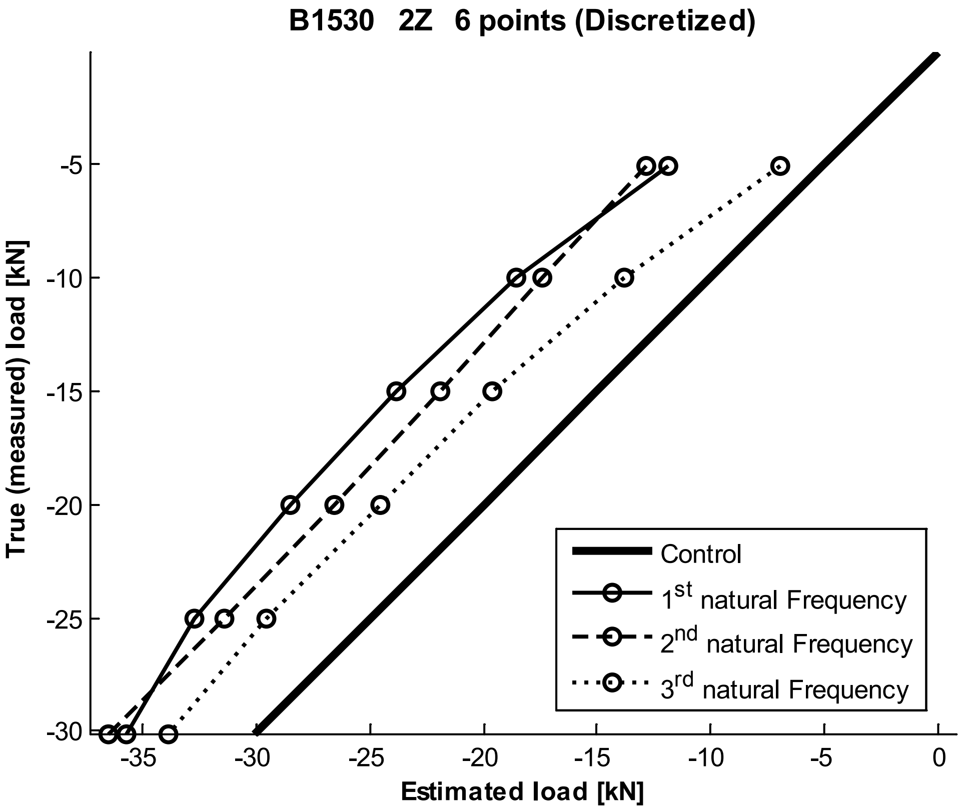
B1530 2Z 6 points (Discretized)
True (measured) load [kN]
-5
-10
-15
-20
-25
-30
-35
-30
-25
-20
-15
-10
-5
0
Estimated load [kN]
Control
1st natural Frequency
2nd natural Frequency
3rd natural Frequency

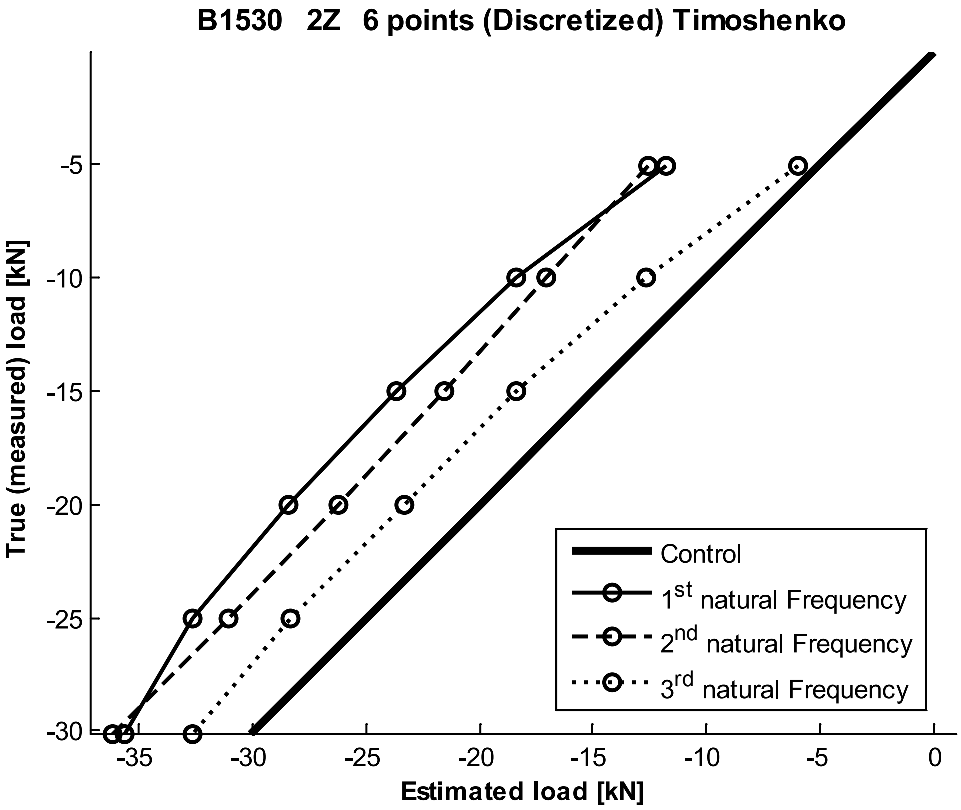
B1530 2Z 6 points (Discretized) Timoshenko
True (measured) load [kN]
-5
-10
-15
-20
-25
-30
-35
-30
-25
-20
-15
-10
-5
0
Estimated load [kN]
Control
1st natural Frequency
2nd natural Frequency
3rd natural Frequency

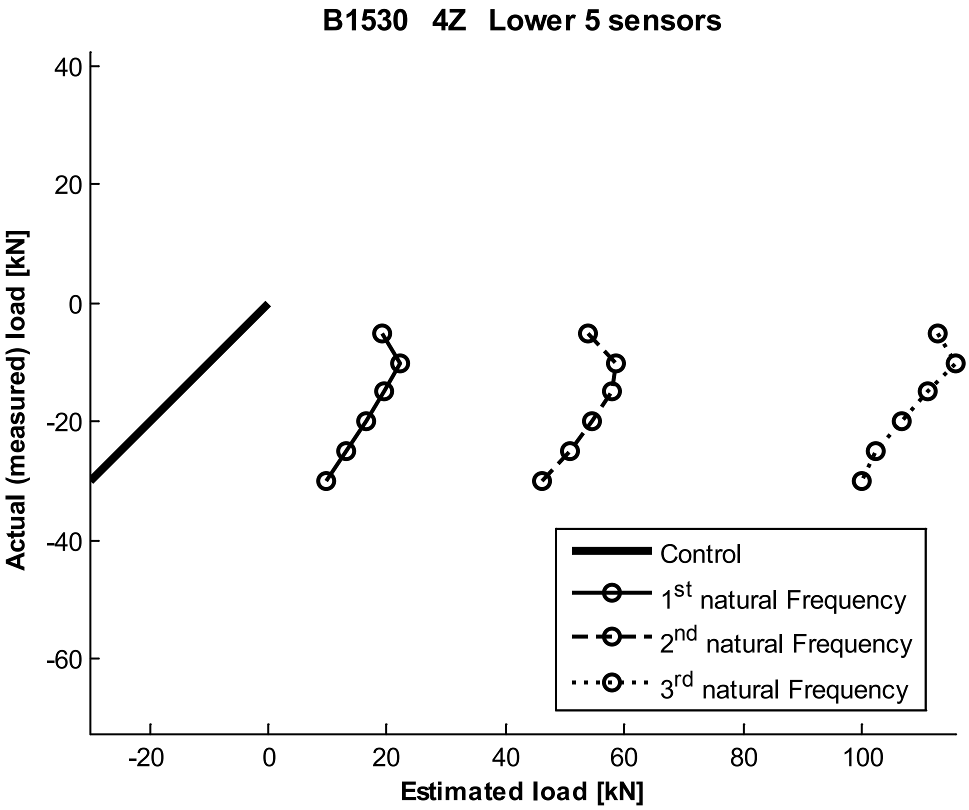
B1530 4Z Lower 5 sensors
Actual (measured) load [kN]
40
20
0
-20
-40
-60
Estimated load [kN]
-20
0
20
40
60
80
100
Control
1st natural Frequency
2nd natural Frequency
3rd natural Frequency

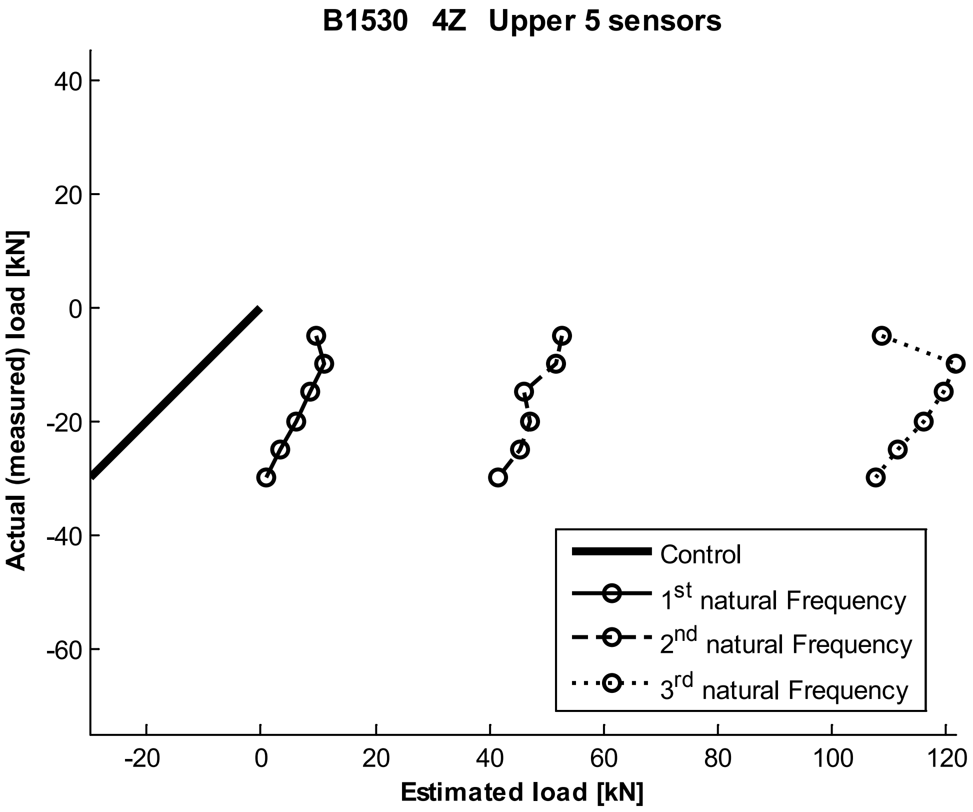
B1530 4Z Upper 5 sensors
Actual (measured) load [kN]
40
20
0
-20
-40
-60
Estimated load [kN]
-20
0
20
40
60
80
100
120
Control
1st natural Frequency
2nd natural Frequency
3rd natural Frequency

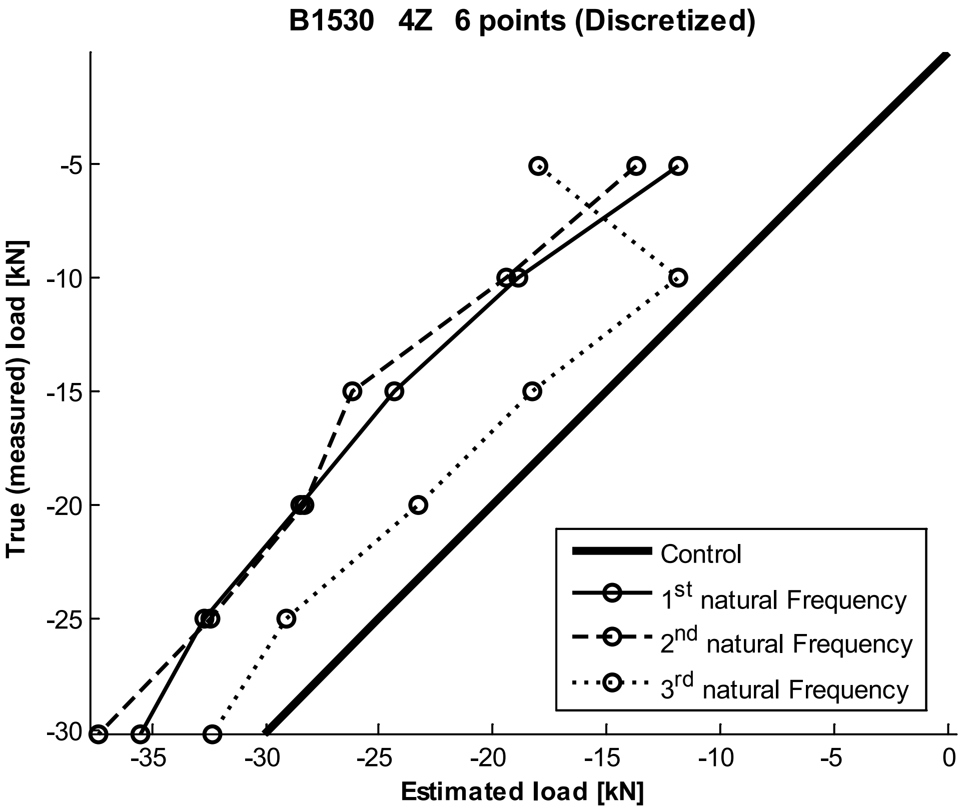
B1530 4Z 6 points (Discretized)
True (measured) load [kN]
Estimated load [kN]
-5
-10
-15
-20
-25
-30
-35
-30
-25
-20
-15
-10
-5
0
Control
1st natural Frequency
2nd natural Frequency
3rd natural Frequency

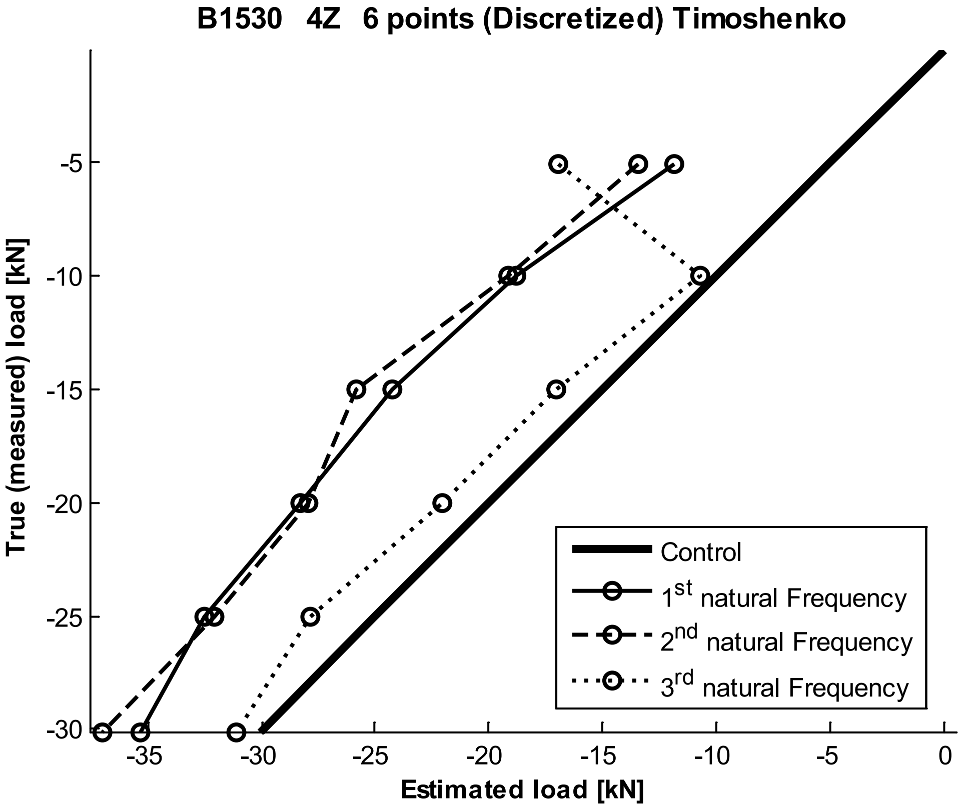
B1530 4Z 6 points (Discretized) Timoshenko
True (measured) load [kN]
Estimated load [kN]
-5
-10
-15
-20
-25
-30
-35
-30
-25
-20
-15
-10
-5
0
Control
1st natural Frequency
2nd natural Frequency
3rd natural Frequency

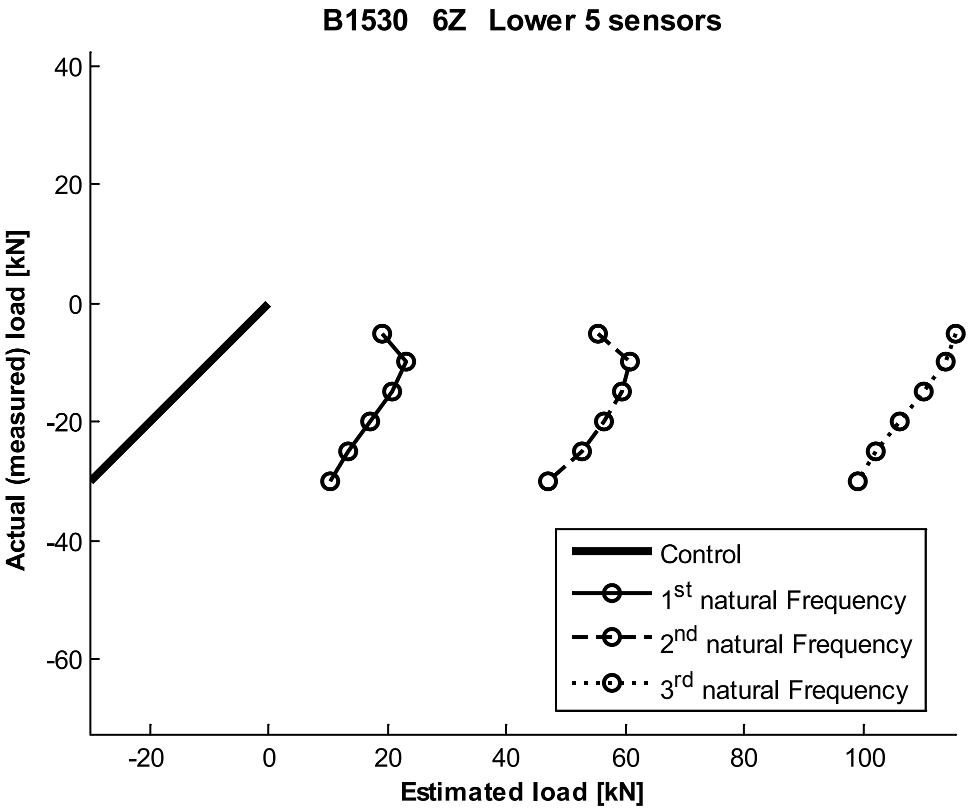
B1530 6Z Lower 5 sensors
Actual (measured) load [kN]
40
20
0
-20
-40
-60
-20
0
20
40
60
80
100
Estimated load [kN]
Control
1st natural Frequency
2nd natural Frequency
3rd natural Frequency

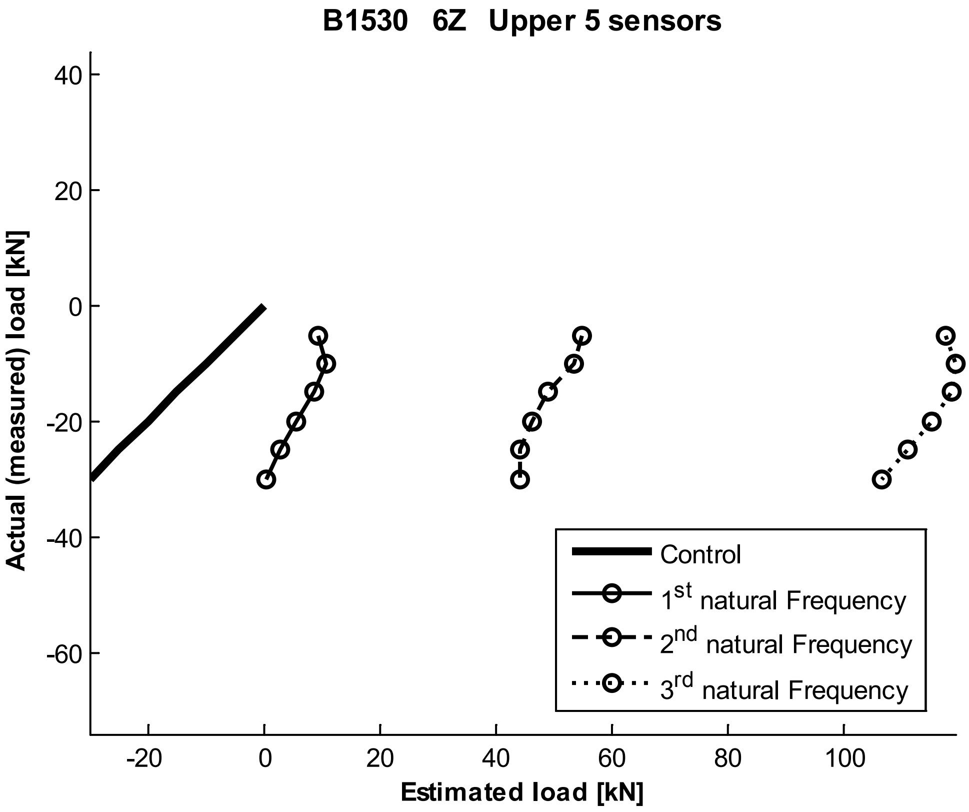
B1530 6Z Upper 5 sensors
Actual (measured) load [kN]
40
20
0
-20
-40
-60
-20
0
20
40
60
80
100
Estimated load [kN]
Control
1st natural Frequency
2nd natural Frequency
3rd natural Frequency

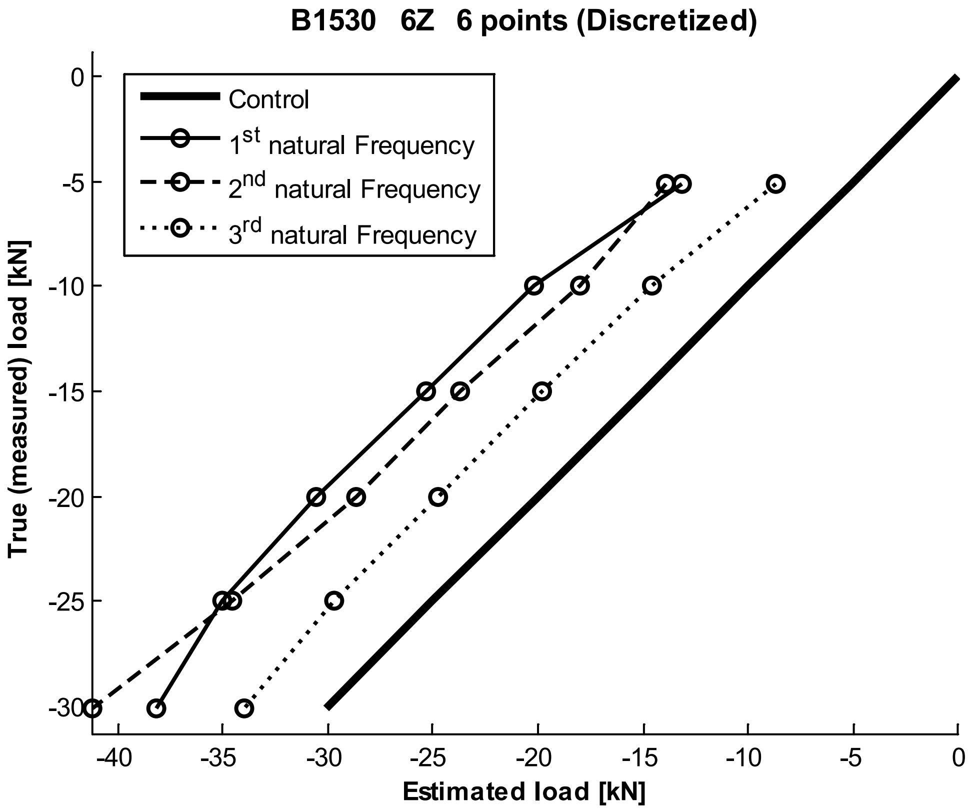
B1530 6Z 6 points (Discretized)
Control
1st natural Frequency
2nd natural Frequency
3rd natural Frequency
True (measured) load [kN]
Estimated load [kN]
0
-5
-10
-15
-20
-25
-30
-40
-35
-30
-25
-20
-15
-10
-5
0

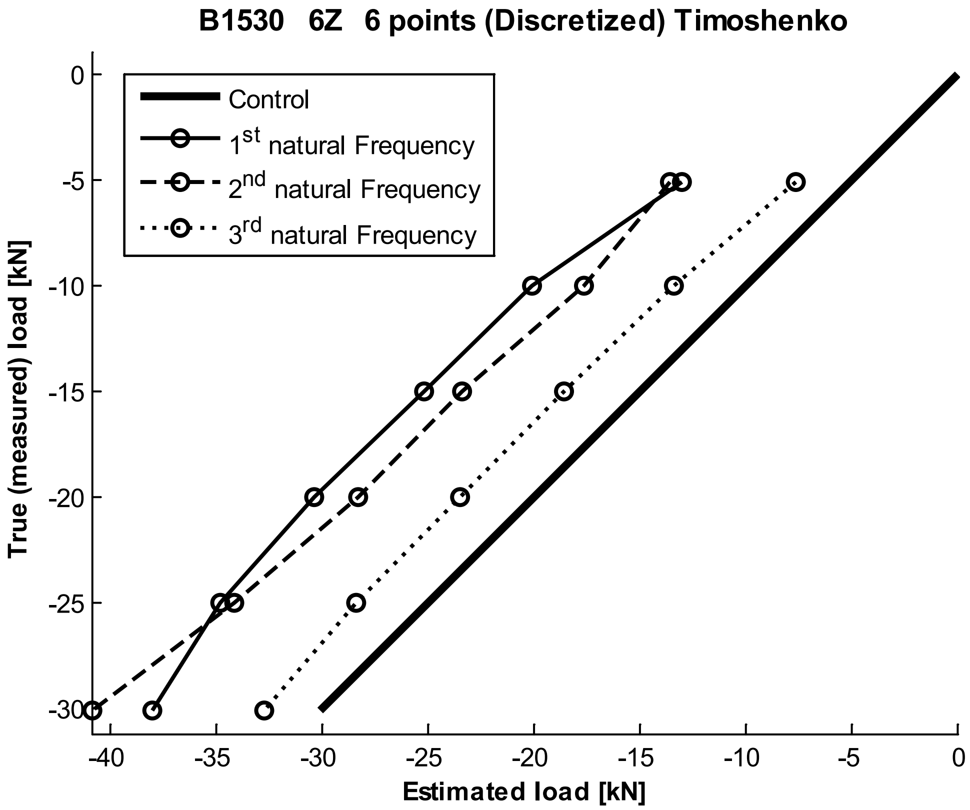
B1530 6Z 6 points (Discretized) Timoshenko
Control
1st natural Frequency
2nd natural Frequency
3rd natural Frequency
True (measured) load [kN]
Estimated load [kN]
0
-5
-10
-15
-20
-25
-30
-40
-35
-30
-25
-20
-15
-10
-5
0

B2040

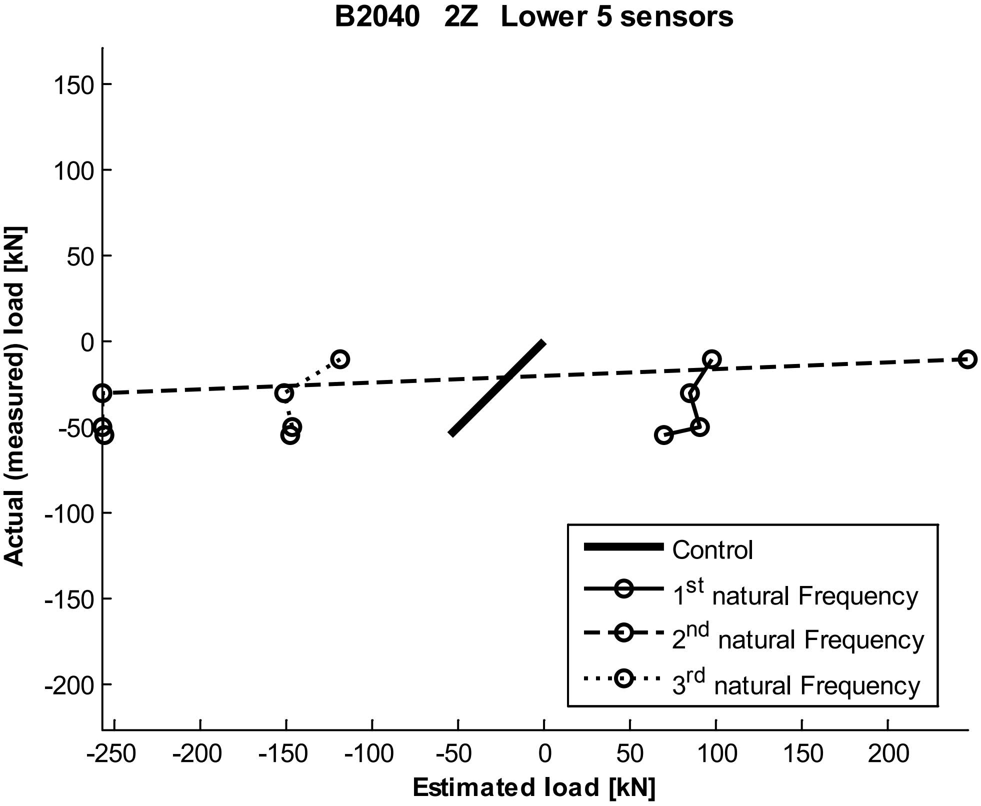
B2040 2Z Lower 5 sensors
Actual (measured) load [kN]
Estimated load [kN]
150
100
50
0
-50
-100
-150
-200
-250
-200
-150
-100
-50
0
50
100
150
200
Control
1st natural Frequency
2nd natural Frequency
3rd natural Frequency

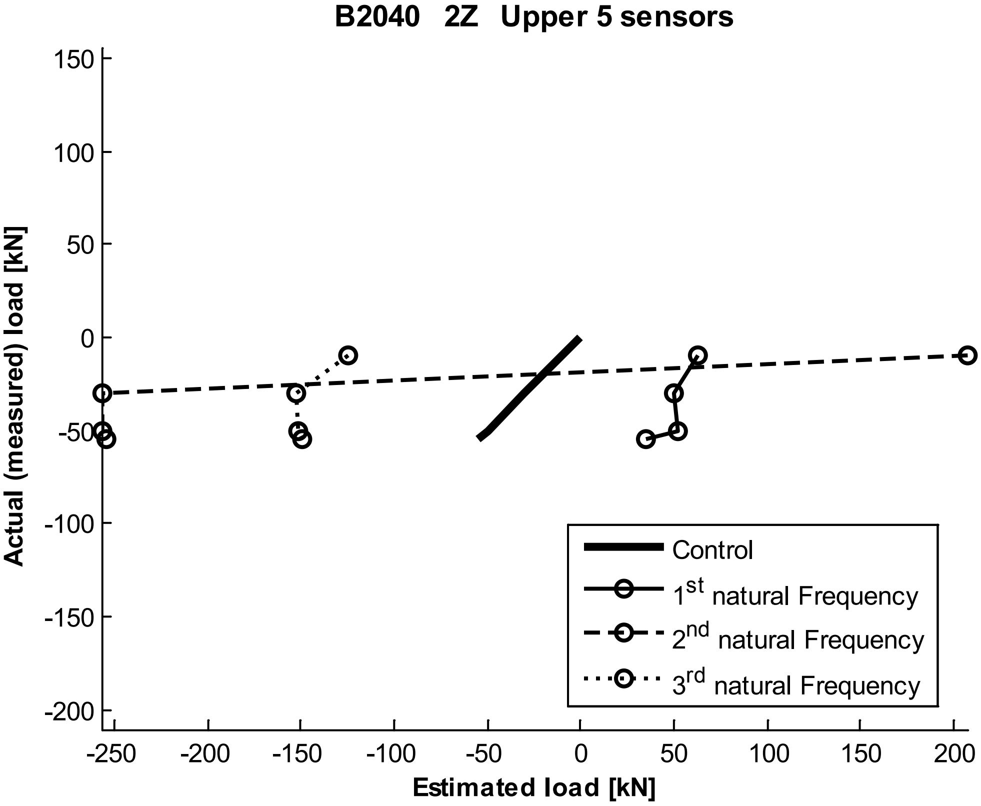
B2040 2Z Upper 5 sensors
Actual (measured) load [kN]
Estimated load [kN]
150
100
50
0
-50
-100
-150
-200
-250
-200
-150
-100
-50
0
50
100
150
200
Control
1st natural Frequency
2nd natural Frequency
3rd natural Frequency

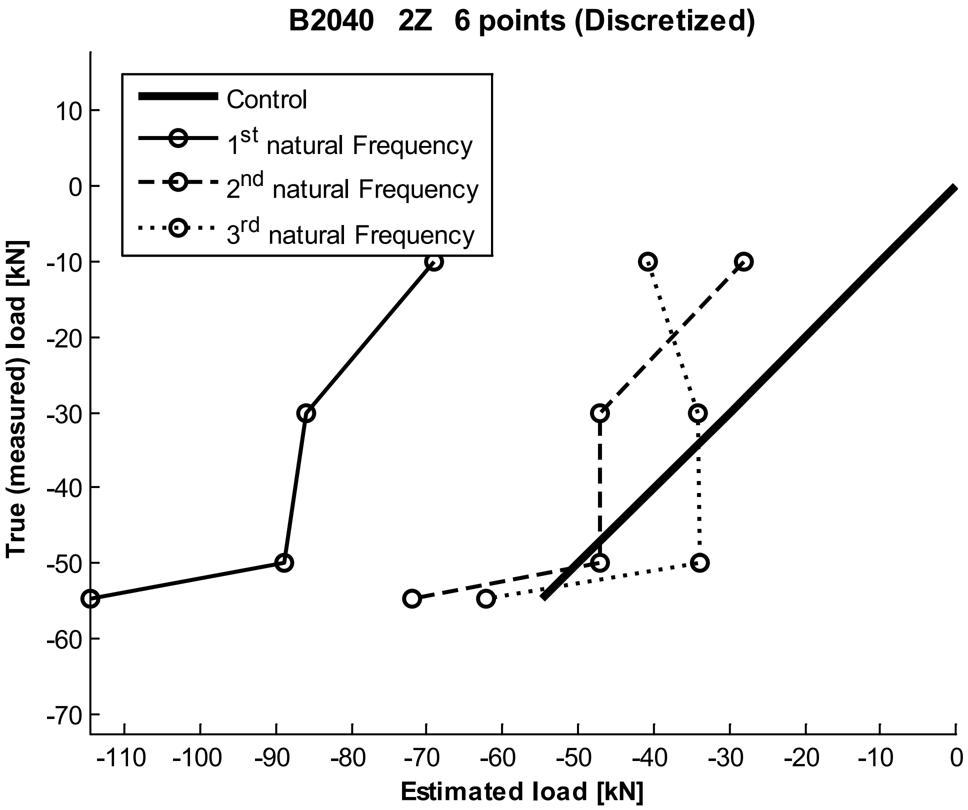
B2040 2Z 6 points (Discretized)
Control
1st natural Frequency
2nd natural Frequency
3rd natural Frequency
True (measured) load [kN]
10
0
-10
-20
-30
-40
-50
-60
-70
-110
-100
-90
-80
-70
-60
-50
-40
-30
-20
-10
0
Estimated load [kN]

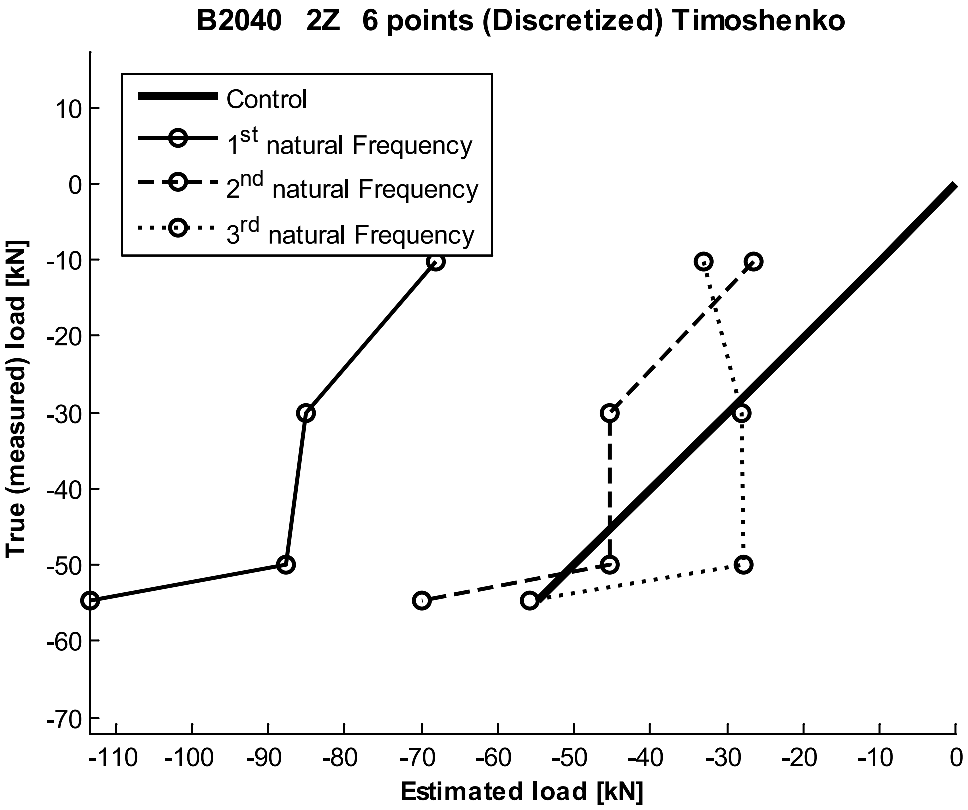
B2040 2Z 6 points (Discretized) Timoshenko
Control
1st natural Frequency
2nd natural Frequency
3rd natural Frequency
True (measured) load [kN]
10
0
-10
-20
-30
-40
-50
-60
-70
-110
-100
-90
-80
-70
-60
-50
-40
-30
-20
-10
0
Estimated load [kN]

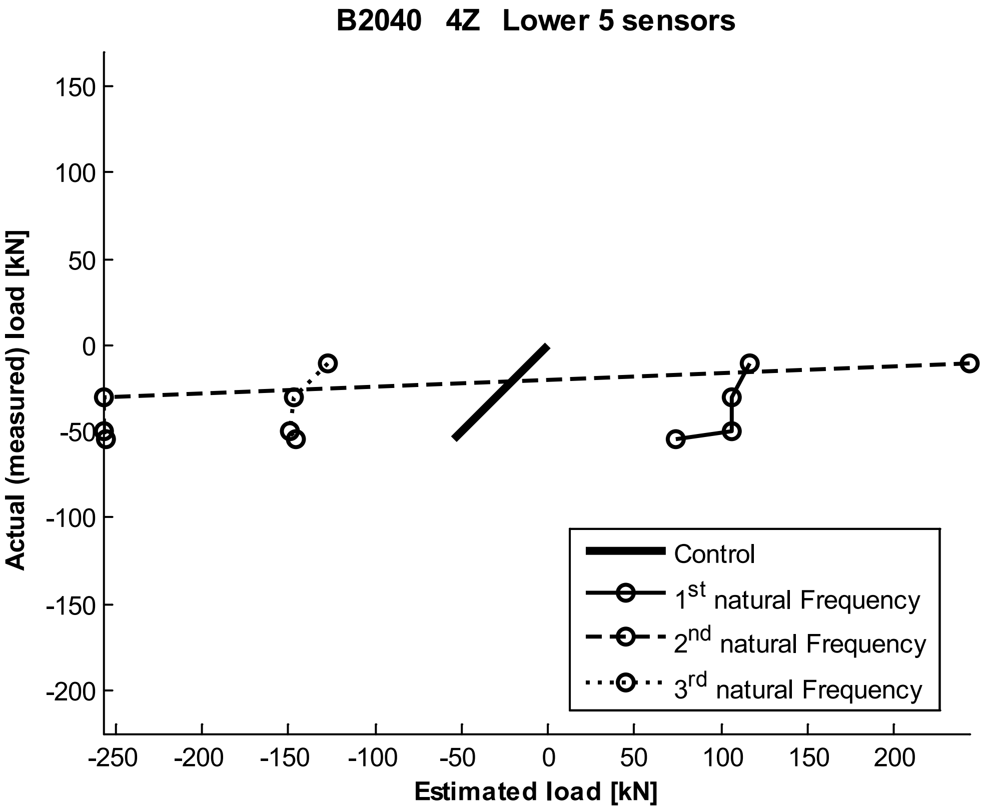
B2040 4Z Lower 5 sensors
Actual (measured) load [kN]
Estimated load [kN]
150
100
50
0
-50
-100
-150
-200
-250
-200
-150
-100
-50
0
50
100
150
200
Control
1st natural Frequency
2nd natural Frequency
3rd natural Frequency

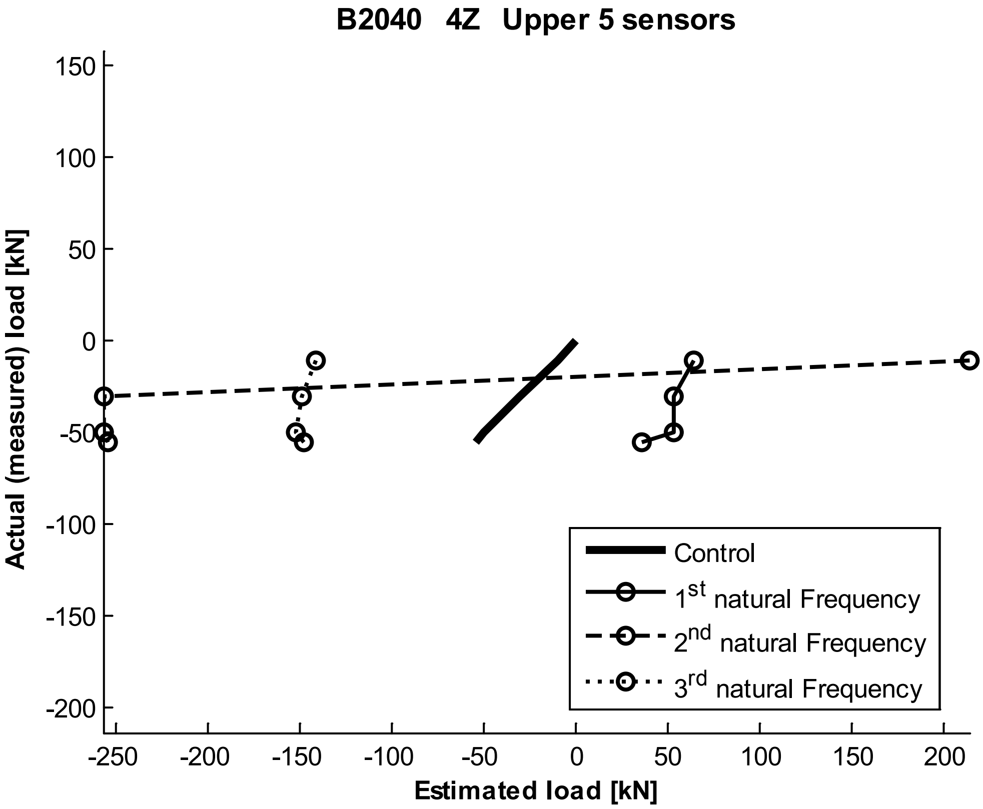
B2040 4Z Upper 5 sensors
Actual (measured) load [kN]
Estimated load [kN]
150
100
50
0
-50
-100
-150
-200
-250
-200
-150
-100
-50
0
50
100
150
200
Control
1st natural Frequency
2nd natural Frequency
3rd natural Frequency

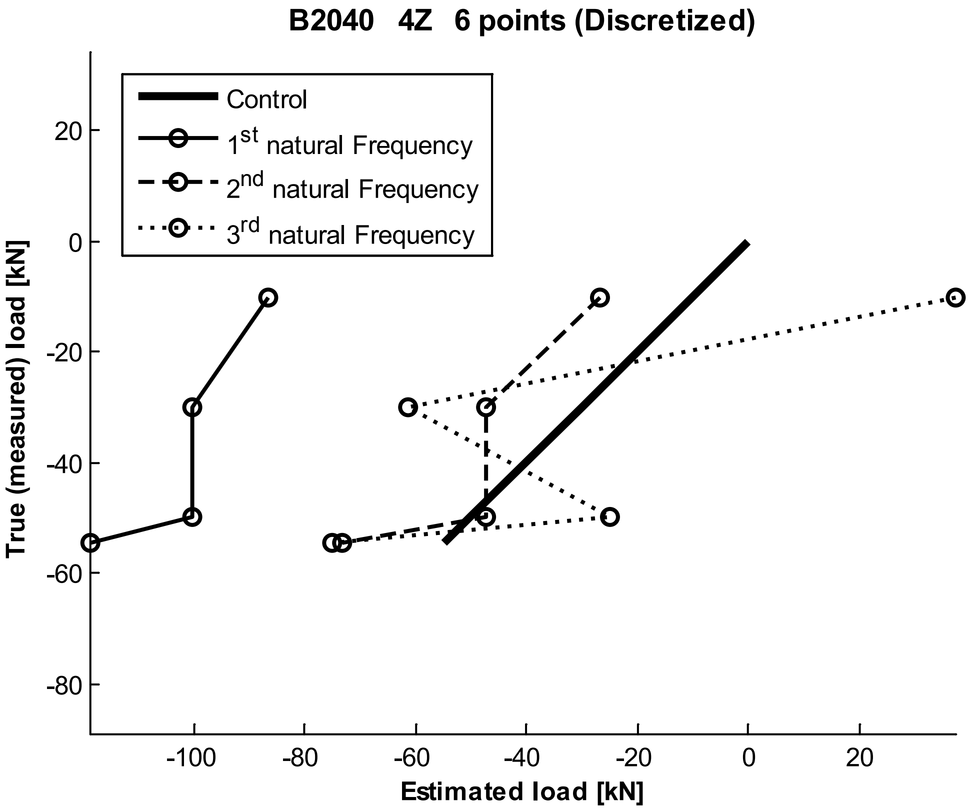
B2040 4Z 6 points (Discretized)
Control
1st natural Frequency
2nd natural Frequency
3rd natural Frequency
True (measured) load [kN]
Estimated load [kN]
20
0
-20
-40
-60
-80
-100
-80
-60
-40
-20
0
20

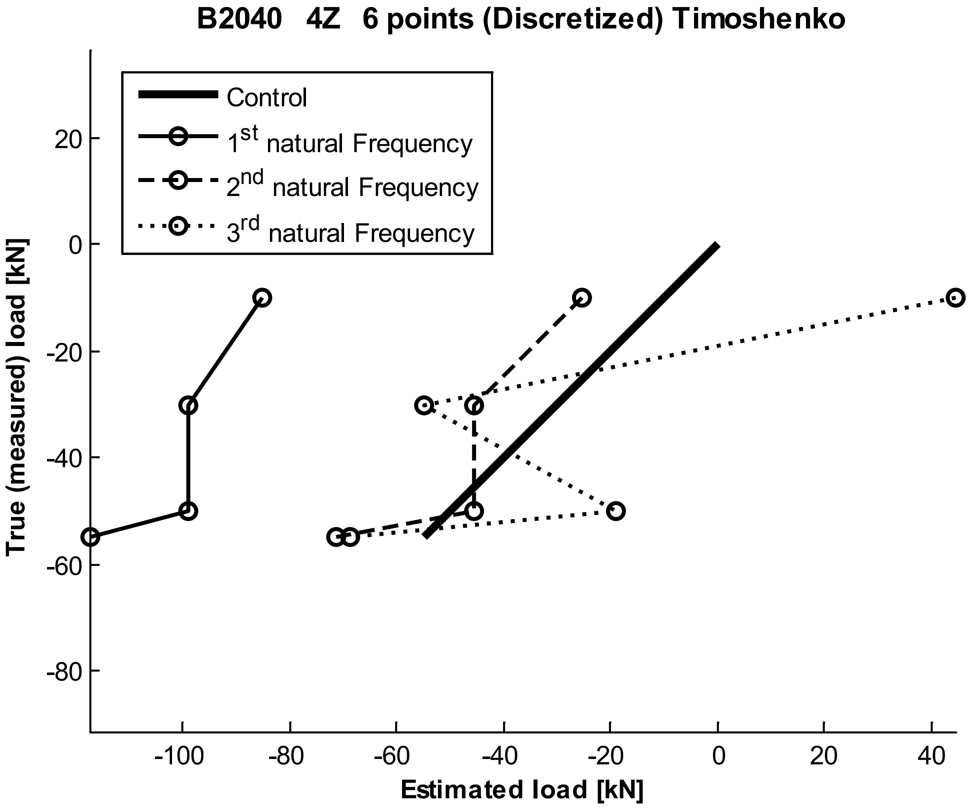
B2040 4Z 6 points (Discretized) Timoshenko
Control
1st natural Frequency
2nd natural Frequency
3rd natural Frequency
True (measured) load [kN]
Estimated load [kN]
20
0
-20
-40
-60
-80
-100
-80
-60
-40
-20
0
20
40

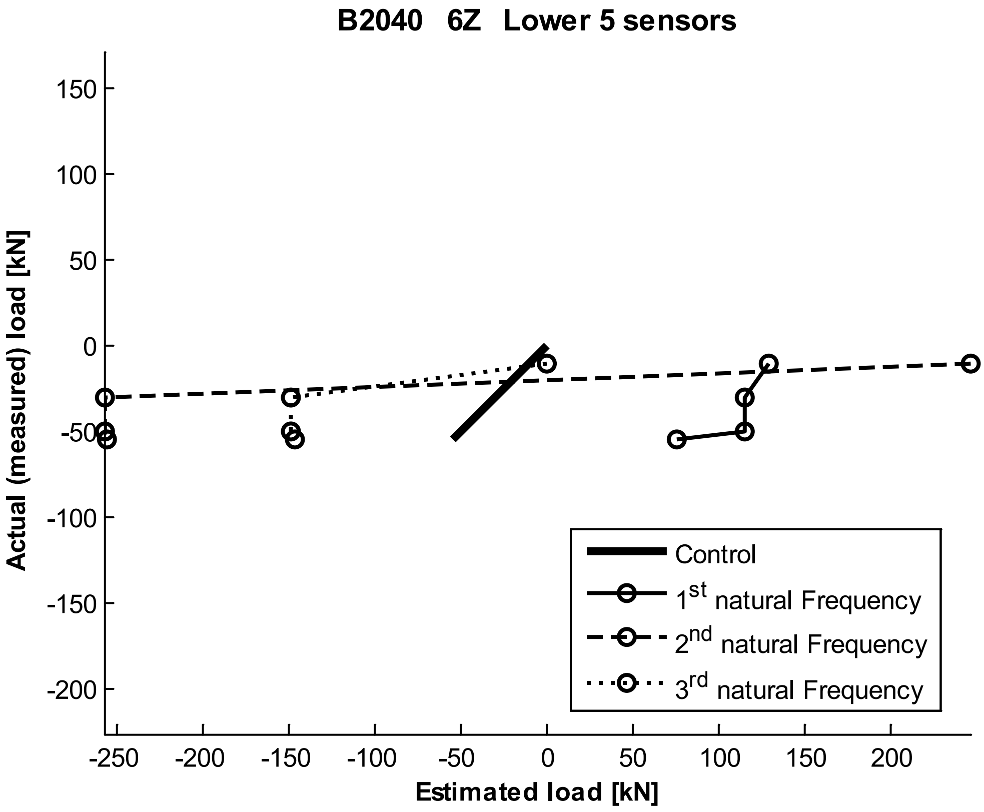
B2040 6Z Lower 5 sensors
Actual (measured) load [kN]
150
100
50
0
-50
-100
-150
-200
Estimated load [kN]
-250
-200
-150
-100
-50
0
50
100
150
200
Control
1st natural Frequency
2nd natural Frequency
3rd natural Frequency

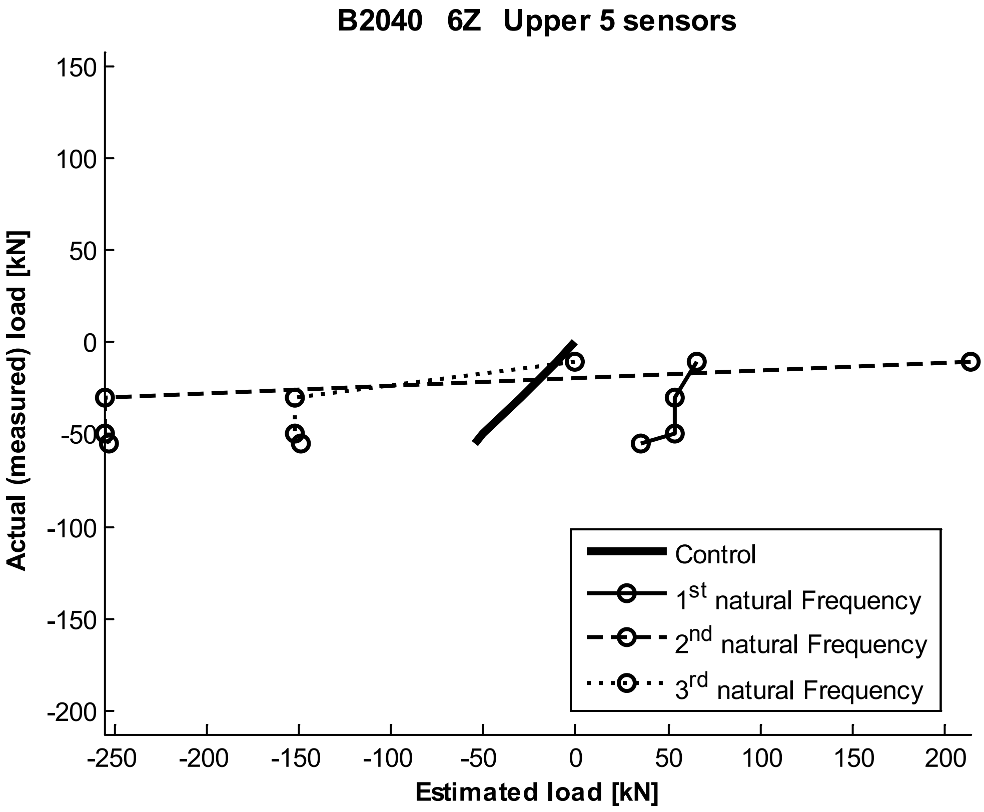
B2040 6Z Upper 5 sensors
Actual (measured) load [kN]
150
100
50
0
-50
-100
-150
-200
Estimated load [kN]
-250
-200
-150
-100
-50
0
50
100
150
200
Control
1st natural Frequency
2nd natural Frequency
3rd natural Frequency

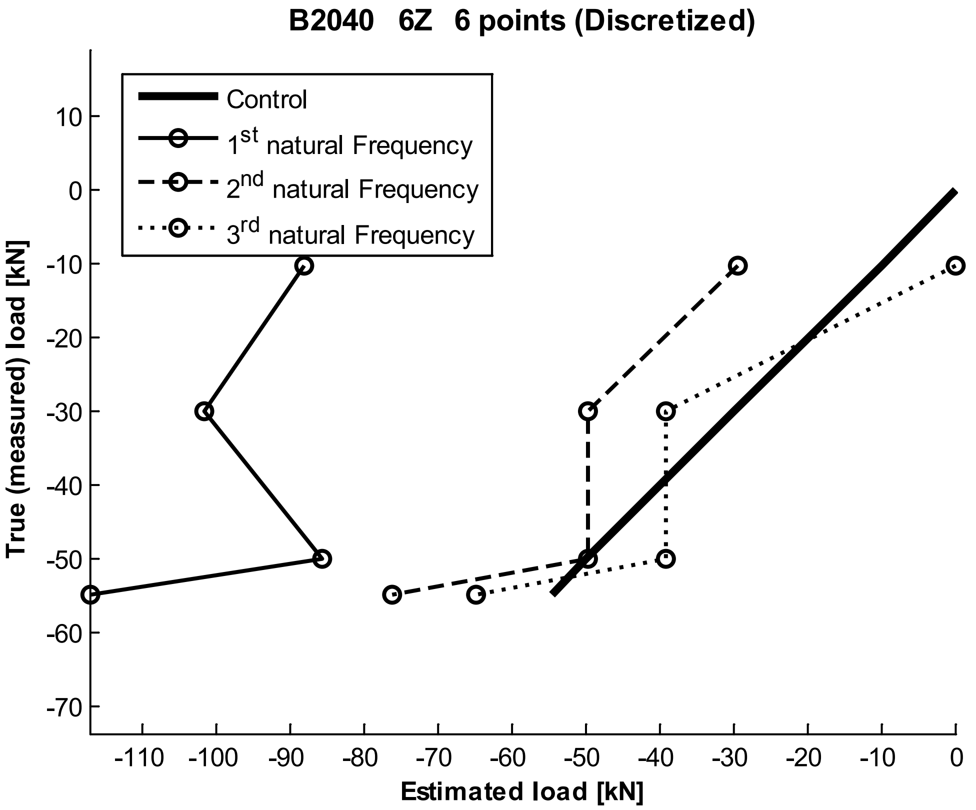
B2040 6Z 6 points (Discretized)
Control
1st natural Frequency
2nd natural Frequency
3rd natural Frequency
True (measured) load [kN]
10
0
-10
-20
-30
-40
-50
-60
-70
-110
-100
-90
-80
-70
-60
-50
-40
-30
-20
-10
0
Estimated load [kN]

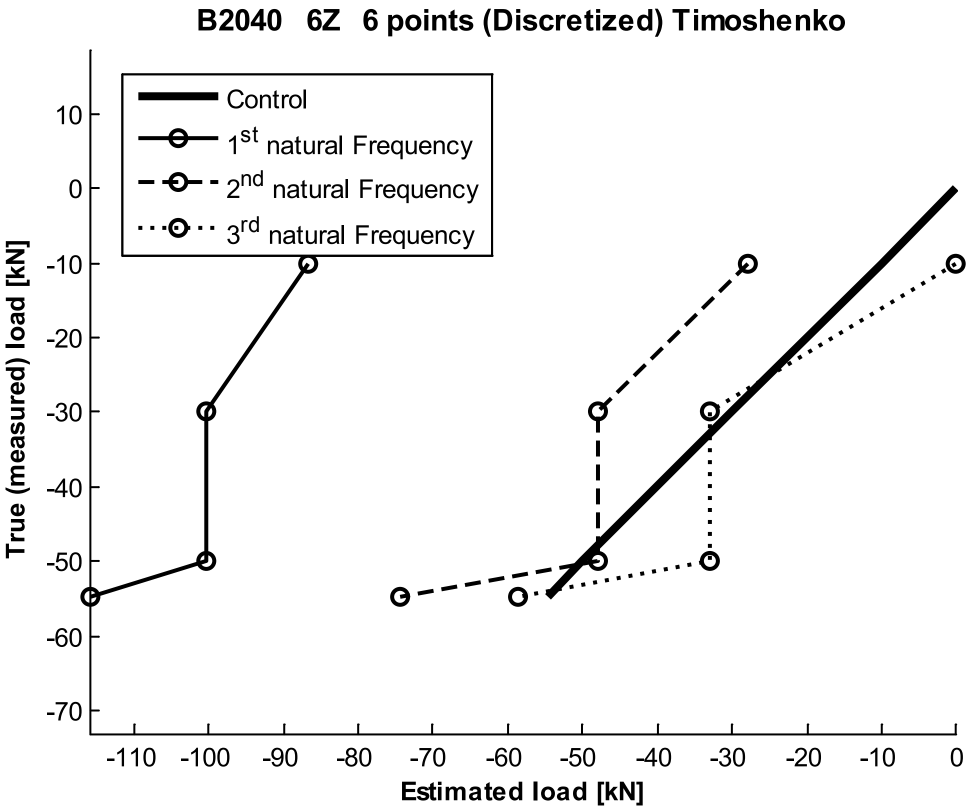
B2040 6Z 6 points (Discretized) Timoshenko
Control
1st natural Frequency
2nd natural Frequency
3rd natural Frequency
True (measured) load [kN]
10
0
-10
-20
-30
-40
-50
-60
-70
-110
-100
-90
-80
-70
-60
-50
-40
-30
-20
-10
0
Estimated load [kN]

B4590

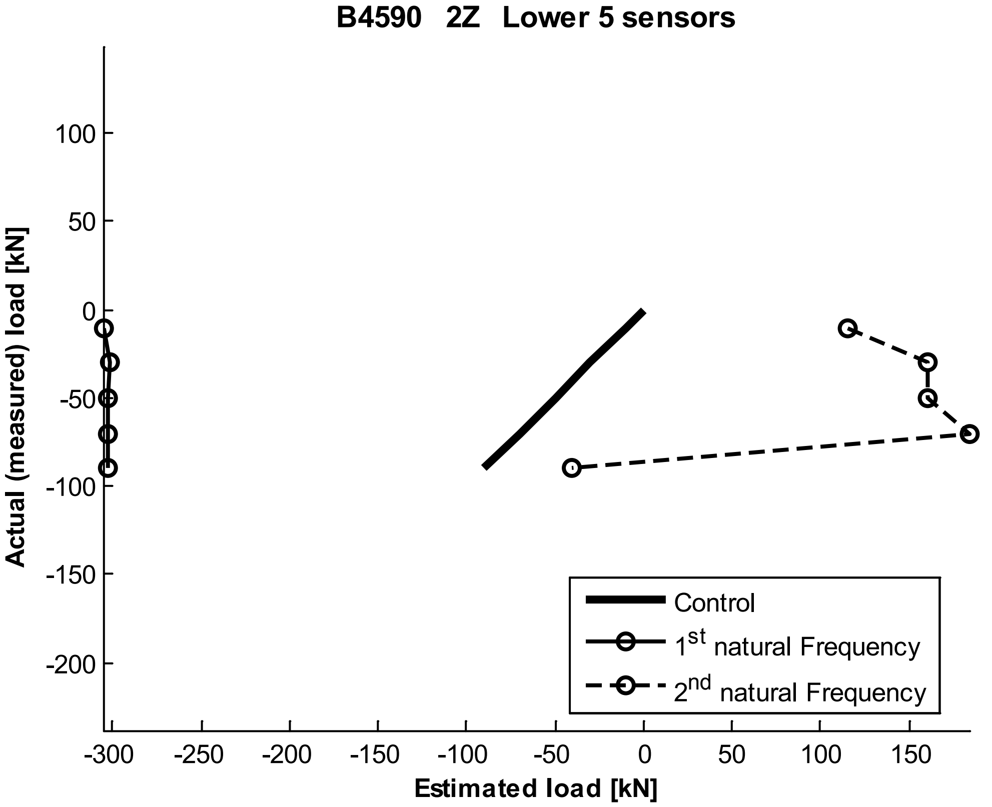
B4590 2Z Lower 5 sensors
Actual (measured) load [kN]
Estimated load [kN]
100
50
0
-50
-100
-150
-200
-300
-250
-200
-150
-100
-50
0
50
100
150
Control
1st natural Frequency
2nd natural Frequency

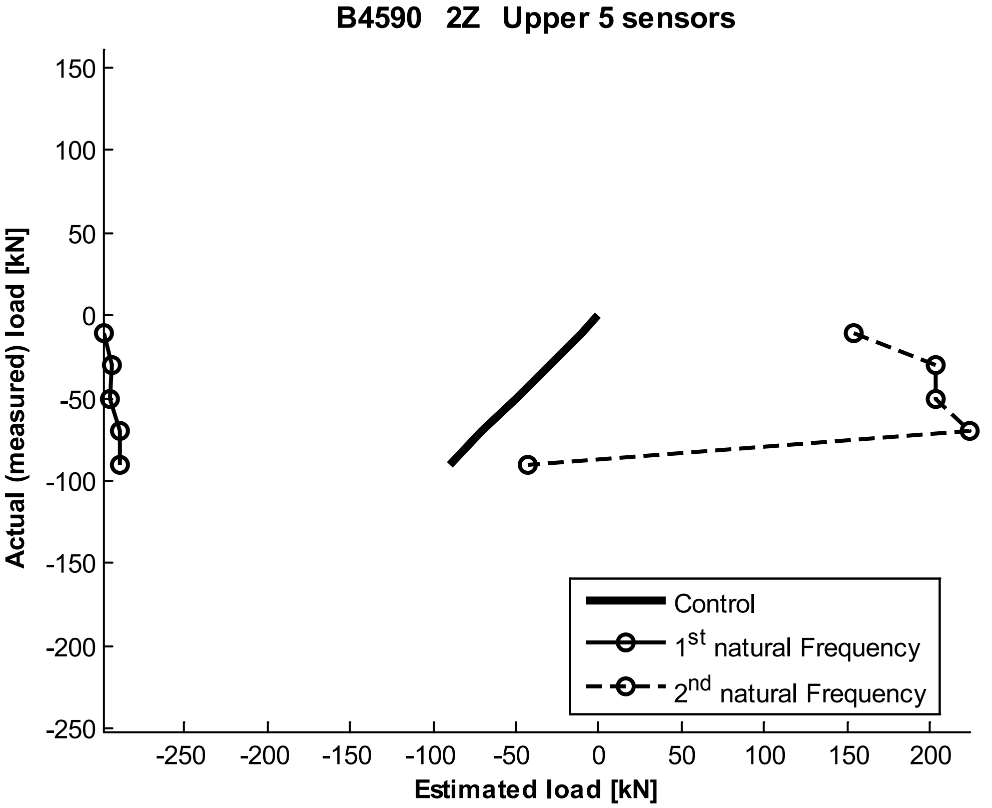
B4590 2Z Upper 5 sensors
Actual (measured) load [kN]
Estimated load [kN]
150
100
50
0
-50
-100
-150
-200
-250
-250
-200
-150
-100
-50
0
50
100
150
200
Control
1st natural Frequency
2nd natural Frequency

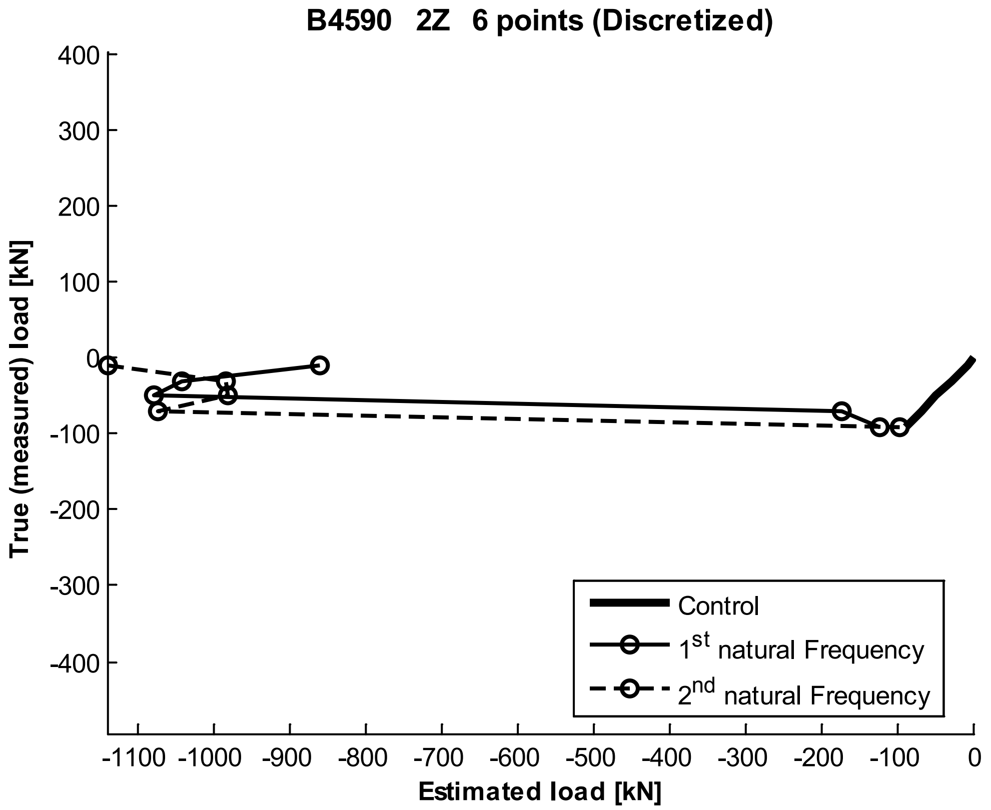
B4590 2Z 6 points (Discretized)
True (measured) load [kN]
400
300
200
100
0
-100
-200
-300
-400
Estimated load [kN]
-1100
-1000
-900
-800
-700
-600
-500
-400
-300
-200
-100
0
Control
1st natural Frequency
2nd natural Frequency

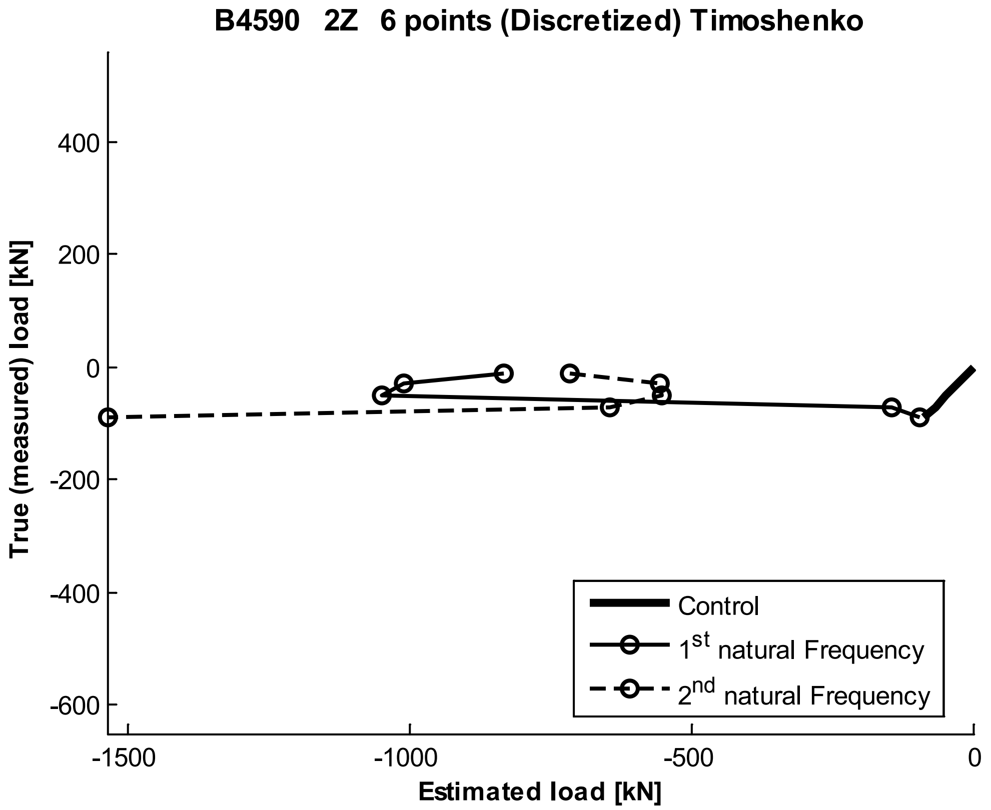
B4590 2Z 6 points (Discretized) Timoshenko
True (measured) load [kN]
400
200
0
-200
-400
-600
Estimated load [kN]
-1500
-1000
-500
0
Control
1st natural Frequency
2nd natural Frequency

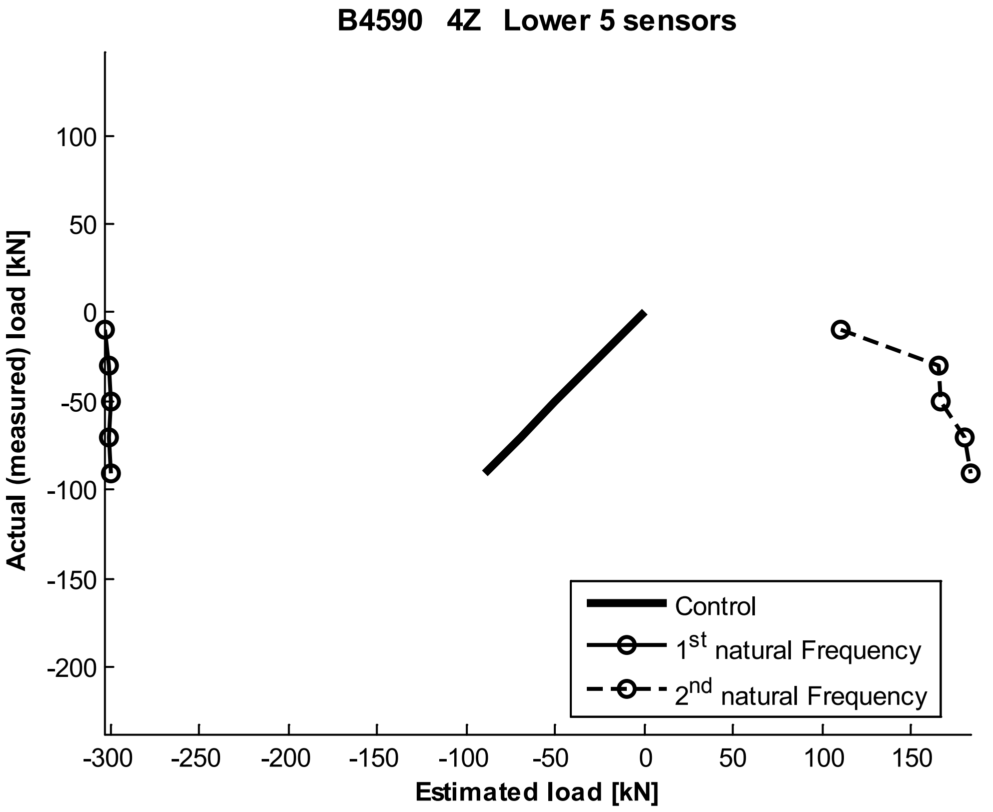
B4590 4Z Lower 5 sensors
Actual (measured) load [kN]
Estimated load [kN]
100
50
0
-50
-100
-150
-200
-300
-250
-200
-150
-100
-50
0
50
100
150
Control
1st natural Frequency
2nd natural Frequency

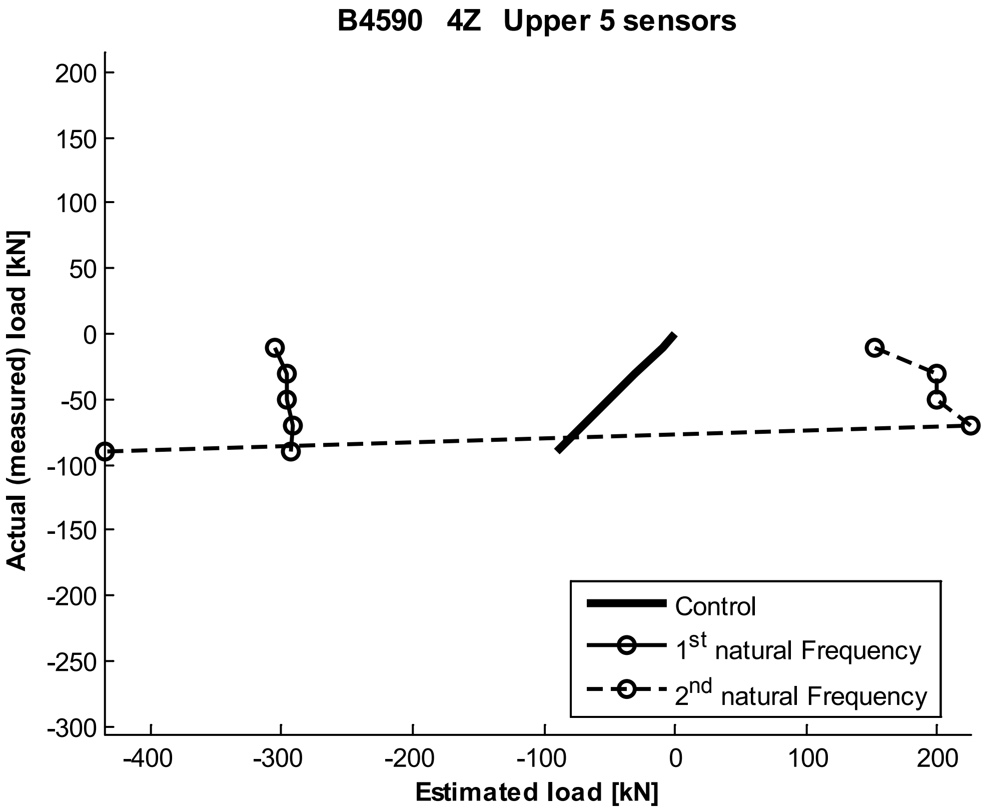
B4590 4Z Upper 5 sensors
Actual (measured) load [kN]
Estimated load [kN]
200
150
100
50
0
-50
-100
-150
-200
-250
-300
-400
-300
-200
-100
0
100
200
Control
1st natural Frequency
2nd natural Frequency

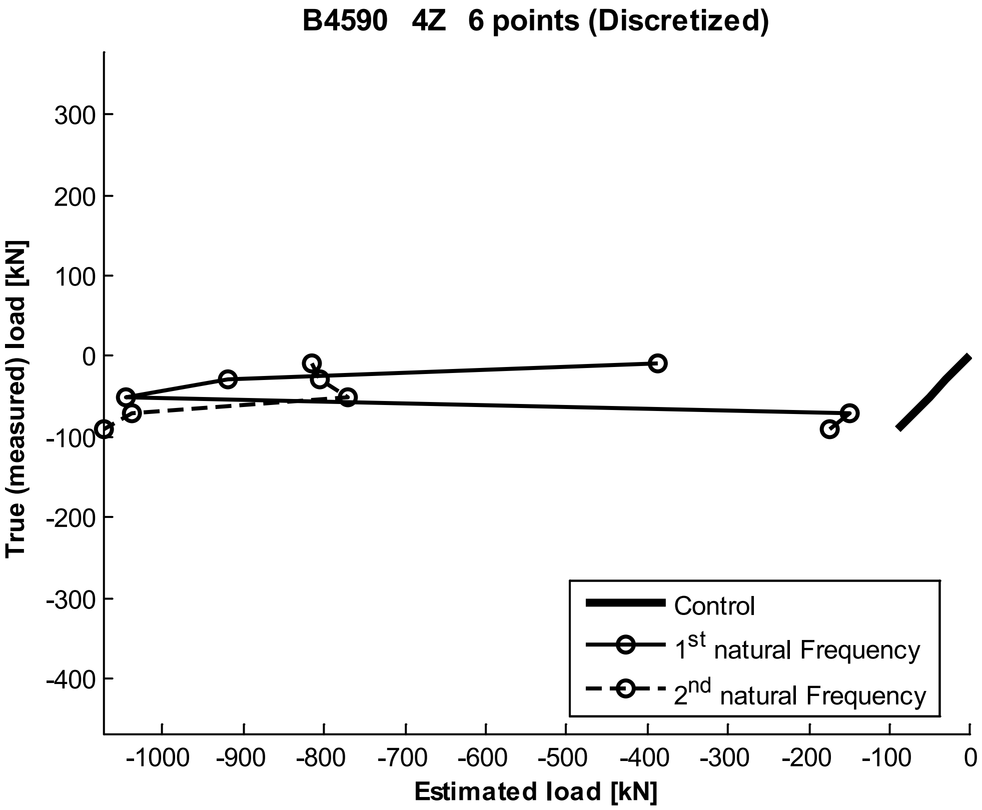
B4590 4Z 6 points (Discretized)
True (measured) load [kN]
300
200
100
0
-100
-200
-300
-400
Estimated load [kN]
-1000
-900
-800
-700
-600
-500
-400
-300
-200
-100
0
Control
1st natural Frequency
2nd natural Frequency

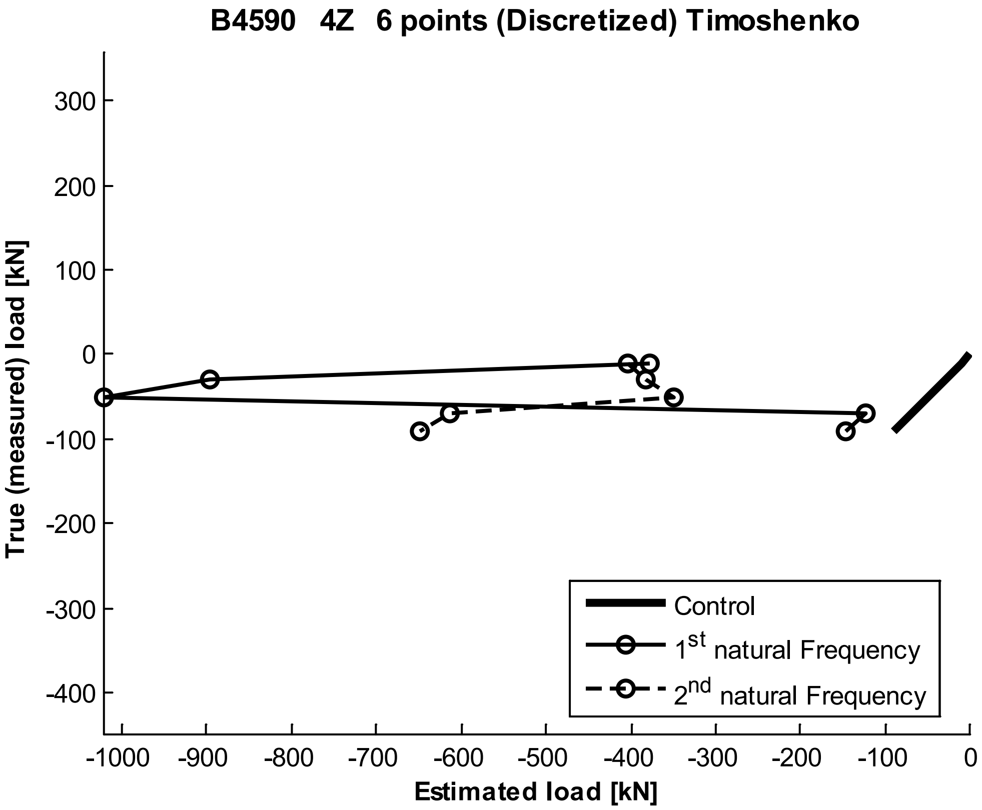
B4590 4Z 6 points (Discretized) Timoshenko
True (measured) load [kN]
300
200
100
0
-100
-200
-300
-400
Estimated load [kN]
-1000
-900
-800
-700
-600
-500
-400
-300
-200
-100
0
Control
1st natural Frequency
2nd natural Frequency

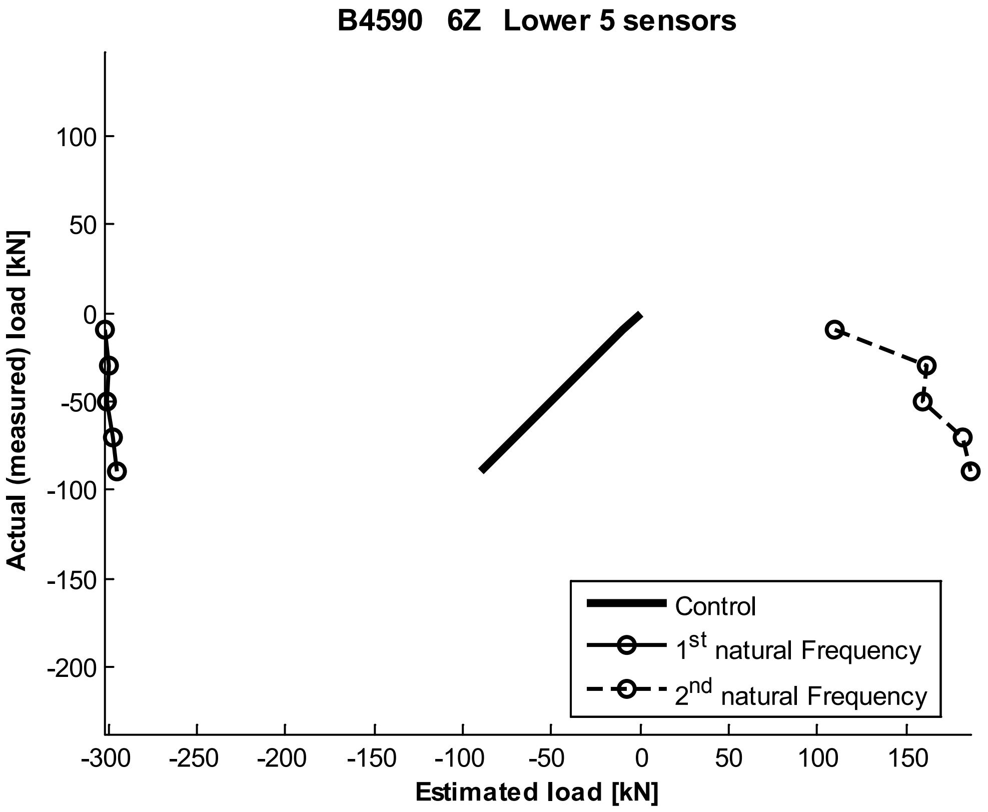
B4590 6Z Lower 5 sensors
Actual (measured) load [kN]
Estimated load [kN]
100
50
0
-50
-100
-150
-200
-300
-250
-200
-150
-100
-50
0
50
100
150
Control
1st natural Frequency
2nd natural Frequency

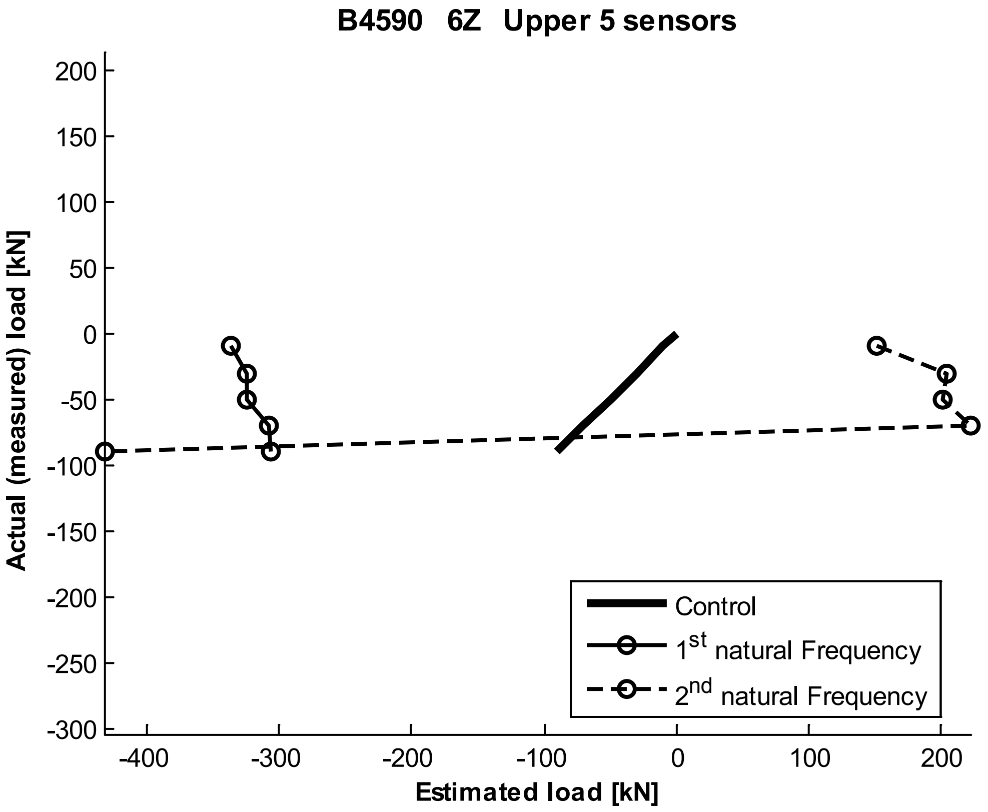
B4590 6Z Upper 5 sensors
Actual (measured) load [kN]
Estimated load [kN]
200
150
100
50
0
-50
-100
-150
-200
-250
-300
-400
-300
-200
-100
0
100
200
Control
1st natural Frequency
2nd natural Frequency

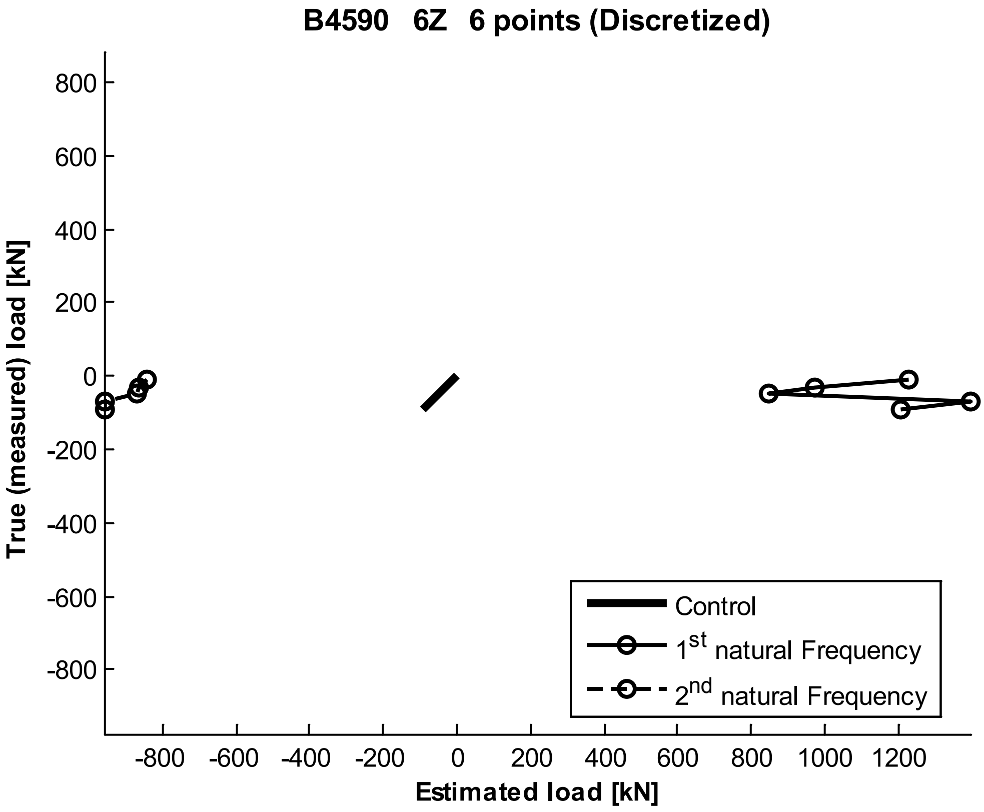
B4590 6Z 6 points (Discretized)

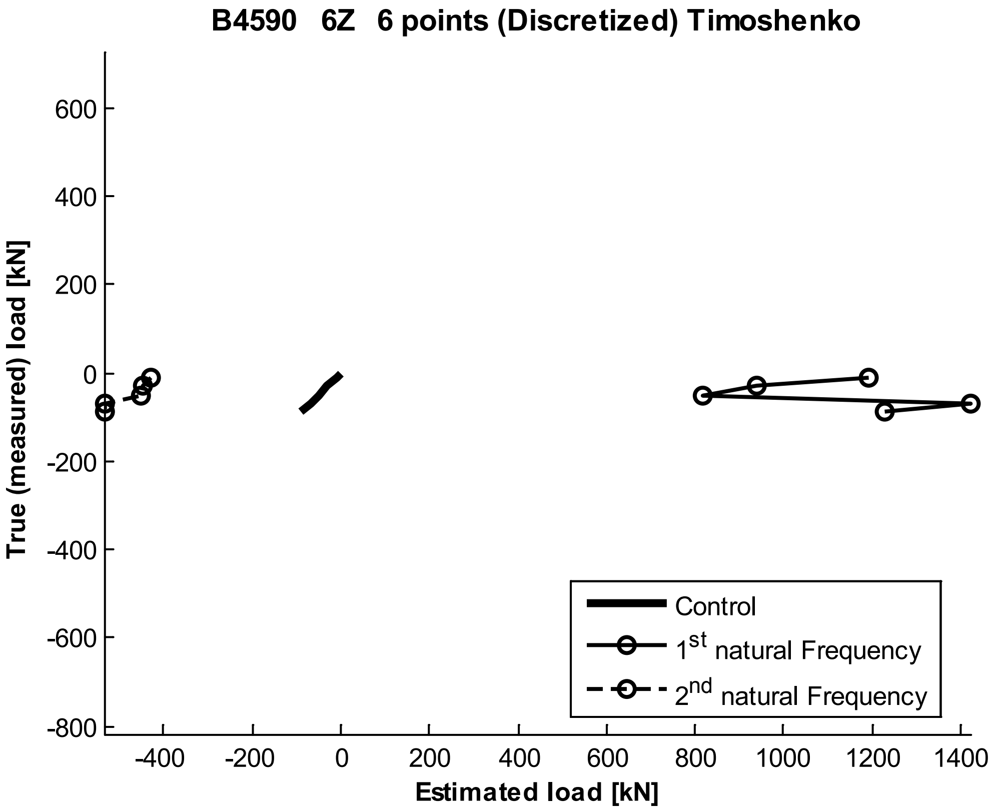
B4590 6Z 6 points (Discretized) Timoshenko